NUNO FILIPE MARCELINO MARTINS

MATHEMATICAL AND NUMERICAL METHODS FOR INVERSE PROBLEMS USING FUNDAMENTAL SOLUTIONS TECHNIQUES

Dissertação apresentada para obtenção do Grau de Doutor em Matemática, especialidade Análise Numérica, pela Universidade Nova de Lisboa, Faculdade de Ciências e Tecnologia.

LISBOA
2008

Acknowledgements

I'm grateful to the Faculdade de Ciências e Tecnologia (UNL) and in particular to the department of mathematics for conceding me a three years leave to do this work. In this period, I was also supported by Fundação para a Ciência e Tecnologia (MCES) through the scholarship SFRH/BD/27914/2006.

I thank my advisor, Professor Carlos Alves, for accepting me at his research group in CEMAT. I was a complete stranger to both inverse problems and meshfree methods (and in fact to Prof. Alves) and he had the patience to guide my first steps in these worlds.

I started my first steps in the world of numerical analysis with Professor Elvira Coimbra, while a licenciatura student. My interest for numerical analysis grew when I became teaching assistant at a numerical analysis course gave by her. It has been a pleasure to be able to work with both.

I thank my "old" friends from the department of mathematics (FCT–UNL), my not so old friend from the Mestrado course in applied mathematics at IST and my (not so new) Ph.D. colleages from IST. Either discussing scientific work or simply talking nonsense at the most strange places it has always been fun.

I can't seem to find the exact word to thank the support of my family (both old and new). It is even harder to fully express my gratitude to my wife Mónica and our son Vasco for the patience (and impatience) as I neared the completion of this work.

Resumo

Neste trabalho são estudados métodos matemáticos e numéricos para problemas inversos relacionados com a identificação e reconstrução de forma, recuperação de coeficientes de Robin e fontes a partir de medições na fronteira. Numa primeira fase, a identificação de formas e coeficientes é estudada num contexto de problemas de valores na fronteira para a equação de Laplace, num domínio limitado Ω_c. A fronteira de Ω_c é dada pela reunião de duas curvas fechadas e regulares Γ (exterior) e γ (interior). Em γ, considera-se uma condição de fronteira homogénea do tipo Dirichlet ou Neumann. Demonstra-se que a partir de dados de Cauchy num conjunto relativamente aberto $\Sigma \subset \Gamma$ é possível identificar γ e a condição de fronteira aí definida. Apresenta-se um critério que permite distinguir a condição de fronteira em γ a partir de um par de dados de Cauchy em Γ. Desenvolvem-se dois métodos numéricos para a resolução do problema inverso geométrico (reconstrução de γ), considerando em $\gamma \subset \mathbb{R}^2$ uma condição de Dirichlet homogénea. O primeiro, é um método que consiste na separação da parte *mal posta* (por intermédio da resolução de um problema de Cauchy) da parte não linear (método de decomposição). O segundo, é um método iterativo do tipo quasi–Newton que requer a resolução de vários problemas directos por cada iterada. Propõe-se a aplicação do método das soluções fundamentais para a resolução numérica problemas anteriores (Cauchy e directos) e são apresentadas várias simulações numéricas para testar estes dois métodos.

Seguidamente, considerando uma condição homogénea mista em γ estuda-se o problema inverso de identificar o coeficiente de Robin na fronteira γ (que agora se supõe ser conhecida) a partir de um par de dados de Cauchy em $\Sigma \subset \Gamma$. Estuda-se uma adaptação dos métodos de decomposição e quasi–Newton anteriormente propostos e apresentam-se várias simulações numéricas para testar e comparar os resultados obtidos através destes métodos.

Os métodos matemáticos e numéricos apresentados para o problema de Laplace são estudados e implementados para os correspondentes problemas geométrico e de Robin em elasticidade linear (sistema de Lamé).

Por fim, estuda-se a identificação de fontes acústicas a partir de medições na fronteira.

Mostra-se que, em geral, tal não é possível a partir de várias medições na fronteira (para um número de onda dado) e propõe-se a utilização de medições obtidas a partir de vários números de onda. Propõe-se a utilização de um método numérico para a resolução deste problema linear baseado no funcional de reciprocidade e apresentam-se resultados de algumas simulações numéricas.

Abstract

In this work we study mathematical and numerical methods for inverse problems related with the identification and reconstruction of shapes, boundary coefficients and sources from boundary measurements. The geometric and coefficient problem is studied in the context of a boundary value problem for the Laplace equation in a non simply connected bounded domain Ω_c. The boundary of Ω_c is the union of two regular closed curves Γ (exterior) and γ (interior). Assuming a homogeneous Dirichlet or Neumann boundary condition on γ, we show that from a single pair of Cauchy data on an accessible part of the boundary $\Sigma \subset \Gamma$ we can identify both the boundary condition and the boundary γ. A criterion is presented to distinguish such situations. We study two numerical methods to retrieve γ in the two dimensional case, when considering a homogeneous Dirichlet condition on γ. The first is a decomposition method requiring at a first step the resolution of a Cauchy problem. The second is a Quasi–Newton method that requires the resolution of several direct problems. For both situations, we propose the method of fundamental solutions as numerical approximation for the Cauchy and direct problems. Several numerical examples are presented and the accuracy and robustness of the methods is discussed. Considering a homogeneous Robin condition on γ, we address the inverse problem that consists in the identification of the Robin coefficient on γ (the boundary is now assumed to be known) from a single pair of Cauchy data on Γ. An adaptation of the decomposition and Quasi–Newton methods is studied and implemented. Several numerical simulations are presented to illustrate and compare the performance of both methods.

The previously developed mathematical and numerical methods are studied in the corresponding geometric and coefficient problems for the Lamé system. The last chapter concerns the identification of acoustic sources from boundary measurements. We show that, from many boundary measurements, identification may not be possible and we propose the use of data generated from many wave numbers. To solve this linear problem, we describe and implement a numerical method based on the reciprocity gap functional. The method is illustrated with several numerical simulations.

Notation and abbreviations

$\| \|$	Euclidean norm of a vector in $\mathbb{R}^d$
$\langle\ ,\ \rangle_H$	inner product in a Hilbert space H
$\|\|\ \|\|_H$	the norm of a vector in a Hilbert space H
$\langle\ ,\ \rangle_{H\times H'}$	duality pairing between H and the dual H'
$\mathbf{u}\cdot\mathbf{v}$	the product defined by $\mathbf{u}\cdot\mathbf{v} := \sum_{i=1}^{d} u_i v_i$
Δ	Laplacian
dx	the infinitesimal volume element $dx_1 \dots dx_d$
$d\varsigma$	the infinitesimal surface element

BVP	boundary value problem(s)
KKM	Kirsch Kress method
MFS	method of fundamental solutions
PDE	partial differential equation(s)

$\mathbf{n},\ \mathbf{n}_x$	the unit normal vector pointing outward on the boundary of a regular bounded domain (at x)
Ω	an open set in $\mathbb{R}^d$: Ω is connected and bounded with regular boundary $\Gamma = \partial\Omega$
$\overline{\Omega}$	the closure of Ω
Ω^{C}	the complement of Ω in $\mathbb{R}^d$

$C^0(\Omega)$	space of continuous functions $f : \Omega \longrightarrow \mathbb{R}$
$C^k(\Omega)$	space of k– times continuously differentiable functions $f : \Omega \longrightarrow \mathbb{R}$
$C^k(\Omega, \mathbb{R}^d)$	k– times continuously differentiable functions $\mathbf{f} : \Omega \longrightarrow \mathbb{R}^d$
$H^r(\Omega)$	the Sobolev space of order r on Ω
$\mathbf{H}^r(\Omega)$	the Sobolev space $(H^r(\Omega))^d$
$L^2(\Omega)$	the Hilbert space of square integrable functions on Ω
$\mathbf{L}^2(\Omega)$	the Hilbert space $(L^2(\Omega))^d$

Contents

List of Figures

List of Tables

1 Introduction

The study of inverse problems in partial differential equations is an area of intensive research in our days. From the mathematical point of view, these problems are quite challenging due to their ill–posed nature. In the early work of Hadamard (cf. [46]), ill–posed problems were believed to be incorrectly posed, "artificial" and that they would not describe physical systems. Many properly formulated inverse problems arise from physical systems. The successful non intrusive medical imaging, discovery of oil reservoirs from seismic measurements (to name a few) are a proof that, despite several mathematical and computational challenges, we can in fact obtain some meaningful information from boundary or exterior measurements. Moreover, one should have in mind that, in practise, a mathematical model (in our case a PDE) is used to describe the physical problem and tested with real measured data. Assuming that the model describes the physical system accurately, two natural questions arise:

1) *How many measurements must we consider in order to identify the object*?

2) *If two measurements that are in some sense close to each other were generated by two objects can we still expect that the objects are "close" to each other ?*

The first is an identifiability question and the second a stability question and are two of the main theoretical questions for the inverse problem.

In inverse problems, the existence issue is inherent to its formulation, in two aspects:

i) we assume that the measured data is given (ie. a solution exists);

ii) the measurements are not exact, are affected by noise (ie. a solution that produces such results does not exist).

Robust numerical methods are also very important. If on one hand we need fast and accurate numerical solvers on the other the method has to be sufficiently robust to deal with the ill posedness. If for the robustness issue regularization methods are usually applied (with good results) the search for a fast accurate (and easy to implement) numerical solver for the underlying PDE is very important.

The method of fundamental solutions (MFS) is a meshfree numerical method usually applied to solve certain boundary value problems. The approximation is given by a linear combination of several shifted fundamental solutions that automatically solve the PDE (here we shall consider Laplace and Helmholtz equations and the Lamé system) and therefore one only has to fit the boundary condition(s). The method has the three aforementioned properties for the addressed problems: is easy to implement, is a fast solver and for sufficiently regular boundaries and boundary data it produces excellent results.

In this work we study several inverse problems related to the identification of sources, boundary coefficients and shape from measurements on an accessible part of the boundary. The study is complemented with several numerical methods relying on the MFS and numerical examples are provided to illustrate the feasibility of the methods. The work is organized as follows:

We start with some useful results or concepts that will be used through the work (Chapter 2).

In Chapter 3 we study two inverse problems that can serve as a model for detection of corrosion from boundary measurements. The domain is a two connected set with interior boundary γ and exterior boundary Γ. Inside, Laplace equation holds and on Γ we have a Dirichlet condition.

First we address a geometric inverse problem: Assuming a null Dirichlet (inclusion) or Neumann (cavity) condition on γ and considering a pair of Cauchy data on part of Γ, *can we identify the shape of γ and the condition on γ from this data* ? If the condition on γ is assumed to be known then there is a result that shows that if the Dirichlet condition on Γ is

not identically constant, a single pair of (compatible) Cauchy data is sufficient to identify γ. We extend this result and show that under the same assumptions we can identify both boundary shape γ and boundary condition on γ. We present a criterion to distinguish such boundary conditions from the Cauchy data on Γ. The well known expression for the domain derivative for the Dirichlet problem is derived and as a consequence, the local Lipschitz stability result.

The second part of this chapter is devoted to the identification of a Robin boundary coefficient Z on γ from Cauchy data on Γ. This Robin problem is similar to other Robin problem addressed by several authors in the literature (eg. [50], [33]) and the identifiability, derivative expression and Local Lipschitz stability results were established using the same type of arguments.

Chapter 4 is devoted to the MFS and its applications to direct and inverse problems and is complemented with several numerical simulations. First a theoretical study of the MFS for the Laplace equation in two connected domains and an application to direct problems in such domains. Several numerical examples are provided with the twofold objective of showing the accuracy of the method for several boundary value problems and to obtain artificially generated boundary measurements for the inverse problem.

The second part is devoted to MFS based methods for the inverse geometric and Robin problems. The methods can be divided in two categories: decomposition based methods and Newton–type of methods.

The first decomposes the ill posedness and non linearity of the inverse problem in two steps. The ill posedness is addressed by solving the linear Cauchy problem. Although several authors have used the MFS as Cauchy problem solver (eg. [52], [67]), to our knowledge, no direct theoretical proofs regarding this numerical approximation have been provided. We provide such results in section 4.2.1 and establish a connection with the MFS approximation for the direct problem. The numerical method for the inverse geometric problem consists in computing an approximate solution for the Cauchy problem and a line search method, based on maximum principle results, to reconstruct the shape of γ. Several numerical examples are presented in order to illustrate the feasibility of the method.

A Levenberg–Marquardt optimization method based on the MFS approximation for direct problems is proposed for the inverse geometric problem. We implemented the proposed method and compared the results with those of the decomposition method. Numerical tests with partial data were also considered.
This study started with the 2006 work [12] and was latter developed and compiled as the paper [15].

The decomposition approach provided a simple reconstruction method for the Robin problem. The Levenberg–Marquardt method was adapted to the Robin problem and a numerical comparison of both methods is presented (for complete and incomplete Cauchy data).

The mathematical study of the geometric and Robin (inverse) problems for the elastostatic problem is addressed in Chapter 5 where the MFS based methods described in the previous chapter are extended to the Lamé system. This chapter is based on the papers [13] and [14].

In the last Chapter, we study the identification and reconstruction of acoustic sources from boundary measurements, following our works [10] and [16].

2

Preliminary results

This introductory chapter surveys useful results concerning the partial differential equations that will be used in the following chapters and some discussion about inverse problems and ill posedness. Since we will be dealing mainly with interior problems, we start with the definition of domain.

Definition 2.1 We define (interior) *domain* as an open, bounded and connected set $\Omega \subset \mathbb{R}^d$ with regular boundary $\Gamma := \partial\Omega$ (at least C^1).

We will address the cases $d = 2, 3$. We recall that on a regular boundary Γ, the normal vector $\mathbf{n}$ is defined at each point. In this work, we will always assume that the normal vector points outward with respect to the domain Ω.

2.1 Poisson equation

Poisson equation or potential equation

$$\Delta u = f \text{ in } \Omega \tag{2.1}$$

is the classical example for second order elliptic partial differential equations and it is a mathematical model to some important physical phenomena. For instance:

- Gravitation problems: u is the gravitation field generated by the mass distribution f.

- Conductivity problems: For a body with constant electric or thermal conductivity K, u is the electric or thermal potential and, for a given source f, we have Poisson's equation

$$\Delta u = f/K.$$

In absence of sources, that is $f \equiv 0$, equation (2.1) is called Laplace equation. These equations may have several solutions and some extra condition(s) must be considered.

The usual boundary conditions for the Poisson equation are:

- **Dirichlet**:

$$u = g \text{ on } \Gamma.$$

  This means that the temperature (in thermal conductivity problems) or the voltage (electrostatic problems) is imposed.

- **Neumann**:

$$\partial_{\mathbf{n}} u = g_1 \text{ on } \Gamma,$$

  where $\mathbf{n}$ is the outward unit normal to the boundary and $\partial_{\mathbf{n}} u$ is the normal derivative on Γ. With this condition we impose heat flux (thermal problems) or current (electrostatic).

- **Robin**:

$$\partial_{\mathbf{n}} u + Zu = g_1 \text{ on } \Gamma,$$

  which is a more general boundary condition. We note that, for the Robin coefficient $Z = 0$ we obtain the Neumann condition and for $Z = \infty$ the Dirichlet condition.

The following are the well known Hopf's lemma and strong maximum principle for Laplace equation. For a proof, see [37].

Lemma 2.2 *(Hopf's lemma) Let $u \in C^2(\Omega) \cap C^0(\overline{\Omega})$ be a function satisfying Laplace's equation in a domain Ω with C^2 boundary. Assume further that $u > 0$ in Ω and that, for some $x_0 \in \partial\Omega$, $u(x_0) = 0$. If the normal derivative $\partial_{\mathbf{n}} u$ at x_0 exists then*

$$\partial_{\mathbf{n}} u(x_0) < 0.$$

Theorem 2.3 *(Maximum principle) If $u \in C^2(\Omega)$ is a solution of Laplace equation in a connected open set Ω, is such that for some $x_0 \in \Omega$*

$$u(x) \leq u(x_0),\ \forall x \in \Omega$$

then u is constant in Ω.

A function $u \in C^2(\Omega)$ that satisfies $\Delta u = 0$ in Ω is called a classical solution of Laplace's equation. However, classical solutions to boundary value problems may not exist and we must consider weak solutions. In this framework, the boundary conditions must be understood in the trace sense. For instance, if Ω is a domain with C^2 boundary and $u \in H^2(\Omega)$ then, by the trace theorem, the trace

$$\tau_\Gamma u := u|_\Gamma$$

is an element in $H^{3/2}(\Gamma) \subset L^2(\Gamma)$ and $\tau_\Gamma : H^2(\Omega) \to H^{3/2}(\Gamma)$ is linear, continuous and surjective. The normal trace of $u \in H^2(\Omega)$,

$$\tau_\Gamma^{\mathbf{n}} u := \partial_{\mathbf{n}} u|_\Gamma$$

is in $H^{1/2}(\Gamma) \subset L^2(\Gamma)$ and $\tau_\Gamma^{\mathbf{n}} : H^2(\Omega) \to H^{1/2}(\Gamma)$ is also linear, continuous and surjective (eg. [37]). For $u \in H^1(\Omega)$ with Ω a domain with C^1 boundary the trace $\tau_\Gamma u$ is an element in $H^{1/2}(\Gamma)$ (trace theorem). In this case, if $u \in H^1_\Delta(\Omega)$ where

$$H^1_\Delta(\Omega) := \left\{ u \in H^1(\Omega) : \Delta u \in L^2(\Omega) \right\},$$

the normal trace $\tau_\Gamma^{\mathbf{n}} u$ can be defined as an element in $H^{-1/2}(\Gamma)$. In both situations, the trace and normal trace are linear and continuous from $H^1(\Omega)$ ($H^1_\Delta(\Omega)$) onto $H^{1/2}(\Gamma)$ ($H^{-1/2}(\Gamma)$). We recall that $H^{-1/2}(\Gamma)$ can be identified with the dual of $H^{1/2}(\Gamma)$ using $L^2(\Gamma)$ as pivot space and that the inclusions

$$H^{1/2}(\Gamma) \subset L^2(\Gamma) \subset H^{-1/2}(\Gamma)$$

hold. The realization of the duality pairing is just the $L^2(\Gamma)$ inner product extended to $H^{1/2}(\Gamma) \times H^{-1/2}(\Gamma)$.

Solutions of Poisson equation can be represented by a sum of convolutions. This leads to an integral representation of the solution in terms of boundary layers and Newton potentials with kernel defined in terms of fundamental solutions. We start with some properties of such solutions.

2.1.1 Fundamental solutions

A fundamental solution for the Laplace equation is a solution of

$$\Delta\Phi = -\delta$$

in $\mathbb{R}^d$, where δ is the Dirac delta distribution centered at the origin. A fundamental solution is not unique and depends on the dimension of the space. When $\Omega \subset \mathbb{R}^2$ (2D case) we consider

$$\Phi(x) := -\frac{1}{2\pi}\log|x|$$

and in the 3D case ($\Omega \subset \mathbb{R}^3$)

$$\Phi(x) := \frac{1}{4\pi|x|}.$$

Fundamental solutions are analytic in $\mathbb{R}^d$ except at the origin, where there is a singularity. We note that a shift of the singularity from the origin to a point y can be obtained by taking the *point source function*

$$\Phi_y(x) := \Phi(y-x),\ x \in \mathbb{R}^d \setminus \{y\}. \tag{2.2}$$

This notation is justified by the fact that $\nabla_x\Phi_y(x) \neq \nabla_y\Phi_y(x)$ (despite $\Phi_y(x) = \Phi_x(y)$). A shift on the fundamental solution is a response to a shift of the mass center on the Dirac delta. More precisely, $\Delta\Phi_y = -\delta_y$ in $\mathbb{R}^d$, where δ_y denotes the Dirac distribution with mass center at y.

2.1.2 Integral representation

Gauss–Green integration by parts formulas are an essential tool in the study of several boundary value problems. Given $u \in H^2(\Omega), v \in H^1(\Omega)$, we have the first Green formula

$$\int_\Omega \nabla u \cdot \nabla v dx - \int_\Gamma \partial_{\mathbf{n}} uv d\varsigma = -\int_\Omega \Delta uv dx$$

and, if $v \in H^2(\Omega)$, the second Green formula

$$\int_\Omega (\Delta uv - u\Delta v)dx = \int_\Gamma (\partial_{\mathbf{n}} uv - u\partial_{\mathbf{n}} v)d\varsigma.$$

The *reciprocity functional* (cf. [31]) is defined by

$$\mathcal{R}(v) := \int_\Gamma (\partial_{\mathbf{n}} u v - u \partial_{\mathbf{n}} v) d\varsigma$$

and by the second formula,

$$\mathcal{R}(v) = \int_\Omega (\Delta u v - u \Delta v) dx, \ \forall u, v \in H^2(\Omega).$$

In the particular case $\Delta u = \Delta v = 0$, we obtain the reciprocity relation

$$\mathcal{R}(v) = 0.$$

Given some integrable density ϕ, the *single layer potential* is defined by

$$L_\Gamma(\phi)(y) := \int_\Gamma \Phi_y(x)\phi(x) d\varsigma_x, \ y \in \mathbb{R}^d \setminus \Gamma$$

and the *double layer potential* by

$$M_\Gamma(\phi)(y) := \int_\Gamma \partial_{\mathbf{n}_x} \Phi_y(x)\phi(x) d\varsigma_x, \ y \in \mathbb{R}^d \setminus \Gamma.$$

We use the notation $(L_\Gamma(\phi))^+$ and $(L_\Gamma(\phi))^-$ to indicate the restriction of $L_\Gamma(\phi)$ to $\overline{\Omega}^{\mathrm{C}}$ and Ω respectively. The same notation will be used for the double layer potential. We denote by $S_\Gamma^\pm$ and $K_\Gamma^\pm$ the trace of the single and double layer potentials, ie.,

$$S_\Gamma^\pm(\phi) := \tau_\Gamma(L_\Gamma(\phi))^\pm \text{ and } K_\Gamma^\pm(\phi) := \tau_\Gamma(M_\Gamma(\phi))^\pm$$

and by $N_\Gamma^\pm$ and $D_\Gamma^\pm$ the normal traces

$$N_\Gamma^\pm(\phi) := \tau_\Gamma^{\mathbf{n}}(L_\Gamma(\phi))^\pm \text{ and } D_\Gamma^\pm(\phi) := \tau_\Gamma^{\mathbf{n}}(M_\Gamma(\phi))^\pm.$$

Define

$$K_\Gamma(\phi)(y) := \int_\Gamma \partial_{\mathbf{n}_y} \Phi_y(x)\phi(x) d\varsigma_x, \ y \in \Gamma. \tag{2.3}$$

Theorem 2.4 *([34]) Given $\phi \in H^{1/2}(\Gamma)$ and $\psi \in H^{3/2}(\Gamma)$ we have,*

(a) $S_\Gamma^+(\phi) = S_\Gamma^-(\phi)$ *(c)* $N_\Gamma^\pm(\phi) = \mp\frac{1}{2}\phi + K_\Gamma^*(\phi)$

(b) $K_\Gamma^\pm(\psi) = \pm\frac{1}{2}\psi + K_\Gamma(\psi)$ *(d)* $D_\Gamma^+(\psi) = D_\Gamma^-(\psi)$

where K_Γ^* denotes the adjoint of K_Γ.

Let f be a source with compact support $\overline{\Omega}_f$ and such that $\Phi_y f$ is integrable in $\mathbb{R}^d$. The *Newton potential* is defined by the improper integral

$$V(f)(y) := \int_{\mathbb{R}^d} \Phi_y(x) f(x) dx.$$

When the previous integration is performed on some open set $\Omega \subset \mathbb{R}^d$ we write $V_\Omega(f)$. Let $u^- \in H^2(\Omega)$ be such that $\Delta u^- = f$ in Ω. Green's formula yield

$$u^-(y) = -V_\Omega(f)(y) + (L_\Gamma(\partial_{\mathbf{n}} u^-))^-(y) - (M_\Gamma(u^-))^-(y),\ y \in \Omega.$$

On the other hand, if $u^+ \in H^2(\overline{\Omega}^{\mathrm{C}})$ is such that $\Delta u^+ = f$ in $\overline{\Omega}^{\mathrm{C}}$ and

$$u^+(y) = O(|y|^{-\alpha}) \ \wedge\ \nabla u^+(y) = O(|y|^{-1-\alpha}) \qquad |y| \to \infty \tag{2.4}$$

then (see [34]), if $\alpha > 0$,

$$u^+(y) = -V_{\overline{\Omega}^{\mathrm{C}}}(f)(y) - (L_\Gamma(\partial_{\mathbf{n}} u^+))^+(y) + (M_\Gamma(u^+))^+(y),\ y \in \overline{\Omega}^{\mathrm{C}}.$$

Thus, if $u := \chi_\Omega u^- + \chi_{\overline{\Omega}^{\mathrm{C}}} u^+$, where χ_Ω denotes the characteristic function on Ω and defining the boundary jumps

$$[u]_\Gamma := u^-|_\Gamma - u^+|_\Gamma, \quad [\partial_{\mathbf{n}} u]_\Gamma := \partial_{\mathbf{n}} u^-|_\Gamma - \partial_{\mathbf{n}} u^+|_\Gamma$$

we conclude that

$$u(y) = -V(f)(y) + L_\Gamma([\partial_{\mathbf{n}} u]_\Gamma)(y) - M_\Gamma([u]_\Gamma)(y),\ y \in \mathbb{R}^d \setminus \Gamma. \tag{2.5}$$

We note that this integral representation is unique, in the sense that, if

$$u(y) = -V(f)(y) + L_\Gamma(\phi)(y) - M_\Gamma(\psi)(y)$$

then

$$[u]_\Gamma = u^-|_\Gamma - u|_\Gamma^+ = S_\Gamma^-(\phi) - K_\Gamma^-(\psi) - S_\Gamma^+(\phi) + K_\Gamma^+(\psi) = \psi$$

and

$$[\partial_{\mathbf{n}} u]_\Gamma = \partial_{\mathbf{n}} u^-|_\Gamma - \partial_{\mathbf{n}} u|_\Gamma^+ = N_\Gamma^-(\phi) - D_\Gamma^-(\psi) - N_\Gamma^+(\phi) + D_\Gamma^+(\psi) = \phi.$$

We finish this section with unique continuation principles and Holmgren lemma which are a useful tool for identification results in inverse problems. Holmgren lemma is a

classical result and a proof can be found in [37]. Our proof, however, is different and gives insight to derive similar results for other problems with solutions admitting integral representations of the form (2.5).

Lemma 2.5 *Let u be defined by (2.5) and suppose that $\overline{\Omega}_f \subset \Omega$ and $u = 0$ in $\overline{\Omega}^{\mathrm{C}}$. If $\Sigma \subset \Gamma$ is a relative (non empty) open set such that*

$$[u]_\Sigma = [\partial_{\mathbf{n}} u]_\Sigma = 0$$

then $u = 0$ in the connected component of $\overline{\Omega} \setminus \overline{\Omega}_f$ containing Γ.

Proof. With this hypothesis, we can write

$$u = \begin{cases} -V_\Omega(f) + L_{\Gamma\setminus\Sigma}([\partial_{\mathbf{n}} u]) - M_{\Gamma\setminus\Sigma}([u]) & \text{in } \Omega \\ 0 & \text{in } \overline{\Omega}^{\mathrm{C}} \cup \Sigma \end{cases}.$$

By analyticity of fundamental solutions, this representation implies that u is analytic in $\mathbb{R}^d \setminus (\overline{\Omega}_f \cup (\Gamma \setminus \Sigma))$. On the other hand, $u = 0$ in $\overline{\Omega}^{\mathrm{C}}$ and by analytic continuation through Σ, we conclude that u is also null in the connected component of $\overline{\Omega} \setminus \overline{\Omega}_f$ containing Γ. □

Corollary 2.6 *Let $u \in H^2(\Omega)$ satisfy*

$$\begin{cases} \Delta u = f & \text{in } \Omega \\ u = \partial_{\mathbf{n}} u = 0 & \text{on } \Sigma \end{cases}$$

for a source f, null in an open and connected set $\overline{\Omega}_f^{\mathrm{C}} \subset \Omega$ such that $\Gamma \subset \partial\overline{\Omega}_f^{\mathrm{C}}$. Then,

$$u = 0 \text{ in } \overline{\Omega}_f^{\mathrm{C}}.$$

In particular, the unique solution of Laplace equation with null Cauchy data on Σ is $u = 0$.

Remark 2.7 We note that the integral representation and Holmgren's lemma are still valid for $u \in H^1_\Delta(\Omega)$. In this situation, the normal trace is in $H^{-1/2}(\Gamma)$ and the single layer potential must be considered in the duality sense.

2.2 Helmholtz equation

In this section we give a brief description of the physical context of the Helmholtz equation and the boundary conditions usually considered in boundary value problems. An application of Green formulas and the previous properties of potentials yields a similar

representation formula for a solution of Helmholtz equation. In particular, the Holmgren lemma is also valid for the Helmholtz case.

The Helmholtz equation

$$\Delta u + \kappa^2 u = 0$$

arises naturally in physical applications related to wave propagation and vibration phenomena. The constant κ is called *wave number* and can be seen as the quotient between the frequency $\omega > 0$ and the speed of the wave propagation c. In the presence of an acoustic source, we have the non homogeneous Helmholtz equation

$$\Delta u + \kappa^2 u = f.$$

For $\kappa = 0$, this non homogeneous equation reduces to Poisson equation. Although the wave number can be a complex function we will consider only the constant and non negative situation.

Plane waves

Plane waves are functions defined by

$$v_{\kappa,\widehat{d}}(x) := e^{i\kappa x\cdot\widehat{d}}, \;\; \widehat{d} \in S^{d-1}$$

where $S^{d-1} := \{x \in \mathbb{R}^d : |x| = 1\}$ and are particular solutions of the homogeneous Helmholtz equation, ie.,

$$(\Delta + \kappa^2 I)v_{\kappa,\widehat{d}} = 0 \text{ in } \mathbb{R}^d$$

in all directions $\widehat{d} \in S^{d-1}$.

Boundary conditions

For a domain Ω with boundary Γ, we consider the Dirichlet and Neumann conditions:

- **Dirichlet**:

  $$u = g \text{ on } \Gamma.$$

  With this condition we are imposing (or measuring) the pressure for the sound wave at the boundary.

- **Neumann**:

  $$\partial_{\mathbf{n}} u = g_1 \text{ on } \Gamma,$$

and this corresponds to the prescription of the normal component of the velocity of the wave at the boundary.

When null pressure is imposed on the boundary we obtain the *eigenvalue problem for the Laplace–Dirichlet operator*

$$\begin{cases} \Delta u = -\kappa^2 u & \text{in } \Omega \\ u = 0 & \text{on } \Gamma \end{cases}.$$

2.2.1 Fundamental solutions

A fundamental solution for the Helmholtz equation satisfies

$$\Delta \Phi_\kappa + \kappa^2 \Phi_\kappa = -\delta$$

in $\mathbb{R}^d$ and the usual expression is (see [34])

$$\Phi_\kappa(x) := \frac{i}{4} H_0^{(1)}(\kappa|x|) \tag{2.6}$$

in the 2D case and

$$\Phi_\kappa(x) := \frac{e^{i\kappa|x|}}{4\pi|x|}$$

in the 3D case, where $H_0^{(1)}$ is the first Hänkel function. When there is no ambiguity about the dependence on κ, we simply write Φ. With this notation, the point source function $\Phi_y : \mathbb{R}^d \setminus \{y\} \longrightarrow \mathbb{C}$ defined by

$$\Phi_y(x) := \Phi(y - x)$$

is analytic and we have

$$\Delta \Phi_y + \kappa^2 \Phi_y = -\delta_y \text{ in } \mathbb{R}^d.$$

2.2.2 Integral representation

Consider the Newton and the boundary layer potentials with kernel given by the aforementioned fundamental solution and the corresponding trace and normal trace. Then, the acoustic version of Theorem 2.4 holds (see [34]) and the asymptotic behavior is now given by the Sommerfeld radiation condition

$$\lim_{r \to \infty} r^{\frac{d-1}{2}} \left(\frac{\partial u}{\partial r} - i\kappa u \right) = 0$$

where $r = |x|$ and the limit is assumed to hold uniformly in all directions $x/|x|$. Thus, for u satisfying the inhomogeneous Helmholtz equation and the Sommerfeld radiation condition we have the integral representation

$$u(y) = -V(f)(y) + L_\Gamma([\partial_{\mathbf{n}} u]_\Gamma)(y) - M_\Gamma([u]_\Gamma)(y),\ y \in \mathbb{R}^d \setminus \Gamma.$$

The following, is the version of corollary 2.6 for the Helmholtz equation.

Lemma 2.8 *Let $u \in H^2(\Omega)$ satisfy*

$$\begin{cases} \Delta u + \kappa^2 u = f & \text{in } \Omega \\ u = \partial_{\mathbf{n}} u = 0 & \text{on } \Sigma \subset \Gamma \end{cases}$$

for a source f, null in an open and connected set $\overline{\Omega}_f^{\mathrm{C}} \subset \Omega$ such that $\Gamma \subset \partial\overline{\Omega}_f^{\mathrm{C}}$. Then,

$$u = 0 \text{ in } \overline{\Omega}_f^{\mathrm{C}}.$$

In particular, the unique solution of the homogeneous Helmholtz equation in Ω with null Cauchy data on Σ is $u = 0$.

Considering the single layer potential defined in a duality sense, the integral representation and the previous lemma are valid for $u \in H^1_\Delta(\Omega)$.

2.3 Elasticity system

An Hookean or linear elastic body has the property that the stress tensor, σ, is zero in the undeformed state and deforms with a linear stress-strain relationship without dissipation of energy. Supposing further that the body is isotropic and homogeneous, we have by Hooke's law

$$[\sigma(\mathbf{u})]_{ij} = [\lambda(\nabla.\mathbf{u})\mathbf{I} + 2\mu\epsilon(\mathbf{u})]_{ij}$$

where:

- $\mathbf{u} = (u_1, \ldots, u_d)$, $d = 2, 3$ is a vectorial function describing the displacement of the body and $\nabla \cdot \mathbf{u}$ is the divergence of the displacement,
- ϵ is the stress-strain tensor of $\mathbf{u}$ and is given by

$$[\epsilon(\mathbf{u})]_{ij} = \frac{1}{2}\left(\frac{\partial u_i}{\partial x_j} + \frac{\partial u_j}{\partial x_i}\right) = \frac{1}{2}\left[\nabla\mathbf{u} + \nabla\mathbf{u}^\top\right]_{ij}$$

and

- λ and μ are the *Lamé coefficients*, which are (positive) parameters describing elastic properties of the body.

The equations of motion of an elastic body under a body force $\mathbf{f}$ are given by

$$\nabla \cdot \sigma(\mathbf{u}) - \mathbf{f} = \rho \frac{\partial^2 \mathbf{u}}{\partial t^2}$$

where ρ is the mass density. When there is no body force and when the body is in static equilibrium the equations of motion reduce to the Lamé system (or Cauchy–Navier equation of elastostatics)

$$\nabla \cdot \sigma(\mathbf{u}) = \mathbf{0}.$$

We define

$$\Delta^* \mathbf{u} := \nabla \cdot \sigma(\mathbf{u}).$$

Using the formal identity $\Delta = \nabla(\nabla\cdot) - \nabla \times \nabla\times$ we can write

$$\begin{aligned} \Delta^* \mathbf{u} &= \mu \nabla \cdot (\nabla \mathbf{u}) + (\lambda + \mu) \nabla(\nabla \cdot \mathbf{u}) \\ &= \mu \Delta \mathbf{u} + (\lambda + \mu) \nabla(\nabla \cdot \mathbf{u}), \end{aligned}$$

where $\Delta \mathbf{u} = (\Delta u_1, \ldots, \Delta u_d)$.

The usual boundary conditions for the Lamé system are:

- **Dirichlet**:

  $$\mathbf{u} = \mathbf{g} \text{ on } \Gamma.$$

  This means that the displacement on the boundary is prescribed.

- **Neumann**:

  $$\partial^*_{\mathbf{n}} \mathbf{u} = \mathbf{g}_1 \text{ on } \Gamma,$$

  where $\partial^*_{\mathbf{n}} \mathbf{u} := \sigma(\mathbf{u})\mathbf{n}$ is the traction vector.

- **Robin**:

  $$\partial^*_{\mathbf{n}} \mathbf{u} + \mathbf{Z}\mathbf{u} = \mathbf{g}_1 \text{ on } \Gamma,$$

  where the Robin coefficient $\mathbf{Z}$ is now a matrix.

2.3.1 Fundamental tensors

A fundamental solution for the Lamé system is a solution of

$$\Delta^* \mathbf{\Phi} = -\delta \mathbb{I}$$

in $\mathbb{R}^d$, where $\mathbb{I}$ is the identity matrix. We consider (eg. [34])

$$[\mathbf{\Phi}(x)]_{i,j} := \frac{\lambda + 3\mu}{4\pi\mu(\lambda + 2\mu)} \left(-\log|x|\delta_{ij} + \frac{\lambda + \mu}{\lambda + 3\mu} \frac{x_i x_j}{|x|^2} \right),\ 1 \leq i, j \leq 2$$

in $\mathbb{R}^2$ and in $\mathbb{R}^3$,

$$[\mathbf{\Phi}(x)]_{i,j} := \frac{\lambda + 3\mu}{8\pi\mu(\lambda + 2\mu)} \left(\frac{1}{|x|}\delta_{ij} + \frac{\lambda + \mu}{\lambda + 3\mu} \frac{x_i x_j}{|x|^3} \right),\ 1 \leq i, j \leq 3,$$

where δ_{ij} is the Kronecker delta. The point source function $\mathbf{\Phi}_y$ is defined as in (2.2).

2.3.2 Elastostatic potentials

Integration by parts formulas are given by:

$$\int_\Omega \sigma(\mathbf{u}) : \epsilon(\mathbf{v}) dx - \int_\Gamma \partial^*_{\mathbf{n}} \mathbf{u} \cdot \mathbf{v} d\varsigma = -\int_\Omega \Delta^* \mathbf{u} \cdot \mathbf{v} dx$$

for $\mathbf{u} \in \mathbf{H}^2(\Omega)$ and $\mathbf{v} \in \mathbf{H}^1(\Omega)$, where

$$\sigma(\mathbf{u}) : \epsilon(\mathbf{v}) := \sum_{i,j} \sigma_{i,j}(\mathbf{u}) \epsilon_{i,j}(\mathbf{v})$$

is the tensorial inner product. The bold notation $\mathbf{H}^2(\Omega)$ represents the product space $(H^2(\Omega))^d$.
If $\mathbf{u},\ \mathbf{v} \in \mathbf{H}^2(\Omega)$,

$$\int_\Omega (\Delta^* \mathbf{u} \cdot \mathbf{v} - \mathbf{u} \cdot \Delta^* \mathbf{v}) dx = \int_\Gamma (\partial^*_{\mathbf{n}} \mathbf{u} \cdot \mathbf{v} - \mathbf{u} \cdot \partial^*_{\mathbf{n}} \mathbf{v}) d\varsigma.$$

Given some integrable density $\phi = (\phi_1, \ldots, \phi_d)$, the *single layer elastostatic potential* is defined by

$$\mathbf{L}_\Gamma(\phi)(y) := \int_\Gamma \mathbf{\Phi}_y(x) \phi(x) d\varsigma_x,\ y \in \mathbb{R}^d \setminus \Gamma$$

understood in the sense

$$\int_\Gamma \mathbf{\Phi}_y(x)\phi(x)d\varsigma_x = \left[\int_\Gamma ([\mathbf{\Phi}_y(x)]_{j,1}\phi_1(x) + \ldots + [\mathbf{\Phi}_y(x)]_{j,d}\phi_d(x))d\varsigma_x\right]_j,\ 1 \le j \le d. \quad (2.7)$$

The *double layer potential* is defined by

$$\mathbf{M}_\Gamma(\phi)(y) := \int_\Gamma \partial^*_{\mathbf{n}_x}\mathbf{\Phi}_y(x)\phi(x)d\varsigma_x,\ y \in \mathbb{R}^d \setminus \Gamma,$$

where

$$\partial^*_{\mathbf{n}_x}\mathbf{\Phi}_y(x) = \left[\partial^*_{\mathbf{n}_x}(\mathbf{\Phi}_y(x)e_i)_j\right]_{i,j}, 1 \le i,j \le d$$

and e_i is the i-th vector of the standard basis in $\mathbb{R}^d$.

The single and double layer elastostatic potentials behave near the boundary like the scalar (harmonic) potentials. Using the "bold letters" for the trace and normal trace notations we have.

Theorem 2.9 *([34]) Given $\phi \in \mathbf{H}^{1/2}(\Gamma)$ and $\psi \in \mathbf{H}^{3/2}(\Gamma)$ we have,*

(a) $\mathbf{S}^+_\Gamma(\phi) = \mathbf{S}^-_\Gamma(\phi)$ *(c)* $\mathbf{N}^\pm_\Gamma(\phi) = \mp\frac{1}{2}\phi + \mathbf{K}^*_\Gamma(\phi)$

(b) $\mathbf{K}^\pm_\Gamma(\psi) = \pm\frac{1}{2}\psi + \mathbf{K}_\Gamma(\psi)$ *(d)* $\mathbf{D}^+_\Gamma(\psi) = \mathbf{D}^-_\Gamma(\psi)$

where $\mathbf{K}^*_\Gamma$ denotes the adjoint of $\mathbf{K}_\Gamma$ and $\mathbf{K}_\Gamma$ is defined as in (2.3).

Let $\mathbf{f}$ be a source with compact support $\overline{\Omega}_\mathbf{f}$ and such that $\mathbf{\Phi}_y\mathbf{f}$ is integrable in $\mathbb{R}^d$. The *Newton potential* is defined by

$$\mathbf{V}(\mathbf{f})(y) := \int_{\mathbb{R}^d} \mathbf{\Phi}_y(x)\mathbf{f}(x)dx$$

where the improper integral is understood in the sense of (2.7). The usual notation $\mathbf{V}_\Omega(\mathbf{f})$ denotes the integration on some open set $\Omega \subset \mathbb{R}^d$.

Theorem 2.10 *If*

$$\mathbf{u} = -\mathbf{V}(\mathbf{f}) + \mathbf{L}_\Gamma(\phi) - \mathbf{M}_\Gamma(\psi)$$

and $\mathbf{u}$ satisfies the asymptotic conditions (2.4) with $\alpha > 0$ then

$$\phi = [\partial^*_\mathbf{n}\mathbf{u}]_\Gamma\ \wedge\ \psi = [\mathbf{u}]_\Gamma.$$

We conclude with the elastostatic version of Holmgren's lemma (also called Almansi's lemma).

Lemma 2.11 *Given a relatively open set $\Sigma \subset \Gamma$ let $\mathbf{u} \in \mathbf{H}^2(\Omega)$ satisfy*

$$\begin{cases} \Delta^* \mathbf{u} = \mathbf{f} & \text{in } \Omega \\ \mathbf{u} = \partial^*_{\mathbf{n}} \mathbf{u} = \mathbf{0} & \text{on } \Sigma \subset \Gamma \end{cases}$$

for a source $\mathbf{f}$, null in an open and connected set $\overline{\Omega}^{\mathrm{C}}_{\mathbf{f}} \subset \Omega$ such that $\Gamma \subset \partial\overline{\Omega}^{\mathrm{C}}_{\mathbf{f}}$. Then,

$$\mathbf{u} = \mathbf{0} \text{ in } \overline{\Omega}^{\mathrm{C}}_{\mathbf{f}}.$$

In particular, the unique solution of Lamé system with null Cauchy data on Σ is $\mathbf{u} = \mathbf{0}$.

2.4 Inverse problems

The aim of collecting data is to gain meaningful information about a physical system or phenomenon of interest. If the collected (measured) data dependents on some inaccessible quantities then it is expected that the data contains, somehow, information about those quantities of the system. Loosely speaking, in an inverse problem we measure an effect and want to determine the cause. As opposite, in a direct or forward problem we have a complete description of a phenomenon (cause) and want to predict the outcome of some measurements (effect). A first remark is that in the inverse problem, one cannot expect to obtain information regarding parameters or other quantities that do not make sense in the actual model. From the mathematical point of view, this means that in the inverse problem one assumes the existence of an associated direct problem.

2.4.1 Ill–posedness and regularization

In general, direct problems are *well–posed* and inverse problems are *ill–posed* (in the sense of Hadamard). We recall that for an operator $F : U \to V$, where $U \subset X$, $V \subset Y$ and X, Y are normed spaces the equation

$$F\phi = g_{\mathbf{n}} \tag{2.8}$$

is well–posed if F is bijective and the inverse F^{-1} is continuous, and ill–posed if at least one of those conditions does not hold. Thus, (2.8) is ill–posed if:

(1) F is not surjective or

(2) F is not injective or

(3) F^{-1} exists but is not continuous.

The surjective question in inverse problems is not the right question to ask. In fact, it is not possible to characterize all the possible outcomes of a given experience. Moreover measurement errors are expected to occur and equation (2.8) may fail to have a solution for noisy right hand side data.
The injectivity question addresses whether the model information, ϕ, can be uniquely identified from the value $F\phi$. This will be the identifiability results presented through this work.
The third point regards instability which is a common feature of inverse problems.

To further analyze ill–posedness, assume that X, Y are Hilbert spaces and $F : X \to Y$ is linear and compact. Denote by $F^* : Y \to X$ its adjoint. The self adjoint and compact operator $F^*F : X \to X$ has a countable number of non negative eigenvalues $(\lambda_n)_{n\in\mathbb{N}}$ with finite (geometric) multiplicity. The scalars

$$\nu_i := \sqrt{\lambda_i},\ i \in \mathbb{N}$$

are called *singular values* of the operator F. As usual, we consider the order (repeating the singular value according to the multiplicity of the corresponding eigenvalue)

$$\nu_1 \geq \nu_2 \geq \dots$$

Theorem 2.12 *In the above conditions, there exists orthonormal sequences (ϕ_n) in X and (ψ_n) in Y such that*

$$F\phi_n = \nu_n\psi_n,\ F^*\psi_n = \nu_n\phi_n,\ \forall n \in \mathbb{N}.$$

For each $\phi \in X$, we have the singular value decomposition

$$\phi = \sum_{n\geq 1} \langle \phi, \phi_i \rangle_X \phi_n + Q\phi$$

with the orthogonal projection operator $Q : X \to \ker F$ and

$$F\phi = \sum_{n\geq 1} \nu_n \langle \phi, \phi_n \rangle_X \psi_n.$$

Proof. See [36]. □

Each system (ν_n, ϕ_n, ψ_n) with these properties is called a *singular system* of F.

Theorem 2.13 *(Picard) Let $F : X \to Y$ be a compact linear operator with singular system (ν_n, ϕ_n, ψ_n). The equation*

$$F\phi = g_{\mathbf{n}}$$

is solvable if and only if $g_{\mathbf{n}}$ belongs to the orthogonal complement $(\ker F^*)^{\perp}$ and satisfies

$$\sum_{i\geq 1} \frac{1}{\nu_i^2} |\langle g_{\mathbf{n}}, \psi_i \rangle_Y|^2 < \infty.$$

In this case a solution is given by

$$\phi = \sum_{i\geq 1} \frac{1}{\nu_i} \langle g_{\mathbf{n}}, \psi_i \rangle_Y \phi_i.$$

Proof. See [36]. □

Now consider a perturbation of $g_{\mathbf{n}}$ in the direction of ψ_i that is,

$$g_{\mathbf{n}}^{\delta} = g_{\mathbf{n}} + \delta\psi_i.$$

A solution to the corresponding perturbed problem is $\phi^{\delta} = \phi + \delta\phi_i/\nu_i$ and we have

$$\frac{||\phi^{\delta} - \phi||_X}{||g_{\mathbf{n}}^{\delta} - g_{\mathbf{n}}||_Y} = \frac{1}{\nu_i}$$

which can be can large because F is compact. Thus, a small perturbation on $g_{\mathbf{n}}$ can induce a large perturbation on the solution.

Regularization methods

Regularization methods are methods for constructing a stable approximate solution. Suppose F is injective and that $g_{\mathbf{n}} \in F(X)$. Given a perturbation $g_{\mathbf{n}}^{\delta}$ with a known error level

$$||g_{\mathbf{n}}^{\delta} - g_{\mathbf{n}}||_Y \leq \delta$$

we want to construct a stable (and reasonable) approximation ϕ^{δ} to the exact solution of (2.8), i.e., we want ϕ^{δ} to depend continuously on $g_{\mathbf{n}}^{\delta}$.

Again, we will mainly follow the exposition presented in [36]. We start with the definition of regularization scheme.

Definition 2.14 Let X, Y be normed spaces and $F : X \to Y$ be an injective bounded linear operator. A family of bounded linear operators $R_\mu : Y \to X$, $\mu > 0$ with the property of pointwise convergence

$$\lim_{\mu \to 0} R_\mu F\phi = \phi,$$

for all $\phi \in X$ is called a regularization scheme for the operator F. The parameter μ is called the *regularization parameter*.

The regularization scheme approximates the solution of (2.8) by

$$\phi_\mu^\delta := R_\mu g_{\mathbf{n}}^\delta.$$

We will now describe one of the most used regularization scheme, the *Tikhonov regularization*.

Theorem 2.15 *Let $F : X \to Y$ be a compact linear operator between Hilbert spaces. Then, for each $\mu > 0$ the operator $\mu I + F^*F : X \to X$ is bijective and has a bounded inverse. Furthermore, if F is injective then*

$$R_\mu := (\mu I + F^*F)^{-1} F^*$$

describes a regularization scheme with $||R_\mu|| \leq 1/2\sqrt{\mu}$.

The next result shows that the stability is achieved by introducing a balance between the residual $||F\phi - g_{\mathbf{n}}||_Y^2$ and the size of the solution $||\phi||_X^2$.

Theorem 2.16 *Let $F : X \to Y$ be a compact linear operator (between Hilbert spaces) and $\mu > 0$. Then for each $g_{\mathbf{n}} \in Y$ there exists a unique $\phi_\mu \in X$ such that*

$$||F\phi_\mu - g_{\mathbf{n}}||_Y^2 + \mu ||\phi_\mu||_X^2 = \inf_{\phi \in X} \left\{ ||F\phi - g_{\mathbf{n}}||_Y^2 + \mu ||\phi||_X^2 \right\}.$$

The minimizer is the unique solution of

$$(\mu I + F^*F)\phi = F^* g_{\mathbf{n}}$$

and depends continously on $g_{\mathbf{n}}$.

In order to implement the Tikhonov scheme, first we must choose a regularization parameter. Since the approximate solution satisfies the error bound

$$||\phi_\mu^\delta - \phi||_X \leq \delta||R_\mu|| + ||R_\mu F\phi - \phi||_Y$$

then, typically, the first right hand side term increases and the second term decreases as $\mu \to 0$. Thus, depending on δ, the choice of regularization parameter μ must be carefull. On one hand, accuracy of the approximation asks for a small parameter μ and on the other stability asks for a large parameter μ.

Quite often, the choice of regularization parameter μ is made by *trial and error*. There are also several practical methods for the choice of μ. The following are two of the most used.

• *Morozov discrepancy principle* The motivation for the Morozov discrepancy principle (cf. [72]) is based on the consideration that, for perturbed data $g_{\mathbf{n}}^\delta$, the residual $||F\phi - g_{\mathbf{n}}||_Y$ should not be smaller than the accuracy of the measurements of $g_{\mathbf{n}}$, i.e., the regularization parameter should be chosen such that

$$||F\phi_\mu^\delta - g_{\mathbf{n}}^\delta||_Y = c\delta$$

with some fixed parameter $c \geq 1$.

• *L–curve criterion* The L–curve (cf. [65]) is perhaps the most convenient graphical tool for displaying the trade-off between the size of the regularized solution and its fit to the given data as the regularization parameter varies. It is a log–log plot of the norm $||F\phi_\mu^\delta - g_{\mathbf{n}}^\delta||_Y$ versus $||\phi_\mu^\delta||_X$, for $\mu > 0$. It has an "L" shape and the criterion to choose the regularization parameter is to find μ such that the pair $(\log(||F\phi_\mu^\delta - g_{\mathbf{n}}^\delta||_Y), \log(||\phi_\mu^\delta||_X))$ lies on the "corner" of the curve.

2.4.2 Ill conditioning in inverse and direct problems

In the following we will consider boundary layer integral operators such as

$$\begin{array}{rccc} F: & L^2(\hat{\Gamma}) & \to & L^2(\Gamma) \\ & \phi & \mapsto & L_{\hat{\Gamma}}(\phi) \end{array}.$$

When Γ and $\hat{\Gamma}$ are different boundaries the kernel of this operator (a fundamental solution) is analytic and F defines a compact operator.

Then, solving the integral equation of the first kind,

$$F\phi = g_{\mathbf{n}}$$

is an inverse problem that fits in the previous general framework for linear operators.

It is interesting to note that this might be seen in two different contexts:

(i) in the inverse problem context – for instance in the decomposition method that we will address;

(ii) in the direct problem context – related to the method of fundamental solutions.

It is clear that (i) is the usual context while dealing with the Cauchy problem. The ill posedness is an unavoidable feature of the inverse problems. On the other hand, it appears in (ii), in the context of direct problems, only as our choice for the forward solver. These two subjects will be related in Section 4.2.

In the classical method of fundamental solutions one may use Tikhonov regularization techniques to overcome the ill posed nature of the first kind integral equation. This has been only considered in the discretized framework, in terms of matrices.

In theoretical terms, density results have been used to prove that the range of F is dense, and therefore show the applicability of the method. It is important to stress here that the application of Tikhonov's regularization scheme R_μ to the operator F also allows to define a pseudo-inverse

$$R_\mu = (\mu I + F^*F)^{-1}F^*$$

here with the adjoint

$$F^*\psi = L_\Gamma(\psi) \quad (\text{on } \hat{\Gamma}).$$

This pseudo-inverse gives the best approximations (in the sense of Theorem 2.16),

$$\phi_\mu = R_\mu g_{\mathbf{n}}$$

and will lead to the solution, whenever $g_{\mathbf{n}}$ lies in the range of F.

3

Obstacle identification from a single measurement for a Laplace problem

In this chapter we study the identification of inclusions or cavities within a conducting medium Ω_c by means of external boundary measurements. This is a nonlinear inverse problem in nondestructive testing and it has been considered in the literature as a mathematical model for detection of corrosion phenomena (eg. [28], [50]). In a simplified model, Laplace equation holds in the medium Ω_c. Measuring data on some part $\Sigma \subset \Gamma$ of the external (accessible) boundary Γ, we aim to detect the occurrence of damage on the inaccessible part of the boundary, γ (note that $\partial\Omega_c = \Gamma \cup \gamma$). Kaup and Santosa introduced and tested in [56] (see also [57]) a model borrowed from *electrical impedance tomography* based on electrostatic data collection. Other model, based on temperature and heat flux boundary data, was described by Bryan and Caudill in [28]. This is an example of *thermal imaging*.

In the aforementioned literature, two models for the damage due to corrosion in γ have been considered:

(a) The effect of corrosion is modeled by a small perturbation, $\delta\gamma$, of γ. The inverse problem consists in retrieving $\delta\gamma$ from data collected at an accessible part of the boundary (eg. [28], [57]).

(b) The corrosion is represented by a non negative exchange coefficient Z in a Robin boundary condition. The inverse problem is to obtain the Robin coefficient Z on γ again from data at an accessible part of the boundary (eg. [50]).

In this chapter, the first section is dedicated to the inverse geometric problem that can model (a) . We start with the statement of the inverse problem (paragraph 3.1.1) and we study the identification of an inclusion or cavity from a single boundary measurement. Then, in paragraph 3.1.2, we present a well known result of the domain derivative for the Dirichlet problem with a twofold objective: first to discuss a local Lipschitz stability result and second to use the derivative expression for an iterative reconstruction method.

The same organization was considered for the Robin problem related to (b) (second section).

3.1 Geometric problem

In this section we analyze the identifiability of an inclusion or cavity from a pair of boundary data and provide a criterion to distinguish them using such data. We start with the statement of the direct problem. Let $\omega, \Omega \subset \mathbb{R}^d$ $(d = 2, 3)$ be two open, simply connected and bounded domains such that $\overline{\omega} \subset \Omega$. The boundaries

$$\Gamma := \partial\Omega \text{ and } \gamma := \partial\omega$$

are assumed to be C^2 closed curves. We define the domain of propagation by

$$\Omega_c := \Omega \setminus \overline{\omega}.$$

Ω_c is a doubly connected domain with regular boundary $\partial\Omega_c = \Gamma \cup \gamma$ (see Fig. 3.1).

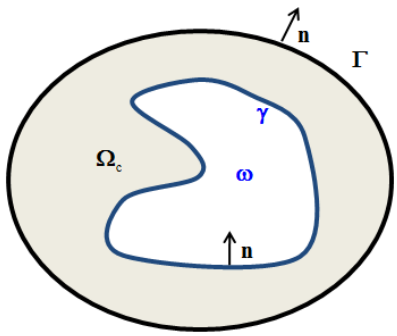

Figure 3.1: Example of a domain of propagation $\Omega_c \subset \mathbb{R}^2$.

Consider the following *direct problem*:

Given g (an input function), measure $g_{\mathbf{n}} := \partial_{\mathbf{n}} u$ on $\Sigma \subset \Gamma$, where u solves the problem

$$\begin{cases} \Delta u = 0 & \text{in } \Omega_c \\ u = g & \text{on } \Gamma \\ \mathcal{B}u = 0 & \text{on } \gamma \end{cases} \tag{3.1}$$

and $\mathcal{B}$ is either the Dirichlet or Neumann boundary operator, ie.:

Dirichlet: $\mathcal{B}$ is the operator

$$\mathcal{B}u = u.$$

The condition

$$u = 0 \quad \text{on } \gamma$$

means that ω is a perfectly conducting or rigid inclusion.

Neumann: $\mathcal{B}$ is the operator

$$\mathcal{B}u = \partial_{\mathbf{n}} u$$

The condition

$$\partial_{\mathbf{n}} u = 0 \quad \text{on } \gamma$$

means that γ is a perfectly insulating inclusion or a cavity.

For these cases, we denote (3.1) by $(\mathcal{P}_D)$ and $(\mathcal{P}_N)$, respectively.
The following is a well known result (eg. [42], [77]).

Theorem 3.1 *If $g \in H^{3/2}(\Gamma)$ then $(\mathcal{P}_D)$ and $(\mathcal{P}_N)$ are well posed, with solution in $H^2(\Omega_c)$.*

Remark 3.2 If the regularity of the boundary is C^1 and $g \in H^{1/2}(\Gamma)$, the previous problem has a unique (weak) solution in $H^1(\Omega_c)$. The stronger assumptions $\gamma \in C^2$ and $u \in H^2(\Omega_c)$ will be needed for the domain derivative calculation.

The same conclusions hold if ω is a finite union of simply connected and disjoint domains. In a more general case, we can have rigid inclusions, cavities or a mixture of both.

3.1.1 Inverse problem

The inverse geometric problem can be stated as:

(IGP): *From a single pair of Cauchy data on* $\Sigma \subset \Gamma$*, identify the inclusion* ω*.*

This is well known to be an ill posed and non linear inverse problem. In fact, without prior assumptions on the boundary data, (IGP) may not even be uniquely solvable. The following definition will give a framework to address (IGP).

Definition 3.3 Let $\Sigma \subset \Gamma$ be a nonempty and open set in the topology of Γ. We define

$$\begin{aligned}\mathcal{G}_D(\Gamma) := \{(\phi,\psi) \in H^{3/2}(\Gamma) \times H^{1/2}(\Gamma) \ \wedge \ \exists u \in H^2(\Omega_c) \text{ solving } (\mathcal{P}_D) \\ \text{with } \phi = u|_\Gamma \ \wedge \ \psi = \partial_{\mathbf{n}} u|_\Gamma\}\end{aligned}$$

as the space of *compatible Cauchy* data for problem $(\mathcal{P}_D)$. Analogously, we define $\mathcal{G}_N(\Gamma)$ as the space of compatible Cauchy data for $(\mathcal{P}_N)$. We denote by $\mathcal{G}_D(\Sigma)$ and $\mathcal{G}_N(\Sigma)$ the restriction of $\mathcal{G}_D(\Gamma)$ and $\mathcal{G}_N(\Gamma)$ to Σ, respectively.

As a consequence of Holmgren's lemma, we can identify compatible boundary data with the solution of $(\mathcal{P}_D)$ (or $(\mathcal{P}_N)$) via

$$u \mapsto (g, \partial_{\mathbf{n}} u) \in \mathcal{G}_D(\Sigma).$$

In particular, results requiring compatible Cauchy data (in $\mathcal{G}_D(\Gamma)$) are also valid for partial boundary data (in $\mathcal{G}_D(\Sigma)$).

Example 3.4 Consider the circular domain of propagation

$$\Omega_c := \{x \in \mathbb{R}^2 : r < |x| < R\},$$

with $0 < r < R$. Let g be a given constant input function on Γ and measure the (constant and non null) data $g_{\mathbf{n}} = \partial_{\mathbf{n}} u$ on Γ, where u is the unique solution of the Dirichlet problem $(\mathcal{P}_D)$. We show that in this simple setting, if we know that ω is a centered circle, then its radius, r, can be explicitly computed from the compatible Cauchy data $(g, g_{\mathbf{n}})$. We consider the radial function

$$u(x) := a + b \log |x|, \ x \in \mathbb{R}^2 \setminus \{0\}$$

and compute $a, b, \ r$ by imposing the homogeneous Dirichlet boundary condition on $\gamma :=$

$\partial B(0,r)$ and the Cauchy conditions on $\Gamma := \partial B(0,R)$. Thus,

$$\left\{\begin{array}{ll} \partial_{\mathbf{n}} u(x) = g_{\mathbf{n}} & \text{on } \Gamma \\ u(x) = g & \text{on } \Gamma \\ u(x) = 0 & \text{on } \gamma \end{array}\right. \Leftrightarrow \left\{\begin{array}{ll} bx/|x| \cdot x/|x|^2 = g_{\mathbf{n}} & \text{on } \Gamma \\ a + b\log R = g \\ a + b\log r = 0 \end{array}\right. \Leftrightarrow \left\{\begin{array}{l} b = Rg_{\mathbf{n}} \\ a = g - Rg_{\mathbf{n}} \log R \\ r = Re^{-g/(Rg_{\mathbf{n}})} \end{array}\right.$$

and the last right hand side equation gives an explicit formula to compute r.

For the general case, the boundary of ω is defined by many parameters and a more subtle analysis for the identification and reconstruction is required. The following lemma will be needed to establish uniqueness of the inverse problem.

Lemma 3.5 *Let Ω be a connected domain with regular boundary Γ and consider the decomposition*

$$\Gamma = \overline{\Gamma}_0 \cup \overline{\Gamma}_1$$

where Γ_0 and Γ_1 are relatively open and disjoint sets. Then, if $\Gamma_0 = \emptyset$, there exists a unique solution of the mixed problem

$$\left\{\begin{array}{ll} \Delta u = 0 & \text{in } \Omega \\ u = 0 & \text{on } \Gamma_0 \\ \partial_{\mathbf{n}} u = 0 & \text{on } \Gamma_1 \end{array}\right. \tag{3.2}$$

in $H^2(\Omega)/\mathbb{R}$. If $\Gamma_0 \neq \emptyset$, the unique solution in $H^2(\Omega)$ is the null function.

Proof. Existence is clear. Considering Green's formula for $u \in H^2(\Omega)$ solving (3.2) we obtain

$$||\nabla u||^2_{L^2(\Omega)} = \int_\Omega \nabla u \cdot \nabla u dx = \int_{\partial\Omega} \partial_{\mathbf{n}} u u d\varsigma - \int_\Omega \Delta u u dx = 0.$$

Therefore, $\nabla u = 0$ in Ω and we conclude that $u = c$ on $\overline{\Omega}$. For a pure Neumann problem ($\Gamma_0 = \emptyset$) this means that the solutions of the mixed problem are only constants. Now if $\Gamma_0 \neq \emptyset$, the condition $u|_{\Gamma_0} = 0$ implies $u = 0$ in $\overline{\Omega}$. □

We now prove that from a single pair of compatible Cauchy data on Σ we can identify and distinguish inclusions from cavities and, in particular, we obtain the uniqueness result for (IGP). Denote by $\mathcal{G}_D^g(\Sigma)$ ($\mathcal{G}_N^g(\Sigma)$) the restriction of $\mathcal{G}_D(\Sigma)$ ($\mathcal{G}_N(\Sigma)$) to the pairs where the first component is $g|_\Sigma$.

Theorem 3.6 *If the restriction of g to Σ is not constant then a single pair of compatible data $(g|_\Sigma, g_{\mathbf{n}}|_\Sigma)$ determines uniquely ω and allows to distinguish between Dirichlet and*

Neumann b.c., more precisely,

$$\mathcal{G}_D^g(\Sigma) \cap \mathcal{G}_N^g(\Sigma) = \emptyset.$$

Proof. We start by proving that ω is determined by a single pair of (compatible) Cauchy data. Consider two domains of propagation Ω_c^1 and Ω_c^2 with regular boundaries

$$\partial\Omega_c^1 = \Gamma \cup \gamma_1 \text{ and } \partial\Omega_c^2 = \Gamma \cup \gamma_2$$

respectively. Take $\gamma_i = \partial\omega_i$ and $\overline{\omega}_i \subset \Omega$.

Let $(g, g_{\mathbf{n}})$ belong to $\mathcal{G}_D(\Sigma)$ or $\mathcal{G}_N(\Sigma)$ for the domains of propagation Ω_c^1 and Ω_c^2. This means that exists $u_i \in H^2(\Omega_c^i)$ solving $(\mathcal{P}_D)$ or $(\mathcal{P}_N)$ in Ω_c^i such that

$$g|_\Sigma = u_1|_\Sigma = u_2|_\Sigma \ \wedge \ g_{\mathbf{n}}|_\Sigma = \partial_{\mathbf{n}} u_1|_\Sigma = \partial_{\mathbf{n}} u_2|_\Sigma. \tag{3.3}$$

Therefore, u_1 and u_2 have the same Cauchy data on Σ hence, by the Holmgren lemma,

$$u_1 = u_2 \text{ in } \widetilde{\Omega}_c,$$

where $\widetilde{\Omega}_c$ denotes the connected component of $\Omega_c^1 \cap \Omega_c^2$ that contains Γ. Now, $\partial\widetilde{\Omega}_c = \Gamma \cup \overline{\widetilde{\gamma}}_1 \cup \overline{\widetilde{\gamma}}_2$ with $\overline{\widetilde{\gamma}}_j \subset \gamma_j$ and $\widetilde{\gamma}_1 \cap \widetilde{\gamma}_2 = \emptyset$. Assume that $\Omega_c^1 \neq \Omega_c^2$ and without loss of generality suppose that $\widetilde{\gamma}_2$ is open and nonempty.

- If $\Omega_c^1 \cap \Omega_c^2$ is connected, ie $\Omega_c^1 \cap \Omega_c^2 = \widetilde{\Omega}_c$, take $\sigma = \omega_2 \setminus \overline{\omega}_1 \subset \Omega_c^1$ which is a nonempty open set with boundary $\partial\sigma \subset \overline{\widetilde{\gamma}}_2 \cup \gamma_1$ (see Fig. 3.2, left).
- If $\Omega_c^1 \cap \Omega_c^2$ is not connected, take σ as a (simply) connected component of $\Omega_c^1 \setminus \overline{\widetilde{\Omega}_c}$. Again, $\partial\sigma \subset \overline{\widetilde{\gamma}}_2 \cup \gamma_1$. (see Fig. 3.2, right).

In both cases, it is clear that $\Delta u_1 = 0$ in σ and on γ_1 we have null Dirichlet or Neumann data. By analytic continuation, u_1 has also null Dirichlet or Neumann data on $\widetilde{\gamma}_2$. Hence, we can consider a decomposition $\partial\sigma = \overline{\eta}_1 \cup \overline{\eta}_2$ where we can apply Lemma 3.5. Thus, u_1 is constant on the open and connected set σ and by analytic continuation, u_1 is constant on $\widetilde{\Omega}_c$. This implies $g|_\Sigma = u_1|_\Sigma$ constant, which contradicts the assumption that $g|_\Sigma$ is not constant. It follows that $\Omega_c^1 = \Omega_c^2$.

For the second part of the theorem, notice that since $\Omega_c^1 = \Omega_c^2$ then $u_1 = u_2$ on $\Omega_c = \Omega_c^1$. In particular, if

$$u_1|_\gamma = 0 \ \wedge \ \partial_{\mathbf{n}} u_1|_\gamma = 0$$

then, by Holmgren's lemma, $u_1 = 0$ in Ω_c and again this contradicts the fact that $g|_\Sigma$ is not constant. We can thus conclude that the boundary condition on γ is also fully identified from the single pair of Cauchy data $(g, g_{\mathbf{n}})$ on Σ. □

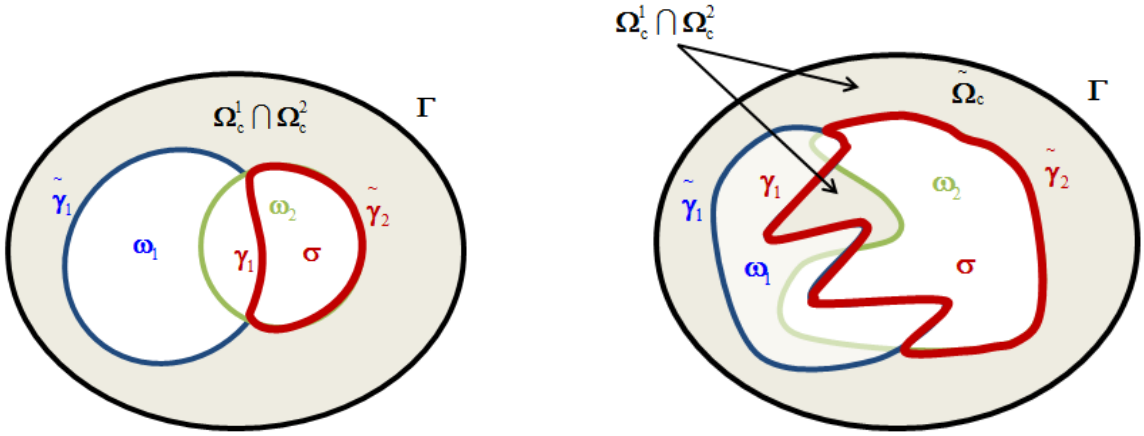

Figure 3.2: Examples for the chosen σ, when $\Omega_c^1 \cap \Omega_c^2$ is connected (left) and not connected (right).

Remark 3.7 If we know *a priori* that ω is a rigid inclusion then it follows from the previous proof that identification can be establish under the assumption that g is not identically null on Σ. Moreover, the result is still valid if ω is a union of simply connected, disjoint open domains.

A criterion to distinguish inclusions from cavities

As previously proved, given a non constant input function, we can distinguish an inclusion from a cavity from compatible Cauchy data. However, the result does not give a criterion to distinguish such boundaries conditions. The next result presents, in a classical solution framework, a criterion for such identification.

Theorem 3.8 *Suppose that ω is a rigid inclusion or a cavity. Let $g \in C^0(\Gamma)$ be a strictly positive input function and $g_{\mathbf{n}} = \partial_{\mathbf{n}} u|_\Gamma$, where u is a classical solution of $(\mathcal{P}_D)$ or $(\mathcal{P}_N)$. Then, ω is a cavity if and only if $\int_\Gamma g_{\mathbf{n}} d\varsigma = 0$.*

Proof. Suppose that ω is a cavity and let u be a solution of $(\mathcal{P}_N)$ in the conditions of the proposition. By Green's formula, we obtain

$$0 = \int_{\partial\Omega_c} \partial_{\mathbf{n}} u d\varsigma = \int_\Gamma \partial_{\mathbf{n}} u d\varsigma + \int_\gamma \partial_{\mathbf{n}} u d\varsigma = \int_\Gamma \partial_{\mathbf{n}} u d\varsigma = \int_\Gamma g_{\mathbf{n}} d\varsigma.$$

Reciprocally, we prove that $\int_\Gamma g_{\mathbf{n}} d\varsigma = 0$ implies that ω is a cavity. By contradiction, assume that ω is a rigid inclusion and let u be the classical solution of $(\mathcal{P}_D)$. Since g is positive, we have by the maximum principle and Hopf's lemma

$$\partial_{\mathbf{n}} u < 0 \text{ at } \gamma. \tag{3.4}$$

By Green's formula

$$\int_\gamma \partial_{\mathbf{n}} u d\varsigma = -\int_\Gamma g_{\mathbf{n}} d\varsigma,$$

and since by hypothesis $\int_\Gamma g_{\mathbf{n}} d\varsigma = 0$, the last equation gives $\int_\gamma \partial_{\mathbf{n}} u d\varsigma = 0$ which, by (3.4), is impossible. □

3.1.2 Local Lipschitz stability

Let

$$\mathcal{C} := \left\{ \gamma \in C^2 : \text{ exists a simply connected domain } \omega \text{ with } \gamma = \partial\omega \ \wedge \ \overline{\omega} \subset \Omega \right\}$$

be the class of admissible shapes. As usual, $\Omega_c = \Omega \setminus \overline{\omega}$ denotes the domain of propagation with C^2 boundary $\partial\Omega_c = \Gamma \cup \gamma$. Consider the nonlinear (injective) operator

$$\begin{aligned} F : \mathcal{C} &\longrightarrow H^{1/2}(\Gamma) \\ \gamma &\mapsto g_{\mathbf{n}} \end{aligned}$$

where, for given $g \in H^{3/2}(\Gamma)$, $(g, g_{\mathbf{n}}) \in \mathcal{G}_D(\Gamma)$.

Consider a perturbation of $F(\gamma)$ in the range of F, say $F(\gamma_\varepsilon)$. In this section we study the effect of this perturbation in the perturbation of the shape γ, γ_ε. The main tool is the *domain derivative* map $F'(\gamma)\Psi$ in the direction of some vector field Ψ (eg. [81]). We start by defining the class of admissible perturbations of γ.

Definition 3.9 A map $\Psi \in C^2(\Omega, \mathbb{R}^d)$ is called an *admissible vectorial field* if supp $\Psi \subset \mathcal{O}$, where $\mathcal{O}$ is an open bounded set with regular boundary such that $\overline{\mathcal{O}} \subset \Omega$.

Given $\varepsilon \in \mathbb{R}$ consider a perturbation of the identity $\Psi_\varepsilon : \Omega \longrightarrow \mathbb{R}^d$ defined by

$$\Psi_\varepsilon = I + \varepsilon\Psi$$

where Ψ is an admissible vectorial field. For small $|\varepsilon|$, Ψ_ε is a C^2 diffeomorphism and we

define the perturbed domain of propagation

$$\Omega_c^\varepsilon := \Psi_\varepsilon(\Omega_c).$$

The boundary of the perturbed inclusion ω_ε is C^2 and will be denoted by γ_ε. We note that Ω_c^0 is the original domain of propagation Ω_c and therefore $\omega_0 = \omega$ and $\gamma_0 = \gamma$ (see Fig. 3.3).

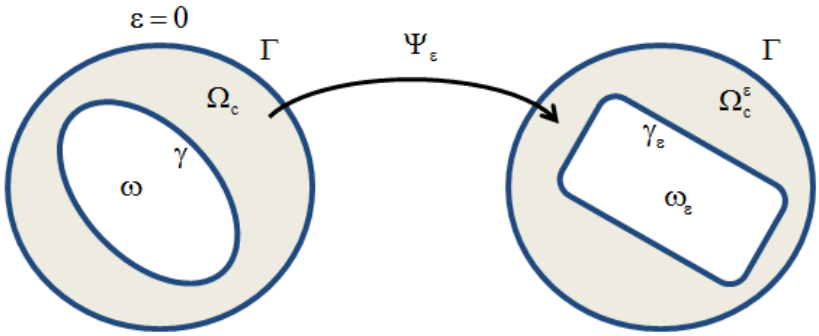

Figure 3.3: A deformation of Ω_c by the diffeomorphism Ψ_ε.

We prove that, for an appropriate admissible vector field, we have the Lipschitz stability result

$$\exists c > 0 : ||F(\gamma_\varepsilon) - F(\gamma)||_{H^{-1/2}(\Gamma)} \geq c|\varepsilon|.$$

This is formulated by the next result.

Theorem 3.10 *(Local Lipschitz stability) Suppose that Ψ is an admissible vector field and $g \in H^{3/2}(\Gamma) \setminus \{0\}$. Then,*

$$F'(\gamma)\Psi = 0 \Leftrightarrow \Psi(x) \perp \mathbf{n}_x, \ \forall x \in \gamma. \tag{3.5}$$

We start by computing the expression of the derivative map $F'(\gamma)$. We will mainly follow the ideas presented in [6] and [58].

Let $\widetilde{u} \in H^2(\Omega)$ be such that

$$\widetilde{u} = 0 \text{ in } \mathcal{O} \text{ and } \widetilde{u}|_\Gamma = g$$

and define $w = u - \widetilde{u}$, where u solves $(\mathcal{P}_D)$. Thus, w is the unique solution of the variational problem

$$\begin{cases} \text{Find } z \in H_0^1(\Omega_c) \text{ such that} \\ S(z, v) = -\int_{\Omega_c} \nabla\widetilde{u} \cdot \nabla v dx, \ \forall v \in H_0^1(\Omega_c) \end{cases} \tag{3.6}$$

with the bilinear form

$$S(z,v) := \int_{\Omega_c} \nabla z.\nabla v dx.$$

Denote by w_ε the unique solution of the following variational problem in the perturbed domain Ω_c^ε

$$\begin{cases} \text{Find } z_\varepsilon \in H_0^1(\Omega_c^\varepsilon) \text{ such that} \\ S_\varepsilon(z_\varepsilon, v_\varepsilon) = -\int_{\Omega_c^\varepsilon} \nabla \widetilde{u} \cdot \nabla v_\varepsilon dy, \ \forall v_\varepsilon \in H_0^1(\Omega_c^\varepsilon) \end{cases}$$

with

$$S_\varepsilon(z_\varepsilon, v_\varepsilon) := \int_{\Omega_c^\varepsilon} \nabla z_\varepsilon.\nabla v_\varepsilon dy.$$

Consider the change of variables $y = \Psi_\varepsilon(x)$ and denote by J_{Ψ_ε} the corresponding Jacobian matrix. We have

$$S_\varepsilon(w_\varepsilon, v_\varepsilon) = \int_{\Omega_c = \Psi_\varepsilon^{-1}(\Omega_c^\varepsilon)} \nabla(w_\varepsilon \circ \Psi_\varepsilon) \cdot (J^\top_{\Psi_\varepsilon^{-1}} J_{\Psi_\varepsilon^{-1}} \nabla(v_\varepsilon \circ \Psi_\varepsilon)) |\det J_{\Psi_\varepsilon}| dx \tag{3.7}$$

and

$$\int_{\Omega_c^\varepsilon} \nabla \widetilde{u}.\nabla v_\varepsilon dy = \int_{\Omega_c = \Psi_\varepsilon^{-1}(\Omega_c^\varepsilon)} \nabla(\widetilde{u} \circ \Psi_\varepsilon) \cdot (J^\top_{\Psi_\varepsilon^{-1}} J_{\Psi_\varepsilon^{-1}} \nabla(v_\varepsilon \circ \Psi_\varepsilon)) |\det J_{\Psi_\varepsilon}| dx. \tag{3.8}$$

On the other hand, the C^2 diffeomorphism $\Psi_\varepsilon : \Omega_c \longrightarrow \Omega_c^\varepsilon$ induces the isomorphism $f \mapsto f \circ \Psi_\varepsilon : H_0^1(\Omega_c^\varepsilon) \longrightarrow H_0^1(\Omega_c)$. We identify $w^\varepsilon = w_\varepsilon \circ \Psi_\varepsilon$ with w_ε and note that $\widetilde{u} \circ \Psi_\varepsilon = \widetilde{u}$, i.e., $\widetilde{u}$ is invariant under this isomorphism.

Lemma 3.11 *There exists w^* and $r(\varepsilon)$ both in $H_0^1(\Omega_c)$ such that*

$$w^\varepsilon = w + \varepsilon w^* + \varepsilon r(\varepsilon) \tag{3.9}$$

and $r(\varepsilon) \underset{\varepsilon}{\to} 0$ in $H_0^1(\Omega_c)$.

Proof. We start by proving that $w^\varepsilon \to w$ in the (equivalent) norm

$$||u||_{H_0^1(\Omega_c)} := \|\nabla u\|_{L^2(\Omega_c)}.$$

From equations (3.7) and (3.8) we conclude that w^ε is a solution of the following variational problem.

• Find $z \in H_0^1(\Omega_c)$ such that:

$$\int_{\Omega_c} |\det J_{\Psi_\varepsilon}| J^\top_{\Psi_\varepsilon^{-1}} J_{\Psi_\varepsilon^{-1}} \nabla z \cdot \nabla v dx = -\int_{\Omega_c} |\det J_{\Psi_\varepsilon}| J^\top_{\Psi_\varepsilon^{-1}} J_{\Psi_\varepsilon^{-1}} \nabla \widetilde{u} \cdot \nabla v dx, \ \forall v \in H_0^1(\Omega_c). \tag{3.10}$$

On the other hand, for small $|\varepsilon|$, we have the expansions,

$$J_{\Psi_\varepsilon} = I + \varepsilon J_\Psi + O(\varepsilon^2),$$

$$\det J_{\Psi_\varepsilon} = 1 + \varepsilon \nabla \cdot \Psi + O(\varepsilon^2) \text{ and}$$

$$J_{\Psi_\varepsilon^{-1}} = I - \varepsilon J_\Psi + O(\varepsilon^2),$$

from where it follows that

$$|\det J_{\Psi_\varepsilon}| J^\top_{\Psi_\varepsilon^{-1}} J_{\Psi_\varepsilon^{-1}} = I - \varepsilon \left(J_\Psi + J_\Psi^\top - \nabla \cdot \Psi I \right) + O(\varepsilon^2).$$

Subtracting (3.10) from (3.6) for the corresponding solutions and inserting the previous expansion we get

$$S(w^\varepsilon - w, v) = \varepsilon \int_{\Omega_c} \left(J_\Psi + J_\Psi^\top - \nabla \cdot \Psi I \right) \nabla (w^\varepsilon + \widetilde{u}) \cdot \nabla v dx + O(\varepsilon^2). \tag{3.11}$$

Since S is invertible and $S(w^\varepsilon - w, \bullet) \in H^{-1}(\Omega_c)$,

$$||w^\varepsilon - w||_{H_0^1(\Omega_c)} \leq C ||S(w^\varepsilon - w, \bullet)||_{H^{-1}(\Omega_c)}$$

for some $C > 0$. Defining $C_\Psi := ||J_\Psi + J_\Psi^\top - \nabla \cdot \Psi I||_\infty$, we get

$$\left| \int_{\Omega_c} \left(J_\Psi + J_\Psi^\top - \nabla \cdot \Psi I \right) \nabla (w^\varepsilon + \widetilde{u}) \cdot \nabla v dx \right| \leq C_\Psi (||w^\varepsilon||_{H_0^1(\Omega_c)} + ||\widetilde{u}||_{H_0^1(\Omega_c)}) ||v||_{H_0^1(\Omega_c)}$$

for all $v \in H_0^1(\Omega_c)$. From these two inequalities and (3.11),

$$||w^\varepsilon - w||_{H_0^1(\Omega_c)} \leq C C_\Psi |\varepsilon| (||w^\varepsilon||_{H_0^1(\Omega_c)} + ||\widetilde{u}||_{H_0^1(\Omega_c)}) + O(\varepsilon^2)$$

and using $||w^\varepsilon||_{H_0^1(\Omega_c)} \leq ||w||_{H_0^1(\Omega_c)} + ||w^\varepsilon - w||_{H_0^1(\Omega_c)}$ we obtain, for small $|\varepsilon|$, the estimate

$$||w^\varepsilon - w||_{H_0^1(\Omega_c)} \leq \frac{C C_\Psi |\varepsilon|}{1 - C C_\Psi |\varepsilon|} (||w||_{H_0^1(\Omega_c)} + ||\widetilde{u}||_{H_0^1(\Omega_c)}) + \frac{O(\varepsilon^2)}{1 - C C_\Psi |\varepsilon|}$$

and we conclude that $w^\varepsilon \to w$ in $H_0^1(\Omega_c)$.
Now, looking at (3.11), w^* should be the solution of the variational equation:

$$S(w^*, v) = \int_{\Omega_c} \left(J_\Psi + J_\Psi^\top - \nabla \cdot \Psi I \right) \nabla (w + \widetilde{u}) \cdot \nabla v dx, \forall v \in H_0^1(\Omega_c). \tag{3.12}$$

In fact, to conclude, we show that, if w^* is the solution of the previous variational equation

then

$$\left|\left|\frac{w^\varepsilon - w}{\varepsilon} - w^*\right|\right|_{H_0^1(\Omega_c)} \to 0.$$

Since

$$S\left(\frac{w^\varepsilon - w}{\varepsilon} - w^*, v\right) = \int_{\Omega_c} \left(J_\Psi + J_\Psi^\top - \nabla\cdot\Psi I\right)\nabla(w^\varepsilon - w)\cdot\nabla v dx + \frac{O(\varepsilon^2)}{\varepsilon}$$

we have

$$\left|\left|\frac{w^\varepsilon - w}{\varepsilon} - w^*\right|\right|_{H_0^1(\Omega_c)} \leq C_1 C_\Psi ||w^\varepsilon - w||_{H_0^1(\Omega_c)} + \frac{O(\varepsilon^2)}{|\varepsilon|}$$

and the conclusion follows. □

It is important to note that w^* does not depend on the choice of $\widetilde{u}$. In fact, since $u = w + \widetilde{u}$ it follows that w^* is the unique solution of the Poisson problem

$$\begin{cases} \Delta w^* = \nabla\cdot[(J_\Psi + J_\Psi^\top - \nabla\cdot\Psi I)\nabla u] \text{ in } \Omega_c \\ w^*|_{\partial\Omega_c} = 0 \end{cases}. \tag{3.13}$$

On the other hand, $\nabla\cdot[(J_\Psi + J_\Psi^\top - \nabla\cdot\Psi I)\nabla u] \in L^2(\Omega_c)$ and since the boundary of Ω_c is C^2 we have, by regularity, that $w^* \in H^2(\Omega_c)\cap H_0^1(\Omega_c)$.

We now analyze the right hand side of problem (3.13).

Lemma 3.12 *We have,*

$$\int_{\Omega_c}(J_\Psi + J_\Psi^\top - \nabla\cdot\Psi I)\nabla u\cdot\nabla v dx = -\int_{\Omega_c}(\Psi\cdot\nabla u)\Delta v dx,\ \forall v\in\mathcal{D}(\Omega_c).$$

Proof. We follow [2]. Let $\Psi = (\Psi_1,\ldots,\Psi_d)$. Given a test function $v\in H^2(\Omega_c)$ consider the decomposition,

$$\begin{aligned}\int_{\Omega_c}(J_\Psi + J_\Psi^\top - \nabla\cdot\Psi I)\nabla u\cdot\nabla v dx = &\int_{\Omega_c}(J_\Psi\nabla u)\cdot\nabla v dx + \int_{\Omega_c}\nabla u\cdot(J_\Psi\nabla v)dx \\ &- \int_{\Omega_c}(\nabla\cdot\Psi I)\nabla u\cdot\nabla v dx.\end{aligned}$$

- For the first integral on the right hand side of the previous decomposition we have,

$$\int_{\Omega_c}(J_\Psi\nabla u)\cdot\nabla v dx = \sum_{j=1}^d\int_{\Omega_c}\nabla\Psi_j\cdot\nabla u\frac{\partial v}{\partial x_j}dx.$$

Applying Green's formula,

$$\begin{aligned}\sum_{j=1}^{d}\int_{\Omega_c}\nabla\Psi_j\cdot\nabla u\frac{\partial v}{\partial x_j}dx &= -\sum_{j=1}^{d}\int_{\Omega_c}\Psi_j\nabla\cdot\left(\nabla u\frac{\partial v}{\partial x_j}\right)dx+\int_{\partial\Omega_c}(\Psi\cdot\nabla v)\nabla u\cdot\mathbf{n}\,d\varsigma\\ &= -\sum_{j=1}^{d}\int_{\Omega_c}\Psi_j\left(\nabla u\cdot\nabla\left(\frac{\partial v}{\partial x_j}\right)+\Delta u\frac{\partial v}{\partial x_j}\right)dx\\ &\quad+\int_{\partial\Omega_c}(\Psi\cdot\nabla v)\nabla u\cdot\mathbf{n}\,d\varsigma\\ &= -\sum_{j=1}^{d}\int_{\Omega_c}\Psi_j\nabla u\cdot\nabla\left(\frac{\partial v}{\partial x_j}\right)dx+\int_{\partial\Omega_c}(\Psi\cdot\nabla v)\nabla u\cdot\mathbf{n}\,d\varsigma.\end{aligned} \tag{3.14}$$

- For the second integral,

$$\begin{aligned}\int_{\Omega_c}\nabla u\cdot(J_\Psi\nabla v)dx &= -\int_{\Omega_c}(\nabla u\cdot\Psi)\Delta v dx-\sum_{j=1}^{d}\int_{\Omega_c}\Psi_j\left(\nabla\left(\frac{\partial u}{\partial x_j}\right)\cdot\nabla v\right)dx\\ &\quad+\int_{\partial\Omega_c}(\Psi\cdot\nabla u)\nabla v\cdot\mathbf{n}\,d\varsigma\end{aligned}$$

Thus,

$$\begin{aligned}\int_{\Omega_c}(J_\Psi+J_\Psi^\top)\nabla u\cdot\nabla v dx &= -\int_{\Omega_c}(\nabla u\cdot\Psi)\Delta v dx-\int_{\Omega_c}\Psi\cdot\nabla(\nabla u\cdot\nabla v)dx\\ &\quad+\int_{\partial\Omega_c}(\Psi\cdot\nabla v)\nabla u\cdot\mathbf{n}\,d\varsigma+\int_{\partial\Omega_c}(\Psi\cdot\nabla u)\nabla v\cdot\mathbf{n}\,d\varsigma\end{aligned} \tag{3.15}$$

On the other hand,

$$\int_{\Omega_c}(\nabla\cdot\Psi I)\nabla u\cdot\nabla v dx = -\int_{\Omega_c}\Psi\cdot\nabla(\nabla u\cdot\nabla v)dx+\int_{\partial\Omega_c}(\nabla u\cdot\nabla v)\Psi\cdot\mathbf{n}\,d\varsigma \tag{3.16}$$

hence,

$$\begin{aligned}\int_{\Omega_c}(J_\Psi+J_\Psi^\top-\nabla\cdot\Psi I)\nabla u\cdot\nabla v dx &= -\int_{\Omega_c}(\nabla u\cdot\Psi)\Delta v dx+\int_{\partial\Omega_c}(\Psi\cdot\nabla v)\nabla u\cdot\mathbf{n}\,d\varsigma\\ &\quad+\int_{\partial\Omega_c}(\Psi\cdot\nabla u)\nabla v\cdot\mathbf{n}\,d\varsigma-\int_{\partial\Omega_c}(\nabla u\cdot\nabla v)\Psi\cdot\mathbf{n}\,d\varsigma\end{aligned} \tag{3.17}$$

and taking $v \in \mathcal{D}(\Omega_c)$,

$$\int_{\Omega_c} (J_\Psi + J_\Psi^\top - \nabla \cdot \Psi I)\nabla u \cdot \nabla v dx = -\int_{\Omega_c} (\Psi \cdot \nabla u)\Delta v dx.$$

□

By (3.13) and the previous lemma we can write, for $v \in \mathcal{D}(\Omega_c)$

$$S(w^*, v) = \int_{\Omega_c} (J_\Psi + J_\Psi^\top - \nabla \cdot \Psi I)\nabla u \cdot \nabla v dx = -\int_{\Omega_c} (\Psi \cdot \nabla u)\Delta v dx = \int_{\Omega_c} \nabla(\Psi \cdot \nabla u).\nabla v dx$$

that is

$$S(w^* - \Psi \cdot \nabla u, v) = 0, \forall v \in \mathcal{D}(\Omega_c). \tag{3.18}$$

Define the *shape derivative* function

$$w' := w^* - \Psi \cdot \nabla u \in H^1(\Omega_c).$$

From (3.18), we have

$$\Delta w' = 0 \text{ in } \Omega_c.$$

Since $\Psi = 0$ in the open set $\Omega \setminus \overline{\mathcal{O}}$ then w', w^* have the same Cauchy data on Γ. On γ, $w^* = 0$ and therefore $w'|_\gamma = -(\Psi \cdot \nabla u)|_\gamma$. On the other hand, $\nabla u \in H^1(\Omega_c)$, $\partial_{\mathbf{n}} u \in H^{1/2}(\gamma) \subset L^2(\gamma)$ (recall that $u \in H^2(\Omega_c)$) and since $u|_\gamma = 0$ we have

$$\nabla u = (\nabla u \cdot \mathbf{n})\mathbf{n} = \partial_{\mathbf{n}} u \, \mathbf{n} \text{ on } \gamma.$$

In conclusion, the shape derivative function w' verifies:

$$\begin{cases} \Delta w' = 0 \text{ in } \Omega_c \\ w'|_\Gamma = w^*|_\Gamma = 0 \\ \partial_{\mathbf{n}} w'|_\Gamma = \partial_{\mathbf{n}} w^*|_\Gamma \\ w'|_\gamma = -(\Psi \cdot \mathbf{n})\partial_{\mathbf{n}} u|_\gamma \end{cases} . \tag{3.19}$$

Proof of Theorem 3.10. Define the operator

$$F'(\gamma)\Psi := \partial_{\mathbf{n}} w'|_\Gamma \in H^{-1/2}(\Gamma).$$

From the previous results and the continuity of the normal trace operator we have

$$\left|\left|\frac{F(\gamma_\varepsilon)-F(\gamma)}{\varepsilon}-F'(\gamma)\Psi\right|\right|_{H^{-1/2}(\Gamma)}\to 0,\qquad \varepsilon\to 0.$$

Suppose that $F'(\gamma)\Psi=0$, i.e., $\partial_{\mathbf{n}}w'|_\Gamma=0$. Then, w' has null Cauchy data on Γ and by Holmgren's lemma, $w'=0$ in Ω_c. In particular, $0=w'|_\gamma=-(\Psi\cdot\mathbf{n})\partial_{\mathbf{n}}u|_\gamma$. If $\Psi(x)\cdot\mathbf{n}_x\neq 0$ for some $x\in\gamma$ then, by continuity, $\Psi(x)\cdot\mathbf{n}_x\neq 0$ on some relatively open set $\sigma\subset\gamma$. Then, we must have $\partial_{\mathbf{n}}u|_\sigma=0$ and again by Holmgren (recall that $u|_\gamma=0$), $u=0$ in Ω_c. In particular, $g=u|_\Gamma=0$ which contradicts the hypothesis.

Reciprocally, if $\Psi\cdot\mathbf{n}$ is identical null on γ then $w'|_\gamma=0$ and therefore $w'|_{\partial\Omega_c}=0$. Thus, $w'=0$ in Ω_c and we conclude that

$$F'(\gamma)\Psi=\partial_{\mathbf{n}}w'|_\Gamma=0.$$

□

3.2 Robin problem

Let Ω_c be a C^1 domain of propagation defined as in section 3.1.

Consider the *direct problem*:

Given g compute $g_{\mathbf{n}}=\partial_{\mathbf{n}}u$ on $\Sigma\subset\Gamma$ where u solves the mixed problem

$$(\mathcal{P}_R)\begin{cases}\Delta u=0 & \text{in } \Omega_c=\Omega\setminus\overline{\omega}\\ u=g & \text{on } \Gamma=\partial\Omega\\ \partial_{\mathbf{n}}u+Zu=0 & \text{on } \gamma=\partial\omega\end{cases}. \tag{3.20}$$

Again, $\mathbf{n}$ denotes the normal vector on γ, pointing outwards with respect to Ω_c(or inward, with respect to ω).

Theorem 3.13 *If $g\in H^{1/2}(\Gamma)$ and $Z\in L^\infty(\gamma)$ is such that $Z\geq 0$ then $(\mathcal{P}_R)$ is well posed, with solution in $H^1(\Omega_c)$.*

Proof. Let $\widetilde{u}\in H^1(\Omega)$ be the solution of

$$\begin{cases}\Delta\widetilde{u}=0 & \text{in } \Omega\\ \widetilde{u}=g & \text{on } \Gamma\end{cases}.$$

Considering $w = u - \widetilde{u}$, $(\mathcal{P}_R)$ is well posed if and only if the problem

$$\begin{cases} \Delta w = 0 & \text{in } \Omega \\ w = 0 & \text{on } \Gamma \\ \partial_{\mathbf{n}} w + Zw = h & \text{on } \gamma \end{cases}, \tag{3.21}$$

where $h := \partial_{\mathbf{n}}\widetilde{u} + Z\widetilde{u}$, is well posed. Define the subspace

$$V = \{s \in H^1(\Omega_c) : s|_\Gamma = 0\}. \tag{3.22}$$

It is well known that V is a closed subspace of $H^1(\Omega_c)$ and that

$$\langle w, s\rangle_V := \int_{\Omega_c} \nabla w \cdot \nabla s dx, \ \forall w, s \in V \tag{3.23}$$

defines an inner product on V. Denote by $||\cdot||_V$ the norm induced by this inner product. By Poincaré inequality, this norm is equivalent to the norm induced by $H^1(\Omega_c)$, hence, V equipped with this inner product is an Hilbert space.

The variational formulation of problem (3.21) is:

$$\begin{cases} \text{Find } w \in V \text{ such that} \\ S(w, s) = \displaystyle\int_\gamma h s d\varsigma, \ \forall s \in V \end{cases} \tag{3.24}$$

where S is the bilinear continuous and symmetric form on $V \times V$ defined by

$$S(w, s) := \int_{\Omega_c} \nabla w \cdot \nabla s dx + \int_\gamma Zws d\varsigma.$$

Given $s \in V$,

$$S(s, s) = ||s||_V^2 + ||\sqrt{Z}s||_{L^2(\gamma)}^2 \geq ||s||_V^2$$

therefore S is V-coercive. It follows from the Riesz theorem that $w \mapsto S(w, \cdot)$ is an isomorphism between V and V'. On the other hand, the linear form

$$s \mapsto J(s) := \int_\gamma h s d\varsigma$$

is continuous on V. Therefore, exists a unique $w \in V$ such that

$$S(w, s) = J(s)$$

and this concludes the proof. □

Remark 3.14 The problem $(\mathcal{P}_R)$ is not well posed for a general $Z \in L^\infty(\gamma)$. For instance, the following harmonic function in $\mathbb{R}^2 \setminus \{0\}$,

$$u(x) = \log(|x|),$$

satisfies

$$u(x) = 0, \ \forall x \in \Gamma := \partial B(0,1)$$

and, on $\gamma = \partial B(0,\rho)$, $\rho > 0$,

$$\partial_{\mathbf{n}} u = -\frac{1}{\rho} \ \wedge \ u = \log \rho$$

where $\mathbf{n}$ points inwards with respect to the domain $\omega := B(0,\rho)$. Considering $\rho < 1$ and defining

$$Z := \frac{1}{\rho \log \rho} (< 0)$$

we conclude that both the null function and u solves $(\mathcal{P}_R)$ in $\Omega_c = B(0,1) \setminus \overline{B(0,\rho)}$ for $g = 0$ and the aforementioned function Z.

3.2.1 Inverse problem

In this section we study the identification of the Robin coefficient from a boundary measurement on Σ. A first question that arises is:

Can we identify the shape of ω for the mixed problem $(\mathcal{P}_R)$?

The previous Remark 3.14 and an analysis of the proof of Theorem 3.6 suggests a negative answer.

Example 3.15 (*Non uniqueness of the geometric inverse problem for Robin b.c.*) Consider the harmonic function in $\mathbb{R}^2 \setminus \{\mathbf{0}\}$ defined by

$$u(x_1, x_2) = x_1 + \frac{x_1}{x_1^2 + x_2^2}$$

and the annular domain

$$\Omega_c = B(0, \mathrm{P}) \setminus \overline{B(0,\rho)}$$

where $0 < \rho < \mathrm{P}$ (see Fig. 3.4, left plot). On $\gamma = \partial B(0, \rho)$, we have

$$\partial_{\mathbf{n}} u|_\gamma = \frac{\rho^2 - 1}{\rho^2} \mathbf{n} \cdot e_1 \ \wedge \ u|_\gamma = -\frac{(\rho^2 + 1)}{\rho} \mathbf{n} \cdot e_1.$$

Hence, u solves the problem

$$\begin{cases} \Delta u = 0 & \text{in } \Omega_c \\ u = g & \text{on } \Gamma = \partial B(0, \mathrm{P}) \\ \partial_{\mathbf{n}} u + Z_\rho u = 0 & \text{on } \gamma \end{cases}$$

where g is the restriction of u to Γ and

$$Z_\rho \equiv \frac{\rho^2 - 1}{\rho^3 + \rho}.$$

The restriction of $\rho \to Z_\rho$ to the interval $]1, 3[$ is positive and non injective (see Fig. 3.4, right plot). This means that at least two circular inclusions generate the same Cauchy data on Γ. Hence, no identification is possible for this problem considering the non null input function g.

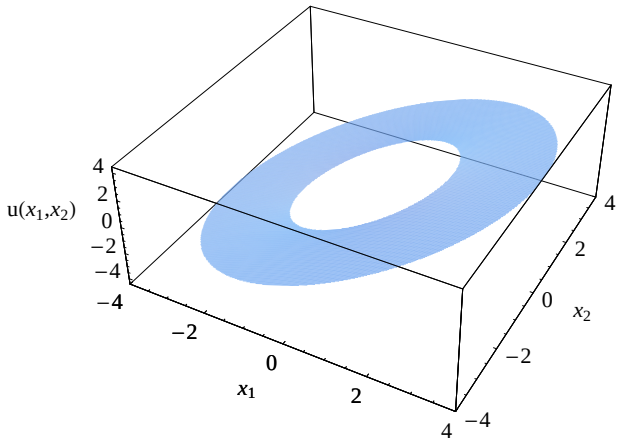

(a) Plot of u considering $\rho = 1.9$ and P= 4.

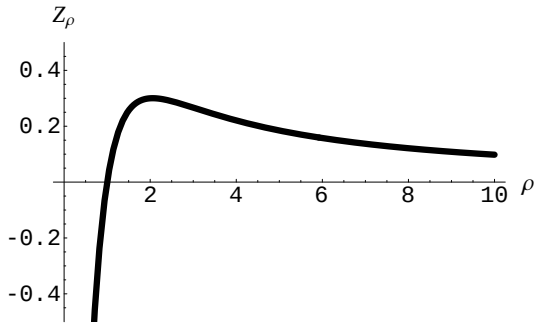

(b) Plot of Z_ρ as a function of ρ.

Figure 3.4: Plot of the functions from Example 3.15.

The inverse Robin problem can be formulated as:

(IRP) : *Assuming that ω is known, identify the Robin coefficient Z from a single pair of Cauchy boundary data on $\Sigma \subset \Gamma$.*

As in (3.3), we denote by $\mathcal{G}_R(\Sigma)$ the space of admissible Cauchy data on an open set $\Sigma \subset \Gamma$, for problem $(\mathcal{P}_R)$. Define the class of admissible Robin coefficients

$$\mathcal{C}_R := \left\{ Z \in C^0(\gamma) : Z \geq 0 \right\}.$$

Theorem 3.16 *(Uniqueness for (IRP)) If g is not identically null on Γ then a single pair of compatible data $(g, g_{\mathbf{n}}) \in \mathcal{G}_R(\Sigma)$ determines uniquely $Z \in \mathcal{C}_R$.*

Proof. This result is well known and, for the sake of completeness we present a proof following [33].

Suppose that exists $u_1, u_2 \in H^1(\Omega_c)$ solving $(\mathcal{P}_R)$ for $Z_1, Z_2 \in \mathcal{C}_R$ respectively such that

$$(g|_\Sigma, \partial_{\mathbf{n}} u_1|_\Sigma) = (g|_\Sigma, \partial_{\mathbf{n}} u_2|_\Sigma).$$

By Holmgren's Lemma, $u_1 = u_2$ in Ω_c. Thus, $u_1|_\gamma = u_2|_\gamma$ and $\partial_{\mathbf{n}} u_1|_\gamma = \partial_{\mathbf{n}} u_2|_\gamma$, and we have

$$(Z_1 - Z_2)u_1 = 0 \text{ on } \gamma. \tag{3.25}$$

Assume by contradiction that $Z_1(x) \neq Z_2(x)$, for some $x \in \gamma$. By continuity, there exists a non empty open set σ in the topology of γ such that $(Z_1 - Z_2)|_\sigma \neq 0$. From (3.25) we obtain $u_1 = 0$ on σ and the Robin boundary condition gives $\partial_{\mathbf{n}} u = 0$ on σ. Using Holmgren's Lemma we get $u_1 = 0$ in Ω_c and in particular $g|_\Sigma = u_1|_\Sigma = 0$, which contradicts the hypothesis. □

Remark 3.17 Due to sign limitations on Z, the Robin inverse problem can not be considered linear. In fact, consider the (injective) operator

$$\begin{aligned} G : \mathcal{C}_R &\longrightarrow H^{-1/2}(\Gamma) \\ Z &\mapsto g_{\mathbf{n}} \end{aligned} \tag{3.26}$$

where $\mathcal{C}_R$ is the cone of admissible coefficients and, for given and fixed $g \in H^{1/2}(\Gamma)$, we have $(g, g_{\mathbf{n}}) \in \mathcal{G}_R(\Gamma)$. It is clear that, in order to have the property

$$G(Z_1 + Z_2) = G(Z_1) + G(Z_2)$$

then $g \equiv 0$ should be considered.

3.2.2 Local Lipschitz stability

In this section, we follow the ideas in [33] and [50] to compute the directional derivative of the map G defined in (3.26) and to present a local Lipschitz stability result.

Given $Z > 0 \in \mathcal{C}_R$ define the perturbation in a given direction $R \in C^0(\gamma)$,

$$Z_\varepsilon := Z + \varepsilon R.$$

Notice that, for sufficient small $|\varepsilon|$, $Z_\varepsilon \in \mathcal{C}_R$. Let $\widetilde{u} \in H^1(\Omega_c)$ be the unique solution of

$$\begin{cases} \Delta\widetilde{u} = 0 & \text{in } \Omega_c \\ \widetilde{u} = g & \text{in } \Gamma \\ \widetilde{u} = 0 & \text{in } \gamma \end{cases}$$

and define $w = u - \widetilde{u}$. We have

$$\begin{cases} \Delta w = 0 & \text{in } \Omega_c \\ w = 0 & \text{in } \Gamma \\ \partial_{\mathbf{n}} w + Zw = h & \text{in } \gamma \end{cases}$$

with $h = -\partial_{\mathbf{n}}\widetilde{u}$. Thus, w is the unique solution of the variational problem

$$\begin{cases} \text{Find } v \in V \text{ such that} \\ S(v,s) = \displaystyle\int_\gamma hs d\varsigma, \ \forall s \in V \end{cases} \tag{3.27}$$

where S is the bilinear form and V the Hilbert space considered in the proof of Theorem 3.13.

In terms of the perturbed problem, $w_\varepsilon = u_\varepsilon - \widetilde{u}$ is the unique solution of

$$\begin{cases} \text{Find } v \in V \text{ such that} \\ S_\varepsilon(v,s) = \displaystyle\int_\gamma hs d\varsigma, \ \forall s \in V \end{cases} \tag{3.28}$$

with

$$S_\varepsilon(v,s) := \int_{\Omega_c} \nabla v \cdot \nabla s dx + \int_\gamma (Z + \varepsilon R) vs d\varsigma.$$

Subtracting the variational equations (3.28) and (3.27) with the corresponding solutions we get

$$S(w_\varepsilon - w, s) = -\varepsilon \int_\gamma R w_\varepsilon s d\varsigma. \tag{3.29}$$

Lemma 3.18 *There exists w' and $r(\varepsilon)$ both in V such that*

$$w_\varepsilon = w + \varepsilon w' + \varepsilon r(\varepsilon)$$

and $r(\varepsilon) \to 0$ in V.

Proof. We follow the proof of Lemma 3.11. By the invertibility of S and equation (3.29) we have

$$||w_\varepsilon - w||_V \leq CC_R|\varepsilon|||w_\varepsilon||_V$$

with $C > 0$ and $C_R = ||R||_\infty$. Since

$$||w_\varepsilon||_V \leq ||w_\varepsilon - w||_V + ||w||_V$$

then, for small $|\varepsilon|$,

$$||w_\varepsilon - w||_V \leq \frac{CC_R|\varepsilon|}{1 - CC_R|\varepsilon|}||w||_V$$

hence $w_\varepsilon \underset{\varepsilon\to 0}{\longrightarrow} w$ in V. Let w' be the unique solution of the variational problem

$$\begin{cases} \text{Find } v \in V \text{ such that} \\ S(v,s) = -\displaystyle\int_\gamma Rwsd\varsigma, \ \forall s \in V \end{cases} . \tag{3.30}$$

We have

$$S(\frac{w_\varepsilon - w}{\varepsilon} - w', s) = -\int_\gamma R(w_\varepsilon - w)sd\varsigma$$

hence

$$\left|\left|\frac{w_\varepsilon - w}{\varepsilon} - w'\right|\right|_V \leq C_1C_R||w_\varepsilon - w||_V$$

and we conclude that $r(\varepsilon) = \frac{w_\varepsilon - w}{\varepsilon} - w' \longrightarrow 0$ in V. □

In conclusion:

Theorem 3.19 *The derivative map $G'(Z) : C^0(\gamma) \to H^{-1/2}(\Gamma)$ is given by $G'(Z)R = \partial_{\mathbf{n}}w'$, where $w' \in H^1(\Omega_c)$ is the unique solution of the mixed problem*

$$\begin{cases} \Delta w' = 0 & \text{in } \Omega_c \\ w' = 0 & \text{on } \Gamma \\ \partial_{\mathbf{n}}w' + Zw' = -Ru & \text{on } \gamma \end{cases} .$$

Theorem 3.20 *(Local Lipschitz stability) Let $R \in C^0(\gamma) \setminus \{0\}$ and $g \in H^{1/2}(\Gamma) \setminus \{0\}$. There exists $c > 0$ such that, for small $|\varepsilon|$,*

$$||G(Z_\varepsilon) - G(Z)||_{H^{-1/2}(\Gamma)} \geq c|\varepsilon|$$

Proof. By contradiction, assume that

$$\lim_{\varepsilon \to 0} \frac{1}{|\varepsilon|} ||G(Z_\varepsilon) - G(Z)||_{H^{-1/2}(\Gamma)} = ||G'(Z)R||_{H^{-1/2}(\Gamma)} = 0.$$

This means $\partial_{\mathbf{n}} w' = 0$ on Γ. Applying Holmgren's Lemma (recall that $w' = 0$ on Γ) we get $w' = 0$ in Ω_c. In particular,

$$0 = \partial_{\mathbf{n}} w + Zw = -Ru \text{ on } \gamma. \tag{3.31}$$

Since by hypothesis $R \not\equiv 0$ then, by continuity, $R|_\sigma \neq 0$ on some open set σ. From (3.31) we get $u = 0$ on σ and it follows $\partial_{\mathbf{n}} u = 0$ on σ because u satisfies a Robin condition on $\gamma \supset \sigma$. Again by Holmgren, $u = 0$ in Ω_c therefore $g = u|_\Gamma = 0$, which contradicts the hypothesis. □

3.3 Conclusions

In this chapter, we addressed two inverse problems:

1. A non linear geometric problem, consisting in the identification of an inclusion or cavity from a single pair of Cauchy data. It was proved that a single pair of compatible Cauchy data $(g, g_{\mathbf{n}})$ with non constant g determines the obstacle and the boundary condition (Dirichlet or Neumann) defined on it. A criterion to distinguish these two situations was provided. Using the domain derivative, we presented a local Lipschitz stability result for the determination of inclusions.

2. The identification of a Robin coefficient problem from a single pair of Cauchy data. It was proved for this non linear problem that for non negative and continuous coefficients a single pair of compatible data determines the coefficient. A local Lipschitz stability result was also obtained.

In the next chapter we focus on the numerical approximation for both direct and inverse problems using methods based on the MFS.

4

The MFS for direct and inverse problems - Laplace equation

The MFS is a meshfree boundary method and has been mostly considered as a numerical method for (elliptic) direct boundary value problems since the first papers by Kupradze and Alekside [64], Oliveira [24] or Mathon and Johnston [69]. Being a boundary method, it does not require any sort of domain discretization technique. On the other hand, no singular integration is performed which is an advantage over the boundary element method. Numerically, the method can be seen as a discretization of a single layer potential on an exterior artificial boundary. Nevertheless it should be noticed that this connection only exists as a term in a sequence of boundary layer densities aimed to fit the given boundary data. In practice, it consists in taking a linear combination of fundamental solutions centered at some (chosen) exterior point sources and then the coefficients can be computed by taking into account the boundary condition(s), for instance by collocation on some boundary points. For the Laplace equation, exponential convergence of the MFS, for smooth data and appropriate chosen collocation and source points, has been proven for circles or its conformal mapped domains (eg. [26], [54], [55], [69]). This optimal exponential decay of the error $O(R^{-n})$ has a counterpart of exponential increase of the condition number $O(R^n)$, for a circle of radius R (cf. [61]). This leads to an "uncertainty principle", already pointed out for radial basis functions (RBF) approximations (cf. [80]):

we can not get both accurate approximations and low condition numbers.

A review on the MFS for direct problems can be found in the recent thesis [84].

On the other hand the MFS is also being considered as a tool for inverse problems, mainly for Cauchy data reconstruction. An example of this application can be found in the early work by Kirsch and Kress [60], twenty years ago, where it was used to fit the boundary data in an external problem, in the context of obstacle detection for exterior acoustic inverse scattering problems. A recent application of the method for linear inverse problems can be found in the references [52] and [67].

In this Chapter we show some theoretical results for the single layer potential to justify the MFS approximation for direct and Cauchy (data reconstruction) problems. An application to the direct problems discussed in Chapter 3 is given and some numerical simulations are presented to illustrate the performance of the method. Concerning the inverse problems, the MFS is applied for Cauchy data reconstruction in a decomposition method and also as numerical approximation for direct problems, in an iterative method. Numerical results are given in order to compare both approaches.

4.1 The MFS for direct problems

For simplicity, we start by recasting the problems $(\mathcal{P}_D)$, $(\mathcal{P}_N)$ and $(\mathcal{P}_R)$ in terms of a single boundary value problem. Let $\Omega_c = \Omega \setminus \overline{\omega} \subset \mathbb{R}^d$ be a doubly connected domain of propagation with C^1 boundary. Consider the following (direct) problem:

Given $g \in H^{1/2}(\Gamma)$, solve

$$(\mathcal{P}) \begin{cases} \Delta u = 0 & \text{in } \Omega_c \\ u = g & \text{on } \Gamma \\ \mathcal{B}u = 0 & \text{on } \gamma \end{cases} \tag{4.1}$$

where $\mathcal{B}$ is the boundary operator defined by $\mathcal{B} := a\tau_\gamma^{\mathbf{n}} + Z_a\tau_\gamma$ and

- a is a constant coefficient in $\{0, 1\}$,
- Z_a is bounded and non negative such that $Z_0 = 1$.

This problem is well posed in $H^1(\Omega_c)$. Notice that, for $a = 0$ we obtain problem $(\mathcal{P}_D)$. When $a \neq 0$ we obtain $(\mathcal{P}_R)$ and, in particular, $(\mathcal{P}_N)$ when $Z_1 = 0$.

To apply the Method of Fundamental Solutions, we consider C^1 artificial boundaries $\partial\widehat{\Omega}_c := \widehat{\Gamma} \cup \widehat{\gamma}$ outside $\overline{\Omega}_c$ that will be used to define the point-sources location. These curves will be called *admissible source set*.

The complementary set $\mathbb{R}^d \setminus \overline{\Omega}_c$ has two connected components, one exterior $\Omega^{\mathrm{C}} = \mathbb{R}^d \setminus \bar{\Omega}$ and one interior, ω. In ω, we consider as admissible sets, $\widehat{\gamma} = \partial\widehat{\omega} \in C^1$ internal regular boundary of $\widehat{\omega}$ simply connected open set such that $\overline{\widehat{\omega}} \subset \omega$. In the exterior of Ω, we define an external boundary $\widehat{\Gamma} = \partial\widehat{\Omega}^{\mathrm{C}} \in C^1$ with $\widehat{\Omega}^{\mathrm{C}}$ an open unbounded set contained in Ω^{C} with a boundary that encloses the domain, $\Omega \subset \mathbb{R}^d \setminus \widehat{\Omega}^{\mathrm{C}}$. The artificial domain of propagation is thus defined by $\widehat{\Omega}_c := \widehat{\Omega} \setminus \overline{\widehat{\omega}}$ where $\widehat{\Omega} := \mathbb{R}^d \setminus \overline{\widehat{\Omega}^{\mathrm{C}}}$ (see Fig. 4.1).

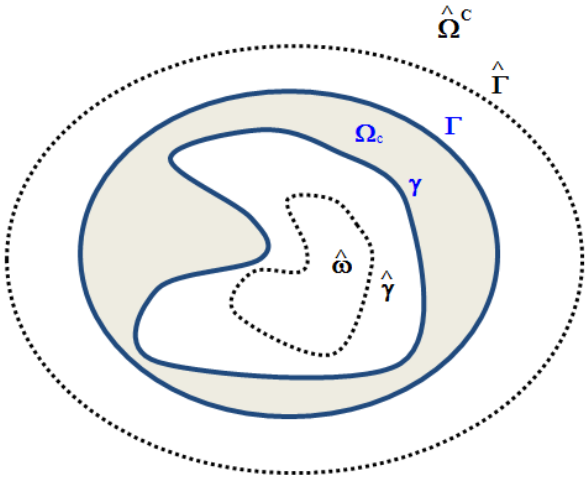

Figure 4.1: A doubly connected domain Ω_c and an artificial boundary $\widehat{\Gamma} \cup \widehat{\gamma}$.

Consider the single layer representation

$$u := L_{\widehat{\Gamma}}\phi + L_{\widehat{\gamma}}\psi. \tag{4.2}$$

Notice that the singularities of u are placed outside $\overline{\Omega}_c$ and that $\Delta u = 0$ in $\mathbb{R}^d \setminus (\widehat{\Gamma} \cup \widehat{\gamma})$. Thus, to approximate the solution of $(\mathcal{P})$ using the single layer representation we have to consider the integral equations

$$S_{\Gamma,\widehat{\Gamma}}\phi + S_{\Gamma,\widehat{\gamma}}\psi = g \qquad \wedge \qquad \mathcal{B}L_{\widehat{\Gamma}}\phi + \mathcal{B}L_{\widehat{\gamma}}\psi = 0. \tag{4.3}$$

where we used the notation for the single layer potentials

$$S_{\Gamma,\widehat{\Gamma}}\phi := \tau_{\Gamma} L_{\widehat{\Gamma}}\phi.$$

However, in general, such equations are not solvable. Nevertheless, we prove that, in a

proper functional space containing the boundary data $(g, 0)$, the set

$$\left\{\left(S_{\Gamma,\widehat{\Gamma}}\phi + S_{\Gamma,\widehat{\gamma}}\psi, \mathcal{B}L_{\widehat{\Gamma}}\phi + \mathcal{B}L_{\widehat{\gamma}}\psi\right)\right\}$$

is dense. Although the steps of the density proof are similar, there are some slightly differences between the 2D and 3D cases. This is related to the different asymptotic behavior of the fundamental solutions in 2D and 3D.

Lemma 4.1 *Given $c \in \mathbb{R}$ and $g \in H^{1/2}(\widehat{\Gamma})$ the exterior problem*

$$\begin{cases} \Delta u = 0 & \text{in } \widehat{\Omega}^{\mathrm{C}} \subset \mathbb{R}^2 \\ u = g & \text{on } \widehat{\Gamma} \\ u(x) = c \log|x| + O(1) & |x| \to \infty \end{cases} \tag{4.4}$$

is well posed in $H^1_{loc}(\widehat{\Omega}^{\mathrm{C}})$. In $\mathbb{R}^3$ the same conclusion holds if u satisfies

$$u(x) = O(|x|^{-1}), \qquad |x| \to \infty$$

instead.

Proof. See [34]. □

We focus on the 2D case. Given a boundary Υ, $Z \in L^\infty(\Upsilon)$, define the closed space

$$\mathcal{H}_Z^{1/2}(\Upsilon) := \left\{\phi \in H^{1/2}(\Upsilon) : \int_\Upsilon Z(x)\phi(x)d\varsigma_x = 0\right\}.$$

It is clear that $Z \equiv 0$ implies $\mathcal{H}_Z^{1/2}(\Upsilon) = H^{1/2}(\Upsilon)$ and

$$\int_\Upsilon Z(x)d\varsigma_x \neq 0 \implies \mathcal{H}_Z^{1/2}(\Upsilon) \cong H^{1/2}(\Upsilon)/\mathbb{R}$$

by taking

$$\phi - \frac{1}{\int_\Upsilon Z(x)d\varsigma_x}\int_\Upsilon Z(x)\phi(x)d\varsigma_x \in \mathcal{H}_Z^{1/2}(\Upsilon),$$

for each $\phi \in H^{1/2}(\Upsilon)$.
By duality, we define the space $\mathcal{H}_Z^{-1/2}(\Upsilon)$ consisting of $\psi \in H^{-1/2}(\Upsilon)$ such that

$$\int_\gamma Z(x)\psi(x)d\varsigma_x = 0.$$

We note that, for $Z \in L^\infty(\Upsilon) \setminus \{0\}$ non negative, the dual of $\mathcal{H}_Z^{1/2}(\Upsilon)$ can be identified with $\mathcal{H}_Z^{-1/2}(\Upsilon)$.

Consider the operator

$$\mathcal{M}(\Gamma,\gamma) : H^{-1/2}(\widehat{\Gamma}) \times H^{-1/2}(\widehat{\gamma}) \longrightarrow H^{1/2}(\Gamma) \times H^{-1/2}(\gamma)$$

defined by

$$\mathcal{M}(\Gamma,\gamma)(\phi,\psi) = \begin{bmatrix} S_{\Gamma,\widehat{\Gamma}} & S_{\Gamma,\widehat{\gamma}} \\ \mathcal{B}L_{\widehat{\Gamma}} & \mathcal{B}L_{\widehat{\gamma}} \end{bmatrix} \begin{bmatrix} \phi \\ \psi \end{bmatrix}. \tag{4.5}$$

Equations (4.3) can now be written in the form

$$\mathcal{M}(\Gamma,\gamma)(\phi,\psi) = \mathcal{D}(\Gamma,\gamma) \tag{4.6}$$

where

$$\mathcal{D}(\Gamma,\gamma) := \begin{bmatrix} g \\ 0 \end{bmatrix}.$$

Theorem 4.2 *The restriction of $\mathcal{M}(\Gamma,\gamma)$ to $\mathcal{H}_1^{-1/2}(\widehat{\Gamma}) \times \mathcal{H}_1^{-1/2}(\widehat{\gamma})$ is injective.*

Proof. Let $(\phi,\psi) \in \mathcal{H}_1^{-1/2}(\widehat{\Gamma}) \times \mathcal{H}_1^{-1/2}(\widehat{\gamma})$ be such that $\mathcal{M}(\Gamma,\gamma)(\phi,\psi) = \mathbf{0}$. Denote by u the single layer potential defined in (4.2). Then,

$$[u]_{\widehat{\Gamma}} = [u]_{\widehat{\gamma}} = 0, \quad \phi = [\partial_{\mathbf{n}} u]_{\widehat{\Gamma}}, \quad \psi = [\partial_{\mathbf{n}} u]_{\widehat{\gamma}}, \tag{4.7}$$

where u^- is the restriction of u to $\widehat{\Omega}_c$ and u^+ the restriction of u to $\mathbb{R}^2 \setminus \overline{\widehat{\Omega}}_c$. On the other hand,

$$\mathcal{M}(\Gamma,\gamma)(\phi,\psi) = \mathbf{0} \Longrightarrow (u = 0 \text{ on } \Gamma \quad \wedge \quad \mathcal{B}u = 0 \text{ on } \gamma).$$

To prove the injectivity we show $u = 0$ in $\mathbb{R}^2 \setminus (\widehat{\Gamma} \cup \widehat{\gamma})$ from where it follows that the jumps ϕ, ψ are null. We split the proof in the analysis of three problems:

- In $\Omega_c \subset \widehat{\Omega}_c$, u^- satisfies the well posed problem in $H^1(\Omega_c)$

$$\begin{cases} \Delta u = 0 & \text{in } \Omega_c \\ u = 0 & \text{on } \Gamma \\ \mathcal{B}u = 0 & \text{on } \gamma \end{cases} \tag{4.8}$$

  hence $u^- = 0$ in Ω_c and, by analytic continuation, $u^- = 0$ in $\widehat{\Omega}_c$. In particular, $u^-|_{\widehat{\Gamma}} = u^-|_{\widehat{\gamma}} = 0$ and since u is continuous across $\widehat{\Gamma} \cup \widehat{\gamma}$, we must have $u^+|_{\widehat{\Gamma}} = u^+|_{\widehat{\gamma}} = 0$.

- Regarding the unbounded component $\widehat{\Omega}^{\mathrm{C}}$ we consider the well posed problem in $H^1_{loc}(\widehat{\Omega}^{\mathrm{C}})$

$$\begin{cases} \Delta u = 0 & \text{in } \widehat{\Omega}^{\mathrm{C}} \\ u = 0 & \text{on } \widehat{\Gamma} = \partial\widehat{\Omega}^{\mathrm{C}} \\ u(y) = c\log|y| + O(1) & |y| \to \infty \end{cases} \tag{4.9}$$

with

$$c = -\frac{1}{2\pi}\left(\int_{\widehat{\Gamma}} \phi(x) d\varsigma_x + \int_{\widehat{\gamma}} \psi(x) d\varsigma_x\right).$$

Now u^+ satisfies this exterior problem with $c = 0$ (recall that $\phi \in \mathcal{H}_1^{-1/2}(\widehat{\Gamma})$, $\psi \in \mathcal{H}_1^{-1/2}(\widehat{\gamma})$) therefore, $u^+ = 0$ in $\widehat{\Omega}^{\mathrm{C}}$.

- For the exterior and bounded component $\widehat{\omega}$, the well posed problem in $H^1(\widehat{\omega})$

$$\begin{cases} \Delta u = 0 & \text{in } \widehat{\omega} \\ u = 0 & \text{on } \widehat{\gamma} = \partial\widehat{\omega} \end{cases} \tag{4.10}$$

is satisfied by u^+ and this gives $u^+ = 0$ in $\widehat{\omega}$.

Thus, $u = 0$ in $\widehat{\Omega}_c \cup \widehat{\Omega}^{\mathrm{C}} \cup \widehat{\omega} = \mathbb{R}^2 \setminus (\widehat{\Gamma} \cup \widehat{\gamma})$ hence, $\phi = \psi = 0$. □

Since $\mathcal{M}(\Gamma, \gamma)$ is a bounded linear operator between Hilbert spaces, we use the property (eg. [78])

$$\mathrm{R}(\mathcal{M}(\Gamma,\gamma))^{\perp} = \ker(\mathcal{M}(\Gamma,\gamma)^*),$$

where $\mathcal{M}(\Gamma,\gamma)^*$ is the adjoint of $\mathcal{M}(\Gamma,\gamma)$, to establish the density result. We start with the expression for the adjoint operator.

Lemma 4.3 *The adjoint of $\mathcal{M}(\Gamma,\gamma)$ is given by*

$$\mathcal{M}(\Gamma,\gamma)^* = \begin{bmatrix} S_{\widehat{\Gamma},\Gamma} & aK_{\widehat{\Gamma},\gamma} + S_{\widehat{\Gamma},\gamma} Z_a \\ S_{\widehat{\gamma},\Gamma} & aK_{\widehat{\gamma},\gamma} + S_{\widehat{\gamma},\gamma} Z_a \end{bmatrix}$$

Proof. We have

$$\begin{aligned} \left\langle \mathcal{B} L_{\widehat{\Gamma}} \phi, \psi \right\rangle_{H^{1/2}(\gamma)\times H^{-1/2}(\gamma)} &= \int_{\gamma} (a\partial_{\mathbf{n}_y} + Z_a(y)) \int_{\widehat{\Gamma}} \Phi_y(x)\phi(x) d\varsigma_x \psi(y) d\varsigma_y \\ &= \int_{\gamma}\int_{\widehat{\Gamma}} (a\partial_{\mathbf{n}_y} + Z_a(y))\Phi_y(x)\phi(x)\psi(y) d\varsigma_x d\varsigma_y \\ &= \int_{\widehat{\Gamma}}\int_{\gamma} (a\partial_{\mathbf{n}_y} + Z_a(y))\Phi_x(y)\psi(y) d\varsigma_y \phi(x) d\varsigma_x \\ &= \left\langle \tau_{\widehat{\Gamma}} \left((aM_\gamma + L_\gamma Z_a)\psi \right), \phi \right\rangle_{H^{1/2}(\widehat{\Gamma})\times H^{-1/2}(\widehat{\Gamma})} \end{aligned}$$

therefore $(\mathcal{B}L_{\widehat{\Gamma}})^* = \tau_{\widehat{\Gamma}}(aM_\gamma + L_\gamma Z_a) = aK_{\widehat{\Gamma},\gamma} + S_{\widehat{\Gamma},\gamma}Z_a$. Using the same argument we get $(S_{\Gamma,\widehat{\gamma}})^* = S_{\widehat{\gamma},\Gamma}$. Thus,

$$\mathcal{M}(\Gamma,\gamma)^* = \begin{bmatrix} (S_{\Gamma,\widehat{\Gamma}})^* & (S_{\Gamma,\widehat{\gamma}})^* \\ (\mathcal{B}L_{\widehat{\Gamma}})^* & (\mathcal{B}L_{\widehat{\gamma}})^* \end{bmatrix}^\top = \begin{bmatrix} S_{\widehat{\Gamma},\Gamma} & aK_{\widehat{\Gamma},\gamma} + S_{\widehat{\Gamma},\gamma}Z_a \\ S_{\widehat{\gamma},\Gamma} & aK_{\widehat{\gamma},\gamma} + S_{\widehat{\gamma},\gamma}Z_a \end{bmatrix}.$$

□

Theorem 4.4 *The operator $\mathcal{M}(\Gamma,\gamma)$ has dense range in $\mathcal{H}_1^{1/2}(\Gamma) \times \mathcal{H}_{Z_a}^{-1/2}(\gamma)$.*

Proof. To prove the density we show that the restriction of the adjoint $\mathcal{M}(\Gamma,\gamma)^*$ to $\mathcal{H}_1^{-1/2}(\widehat{\Gamma})\times\mathcal{H}_{Z_a}^{1/2}(\widehat{\gamma})$ is injective. Let $(\phi,\psi) \in \mathcal{H}_1^{-1/2}(\widehat{\Gamma})\times\mathcal{H}_{Z_a}^{1/2}(\widehat{\gamma})$ such that $M(\Gamma,\gamma)^*(\phi,\psi) = \mathbf{0}$. Define the boundary layer

$$u = L_\Gamma\phi + (aM_\gamma + L_\gamma Z_a)\psi$$

ie.,

$$u(y) = \int_\Gamma \phi(x)\Phi_y(x)d\varsigma_x + \int_\gamma a\psi(x)\partial_{\mathbf{n}_x}\Phi_y(x)d\varsigma_x + \int_\gamma Z_a(x)\psi(x)\Phi_y(x)d\varsigma_x,\ y \in \mathbb{R}^2 \setminus (\Gamma\cup\gamma).$$

It is clear that u is harmonic in $\mathbb{R}^2\setminus(\Gamma\cup\gamma)$ and since by hypothesis $(\phi,\psi)\in\ker\mathcal{M}(\Gamma,\gamma)^*$, we have $u = 0$ in $\widehat{\Gamma}$ and $\widehat{\gamma}$. On the other hand,

$$[u]_\Gamma = 0, \quad [\partial_{\mathbf{n}}u]_\Gamma = \phi, \quad [u]_\gamma = -a\psi \quad \wedge \quad [\partial_{\mathbf{n}}u]_\gamma = Z_a\psi. \tag{4.11}$$

To show that $\phi = \psi = 0$ we follow the proof of Theorem 4.2.

- First notice that the well posed exterior problem (4.9) (now the constant is $c = -\frac{1}{2\pi}(\int_\Gamma \phi(x)d\varsigma_x + \int_\gamma Z_a(x)\psi(x)d\varsigma_x)$) is satisfied by u^+ with $c = 0$. By analytic continuation, it follows that $u^+ = 0$ in Ω^{C} hence, $u^+|_\Gamma = 0$ and $\partial_{\mathbf{n}}u^+|_\Gamma = 0$.

- From $\Delta u^+ = 0$ in $\widehat{\omega}$ and $u^+ = 0$ on $\widehat{\gamma} = \partial\widehat{\omega}$ we conclude that $u^+|_\gamma = 0$ and $\partial_{\mathbf{n}}u^+|_\gamma = 0$.

- Using the jump relations (4.11), we get $u^-|_\Gamma = 0$, $u^-|_\gamma = -a\psi$ and $\partial_{\mathbf{n}}u^-|_\gamma = Z_a\psi$. Thus, u^- satisfies the well posed problem in $H^1(\Omega_c)$

$$\begin{cases} \Delta u = 0 & \text{in } \Omega_c \\ u = 0 & \text{on } \Gamma \\ \mathcal{B}u = 0 & \text{on } \gamma \end{cases} \tag{4.12}$$

hence, $u^-|_\gamma = 0$ and $\partial_{\mathbf{n}} u^-|_\Gamma = \partial_{\mathbf{n}} u^-|_\gamma = 0$.

We conclude that $\phi = 0$, $a\psi = 0$ and $Z_a\psi = 0$ and it follows (recall that $a \in \{0, 1\}$ is constant and $Z_0 = 1$)

$$\phi = \psi = 0.$$

□

Remark 4.5

1. It follows from the previous results that the constants must be added to the approximation for the 2D case. This is justified by the asymptotic behavior of the fundamental solution in the (unbounded) domain $\widehat{\Omega}^{\mathrm{C}}$. Instead, if we consider for instance $\widehat{\Omega}^{\mathrm{C}}$ bounded this restriction can be dropped. Although theoretically simpler, this choice leads to (for instance, when $\widehat{\Gamma}$ does not enclose the domain Ω) worst numerical results.

2. In the 3D case, the asymptotic behavior for the exterior problem is automatically satisfied by the fundamental solution. In this case, the previous injectivity and density results hold in the whole functional spaces and can be obtained using the same arguments.

3. The above results are also valid when Ω_c is a multiply connected domain. In this case, an artificial curve must be considered inside each component of ω.

4.1.1 Numerical implementation

We now describe the implementation of the MFS approximation for $(\mathcal{P})$. For numerical computations we must consider a discrete version of (4.6). In particular, only a finite number of source points $y_1, \ldots, y_m \in \widehat{\Gamma} \cup \widehat{\gamma}$ can be considered. For simplicity we drop the constants.

Consider the discretization of the single boundary layer given by

$$\widetilde{u} = \sum_{j=1}^{m} \alpha_j \Phi_{y_j}, \quad \alpha_1, \ldots, \alpha_m \in \mathbb{R},\ y_j \in \widehat{\Gamma} \cup \widehat{\gamma} \tag{4.13}$$

and the corresponding discretization of (4.5), $\widetilde{\mathcal{M}}(\Gamma, \gamma) : \mathbb{R}^m \longrightarrow L^2(\Gamma) \times L^2(\gamma)$ given by

$$\widetilde{\mathcal{M}}(\Gamma,\gamma)=\begin{bmatrix} \Phi_{y_1}|_\Gamma & \cdots & \Phi_{y_m}|_\Gamma \\ (a\partial_{\mathbf{n}}\Phi_{y_1}+Z_a\Phi_{y_1})|_\gamma & \cdots & (a\partial_{\mathbf{n}}\Phi_{y_m}+Z_a\Phi_{y_m})|_\gamma \end{bmatrix}.$$

Thus, the system (4.6) in this discrete form is given by

$$\widetilde{\mathcal{M}}(\Gamma,\gamma)(\alpha_1,\ldots,\alpha_m)=\mathcal{D}(\Gamma,\gamma). \tag{4.14}$$

We now establish an injectivity result similar to Theorem 4.2.

Theorem 4.6 *$\widetilde{\mathcal{M}}(\Gamma,\gamma)$ is injective.*

Proof. We show that if $\mathbf{X}=(\alpha_1,\ldots,\alpha_m)\in\ker\widetilde{\mathcal{M}}(\Gamma,\gamma)$ then $\mathbf{X}=\mathbf{0}$. Let $\widetilde{u}$ be the harmonic function in $\mathbb{R}^d\setminus\{y_1,\ldots,y_m\}$ defined above. Since

$$\widetilde{\mathcal{M}}(\Gamma,\gamma)(\alpha_1,\ldots,\alpha_m)=(\widetilde{u}|_\Gamma,\mathcal{B}\widetilde{u})$$

then $\mathbf{X}\in\ker\widetilde{\mathcal{M}}(\Gamma,\gamma)$ means that $\widetilde{u}$ solves the well posed problem $(\mathcal{P})$ for $g=0$. Therefore $\widetilde{u}=0$ in Ω_c and by analytic continuation,

$$\widetilde{u}=0 \text{ in } \mathbb{R}^d\setminus\{y_1,\ldots,y_m\}.$$

The conclusion follows from the fact that $\{\Phi_{y_1},\ldots,\Phi_{y_m}\}$ is a linearly independent set in $\mathbb{R}^d\setminus\{y_1,\ldots,y_m\}$. □

However, it is clear that a density result of the range of $\widetilde{\mathcal{M}}(\Gamma,\gamma)$ in $L^2(\Gamma)\times L^2(\gamma)$ can not be obtained. In fact, the adjoint operator of $\widetilde{\mathcal{M}}(\Gamma,\gamma)$ is given by $\widetilde{\mathcal{M}}(\Gamma,\gamma)^*: L^2(\Gamma)\times L^2(\gamma)\longrightarrow\mathbb{R}^m$, with

$$\widetilde{\mathcal{M}}(\Gamma,\gamma)^*(\phi,\psi)=\begin{bmatrix} L_\Gamma(\phi)(y_1)+(aM_\gamma+L_\gamma Z_a)(\psi)(y_1) \\ L_\Gamma(\phi)(y_2)+(aM_\gamma+L_\gamma Z_a)(\psi)(y_2) \\ \cdots \\ L_\Gamma(\phi)(y_m)+(aM_\gamma+L_\gamma Z_a)(\psi)(y_m) \end{bmatrix}$$

maps to a finite dimensional space.

For the numerical implementation of the MFS we consider the discretized version of

$\widetilde{\mathcal{M}}(\Gamma,\gamma)$ and $\mathcal{D}(\Gamma,\gamma)$ given by

$$\mathbb{M}(\Gamma,\gamma)=\begin{bmatrix} \Phi_{y_1}(x_1^\Gamma) & \cdots & \Phi_{y_m}(x_1^\Gamma) \\ \cdots & \cdots & \cdots \\ \Phi_{y_1}(x_{n_1}^\Gamma) & \cdots & \Phi_{y_m}(x_{n_1}^\Gamma) \\ a\partial_{\mathbf{n}}\Phi_{y_1}(x_1^\gamma)+Z_a(x_1^\gamma)\Phi_{y_1}(x_1^\gamma) & \cdots & a\partial_{\mathbf{n}}\Phi_{y_m}(x_1^\gamma)+Z_a(x_1^\gamma)\Phi_{y_m}(x_1^\gamma) \\ \cdots & \cdots & \cdots \\ a\partial_{\mathbf{n}}\Phi_{y_1}(x_{n_2}^\gamma)+Z_a(x_{n_2}^\gamma)\Phi_{y_1}(x_{n_2}^\gamma) & \cdots & a\partial_{\mathbf{n}}\Phi_{y_m}(x_{n_2}^\gamma)+Z_a(x_{n_2}^\gamma)\Phi_{y_m}(x_{n_2}^\gamma) \end{bmatrix}$$

and

$$\mathbb{D}(\Gamma,\gamma)=\begin{bmatrix} g(x_1^\Gamma) \\ \vdots \\ g(x_{n_1}^\Gamma) \\ 0 \\ \vdots \\ 0 \end{bmatrix}$$

on some collocation points $x_1^\Gamma,\ldots,x_{n_1}^\Gamma\in\Gamma$, $x_1^\gamma,\ldots,x_{n_2}^\gamma\in\gamma$ and source points $y_1,\ldots,y_m\in\widehat{\Gamma}\cup\widehat{\gamma}$. When $n_1+n_2=:n=m$ the coefficients $\alpha_1,\ \ldots,\ \alpha_m\in\mathbb{R}$ can be computed by solving the linear system

$$\mathbb{M}(\Gamma,\gamma)\mathbf{X}=\mathbb{D}(\Gamma,\gamma) \tag{4.15}$$

or using the Tikhonov regularization

$$\left(\mu\mathbb{I}+\mathbb{M}(\Gamma,\gamma)^*\mathbb{M}(\Gamma,\gamma)\right)\mathbf{X}=\mathbb{M}(\Gamma,\gamma)^*\mathbb{D}(\Gamma,\gamma)$$

for overdetermined systems ($n>m$).

4.1.2 Numerical simulations

Dirichlet boundary condition

We illustrate the accuracy of the Method of Fundamental Solutions with four numerical examples regarding $(\mathcal{P}_D)$. The accessible part of the boundary, Γ, is $\partial B(0,3.5)$. On this part of the boundary, we consider the input function

$$g\equiv 1.$$

The boundary of the inclusion is given by the parametrization :

- Example 1 (Ellipsis):

$$\gamma_1(t) = (-1, -1.3) + (1.6\cos t, \sin t),\ 0 \leq t \leq 2\pi$$

- Example 2 (Star):

$$\gamma_2(t) = (1, -1.0) + (1.0 + 0.3\sin 4t)(\cos t, \sin t),\ 0 \leq t \leq 2\pi$$

- Example 3 (Bean):

$$\gamma_3(t) = (0.8 + 1.8\sin t\cos t/2)(\cos t, \sin t),\ 0 \leq t \leq 2\pi$$

- Example 4 (Kite):

$$\gamma_4(t) = (-1.2, 0.5) + (0.9\cos t + 0.3\cos 2t - 0.2, \sin t),\ 0 \leq t \leq 2\pi$$

The numerical approximation for the direct problem using the MFS is given by (4.13) where the coefficients α_j are the solution of the linear system (4.15). The matrix of this system, $\mathbb{M}(\Gamma, \gamma)$, is obtained by considering 1300 equally spaced collocation points $x_1^\Gamma, \ldots, x_{650}^\Gamma \in \Gamma$, $x_1^\gamma, \ldots, x_{650}^\gamma \in \gamma$ and the same amount of source points. The external source points were uniformly distributed on $\widehat{\Gamma} = \partial B(0, 4.5)$ and for the internal source points we considered

$$y_i = x_i^\gamma - \frac{0.1}{|x_{i+1}^\gamma - x_i^\gamma|}\frac{x_{i+1,2}^\gamma - x_{i,2}^\gamma}{x_{i+1,1}^\gamma - x_{i,1}^\gamma},\ i = 1, \ldots, 649. \tag{4.16}$$

This distribution of source points is represented in Fig. 4.2 (black dots).

Since the numerical solution, $\widetilde{u}$, satisfies Laplace's equation in Ω_c then, by the maximum principle, we can control the error

$$|E_{\overline{\Omega}_c}(x)| = |u(x) - \widetilde{u}(x)|,\ x \in \overline{\Omega}_c$$

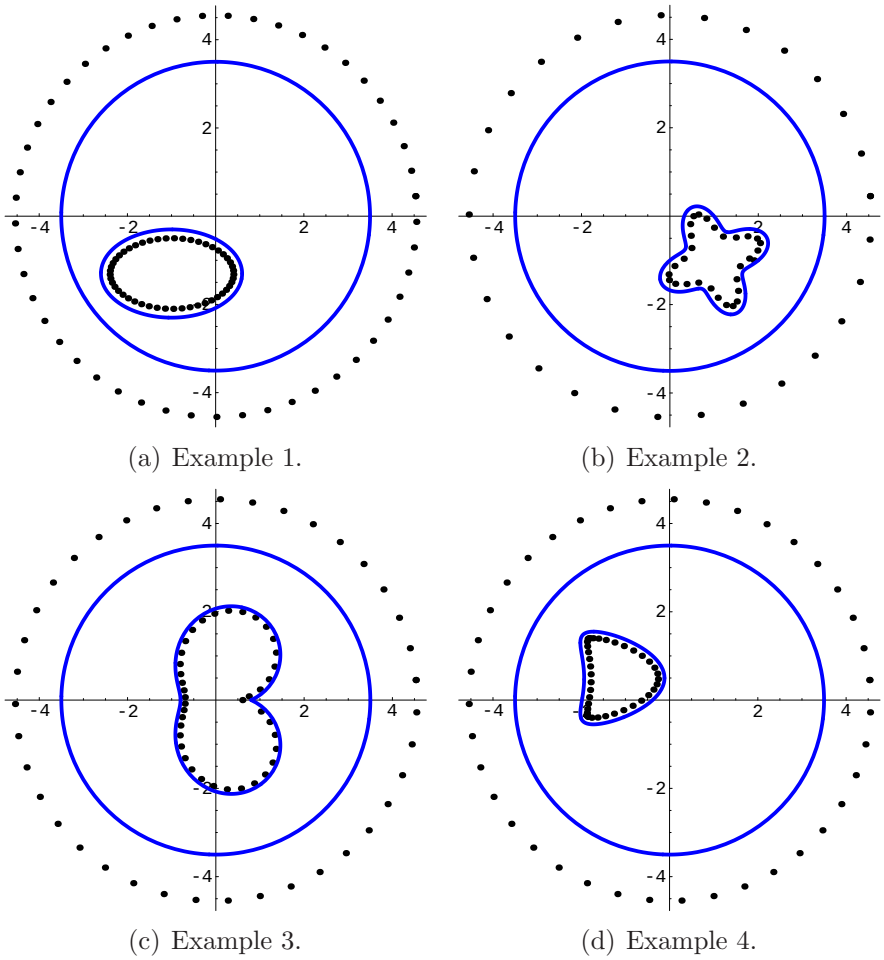

(a) Example 1. (b) Example 2.

(c) Example 3. (d) Example 4.

Figure 4.2: Geometry of the domains. The black dots represent the source points (direct problem).

by the error on the boundary, $|E_{\partial\Omega_c}|$. In Figs. 4.3, 4.4, 4.5 and 4.6 we present the values of $|E_\Gamma|$ on the left and $|E_{\gamma_i}|$ on the right, for the previous examples.

Finally, the ill conditioned feature of the method is illustrated on Table 4.1 where we present the evolution of the condition number $\text{cond}_\infty \mathbb{M}(\Gamma, \gamma)$ and the maximum of the error on the boundary in terms of the number of collocation points. In this table we may notice that despite early high condition numbers, the MFS presents increasing accurate approximations.

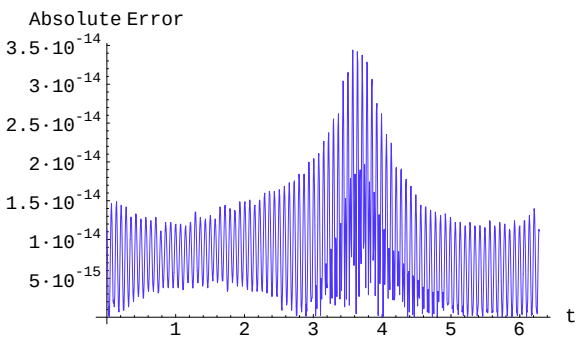

(a) Error on Γ.

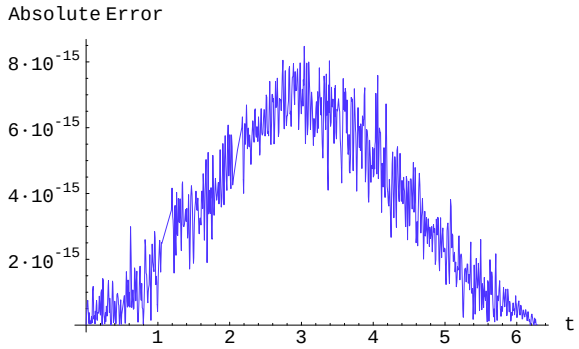

(b) Error on γ_1.

Figure 4.3: Absolute error on the boundary (direct problem).

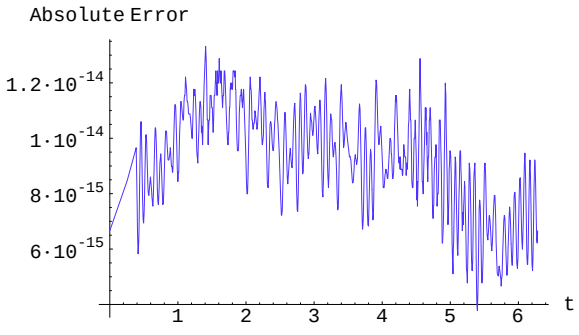

(a) Error on Γ.

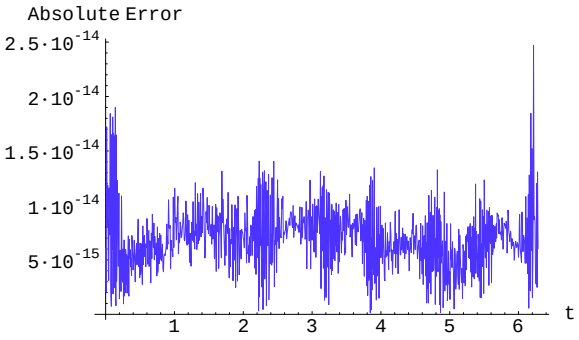

(b) Error on γ_2.

Figure 4.4: Absolute error on the boundary (direct problem).

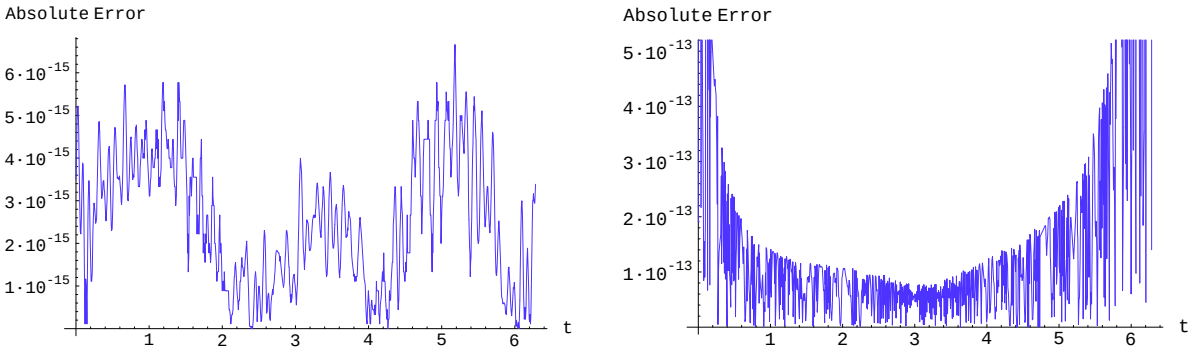

(a) Error on Γ. (b) Error on γ_3.

Figure 4.5: Absolute error on the boundary (direct problem).

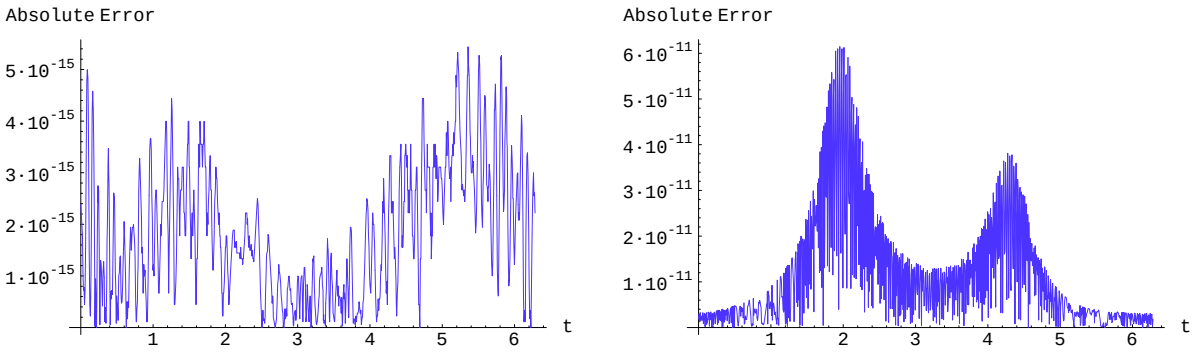

(a) Error on Γ. (b) Error on γ_4.

Figure 4.6: Absolute error on the boundary (direct problem).

Collocation Points	$\text{cond}_\infty(\mathbb{M}(\Gamma,\gamma))$	$\text{Max}\lvert E_{\partial\Omega_c}\rvert$
100	5.3×10^{33}	1.8×10^{-2}
500	1.3×10^{24}	1.8×10^{-5}
1000	3.3×10^{22}	7.5×10^{-8}
1300	5.2×10^{21}	6.1×10^{-11}
1500	1.1×10^{21}	6.1×10^{-11}
2000	7.7×10^{21}	6.1×10^{-11}

Table 4.1: Evolution of the condition number and the error on the boundary with the number of collocation points, for example 2.

Robin boundary condition

Regarding the MFS simulations for the direct Robin problem we present three examples. The boundary of the domain Ω_c is $\Gamma = \partial B(0, 3.5)$ and γ is a centered ellipsis. The artificial boundary is $\widehat{\Gamma} = \partial B(0, 4.5)$ and $\widehat{\gamma}$ is also an ellipsis (see Fig. 4.7). The input function is

$$g \equiv 1.$$

The considered Robin coefficient is (see Fig. 4.8):

- Example 1 (constant):

$$Z_1 \equiv 3$$

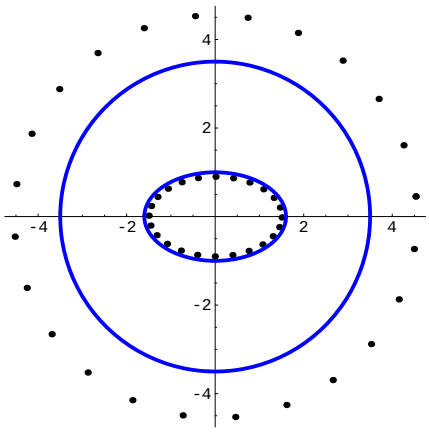

Figure 4.7: Geometry of the domain for the Robin problem. The blue line represents the boundary of $\partial\Omega_c$ and black dots the location of the point sources (direct problem).

- Example 2 (smooth):

$$Z_2(t) = 0.9 + \sin^2 t \cos(t/2),\ 0 \le t \le 2\pi$$

- Example 3 (non-smooth spline):

$$Z_3(t) = \begin{cases} \dfrac{t}{\pi} + \dfrac{1}{2} & 0 \le t < \frac{\pi}{2} \\ 1 + \dfrac{4(\frac{-\pi}{2} + t)}{\pi} & \frac{\pi}{2} \le t < \pi \\ 3 - \dfrac{4(-\pi + t)}{\pi} & \pi \le t < \frac{3\pi}{2} \\ 1 - \dfrac{-\frac{3\pi}{2} + t}{\pi} & \frac{3\pi}{2} \le t \le 2\pi \end{cases}$$

In Figs. 4.9, 4.10 and 4.11 we present the absolute error on the boundary. On Γ the absolute error is given by

$$|\widetilde{u}_i(x) - g(x)|,\ x \in \Gamma$$

and on γ,

$$|\partial_{\mathbf{n}} u_i + Z_i u_i|,\ x \in \gamma$$

where $\widetilde{u}_i$ is the MFS approximation of the solution of the i-th example. We can see that for the smooth coefficients, the boundary error is small. For the non smooth example, we get a bigger boundary error precisely at the non smooth points (Fig. 4.11, right). This is due to the fact that the non smoothness is transferred to the normal derivative appearing on the boundary condition and the approximation is sought in terms of smooth

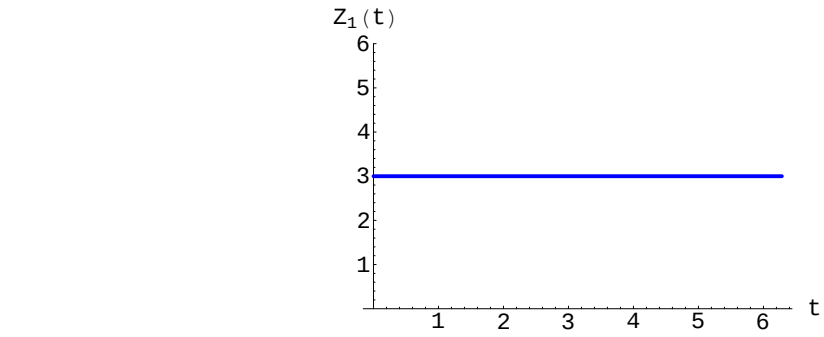

(a) Z_1.

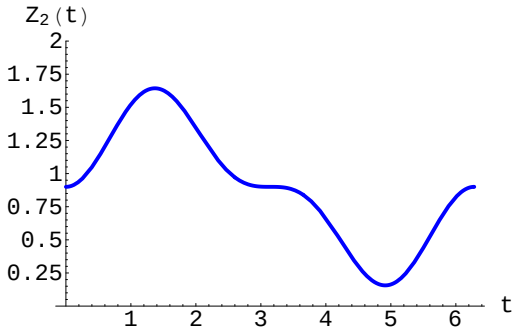

(b) Z_2.

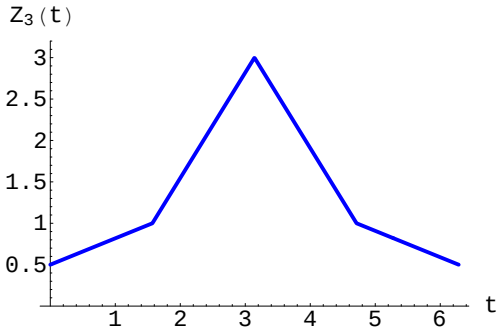

(c) Z_3.

Figure 4.8: Considered Robin coefficients.

basis functions. This problem can be overcome by enriching the approximation space with appropriate particular solutions (adapted to the "corners"). This is beyond the scope of this work.

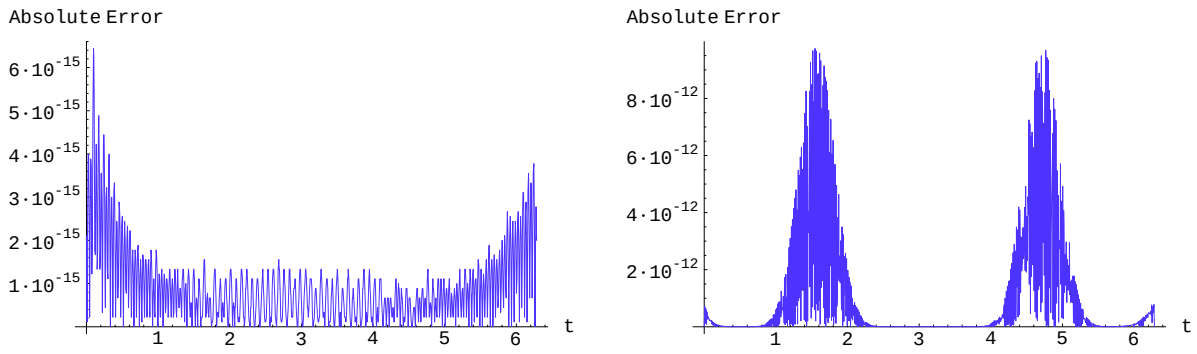

(a) Absolute error on Γ. (b) Absolute error on γ.

Figure 4.9: Error on the boundary - Example 1 (direct problem).

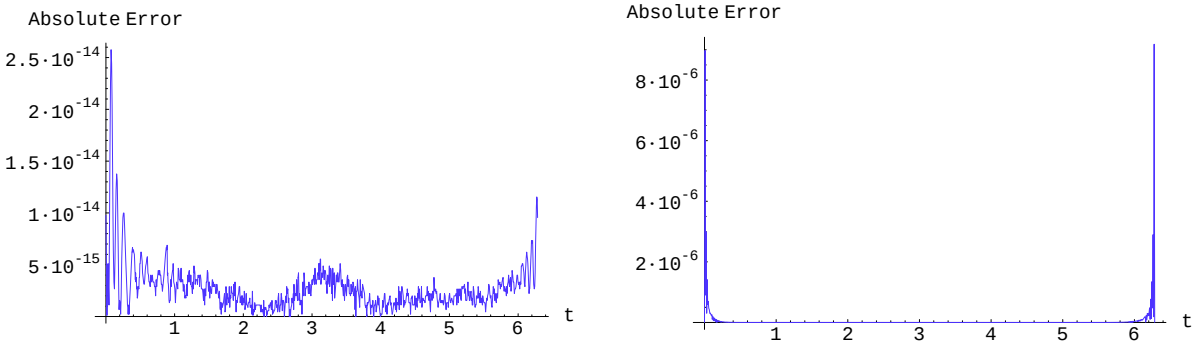

(a) Absolute error on Γ. (b) Absolute error on γ.

Figure 4.10: Error on the boundary - Example 2 (direct problem).

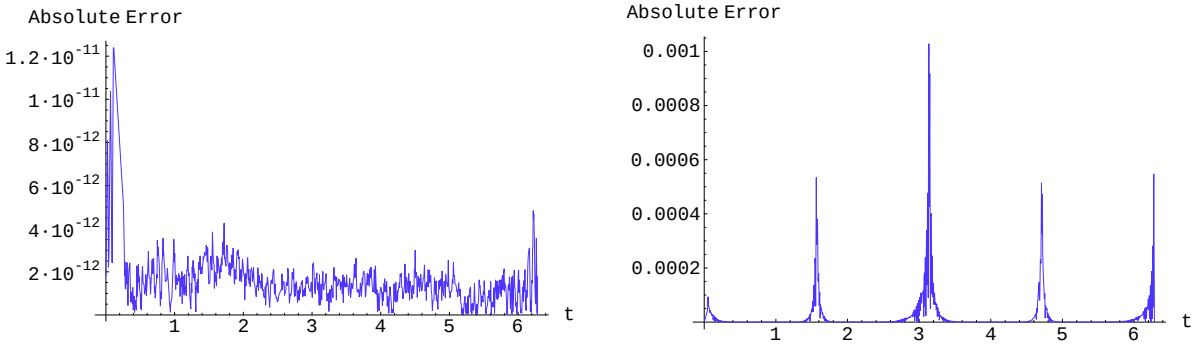

(a) Absolute error on Γ. (b) Absolute error on γ.

Figure 4.11: Error on the boundary - Example 3 (direct problem).

4.2 A MFS based decomposition method for the inverse geometric problem

We now consider the problem of retrieving the shape of the inclusion from the Cauchy data $(g, g_{\mathbf{n}})$ on Γ. Two difficulties are expected to occur:

1. Ill posedness and

2. non linearity of the inverse problem.

The decomposition methods for these inverse problems consists in addressing the aforementioned difficulties separately:

- First (Ill posedness): Computation of a solution of Laplace's equation (in an appropriate domain) that fits the given Cauchy data.

- Second (Non linearity): Reconstruction of γ using the solution computed in step one.

For the first step we apply the MFS. This can be seen as an adaptation of the Kirsch Kress Method (cf. [60]). On the original formulation of the KKM (in the context of acoustic scattering) the boundary layer was defined on an artificial boundary inside the obstacle and the density was computed by fitting the available far field pattern data. However, for interior problems, we have two types of data to fit: Dirichlet and Neumann boundary data. This motivates the MFS adaptation of the KKM that consists in using the single boundary layer representation on two artificial curves instead. An external, $\widehat{\Gamma} \subset \overline{\Omega}^C$, and an internal, $\widehat{\gamma} \subset \omega$. The theoretical results for this MFS approximation are presented in the first paragraph. The numerical implementation is described in the second paragraph and in the third, we present some numerical simulations.

4.2.1 The MFS for the inverse (Cauchy) problem

Consider the single layer potential

$$u = L_{\widehat{\Gamma}}(\phi) + L_{\widehat{\gamma}}(\psi)$$

where $\widehat{\Gamma}$, $\widehat{\gamma}$ are two artificial boundaries defined as in the beginning of section 4.1. On the boundary Γ we have to fit the Cauchy data $(g, g_{\mathbf{n}})$, which we will assume to be in $H^{1/2}(\Gamma) \times H^{-1/2}(\Gamma)$. Thus, using the previous integral representation, we obtain the

integral equations,

$$S_{\Gamma,\widehat{\Gamma}}(\phi) + S_{\Gamma,\widehat{\gamma}}(\psi) = g \quad \wedge \quad N_{\Gamma,\widehat{\Gamma}}(\phi) + N_{\Gamma,\widehat{\gamma}}(\psi) = g_{\mathbf{n}}.$$

In other words, defining the boundary operator $\mathcal{K}(\Gamma,\Gamma) : H^{-1/2}(\widehat{\Gamma}) \times H^{-1/2}(\widehat{\gamma}) \longrightarrow H^{1/2}(\Gamma) \times H^{-1/2}(\Gamma)$ by

$$\mathcal{K}(\Gamma,\Gamma)(\phi,\psi) := \begin{bmatrix} S_{\Gamma,\widehat{\Gamma}} & S_{\Gamma,\widehat{\gamma}} \\ N_{\Gamma,\widehat{\Gamma}} & N_{\Gamma,\widehat{\gamma}} \end{bmatrix} \begin{bmatrix} \phi \\ \psi \end{bmatrix} \tag{4.17}$$

we obtain the equations

$$\mathcal{K}(\Gamma,\Gamma)(\phi,\psi) = \mathcal{D}^{\mathbf{n}}(\Gamma,\Gamma) \tag{4.18}$$

where

$$\mathcal{D}^{\mathbf{n}}(\Gamma,\Gamma) := \begin{bmatrix} g \\ g_{\mathbf{n}} \end{bmatrix}.$$

Remark 4.7 Like in the MFS system for the direct problems (4.6), this system may not be solvable, even for compatible Cauchy data $(g, g_{\mathbf{n}})$. However, if both (4.6) and (4.18) are solvable then, considering the same artificial boundaries on both cases, the same densities will satisfy these systems and the first line of $\mathcal{M}(\Gamma,\gamma)$ is equal to the first line of $\mathcal{K}(\Gamma,\Gamma)$. In the limit situation $\gamma = \Gamma$, if $\mathcal{B} = \tau_\Gamma^{\mathbf{n}}$ then $\mathcal{M}(\Gamma,\Gamma) = \mathcal{K}(\Gamma,\Gamma)$ (see Fig. 4.12).

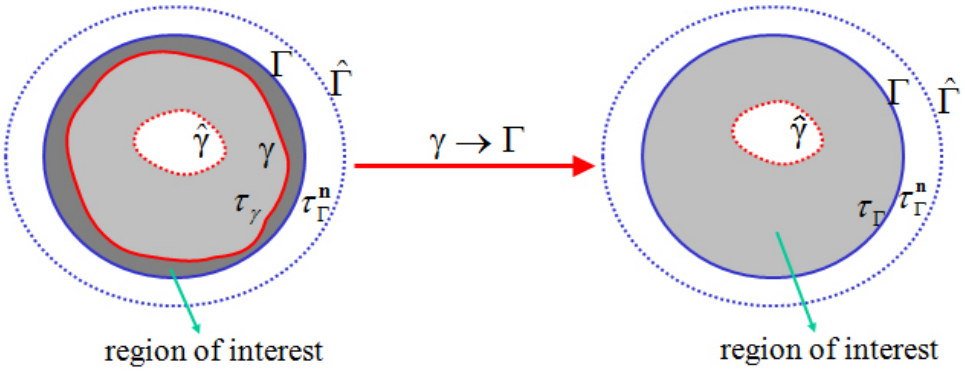

Figure 4.12: Limit situation where the operator matrix arising from the direct MFS (on the left), $\mathcal{M}(\Gamma,\gamma)$, formally tends to $\mathcal{M}(\Gamma,\Gamma)$, the matrix arising from the KKM, used as a Cauchy solver in a different region of interest (on the right).

The next injectivity and density results concerns the two dimensional situation and again we consider the identification $\mathcal{H}^r_Z(\Upsilon) \cong H^r(\Upsilon)/\mathbb{R}$ when $\int_\Upsilon Z(x)d\varsigma_x \neq 0$.

Theorem 4.8 *Let $\Sigma \subset \Gamma$ be an open set in (the topology of) Γ. The restriction of the operator $\mathcal{K}(\Sigma,\Sigma)$ to $H^{-1/2}(\widehat{\Gamma})/\mathbb{R} \times H^{-1/2}(\widehat{\gamma})/\mathbb{R}$ is injective.*

Proof. We follow the proof of Theorem 4.2. Consider two potentials $(\phi,\psi)\in \mathcal{H}_1^{-1/2}(\widehat{\Gamma})\times \mathcal{H}_1^{-1/2}(\widehat{\gamma})$ such that $\mathcal{K}(\Sigma,\Sigma)(\phi,\psi)=\mathbf{0}$. For such potentials, denote by u the harmonic function in $\mathbb{R}^2\setminus(\widehat{\Gamma}\cup\widehat{\gamma})$ represented in terms of the single boundary layer on $\widehat{\Gamma}\cup\widehat{\gamma}$, ie.,

$$u=L_{\widehat{\Gamma}}(\phi)+L_{\widehat{\gamma}}(\psi).$$

Since by hypothesis $(\phi,\psi)\in\ker\mathcal{K}(\Sigma,\Sigma)$ then,

$$\left\{\begin{array}{ll}\Delta u=0 & \text{in } \mathbb{R}^2\setminus(\widehat{\Gamma}\cup\widehat{\gamma})\\ u=0 & \text{on } \Sigma\\ \partial_{\mathbf{n}}u=0 & \text{on } \Sigma\end{array}\right. .$$

Using Holmgren's lemma and analytic continuation, we conclude that $u=0$ in the open connected set $\widehat{\Omega}_c$. Thus, the traces $u^-|_{\widehat{\Gamma}}$, $u^-|_{\widehat{\gamma}}$ and normal traces $\partial_{\mathbf{n}}u^-|_{\widehat{\Gamma}}$,$\partial_{\mathbf{n}}u^-|_{\widehat{\gamma}}$ are null. On the other hand, the boundary jumps across $\widehat{\Gamma}$ and $\widehat{\gamma}$ are given by

$$[u]_{\widehat{\Gamma}}=[u]_{\widehat{\gamma}}=0,\ [\partial_{\mathbf{n}}u]_{\widehat{\Gamma}}=\phi\ \text{ and }\ [\partial_{\mathbf{n}}u]_{\widehat{\gamma}}=\psi$$

and therefore, $u^+|_{\widehat{\Gamma}}$ and $u^+|_{\widehat{\gamma}}$ are null. In particular, for $c=-\frac{1}{2\pi}(\int_{\widehat{\Gamma}}\phi d\varsigma_x+\int_{\widehat{\gamma}}\psi d\varsigma_x)=0$ and $g=0$, u^+ solves the well posed exterior problem (4.4) hence $u^+=0$ in $\widehat{\Omega}^{\mathrm{C}}$. We have also $u^+=0$ in $\widehat{\omega}$, because of the continuity of the jump on $\widehat{\gamma}$. Therefore,

$$\partial_{\mathbf{n}}u^+|_{\widehat{\Gamma}}=\partial_{\mathbf{n}}u^+|_{\widehat{\gamma}}=0$$

and it follows that $\phi=\psi=0$. □

It is clear that the previous injectivity result is still valid for a boundary layer defined on a single artificial boundary $\widehat{\Gamma}\subset\mathbb{R}^2\setminus\overline{\Omega}$. It is only for the density result that the extra artificial boundary $\widehat{\gamma}$ is needed.

Lemma 4.9 *The adjoint of* $\mathcal{K}(\Gamma,\Gamma)$ *is given by*

$$\mathcal{K}(\Gamma,\Gamma)^*=\left[\begin{array}{cc}S_{\hat{\Gamma},\Gamma} & K_{\hat{\Gamma},\Gamma}\\ S_{\hat{\gamma},\Gamma} & K_{\hat{\gamma},\Gamma}\end{array}\right].$$

Proof. The adjoint can be computed following the proof of Lemma 4.3. □

Theorem 4.10 *The matrix operator* $\mathcal{K}(\Gamma,\Gamma)$ *has dense range in* $H^{1/2}(\Gamma)/\mathbb{R}\times H^{-1/2}(\Gamma)$.

Proof. Again, we follow the proof of Theorem 4.2. Let $\phi\in\mathcal{H}_1^{-1/2}(\Gamma)$, $\psi\in H^{1/2}(\Gamma)$ be

densities such that $\mathcal{K}(\Gamma,\Gamma)^*(\phi,\psi)= \mathbf{0}$. Define the function

$$u = L_\Gamma(\phi) + M_\Gamma(\psi),$$

a combination of single and double layer potentials defined on Γ. Now, since $\Delta u = 0$ in $\mathbb{R}^2 \setminus \Gamma$ and $u = 0$ on $\widehat{\Gamma} \cup \widehat{\gamma}$ then by analytic continuation of the unique null solution of the interior and exterior problems ($c = -\frac{1}{2\pi}\int_\Gamma \phi(x) d\varsigma_x = 0$), we obtain $u = 0$ in $\mathbb{R}^2 \setminus \Gamma$. Then $\phi = [\partial_{\mathbf{n}} u]_\Gamma = 0$, $\psi = -[u]_\Gamma = 0$ and the result follows. □

Remark 4.11 Again, the constants can be dropped by taking a bounded $\widehat{\Omega}^{\mathrm{C}}$. For the 3D case, there is no need to add the constants and the results can be proved using the same arguments.

4.2.2 Numerical implementation

We start with the implementation of the first step (linear part) of the decomposition method. Consider the discretization of the single layer given by

$$\widetilde{u} = \sum_{j=1}^{m} \alpha_j \Phi_{y_j}, \quad \alpha_1, \ldots, \alpha_m \in \mathbb{R},\ y_j \in \widehat{\Gamma} \cup \widehat{\gamma}$$

and $\widetilde{\mathcal{K}}(\Gamma,\Gamma) : \mathbb{R}^m \longrightarrow L^2(\Gamma) \times L^2(\Gamma)$ defined by

$$\widetilde{\mathcal{K}}(\Gamma,\Gamma) := \begin{bmatrix} \Phi_{y_1}|_\Gamma & \cdots & \Phi_{y_m}|_\Gamma \\ \partial_{\mathbf{n}}\Phi_{y_1}|_\Gamma & \cdots & \partial_{\mathbf{n}}\Phi_{y_m}|_\Gamma \end{bmatrix}.$$

Lemma 4.12 *Given an open set $\Sigma \subset \Gamma$ in the topology of Γ, the restriction $\widetilde{\mathcal{K}}(\Sigma,\Sigma)$ is an injective operator.*

Proof. We show that if $\mathbf{X} = (\alpha_1, \ldots, \alpha_m) \in \ker \widetilde{\mathcal{K}}(\Sigma,\Sigma)$ then $\mathbf{X} = \mathbf{0}$. Let $\widetilde{u}$ be the harmonic function in $\mathbb{R}^d \setminus \{y_1, \ldots, y_m\}$ defined above. Since

$$\widetilde{\mathcal{K}}(\Sigma,\Sigma)(\alpha_1, \ldots, \alpha_m) = (\widetilde{u}|_\Sigma, \partial_{\mathbf{n}}\widetilde{u}|_\Sigma)$$

then $\mathbf{X} \in \ker \widetilde{\mathcal{K}}(\Sigma,\Sigma)$ means that the Cauchy data $(\widetilde{u}|_\Sigma, \partial_{\mathbf{n}}\widetilde{u}|_\Sigma)$ is null. Applying Holmgren's lemma and uniqueness of the analytic continuation we obtain

$$\widetilde{u} \equiv 0 \text{ in } \mathbb{R}^d \setminus \{y_1, \ldots, y_m\}.$$

The conclusion now follows from the fact that $\{\Phi_{y_1}, \ldots, \Phi_{y_m}\}$ is a linearly independent set in $\mathbb{R}^d \setminus \{y_1, \ldots, y_m\}$. □

For the choice of $\widehat{\gamma} \subset \omega$ we must consider some *a priori* information regarding the location and dimension of ω. We consider

$$\widehat{\gamma} = \partial B(\widetilde{c}, r)$$

and use the following method to obtain $\widetilde{c}$, an approximation of the inclusion's centroid.

Approximation of the centroid

Let $f \neq 0$ be a nonnegative and integrable function defined in ω. The barycenter (centroid, when f is constant) of ω, $c = (c_1, c_2)$, is given by

$$c_i = \frac{\int_\omega x_i f dx}{\int_\omega f dx}.$$

Using Green's formula, we can compute the coordinates of the centroid by

$$c_i = \frac{\int_\gamma (\mathbf{n}_i v_i(x) - x_i \partial_{\mathbf{n}} v_i(x)) d\varsigma_x}{\int_\gamma \partial_{\mathbf{n}} v_i d\varsigma}$$

where $v_i(x_1, x_2) = x_{3-i}^2/2$ and $\mathbf{n}_i$ is the i-th component of the normal to γ.
Considering the reciprocity functional

$$\mathcal{R}(v) = \int_\Gamma (g_{\mathbf{n}} v - g \partial_{\mathbf{n}} v) d\varsigma$$

we have

$$\mathcal{R}(v) = -\int_{\Omega_c} u \Delta v dx - \int_\gamma \partial_{\mathbf{n}} u v d\varsigma$$

where we used $\Delta u = 0$ in Ω_c and $u = 0$ on γ. In particular, considering an harmonic test function v, we have

$$\mathcal{R}(v) = -\int_\gamma \partial_{\mathbf{n}} u v d\varsigma$$

and we compute an approximation $\widetilde{c} = (\widetilde{c}_1, \widetilde{c}_2)$ of the centroid by

$$\widetilde{c}_i := \frac{\mathcal{R}(x_i)}{\mathcal{R}(1)}. \tag{4.19}$$

In discrete terms, $\widetilde{c}$ is a weighted sum of points in $\overline{\omega}$. Considering a positive $C^0(\Gamma)$ input function g, by Hopf's lemma

$$\partial_{\mathbf{n}} u|_\gamma < 0.$$

Thus, we have a convex linear combination of points in $\overline{\omega}$. Therefore, the sum is an element in the convex hull of $\overline{\omega}$.

Remark 4.13 In general, we can not obtain $\widetilde{c}$ and $r > 0$ from the boundary data, such that $\partial B(\widetilde{c}, r) \subset \omega$. For some particular cases, the formula (4.19) provides a point $\widetilde{c}$ inside ω. However, the radius r must be provided.

For the numerical implementation of (4.18) we consider the discretized version of $\widetilde{\mathcal{K}}(\Gamma, \Gamma)$ and $\mathcal{D}^{\mathbf{n}}(\Gamma, \Gamma)$ given by

$$\mathbb{K}(\Gamma,\Gamma) = \begin{bmatrix} \Phi_{y_1}(x_1) & \cdots & \Phi_{y_m}(x_1) \\ \cdots & \cdots & \cdots \\ \Phi_{y_1}(x_n) & \cdots & \Phi_{y_m}(x_n) \\ \partial_{\mathbf{n}}\Phi_{y_1}(x_1) & \cdots & \partial_{\mathbf{n}}\Phi_{y_m}(x_1) \\ \cdots & \cdots & \cdots \\ \partial_{\mathbf{n}}\Phi_{y_1}(x_n) & \cdots & \partial_{\mathbf{n}}\Phi_{y_m}(x_n) \end{bmatrix} \text{ and } \mathbb{D}^{\mathbf{n}}(\Gamma,\Gamma) = \begin{bmatrix} g(x_1) \\ \vdots \\ g(x_n) \\ g_{\mathbf{n}}(x_1) \\ \vdots \\ g_{\mathbf{n}}(x_n) \end{bmatrix}$$

on some collocation $x_1, \ldots, x_n \in \Gamma$ and source points $y_1, \ldots, y_m \in \widehat{\Gamma} \cup \widehat{\gamma}$. Since measurement errors are expected to occur, we apply the Tikhonov regularization scheme and solve

$$(\mu \mathbb{I} + \mathbb{K}(\Gamma,\Gamma)^* \mathbb{K}(\Gamma,\Gamma))\, \mathbf{X}_\mu = \mathbb{K}(\Gamma,\Gamma)^* \mathbb{D}^{\mathbf{n}}(\Gamma,\Gamma) \tag{4.20}$$

where $\mu > 0$ is the regularization parameter.

Using the approximation $\widetilde{u}$ provided by the first step we can now compute the shape of the inclusion as the level curve

$$\widetilde{u}^{-1}(0) = \{x \in \Omega \setminus \overline{\widetilde{\omega}} : \widetilde{u}(x) = 0\}.$$

We note that, since the input function g is positive then, by the maximum principle, the (classical) solution u of $(\mathcal{P}_D)$ is strictly positive in $\Omega_c \cup \Gamma$ and therefore $\gamma = u^{-1}(0)$. In this framework, the numerical method for locating γ consists in searching for the zeros of $\widetilde{u}$ on a domain containing γ. The considered domain is bounded by Γ and the inner artificial curve $\widehat{\gamma}$. The search is performed along segments joining Γ to $\widehat{\gamma}$ (see Fig. 4.15, left plot).

Measured data and noise

Denote by

$$\mathfrak{m} = [\partial_{\mathbf{n}} u(x_i)]_i$$

the vector of measurements on the observation points $x_i \in \Gamma$ generated (artificially) from the numerical solution of the direct problem using the MFS. In order to simulate measurement errors, it is common to consider pointwise relative noise, using

$$\mathfrak{m}_\varepsilon^P := \mathfrak{m} + [\varepsilon_i \mathfrak{m}_i]_i$$

with random values ε_i such that,

$$\max |\varepsilon_i| \leq \varepsilon. \tag{4.21}$$

In this situation, 100ε is the percentage level of relative pointwise noise. This pointwise noise is a sort of noise simplification since it means that the noise follows the solution, and almost no noise will be considered at the locations for which $\mathfrak{m}_i$ is small. To better simulate noise, we also need to consider some amount of absolute noise, using the notion of norm noise. Instead of $\mathfrak{m}^P$ we will consider

$$\mathfrak{m}_\varepsilon^\infty := \mathfrak{m} + ||\mathfrak{m}||_\infty [\varepsilon_i]_i$$

where the random values ε_i satisfy (4.21).

Thus, even at the points where $\mathfrak{m}_i$ is small we can have perturbations as high as in the largest values of $\mathfrak{m}$ (see Figs. 4.13 and 4.14). For both cases, 100ε will be called *noise level* or more simply *pointwise* or *norm noise*. When $\varepsilon = 0$, we obtain $\mathfrak{m}$ which will be called the vector of noise free data.

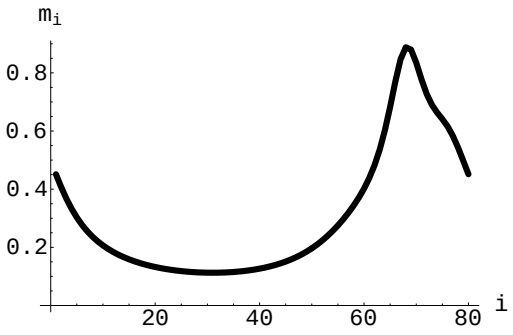

Figure 4.13: Example of noise free data.

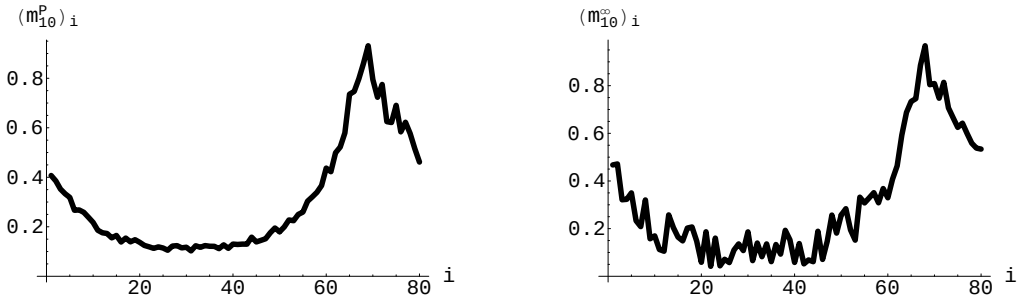

(a) 10 % of pointwise noise.

(b) 10 % of norm $||\cdot||_\infty$ noise.

Figure 4.14: Example of the above data with noise.

4.2.3 Numerical simulations

To test the proposed algorithm we consider the four domains defined at the beginning of section 4.1.2 and the data vector $\mathfrak{m}_\varepsilon^\infty$ at 60 equally distributed points on Γ, for several levels of noise ε. We start with two comparative examples where is it clear when we have an inclusion or a cavity. In these examples the geometry of the domain corresponds to the first (ellipsis) and third (bean) examples. Since the considered input function $g \equiv 1$ is positive then, from Theorem 3.8 we have a cavity if and only if the generated Neumann data $g_{\mathbf{n}}$ satisfies $\int_\Gamma g_{\mathbf{n}} d\varsigma = 0$. This is clear in Table 4.2 where the previous integral is numerically computed using the trapezoidal rule with 60 points for Neumann data affected by several levels of noise.

To apply the MFS approximation to fit the Cauchy data, we considered the external artificial curve $\widehat{\Gamma} = \partial B(0, 5.5)$ and the internal $\widehat{\gamma} = \partial(\widetilde{c}, r)$, where $\widetilde{c}$ is computed by (4.19) using the trapezoidal rule (with 60 points). The radius was $r = 0.3$. The MFS approximation, $\widetilde{u}$, was obtained by solving the system (4.20) at 120 equally distributed source points on $\widehat{\Gamma} \cup \widehat{\gamma}$, 60 collocation points on Γ and choosing the regularization parameter μ accordingly to the L–curve criterion.

To retrieve the shape of the inclusion we considered, for $t \in [0, 2\pi]$, the restriction of $\widetilde{u}$ to the segment defined by the points $\Gamma(t)$ and $\widehat{\gamma}(t)$, that is, the function

$$v_t(\lambda) := \widetilde{u}((1-\lambda)\Gamma(t) + \lambda\widehat{\gamma}(t)),\ \lambda \in]0, 1[.$$

On the nodes $\lambda_i = 0.01i$ we search for $(1-\lambda_{i^*})\Gamma(t) + \lambda_{i^*}\widehat{\gamma}(t)$ such that $v_t(\lambda_{i^*})$ is the small positive value. The curve is reconstructed by repeating this process for several values of t.

	Exact data	5% norm noise	10% norm noise
Ex. 1 (inclusion)	24.8	24.8	24.2
Ex. 1 (cavity)	7.9×10^{-11}	-3.3×10^{-2}	3.6×10^{-1}
Ex. 3 (inclusion)	8.6	8.6	8.6
Ex. 3 (cavity)	8.8×10^{-9}	4.5×10^{-3}	-8.9×10^{-2}

Table 4.2: Distinguishing an inclusion from a cavity by the value of $\int_\Gamma g_{\mathbf{n}} d\varsigma$.

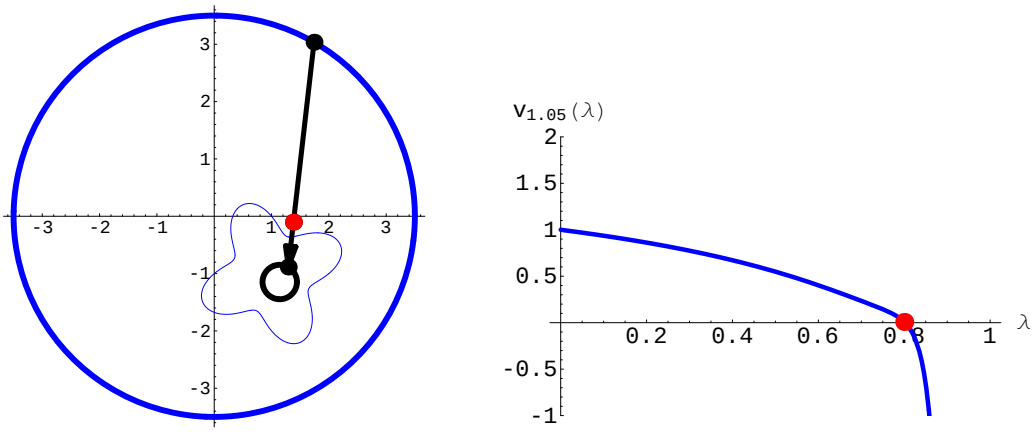

Figure 4.15: Left– segment defined by two points on Γ and $\widehat{\gamma}_2$ (black dots). Right– solution of the inverse problem along the line of the left plot. The red dot is the computed approximation.

On the following plots we present the numerical reconstructions for the aforementioned domains. The red dots represents the computed approximation and the full blue line the curve to reconstruct. The black dot is the computed centroid $\widetilde{c}_i$ and the black dashed line the internal artificial curve. First, we plot the results obtained for noise free data (Figs. 4.16 and 4.17). On the right plot of Fig. 4.16 we can see some difficulties to reconstruct the non convex part of ω_2.

Regarding data with noise, we present, for the first example, a comparison between the reconstruction obtained for data with pointwise and norm random noise. The considered Tikhonov regularization parameter was $\mu = 5 \times 10^{-6}$ and $\mu = 5 \times 10^{-5}$ for data with pointwise and norm noise, respectively (see Fig. 4.18).

The fitting of the Cauchy data by the MFS was, slightly better for the pointwise case. This can be seen in Figs. 4.19 and 4.20 where we plotted the absolute error for the Dirichlet and Neumann data (with 5 % of noise) fitting. We obtained stable results, for data with 5 % (Fig. 4.21) and 10 % (Fig. 4.22) of noise, for both shape and location (centroid). The quality of the reconstructions is identical in both cases.

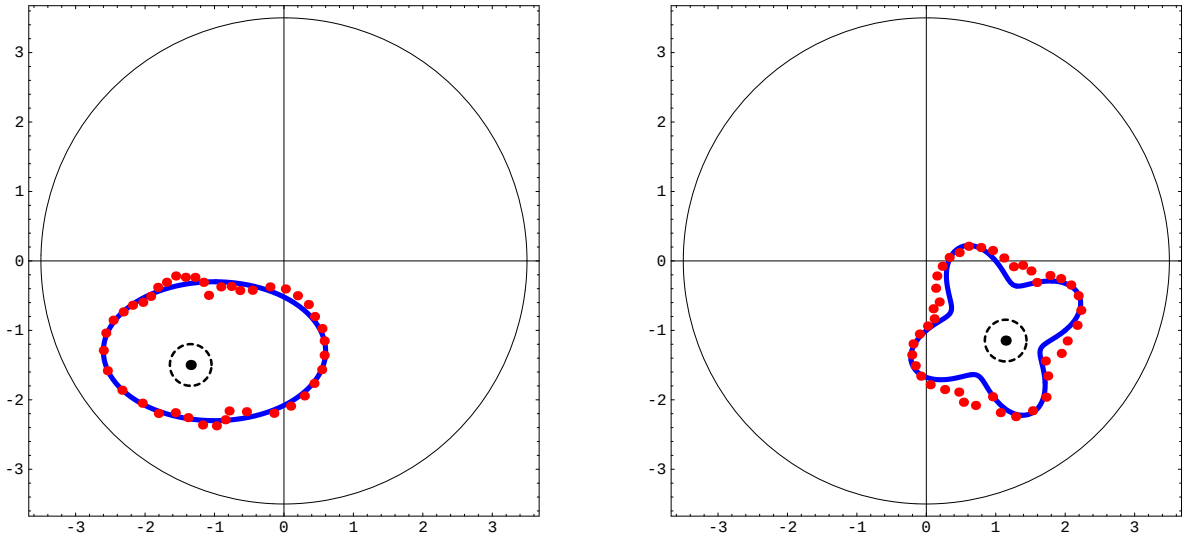

(a) Example 1. (b) Example 2.

Figure 4.16: Reconstruction of the shape considering noise free data.

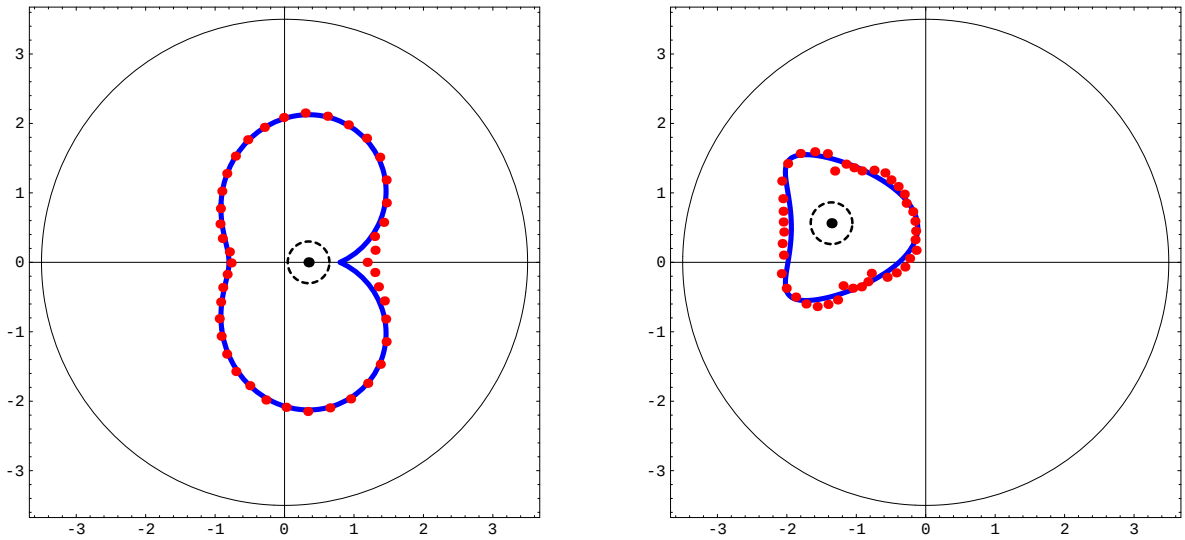

(a) Example 3. (b) Example 4.

Figure 4.17: Reconstruction of the shape considering noise free data.

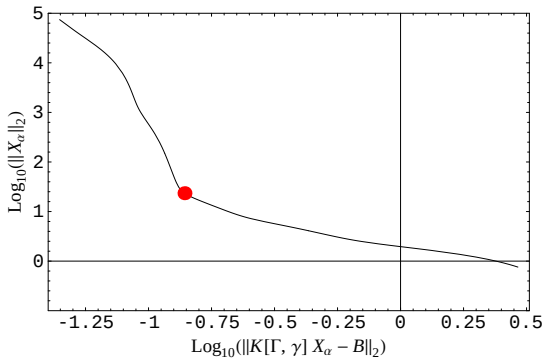

(a) Data with 5 % of pointwise noise.

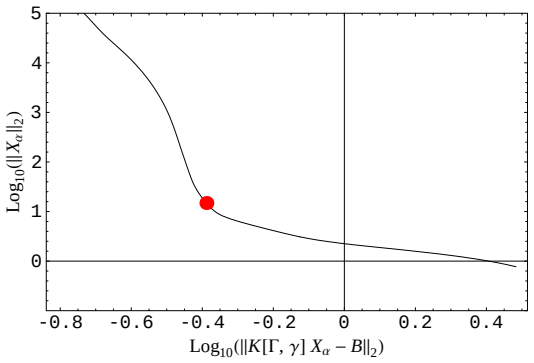

(b) Data with 5 % of norm noise.

Figure 4.18: L–curve for the first example. The red dot corresponds to the selected value for regularization parameter.

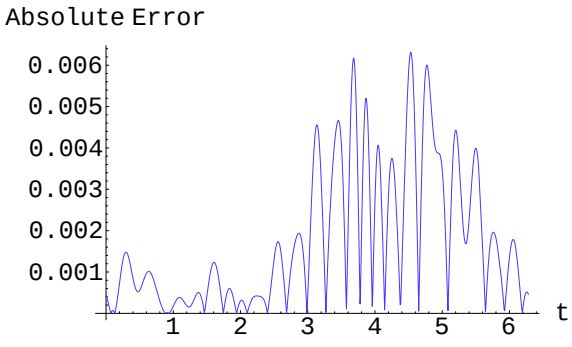

(a) Data with 5 % of pointwise noise.

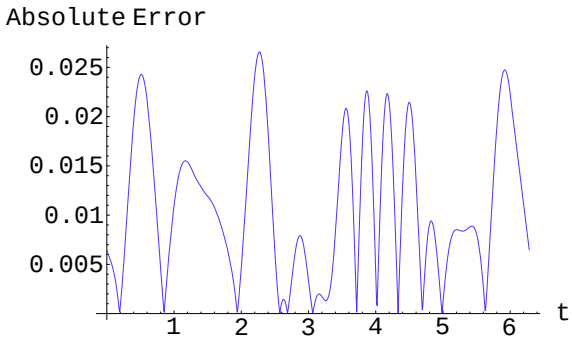

(b) Data with 5 % of norm noise.

Figure 4.19: Dirichlet data fitting with the MFS.

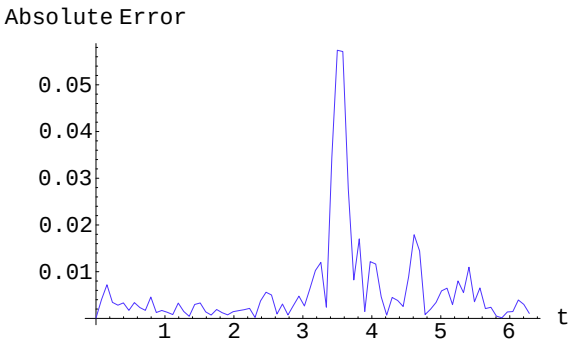

(a) Data with 5 % of pointwise noise.

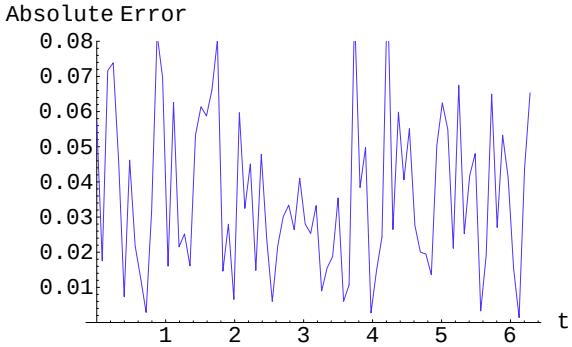

(b) Data with 5 % of norm noise.

Figure 4.20: Neumann data fitting with the MFS.

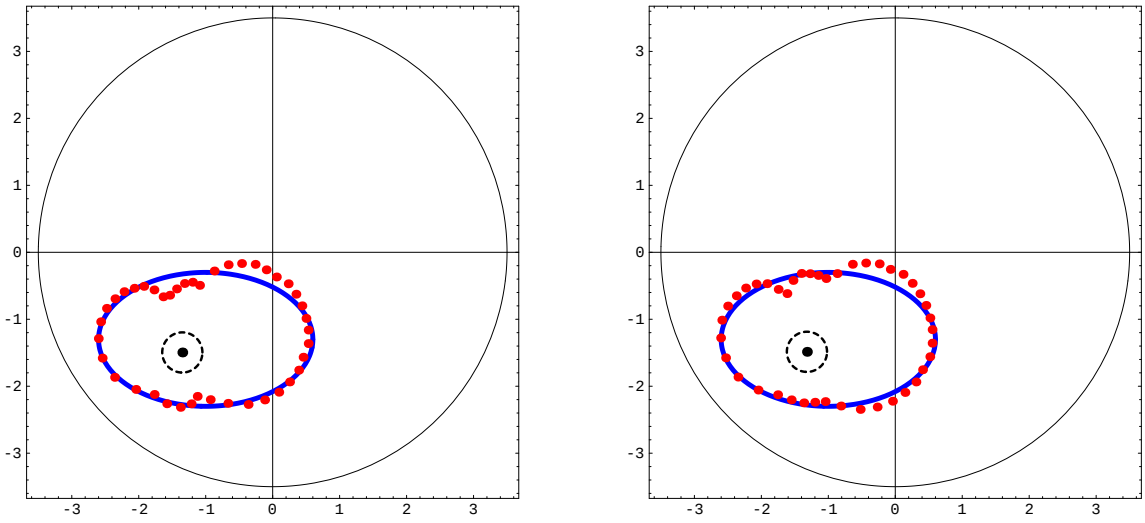

(a) Data with 5 % of pointwise noise.

(b) Data with 5 % of norm noise.

Figure 4.21: Reconstruction of the ellipsis from noisy data.

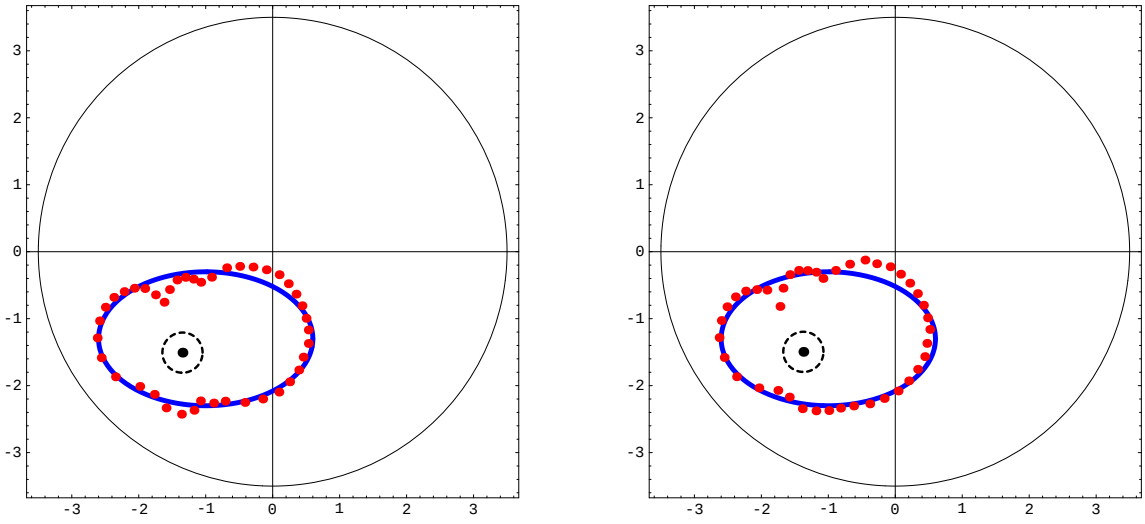

(a) Data with 10 % of pointwise noise.

(b) Data with 10 % of norm noise.

Figure 4.22: Reconstruction of the ellipsis from noisy data.

For the other examples we obtained the results showed in Figs. 4.23 (left), 4.24, 4.25 and 4.26 for 5 % and 10 % of norm noise. For the second example the reconstruction is worst. In this case the approximation of the centroid was $\widetilde{c}_2 = (1.15, -1.15)$ and the reconstruction is not very sensitive to the location and dimension of the internal circle (see Fig. 4.23, right plot for a simulation with a different internal circle). The third example shows that the results are more stable when the inclusion is centered with the accessible part of the boundary Γ.

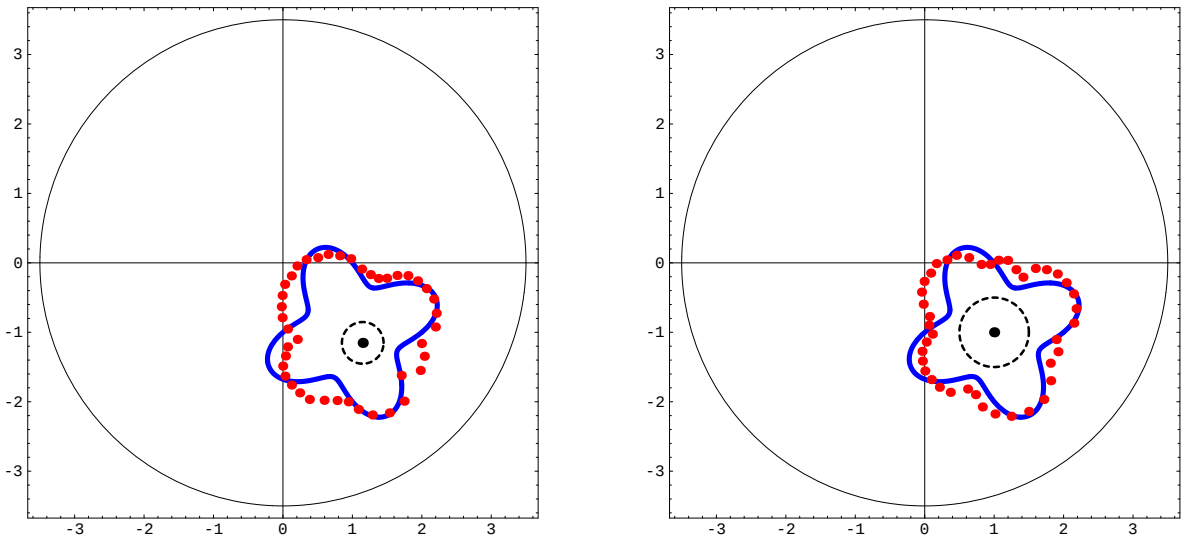

Figure 4.23: Comparison between the reconstruction of γ_2 using the proposed internal curve (left) and $\widehat{\gamma}_2 = \partial B(c_2, 0.5)$ (right). Noise level: 5%.

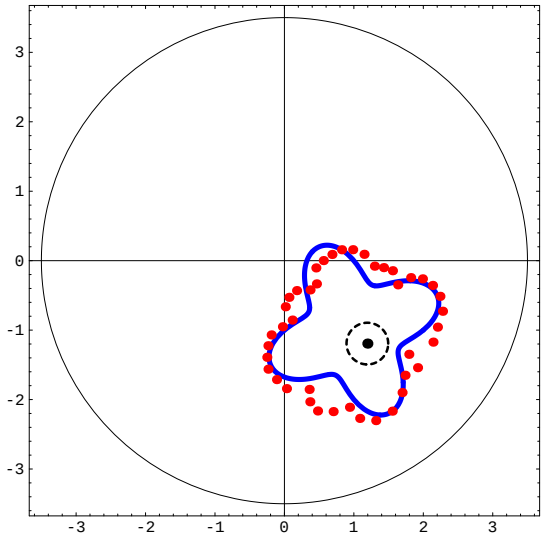

Figure 4.24: Reconstruction of γ_2 from noisy data (Noise level: 10 %).

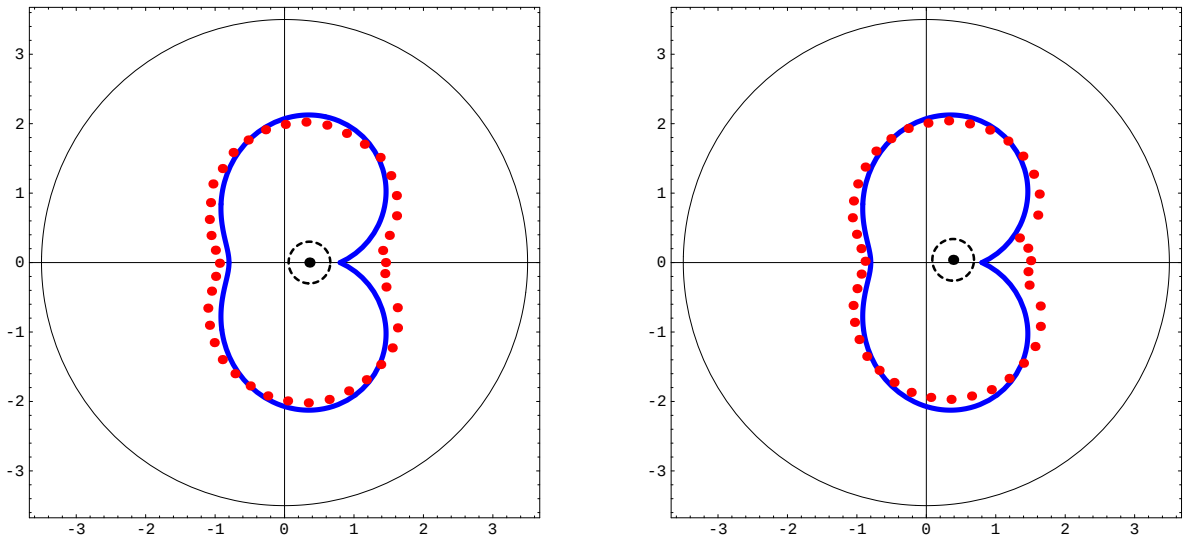

(a) Data with 5 % of noise.

(b) Data with 10 % of noise.

Figure 4.25: Reconstruction of γ_3 from noisy data.

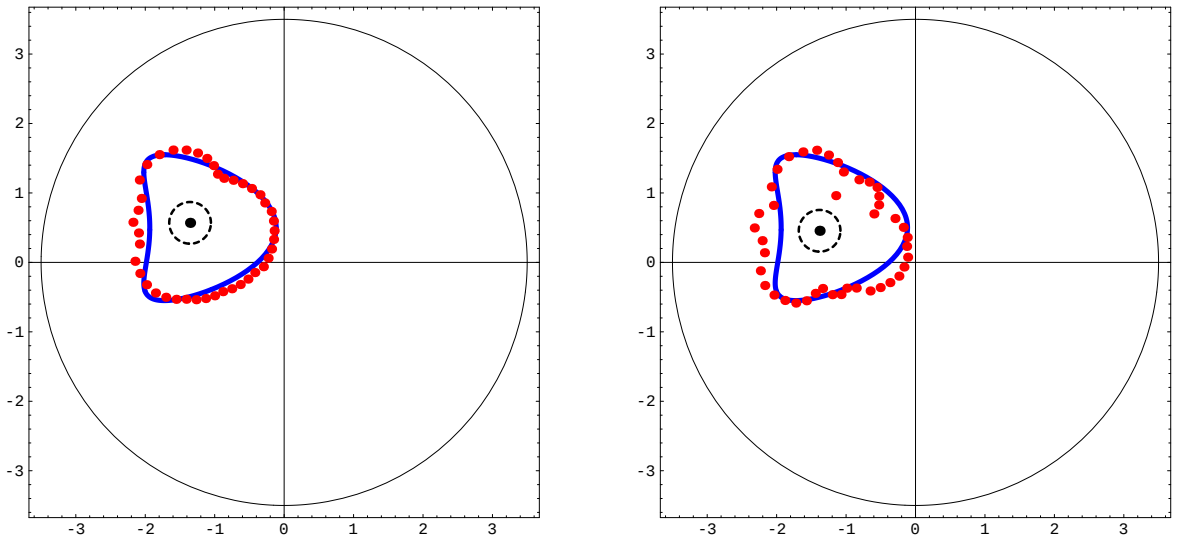

(a) Data with 5 % of noise.

(b) Data with 10 % of noise.

Figure 4.26: Reconstruction of γ_4 from noisy data.

We obtained stable results, taking into account the perturbation introduced in the data. The proposed method was easy to implement and required little computational effort.

4.3 Iterative reconstruction of the inclusion by a Quasi–Newton method

In this section we describe an iterative method to reconstruct the shape of the inclusion. It is based on the optimization of both density and shape and relies on the directional derivative of the map F. The MFS will be used as numerical solver for the arising direct problems.

Consider the non linear equation:
Find the boundary γ_0 such that

$$F(\gamma_0) = g_{\mathbf{n}} \tag{4.22}$$

where $g_{\mathbf{n}} = \partial_{\mathbf{n}} u|_\Gamma$ and u is the solution of $(\mathcal{P}_D)$, for some given and fixed $g \neq 0$. Using the directional derivative of F, we obtain the following linearized equation on Ψ

$$F'(\gamma_0)\Psi = g_{\mathbf{n}} - F(\gamma_0).$$

A Newton type of method can thus be implemented by solving the previous equation (for

given γ_0) and using the update

$$\gamma_{new} = \gamma_0 + \Psi|_{\gamma_0}$$

where $\Psi|_{\gamma_0}$ is the restriction of the admissible vector field Ψ to the boundary γ_0.

However, Newton type of methods applied to ill posed problems tends to, at a first stage, produce a (rapidly) decrease on the norm of the residual but then, increases again. Our approach is to consider the inverse problem formulated instead as the non linear optimization problem

$$\text{argmin}_{\gamma^* \in \mathcal{C}} ||F(\gamma^*) - \partial_{\mathbf{n}} u||_{H^{-1/2}(\Gamma)} \tag{4.23}$$

where $\mathcal{C}$ is a class of admissible shapes containing the solution of (4.22). The uniqueness result for the inverse problem implies that the previous minimization problem has a unique solution, namely the solution of (4.22).

For simplicity, we suppose that ω is a C^2 star shaped inclusion with respect to the origin. Therefore, the boundary $\gamma = \partial\omega$ belongs to the class

$$\mathcal{C} = \left\{ r(t)(\cos t, \sin t) \in \Omega : r \in C^2([0, 2\pi], \mathbb{R}^+) \ \wedge \ r(0) = r(2\pi) \right\}.$$

Such class will be the class of admissible shapes. The class of admissible vector fields on the boundary γ will be

$$\Psi_{ad} := \{ h(t)\,(\cos t, \sin t) : h \in C^2([0, 2\pi], \mathbb{R}) \ \wedge \ h(0) = h(2\pi) \}.$$

The perturbation of the boundary $\gamma(t) = r(t)(\cos t, \sin t) \in \mathcal{C}$ in the direction of $\Psi(t) = h(t)(\cos t, \sin t) \in \Psi_{ad}$ is thus given by

$$\gamma_\varepsilon(t) = r(t)(\cos t, \sin t) + \varepsilon h(t)(\cos t, \sin t), \ t \in [0, 2\pi].$$

With this notations, the directional derivative of F at $\gamma \in \mathcal{C}$,

$$F'(\gamma) : \Psi_{ad} \longrightarrow H^{-1/2}(\Gamma)$$

is the map given by $F'(\gamma)(\Psi) = \partial_{\mathbf{n}} u'|_\Gamma$ where $u' \in H^1(\Omega_c)$ is the solution of the well posed problem

$$\begin{cases} \Delta u' = 0 & \text{in } \Omega_c \\ u' = 0 & \text{on } \Gamma \\ u' = -(\Psi \cdot \mathbf{n}) \partial_{\mathbf{n}} u & \text{on } \gamma \end{cases}.$$

We show some important properties of $F'(\gamma)$.

Lemma 4.14 *$F'(\gamma)$ is injective.*

Proof. Suppose that $F'(\gamma)\Psi = 0$, for some $\Psi \in \Psi_{ad}$. By Theorem 3.10 it is sufficient to show that

$$\forall x \in \gamma, \Psi(x) \perp \mathbf{n}_x \Rightarrow \Psi \equiv 0.$$

Considering the above parameterizations, the normal vector to γ at $t \in [0, 2\pi]$ is given by

$$\mathbf{n}_t = \frac{r'(t)(-\sin t, \cos t) - r(t)(\cos t, \sin t)}{\sqrt{r'(t)^2 + r(t)^2}}$$

and

$$0 = \Psi(t) \cdot \mathbf{n}_t = -\frac{h(t)r(t)}{\sqrt{r'(t)^2 + r(t)^2}} \Rightarrow h(t)r(t) = 0, \ \forall t \in [0, 2\pi].$$

From this we can conclude that $h \equiv 0$ (since by hypothesis $r > 0$), ie., $\Psi \equiv 0$. □

In the following, we identify $\mathcal{C}$ with

$$C^2_\Omega[0, 2\pi]^+ := \{r \in C^2([0, 2\pi], \mathbb{R}^+) : r(t)(\cos t, \sin t) \in \Omega \wedge r(0) = r(2\pi)\}$$

and Ψ_{ad} with

$$C^2_p[0, 2\pi] := \{h \in C^2([0, 2\pi], \mathbb{R}) : h(0) = h(2\pi)\}.$$

The bounded operator $F'(\gamma)$ can be continuously extended to the closure of $C^2_p[0, 2\pi]$ in $L^2([0, 2\pi])$, hence to the whole $L^2([0, 2\pi])$. This extension will still be denoted by $F'(\gamma)$. Since the injection ${}^t i : H^{-1/2}(\Gamma) \longrightarrow H^{-3/2}(\Gamma)$ is continuous, the linear operator

$${}^t iF'(\gamma) = F'(\gamma) : L^2([0, 2\pi]) \longrightarrow H^{-3/2}(\Gamma)$$

is bounded.

Lemma 4.15 *The adjoint of $F'(\gamma)$, $F'(\gamma)^* : H^{3/2}(\Gamma) \longrightarrow L^2([0, 2\pi])$ is given by*

$$(F'(\gamma)^* g_*)(t) = r(t)\partial_{\mathbf{n}_t} u(r(t))\partial_{\mathbf{n}_t} u^*(r(t))$$

where $u^* \in H^2(\Omega_c)$ is the solution of the well posed problem $(\mathcal{P}_D)$ with input function $g_* \in H^{3/2}(\Gamma)$.

Proof. Let $u^* \in H^2(\Omega_c)$ be the solution of the aforementioned problem. We have

$$\begin{aligned}\langle g_*, F'(\gamma)h\rangle_{H^{3/2}(\Gamma)\times H^{-3/2}(\Gamma)} &= \int_\Gamma g_* \partial_{\mathbf{n}} u' d\varsigma \\ &= \int_\Gamma u' \partial_{\mathbf{n}} u^* d\varsigma - \langle u^*, \partial_{\mathbf{n}} u'\rangle_{H^{3/2}(\gamma)\times H^{-3/2}(\gamma)} + \int_\gamma \partial_{\mathbf{n}} u^* u' d\varsigma.\end{aligned}$$

Using the boundary conditions for u' and u^* we get

$$\langle g_*, F'(\gamma)h\rangle_{H^{3/2}(\Gamma)\times H^{-3/2}(\Gamma)} = \int_0^{2\pi} h(t)r(t)\partial_{\mathbf{n}_t}u^*(r(t))\partial_{\mathbf{n}_t}u(r(t))dt.$$

□

Corollary 4.16 *If exists a relatively open set $\sigma \subset \gamma$ where the normal trace $\partial_{\mathbf{n}}u$ does not vanish then, $F'(\gamma)$ has dense range in $H^{-3/2}(\Gamma)$.*

Proof. We show that the adjoint $F'(\gamma)^*$ is injective. Let $g_* \in H^{3/2}(\Gamma)$ be such that $F'(\gamma)^*g_* = 0$. Since $r > 0$ then, by the previous Lemma,

$$\partial_{\mathbf{n}}u\partial_{\mathbf{n}}u^* = 0 \text{ on } \gamma. \tag{4.24}$$

Thus, we must have $\partial_{\mathbf{n}}u^* = 0$ on σ and by Holmgren (notice that we also have $u^* = 0$ in γ), $u^* = 0$ in Ω_c. In particular,

$$0 = u^*|_\Gamma = g_*.$$

□

Remark 4.17 The above hypothesis on the normal trace is not too restrictive. In fact, by Holmgren's theorem, the normal trace of u does not vanish on any relatively open subset of γ.

For numerical purposes, the sets of admissible shapes and vector fields are represented in terms of the (finite dimensional) space defined by the Fourier modes, ie.,

$$\mathcal{C}_N = \left\{ r_\alpha(t)(\cos t, \sin t) \in \Omega : r_\alpha > 0 \wedge r_\alpha(t) = \alpha_0 + \sum_{j=1}^{N} \alpha_j \cos(jt) + \sum_{j=1}^{N} \alpha_{j+N} \sin(jt) \right\}$$

and

$$\Psi_{ad}^N = \left\{ h_\alpha(t)(\cos t, \sin t) : h_\alpha(t) = \alpha_0 + \sum_{j=1}^{N} \alpha_j \cos(jt) + \sum_{j=1}^{N} \alpha_{j+N} \sin(jt) \right\}$$

respectively, with $\alpha := (\alpha_0, \ldots, \alpha_{2N}) \in \mathbb{R}^{2N+1}$. We now formulate the minimization problem (4.23) as a non linear least squares problem. Given a vector of (eventually noisy) data $\mathfrak{m} = [\mathfrak{m}_i]$ on the observation points $x_i \in \Gamma$, the objective function is

$$F_{obj}(\alpha) := \frac{1}{2}\sum_{j=1}^{m}(F_i(\alpha) - \mathfrak{m}_i)^2 = \frac{1}{2}(\mathbf{F}(\alpha) - \mathfrak{m})^\top(\mathbf{F}(\alpha) - \mathfrak{m})$$

where $F_i(\alpha) = F(\alpha)(x_i) = \partial_{\mathbf{n}} u_\alpha(x_i)$,

$$\begin{cases} \Delta u_\alpha = 0 & \text{in } \Omega_c^\alpha \\ u_\alpha = g & \text{on } \Gamma \\ u_\alpha = 0 & \text{on } \gamma_\alpha \end{cases}$$

and γ_α is parameterized by $r_\alpha(t)(\cos t, \sin t) \in \mathcal{C}_N$. The minimization problem is thus

$$\gamma_{\alpha^*} = \text{argmin}_{\gamma_\alpha \in \mathcal{C}_N} F_{obj}(\alpha).$$

We apply the Levenberg–Marquardt (LM) method for this minimization problem. Given an admissible curve $\gamma_\alpha \in \mathcal{C}_N$, the update step $\Psi_{\alpha_s} \in \Psi_{ad}^N$ in the LM method is given by (see appendix)

$$(\mu \mathbb{I} + \mathbb{J}^\top(\alpha)\mathbb{J}(\alpha))\alpha_s = -\mathbb{J}^\top(\alpha)(\mathbf{F}(\alpha) - \mathfrak{m}_i).$$

Lemma 4.18 *The Jacobian matrix $\mathbb{J}(\alpha)$ is given by*

$$\mathbb{J}(\alpha) = \left[\partial_{\mathbf{n}} u_j'(x_i)\right]_{ij}$$

where u_j' solves

$$\begin{cases} \Delta u_j' = 0 & \text{in } \Omega_c^\alpha \\ u_j' = 0 & \text{on } \Gamma \\ u_j' = -(\Psi_{e_j} \cdot \mathbf{n})\partial_{\mathbf{n}} u_\alpha & \text{on } \gamma_\alpha \end{cases}$$

with e_j the jth vector of the standard basis of $\mathbb{R}^{2N+1}$.

Proof. Given a parametrization $r_\alpha(t)(\cos t, \sin t)$ of $\gamma_\alpha \in \mathcal{C}_N$ consider, for sufficient small $|\varepsilon|$, the perturbation $\gamma_\varepsilon \in \mathcal{C}_N$ of γ_α, defined by

$$r_\alpha(t)(\cos t, \sin t) + \varepsilon h_{e_j}(t)(\cos t, \sin t).$$

Thus

$$[\mathbb{J}(\alpha)]_{ij} = \frac{\partial F_i}{\partial \alpha_j}(x_i) = \lim_{\varepsilon \to 0} \frac{F_i(\alpha + \varepsilon e_j) - F_i(\alpha)}{\varepsilon} = (F'(\gamma_\alpha)\Psi_{e_j})(x_i)$$

and the result follows. □

Thus, at each step of the method, we have to solve $2N + 2$ problems (one related to u_α and $2N + 1$ problems related to the Jacobian) and we use the MFS for these problems. Numerically, those $2N + 2$ problems correspond to $2N + 2$ systems of linear equations having in common the same system matrix.

Remark 4.19 Regarding the updated shape $\gamma_{\alpha_{new}} = \gamma_\alpha + \Psi_{\alpha_s}$ some care must be taken in the choice of $\mu > 0$ to assure both descent direction and that $\gamma_{\alpha_{new}}$ is admissible. The first is assured by the algorithm and the second requires the introduction of some control structures in the algorithm. The latter situation can be easily implemented but will not be taken into account since increases computational time and for the tested examples revealed to be unnecessary.

4.3.1 Numerical simulations

In order to test the minimization algorithm we consider the previous four examples. For comparison with the decomposition method, we use the same measured data and computed centroid $\widetilde{c}_i$.

Each direct problem is numerically solved with the MFS approximation. We consider $\widehat{\Gamma} = \partial B(0, 5.5)$ and internal artificial curve obtained by a reduction of the internal boundary by a factor of 0.9. The number of collocation and source points is 120.

We start the iterative process from $\gamma^{(0)} = \partial B(\widetilde{c}_i, 1)$ and the iterations are computed according to the following strategy (cf. [11]).

Algorithm 1

1. `Give an initial curve`
2. `Compute the updates in` $\mathcal{C}_{N_1}$ `with the LM method`
3. `Use the last curve from step 2 in step 1 and repeat the process in` $\mathcal{C}_{N_2}$`, with` $N_2 > N_1$`.`

This strategy avoided the convergence to some local extrema. We used the spaces $\mathcal{C}_0$ (circles) and $\mathcal{C}_4$. This choice of (low dimensional) spaces is related to a trade off between quality and stability. Higher number of Fourier modes increases the quality of the reconstruction (for data without noise) but increases also the instability on the reconstruction (worst reconstructions for noisy data).

As stopping criterion we use the empirically chosen value 10^{-2} in the relative evolution of the objective function, that is we stop at the first α_{new} such that

$$\frac{F_{obj}(\alpha_{old}) - F_{obj}(\alpha_{new})}{F_{obj}(\alpha_{old})} \leq 10^{-2}.$$

We use the full red line to represent the initial curve and the red dashed lines for the intermediate iterations. As usual, the approximation is represented by a red dotted line and the exact by a full blue line.

The first test regards data without noise. For the reconstruction of the ellipsis, we computed 8 iterations in $\mathcal{C}_4$. As we can see in Fig. 4.27 (left), we obtained a good reconstruction.

Regarding the second example, the non convex part is now fully recovered and 8 iterations were computed in $\mathcal{C}_4$ (Fig. 4.27, right). In both cases, no gain was obtained by starting in $\mathcal{C}_0$.

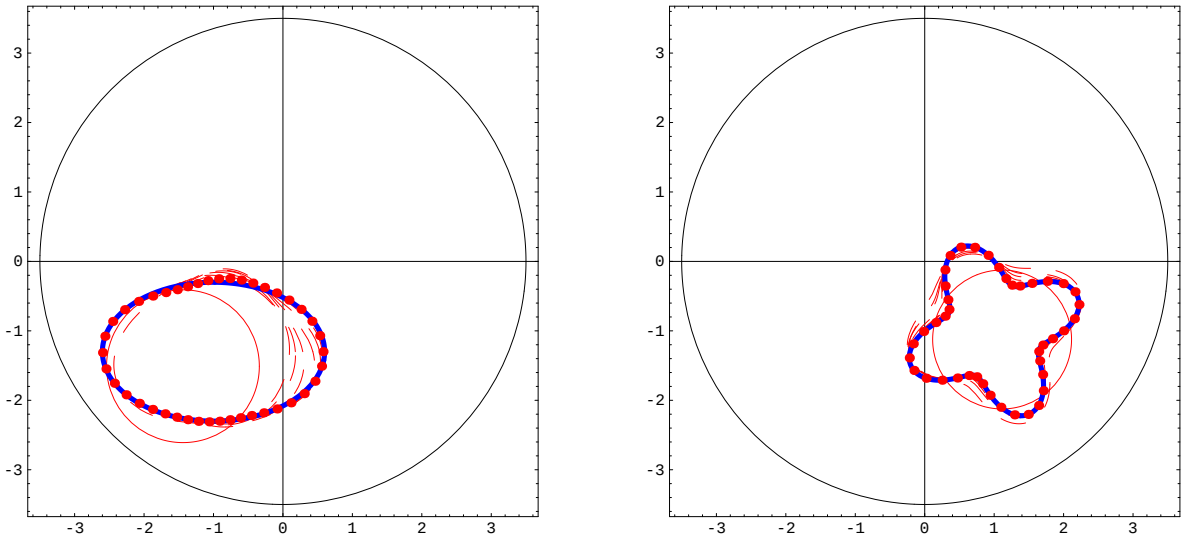

Figure 4.27: Reconstruction of γ_1 (left) and γ_2 (right) in $\mathcal{C}_4$ for data without noise.

For the third simulation, we started in $\mathcal{C}_0$ where 4 circles where computed. Using the last circle, the algorithm computed 6 curves in $\mathcal{C}_4$ (see Fig. 4.28).

The reconstruction of the kite was also good and in this case it took only 4 iterations in $\mathcal{C}_4$ to obtain the result presented in Fig. 4.29. No gain was obtained by starting in $\mathcal{C}_0$.

As expected, the iterative method performed better than the decomposition method for data without noise.

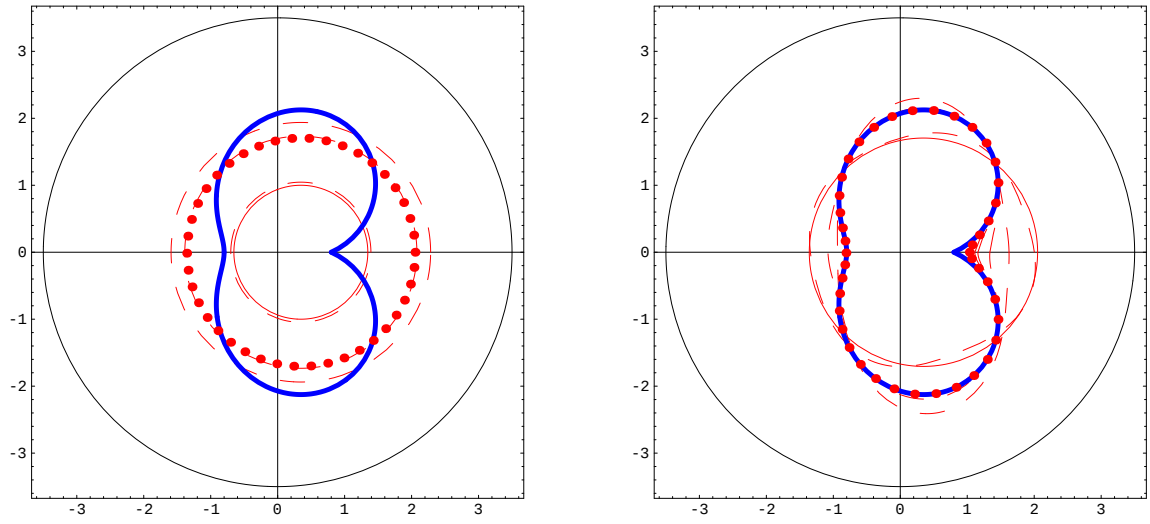

Figure 4.28: Reconstruction of γ_3 in $\mathcal{C}_0$ (left) and $\mathcal{C}_4$ (right) for data without noise.

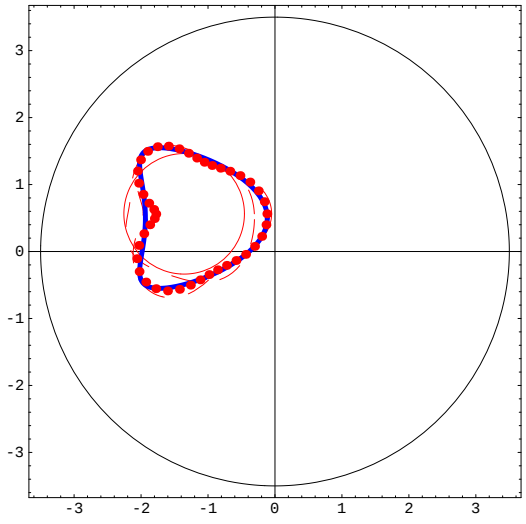

Figure 4.29: Reconstruction of γ_4 in $\mathcal{C}_4$ for data without noise.

For noisy data and concerning the reconstruction of the ellipse, we compare the results for 5 % of pointwise and norm noise. In this case, the results are similar (see Fig. 4.30) and 5 iterations were computed for the pointwise noise simulation and 6 for the norm noise simulation both in $\mathcal{C}_4$. We tested also for 8 % and 10 % of noise and 7 iterations were computed in $\mathcal{C}_4$, for both cases (Fig. 4.31). The reconstructions are stable with the increase of noise and also better when comparing with the decomposition method.

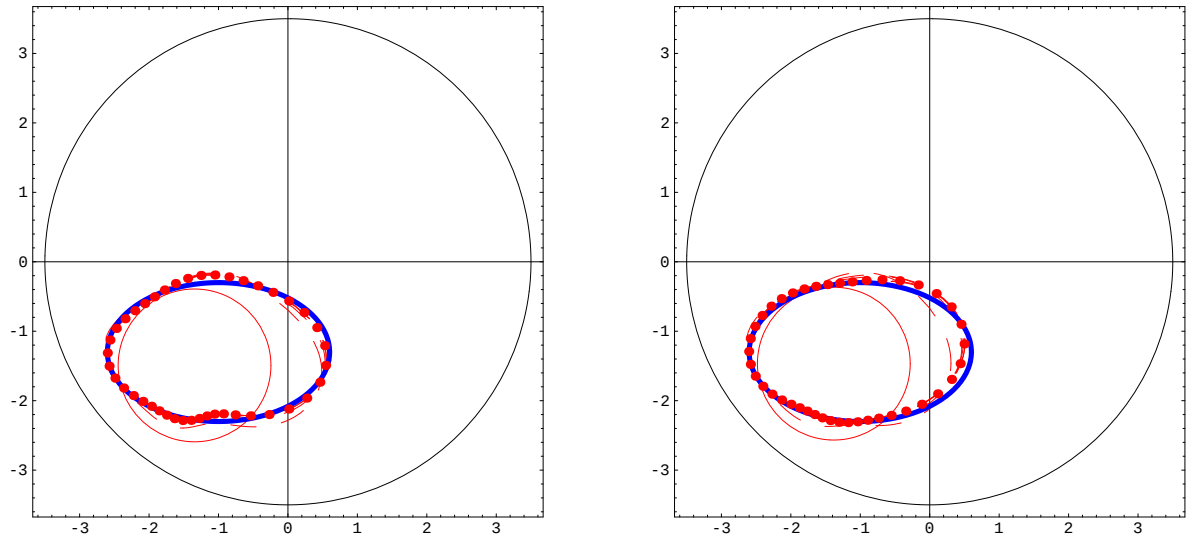

(a) 5 % of pointwise noise.

(b) 5 % of (norm) noise.

Figure 4.30: Reconstruction of γ_1 in $\mathcal{C}_4$.

To further illustrate the stability of the method we present in Fig. 4.32, for the second simulation, the evolution of the reconstruction in $\mathcal{C}_4$ with the noise levels of 5 %, 10%, 15 % and 20 %. For 5 % we computed 4 iterations (Fig. 4.32, (a)) and obtained an approximation with relative error 0.068 (in terms of the L^2 norm). Again 4 iterations were computed for 10 % (Fig. 4.32, (b)) and we obtained an approximation with 0.066 of relative error. When the noise level is 15 % we obtained 0.118 of relative error at the fourth iteration (Fig. 4.32, (c)). Finally, 3 iterations and 0.174 of relative error for 20 % of noise (Fig. 4.32, (d)).

On the third simulation we tested the algorithm with data affected by 5 % and 10 % of noise. For both situations, we started with an approximation by circles and computed 4 iterations in $\mathcal{C}_0$ (Figs. 4.33 and 4.34, left). In $\mathcal{C}_4$ the numerical procedure stopped at the 5th iteration (Figs. 4.33 and 4.34, right).

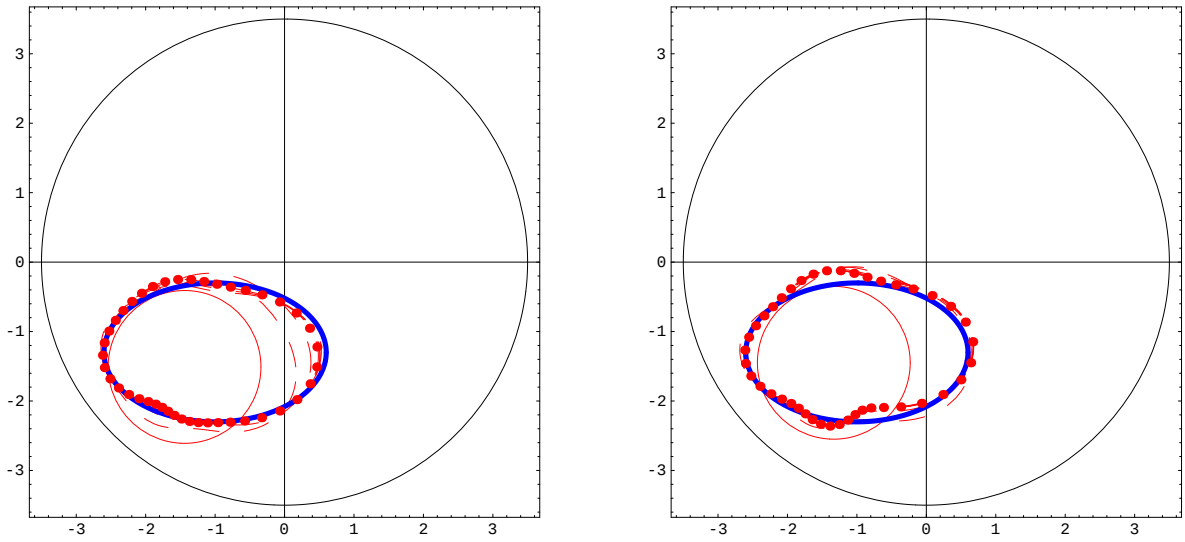

(a) 8 % of noise.

(b) 10 % of noise.

Figure 4.31: Reconstruction of γ_1 in $\mathcal{C}_4$.

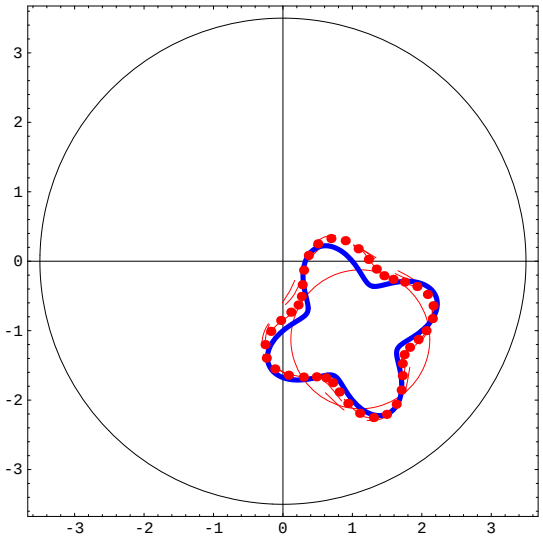

(a) 5% of noise.

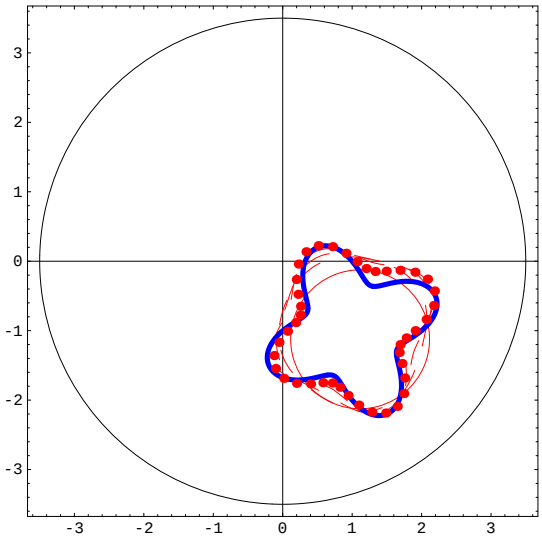

(b) 10% of noise.

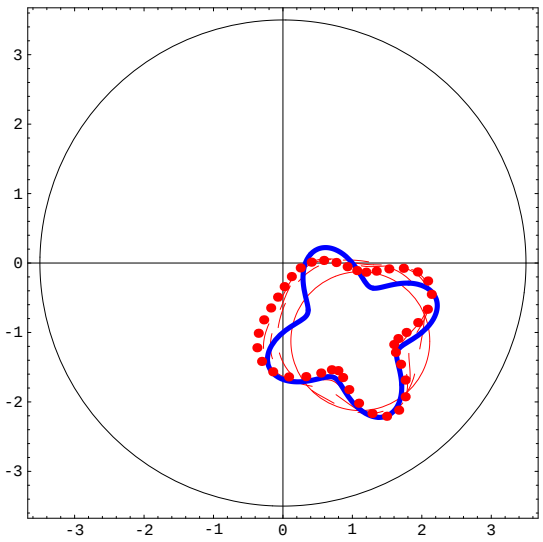

(c) 15% of noise.

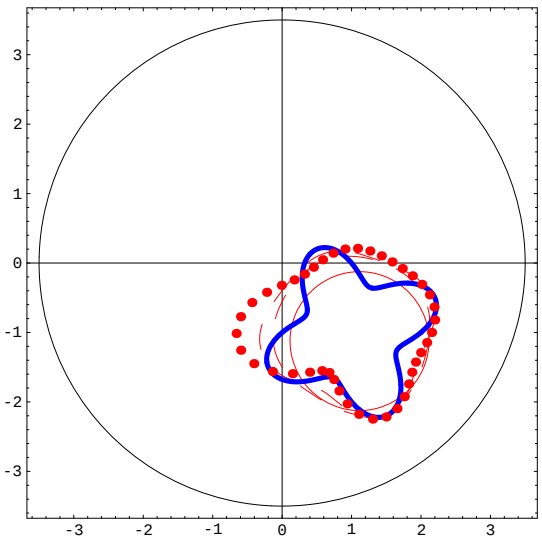

(d) 20% of noise.

Figure 4.32: Reconstruction of γ_2 in $\mathcal{C}_4$.

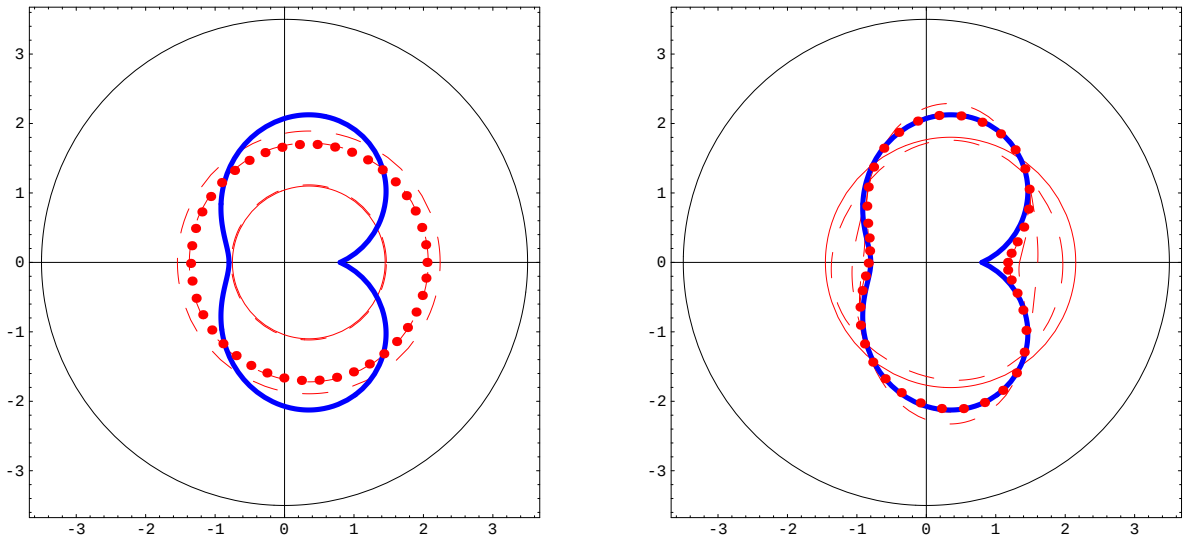

Figure 4.33: Reconstruction of γ_3 in $\mathcal{C}_0$ (left) and $\mathcal{C}_4$ (right). Noise level: 5 %.

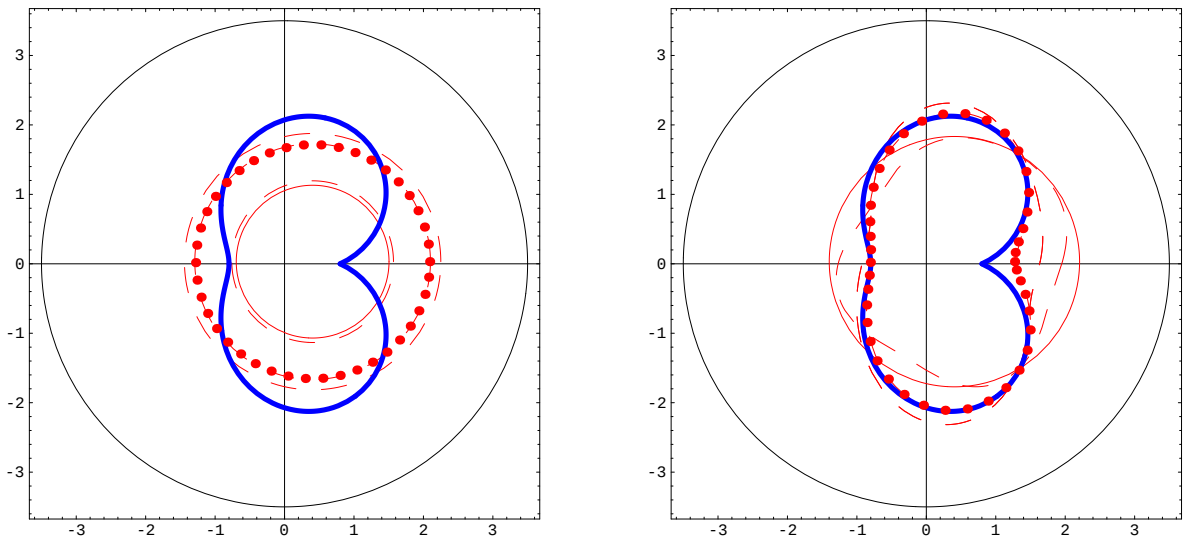

Figure 4.34: Reconstruction of γ_3 in $\mathcal{C}_0$ (left) and $\mathcal{C}_4$ (right). Noise level: 10 %.

The kite was also well recovered from lower noisy data. With a level of 5 % and 10 % it required 5 iterations to obtain the results plotted in Fig. 4.35. The poorer reconstruction with higher noisy data, in the right plot, is expected.

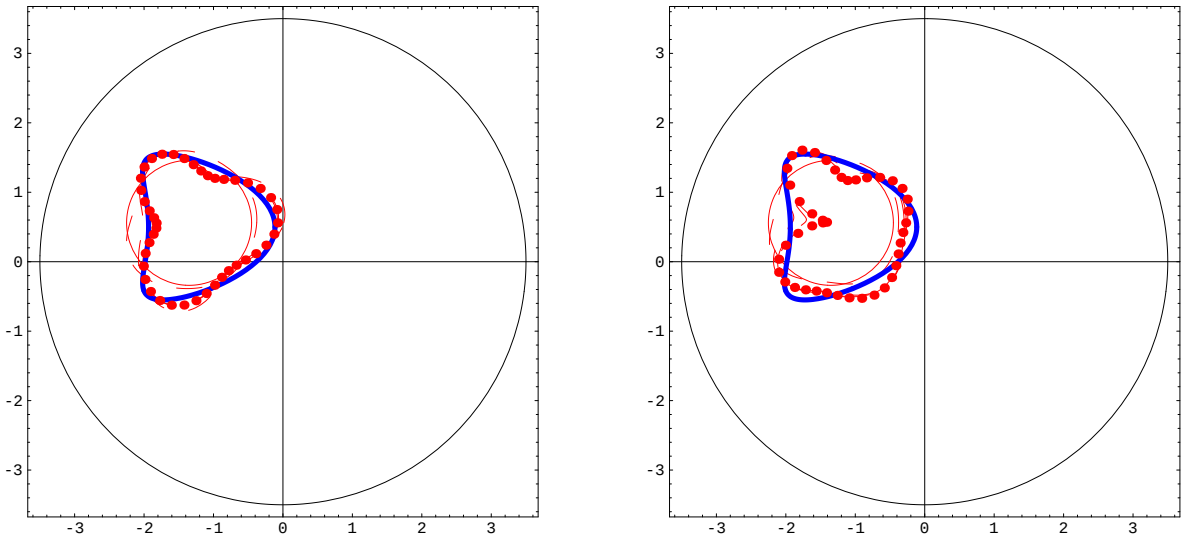

(a) 5 % of noise. (b) 10 % of noise.

Figure 4.35: Reconstruction of γ_4 in $\mathcal{C}_4$.

We now test the same method, but assuming that only part of Γ is accessible for measurements. The location of the inclusion will be included in the minimization scheme as unknown, that is we have two more unknowns corresponding to the coordinates of $\widetilde{c}_i$. Starting from the unitary circle, the first step is to determine the location and dimension using circles as approximating curves. The next step is to recover the shape in $\mathcal{C}_4$.

The following tests concerns the second example and the kite shaped inclusion. The number of observation points is still 60, and the location is represented on the figure by green dots. Starting with noise free data, we first consider, for the second example, 60 uniformly distributed observations on $[0, \pi/2]$. In this interval we were able to retrieve the location $\widetilde{c}_2 = (1.02, -1.11)$ (recall that $c_2 = (1, -1)$) and dimension by computing 4 circles (Fig. 4.36). However, the shape was not recovered by this data. Taking the observation points on $[3\pi/2, 2\pi]$ instead, we were able to obtain a fairly good approximation of the shape with 7 iterations in $\mathcal{C}_4$ (Fig. 4.37, right).

For the kite, we were able to determine the location $\widetilde{c}_4 = (-1.16, 0.48)$ ($c_4 = (-1.2, 0.5)$) from observations on $[0, \pi/4]$ by computing 4 circles (Fig. 4.38). However, we were not able to reconstruct the shape from this boundary data. A good approximation was achieved by taking observation points on $[0, \pi]$ and the algorithm stopped at the fourth iteration in $\mathcal{C}_4$ (Fig. 4.39, right).

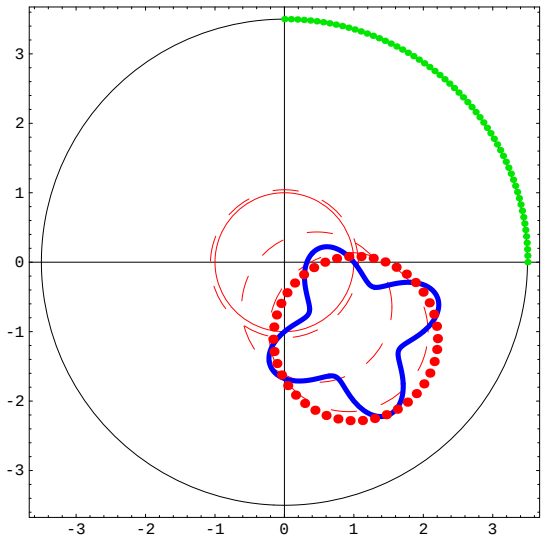

Figure 4.36: Reconstruction of γ_2 in $\mathcal{C}_0$ from incomplete noise free data.

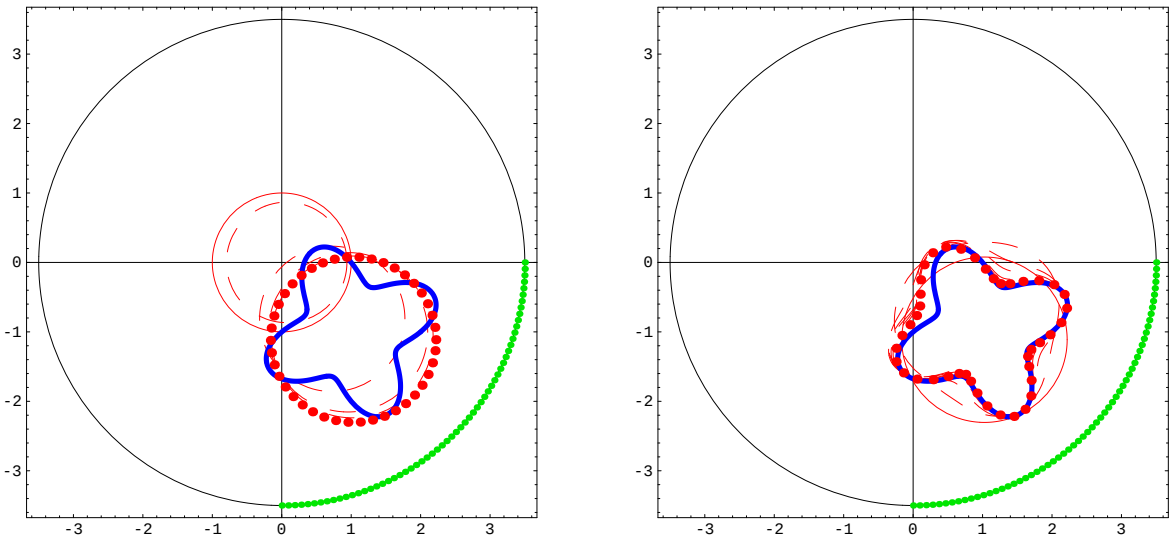

Figure 4.37: Reconstruction of γ_2 in $\mathcal{C}_0$ (left) and $\mathcal{C}_4$ (right) from incomplete noise free data.

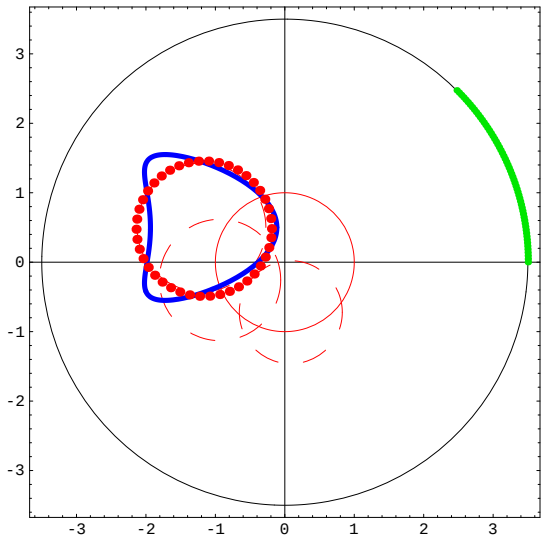

Figure 4.38: Reconstruction of γ_4 in $\mathcal{C}_0$ from incomplete noise free data.

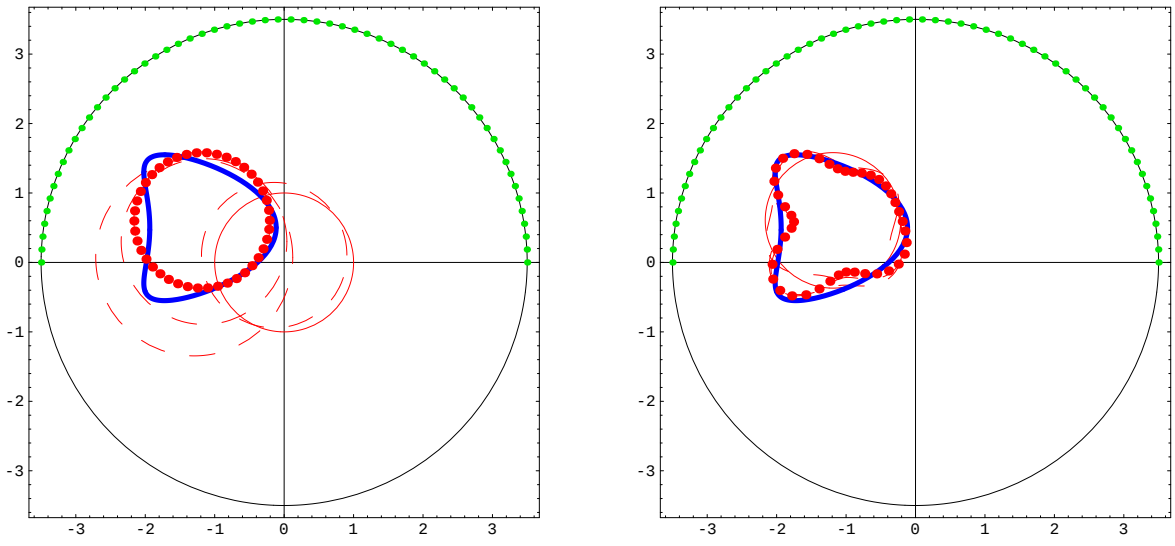

Figure 4.39: Reconstruction of γ_4 in $\mathcal{C}_0$ (left) and $\mathcal{C}_4$ (right) from incomplete noise free data.

From noisy data on the first quadrant, we were still able to retrieve the location (this time $\widetilde{c}_2 = (1.05, -1.08)$) and approximate dimension of γ_2 with four circles (Fig. 4.40). Taking observations on $[3\pi/2, 2\pi]$ we obtain a good approximation of the shape (Fig. 4.41). In this case, the algorithm computed 4 circles and 5 shapes in $\mathcal{C}_4$.

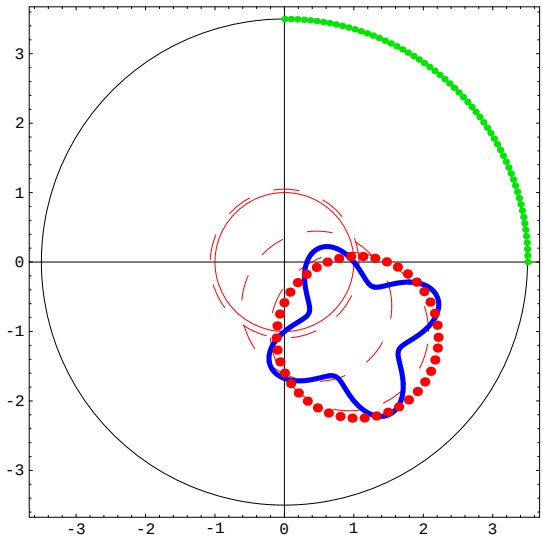

Figure 4.40: Reconstruction of γ_2 in $\mathcal{C}_0$ from incomplete noisy data. Noise level: 5 %.

The location of the kite was retrieved from noisy data on $[0, \pi/2]$ by computing 6 circles (Fig. 4.42). Considering data on $[0, \pi]$ we were able to obtain the approximations plotted in Fig. 4.43.

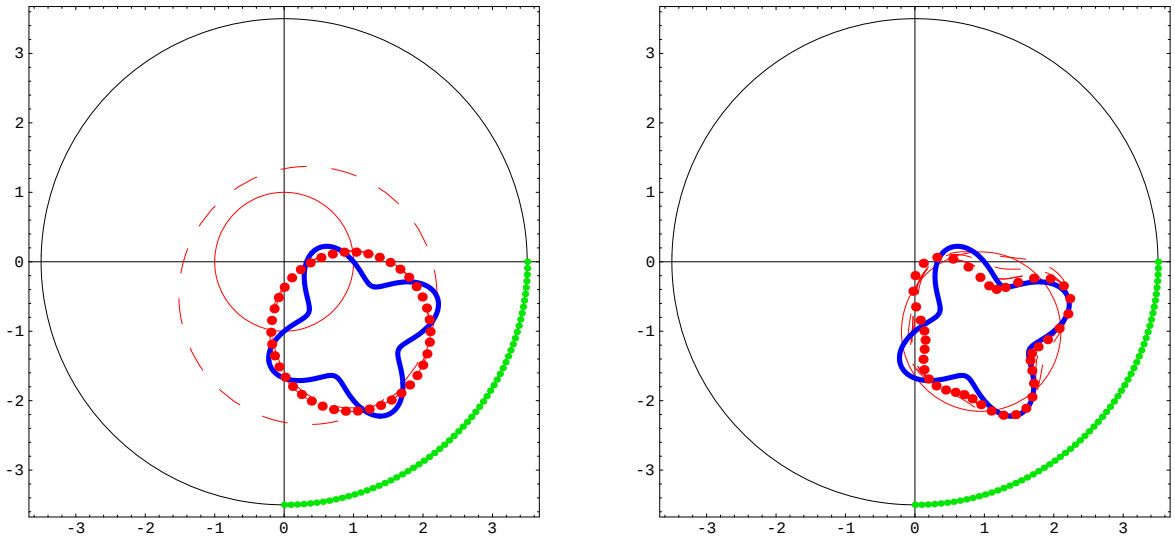

Figure 4.41: Reconstruction of γ_2 in $\mathcal{C}_0$ (left) and $\mathcal{C}_4$ (right) from incomplete noisy data. Noise level: 5 %.

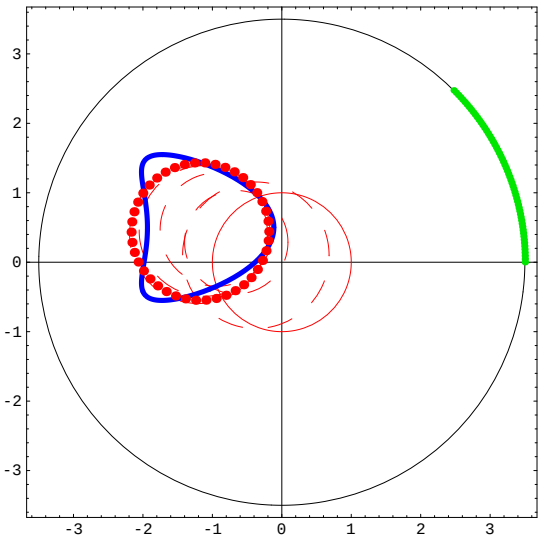

Figure 4.42: Reconstruction of γ_4 in $\mathcal{C}_0$ from incomplete noisy data. Noise level: 5 %.

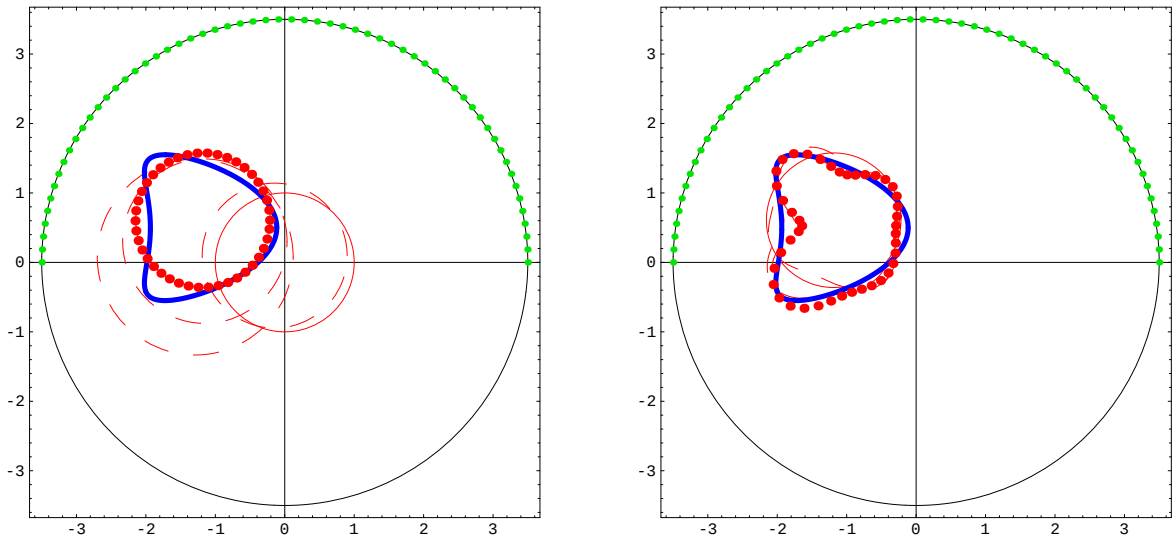

Figure 4.43: Reconstruction of γ_4 in $\mathcal{C}_0$ (left) and $\mathcal{C}_4$ (right) from incomplete noisy data. Noise level: 5 %.

Overall we obtained very accurate and stable results. Despite being slower, the iterative approach provided better results when comparing with the decomposition method. We used the centroid approximation provided by (4.19) but it is clear from the incomplete data simulations that no such *a priori* information is required.

4.4 The MFS applied to the inverse Robin problem

4.4.1 Decomposition method

The decomposition method for the inverse geometric problem can be easily adapted to the Robin inverse problem.

The first step is the same (fitting of the Cauchy data) and is treated using the MFS, as described in section 4.2.1.

The second step is easier than the non linear problem arising in the inverse geometric problem. In fact, since γ is known, then

$$Z = -\frac{\partial_{\mathbf{n}} u|_\gamma}{u|_\gamma} \text{ (when } u \neq 0) \tag{4.25}$$

and an approximation of Z can be explicitly computed by

$$\widetilde{Z} = -\frac{\partial_{\mathbf{n}} \widetilde{u}|_\gamma}{\widetilde{u}|_\gamma} \text{ (when } \widetilde{u} \neq 0), \tag{4.26}$$

where $\widetilde{u}$ is the solution of step 1. Next result shows that for an appropriate input function $g \in C^0(\Gamma)$, the expression (4.25) has no singularities. We start with the following maximum principle (see [37]).

Theorem 4.20 *Let $\partial\Omega_c \in C^2$, $g \in C^0(\Gamma)$ a positive input function, Z an admissible coefficient and u a classical solution of $(\mathcal{P}_R)$. Then,*

$$u > 0 \text{ in } \Omega_c.$$

Corollary 4.21 *We have*

$$u|_\gamma > 0.$$

Proof. It follows from the previous Theorem that $u(x) \geq 0$, $\forall x \in \gamma$. If $u(x_0) = 0$ for some $x_0 \in \gamma$ then, using Hopf's lemma, we must have $\partial_{\mathbf{n}} u < 0$ at such point, which is a contradiction with the fact that u satisfies a Robin boundary condition at γ. □

Next result is based on the two previous results and gives a condition to distinguish a Neumann problem ($Z = 0$) from a general Robin problem.

Corollary 4.22 *In the conditions of Theorem 4.20 we have*

$$Z = 0 \Leftrightarrow \int_\Gamma g_{\mathbf{n}} d\varsigma = 0$$

where $g_{\mathbf{n}} = \partial_{\mathbf{n}} u|_\Gamma$ and u is the classical solution of $(\mathcal{P}_R)$.

Proof. If $Z = 0$ then we have the Neumann problem $(\mathcal{P}_N)$ and it follows, from Green's formula that $\int_\Gamma g_{\mathbf{n}} d\varsigma = 0$.

Now let $\int_\Gamma g_{\mathbf{n}} d\varsigma = 0$. From Green's formula and using the Robin condition,

$$0 = \int_\Gamma g_{\mathbf{n}} d\varsigma = -\int_\gamma \partial_{\mathbf{n}} u d\varsigma = \int_\gamma Z u d\varsigma. \tag{4.27}$$

Since by the previous corollary, $u > 0$ on γ and by hypothesis $Z \geq 0$ we conclude that $Z = 0$. □

Remark 4.23 In the particular case where $Z \neq 0$ is known to be constant, using (4.27), the coefficient can be computed instead by

$$Z = \frac{\displaystyle\int_\Gamma g_{\mathbf{n}} d\varsigma}{\displaystyle\int_\gamma u d\varsigma}. \tag{4.28}$$

4.4.2 Numerical simulations

To show the feasibility of the method we present several numerical simulations regarding the three examples considered in section 4.1.2. To apply the MFS approximation for the Cauchy problem we considered 60 collocation points on the boundary Γ and 120 source points on the artificial boundary curve defined by $\widehat{\Gamma} = \partial B(\mathbf{0}, 5.5)$ and $\widehat{\gamma} = 0.9\gamma$.

We start with the reconstruction from noise free data on 60 equally distributed observation points on Γ. The red dots denotes the reconstruction given by (4.26) and the blue line is the exact coefficient. As we can see in Figs. 4.44 and 4.45 we obtained good results with this fast method.

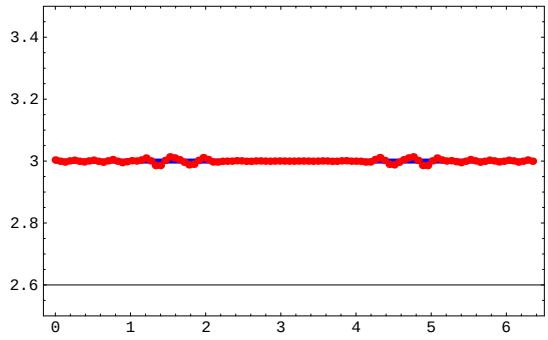

(a) Z_1.

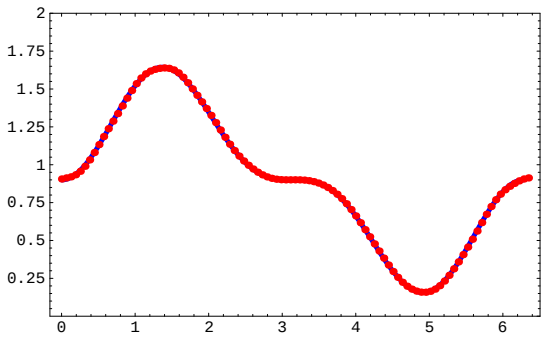

(b) Z_2.

Figure 4.44: Reconstruction of the Robin coefficient from noise free boundary data.

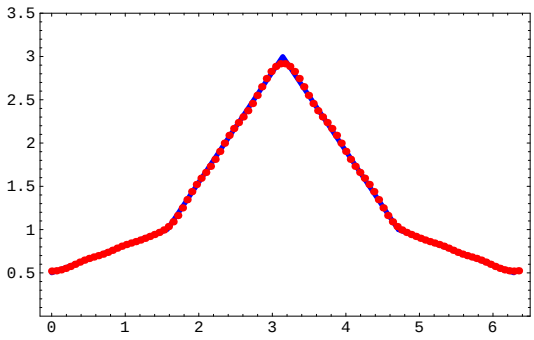

Figure 4.45: Reconstruction of Z_3 from noise free boundary data.

To test the robustness of the method we introduce several levels of random norm noise on the measured data.

The reconstruction of the constant coefficient for data with 5 % and 10 % of noise is presented in Fig. 4.46. For both cases we obtained, via L–curve, the Tikhonov regularization parameter $\mu = 10^{-2}$. If the *a priori* information that Z_1 is constant is assumed

then using (4.28) we get the approximations $\widetilde{Z}_1 = 2.94$ and $\widetilde{Z}_1 = 2.86$ for the previous levels of noise.

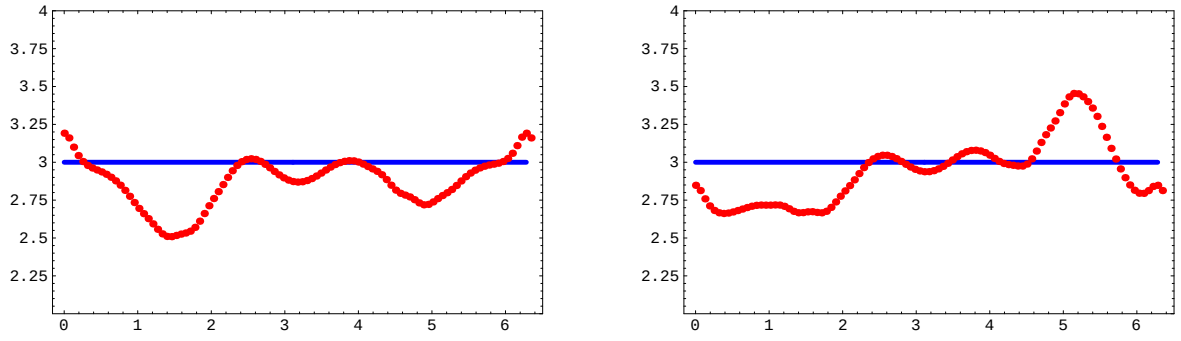

(a) 5 % of noise.

(b) 10 % of noise

Figure 4.46: Reconstruction of Z_1 from noisy data.

For the non constant and smooth coefficient Z_2 we present in Fig. 4.47 the reconstructions for several levels of noise. Starting from the top left (Fig. 4.47 (a)) we have an approximation with 1.2 % of relative ($L^2(\gamma)$ norm) error for 5 % of noise. The regularization parameter was $\mu = 5 \times 10^{-3}$. On the top right plot (Fig. 4.47 (b)), the regularization parameter was the same and the approximation for 10 % of noise has a relative error of 2.3 % . On the bottom the regularization parameter was $\mu = 3 \times 10^{-2}$. From left to right, we have the reconstructions for both 15 % and 20 % of noise, respectively. On the first case, the reconstruction has a relative error of 1.7% and on the second case, 5.3 %.

Regarding the non smooth Robin coefficient Z_3 the regularization parameter was $\mu = 10^{-3}$ for both simulations presented in Fig. 4.48. On the left, the approximation for 5 % of norm noise and on the right, the approximation for 10 % of noise.

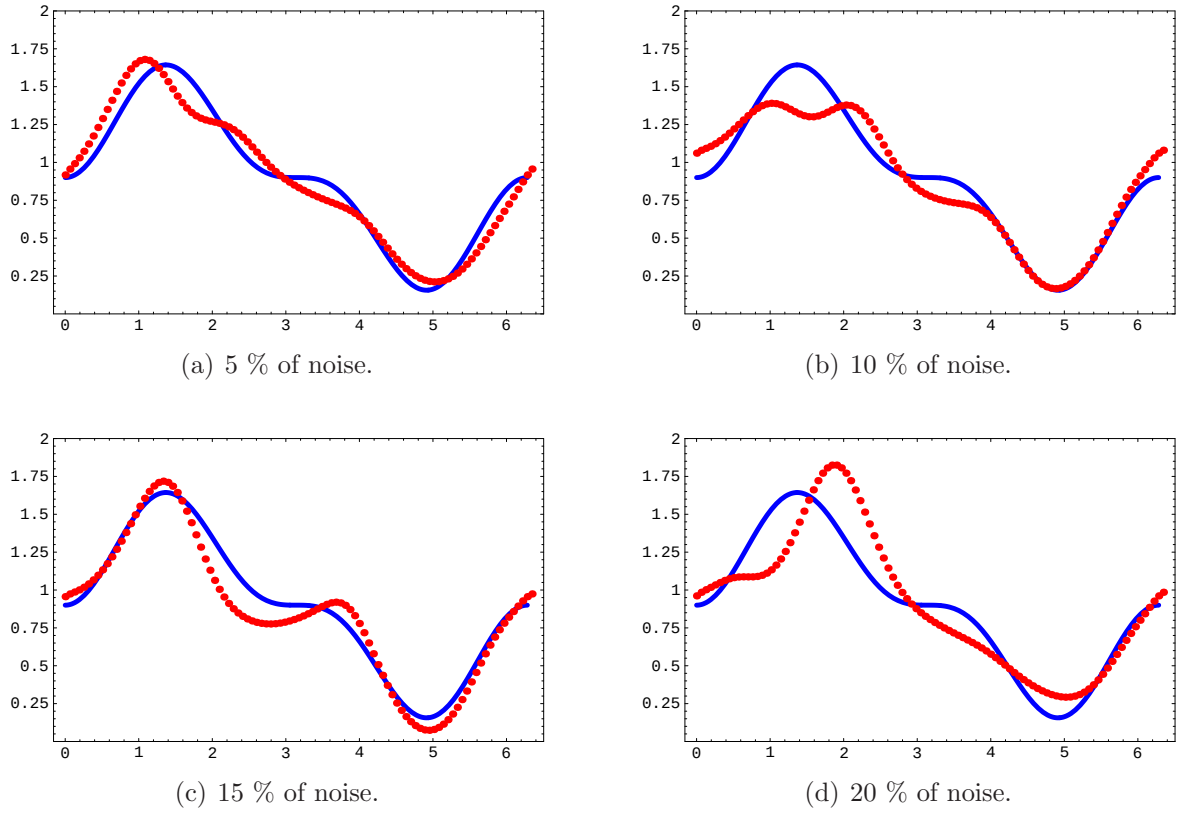

(a) 5 % of noise.

(b) 10 % of noise.

(c) 15 % of noise.

(d) 20 % of noise.

Figure 4.47: Reconstruction of Z_2 from noisy data.

We now consider the situation where only part of the boundary Γ is accessible for measurements. The number of observation points is still 60 (uniformly distributed) but over some specific arcs.

For the smooth coefficient Z_2 we consider the arcs $[0, \pi/2]$ and $[\pi/2, 3\pi/2]$ and show, in Fig. 4.49, the accuracy of the MFS fitting of the (noise free) Cauchy data in the first case. The absolute error on $[0, \pi/2]$ is small, where the maximum value is 3×10^{-8} for the Dirichlet condition and 5×10^{-8} for the Neumann condition. Outside this interval, the error grows and reaches 0.027 which, still, is a good result. This approximation enabled a good reconstruction of Z_2 (Fig. 4.50, left). We note that the part where the reconstruction is worst is contained in the part where no Cauchy data was considered.

On the right plot of Fig. 4.50 we have the reconstruction for noise free data on the arc $[\pi/2, 3\pi/2]$. This time, we were able to retrieve almost the whole coefficient.

Regarding the reconstruction of the non smooth coefficient we present in Fig. 4.51 the results for noise free data on the arcs $[5\pi/4, 3\pi/2]$ (left) and $[\pi/2, \pi]$ (right). In the first case we obtain a good approximation for Z_3 whereas on the second quadrant, almost an exact recovery was achieved.

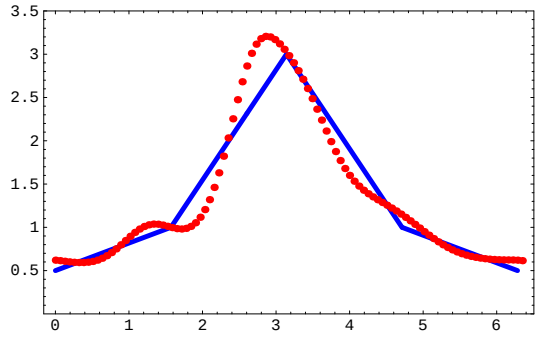

(a) 5 % of noise.

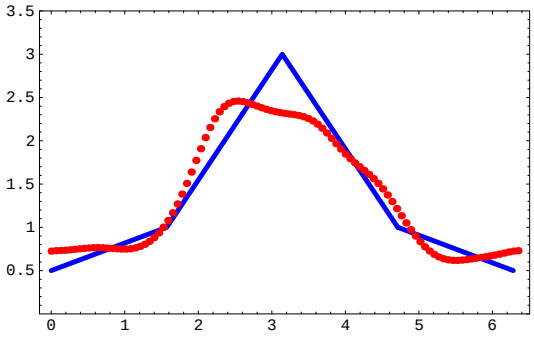

(b) 10 % of noise.

Figure 4.48: Reconstruction of Z_3 from noisy data.

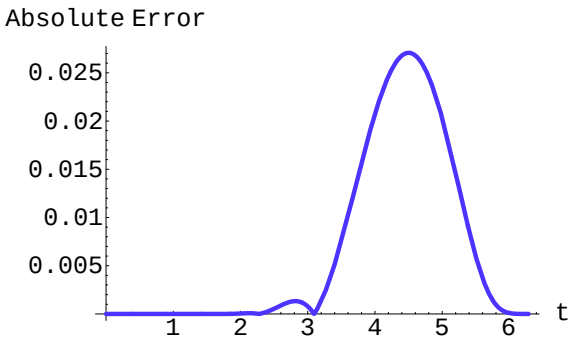

(a) Dirichlet

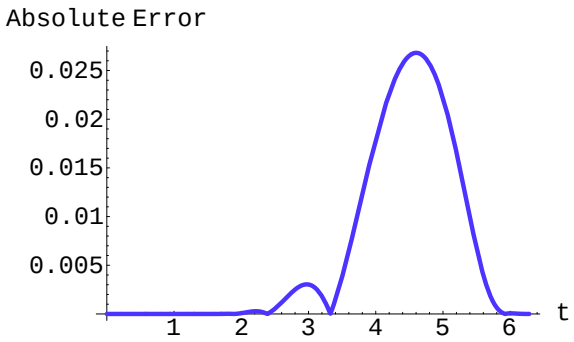

(b) Neumann

Figure 4.49: Error of the Cauchy data fitting from partial data.

Testing the same examples with 5 % of noise we obtained stable results for Z_2. The regularization parameter was $\mu = 10^{-2}$ and on the left plot of Fig. 4.52 we show the reconstruction for data on the arc $[0, \pi/2]$ and on the right, data in the second and third quadrants.

The results for the non smooth coefficient Z_3 are presented in Fig. 4.53. The regularization parameter was 5×10^{-3} and on the left we have the result for noisy data on the arc $[5\pi/4, 3\pi/2]$. On the right, the reconstruction for data on $[\pi/2, \pi]$.

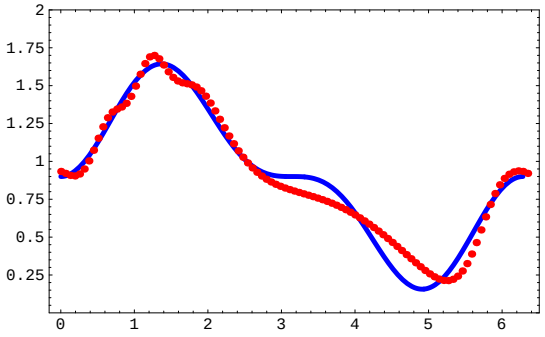

(a) $[0, \pi/2]$.

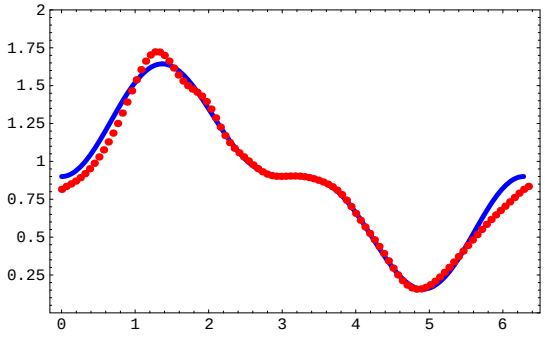

(b) $[\pi/2, 3\pi/2]$.

Figure 4.50: Reconstruction of Z_2 from partial noise free boundary data.

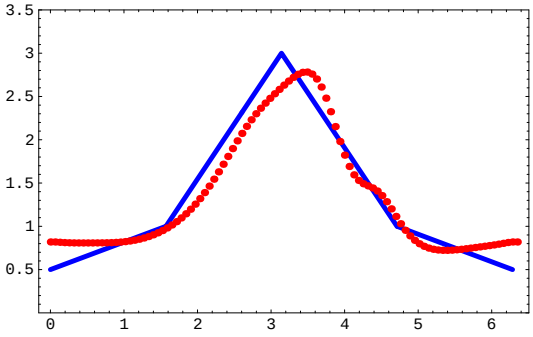

(a) $[5\pi/4, 3\pi/2]$.

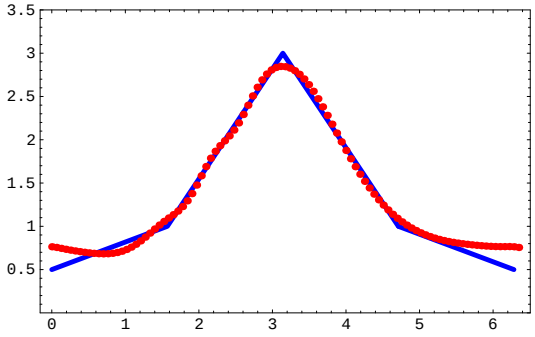

(b) $[\pi/2, \pi]$.

Figure 4.51: Reconstruction of Z_3 from partial noise free boundary data.

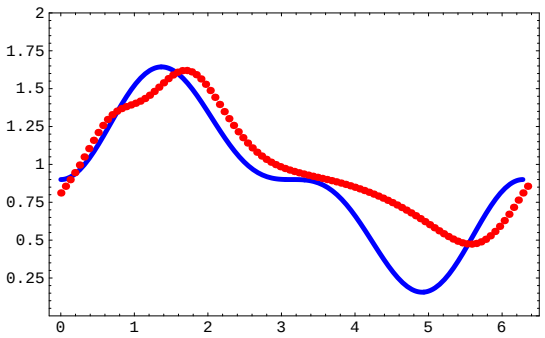

(a) $[0, \pi/2]$.

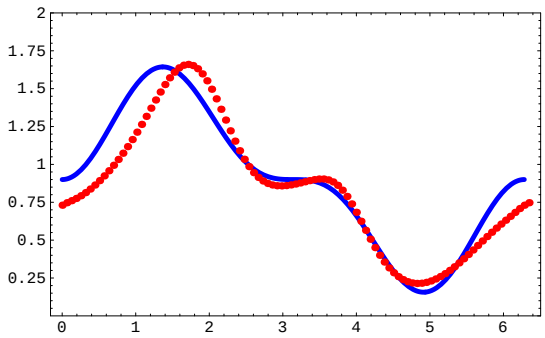

(b) $[\pi/2, 3\pi/2]$.

Figure 4.52: Reconstruction of Z_2 from partial noisy boundary data. Noise: 5%

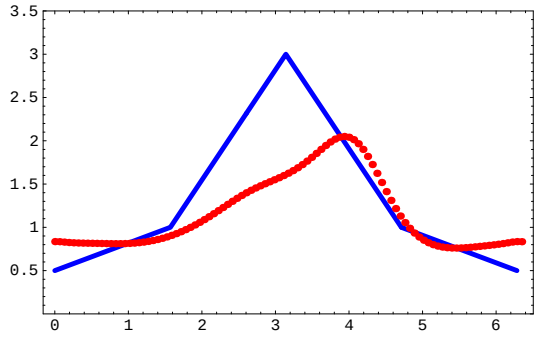

(a) $[5\pi/4, 3\pi/2]$.

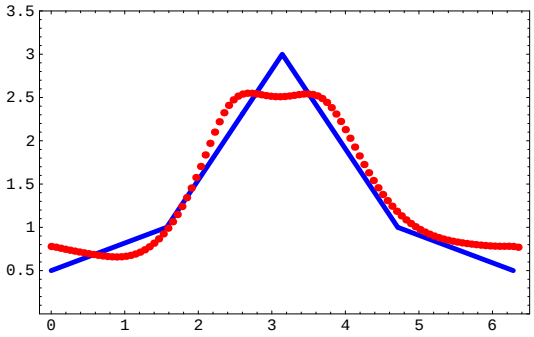

(b) $[\pi/2, \pi]$.

Figure 4.53: Reconstruction of Z_3 from partial noisy boundary data. Noise: 5%

Overall we obtained very accurate and stable results using this decomposition method for the inverse Robin problem. We now compare these results with an iterative approximation for the inverse problem.

4.4.3 Iterative reconstruction of the coefficient by a Quasi–Newton method

Consider the inverse Robin problem formulated in terms of the non linear equation: Given a compatible pair $(g, g_{\mathbf{n}}) \in \mathcal{H}_R(\Gamma)$ with $g \neq 0$, determine $Z \in \mathcal{C}_R$ such that

$$G(Z) = g_{\mathbf{n}}$$

where G is the non linear and injective map defined in (3.26). Following section 4.3, we consider the linearized equation

$$G'(Z)R = g_{\mathbf{n}} - G(Z),$$

where R belongs to the set of admissible directions $R_{ad} = C^0(\gamma)$ and $Z \in \mathcal{C}_R$. The directional derivative of G at Z, $G'(Z) : C^0(\gamma) \to H^{-1/2}(\Gamma)$, is the (injective) linear map defined by (see Lemma 3.18)

$$G'(Z)R = \partial_{\mathbf{n}} u',$$

where $u' \in H^1(\Omega_c)$ is the unique solution of

$$\begin{cases} \Delta u' = 0 & \text{in } \Omega_c \\ u' = 0 & \text{on } \Gamma \\ \partial_{\mathbf{n}} u' + Z u' = -Ru & \text{on } \gamma \end{cases} .$$

We extend this bounded linear map by continuity to the whole $L^2(\gamma)$ and denote it by $G'(Z)$.

Lemma 4.24 *The adjoint of $G'(Z)$, $G'(Z)^* : H^{1/2}(\Gamma) \longrightarrow L^2(\gamma)$ is given by*

$$G'(Z)^*(g_*) = (uu^*)|_\gamma.$$

where $u^* \in H^1(\Omega_c)$ is the solution of the well posed problem $(\mathcal{P}_R)$ with input function $g_* \in H^{1/2}(\Gamma)$.

Proof. We follow the proof of Lemma 4.15. Let $u^* \in H^1(\Omega_c)$ be the solution of the aforementioned problem. We have

$$\begin{aligned} \langle g_*, G'(Z)R\rangle_{H^{1/2}(\Gamma)\times H^{-1/2}(\Gamma)} = \int_\Gamma \partial_{\mathbf{n}} u' g_* d\varsigma = \langle u', \partial_{\mathbf{n}} u^*\rangle_{H^{1/2}(\Gamma)\times H^{-1/2}(\Gamma)} \\ - \langle u^*, \partial_{\mathbf{n}} u'\rangle_{H^{1/2}(\Gamma)\times H^{-1/2}(\gamma)} + \langle u', \partial_{\mathbf{n}} u^*\rangle_{H^{1/2}(\Gamma)\times H^{-1/2}(\gamma)} . \end{aligned}$$

Using the boundary conditions for u' and u^* we get

$$\langle g_*, G'(Z)R\rangle_{H^{1/2}(\Gamma)\times H^{-1/2}(\Gamma)} = \int_\gamma Ruu^* d\varsigma.$$

□

Corollary 4.25 *If exists a relatively open set $\sigma \subset \gamma$ where the trace of u does not vanish then, $G'(Z)$ has dense range in $H^{-1/2}(\Gamma)$.*

Proof. We show that the adjoint $G'(Z)^*$ is injective. Let $g_* \in H^{1/2}(\Gamma)$ be such that $G'(Z)^* g_* = 0$. By the previous Lemma, we must have

$$uu^* = 0 \text{ on } \gamma. \tag{4.29}$$

Thus, the hypothesis on the trace of u implies $u^*|_\sigma = 0$ and since u^* satisfies a Robin condition on γ we must have $u^* = \partial_{\mathbf{n}} u^*$ on σ. This implies $u^* = 0$ in Ω_c and the conclusion

$$g_* = u^*|_\Gamma = 0$$

follows. □

Consider the representation of $\mathcal{C}_R$ and R_{ad} in terms of the Fourier modes, ie.,

$$\mathcal{C}_N = \left\{ Z_\alpha \in C^0([0,2\pi]) : Z_\alpha > 0 \wedge Z_\alpha(t) = \alpha_0 + \sum_{j=1}^{N} \alpha_j \cos(jt) + \sum_{j=1}^{N} \alpha_{j+N} \sin(jt) \right\} \tag{4.30}$$

and

$$R_{ad}^N = \left\{ R_\alpha \in C^0([0,2\pi]) : R_\alpha(t) = \alpha_0 + \sum_{j=1}^{N} \alpha_j \cos(jt) + \sum_{j=1}^{N} \alpha_{j+N} \sin(jt) \right\} \tag{4.31}$$

respectively, with $\alpha := (\alpha_0, \ldots, \alpha_{2N}) \in \mathbb{R}^{2N+1}$. We now formulate the non linear least squares problem. Given a vector of (eventually noisy) data $\mathfrak{m} = [\mathfrak{m}_i]$ on the observation points $x_i \in \Gamma$, the objective function is

$$G_{obj}(\alpha) := \frac{1}{2} \sum_{j=1}^{m} (G_i(\alpha) - \mathfrak{m}_i)^2 = \frac{1}{2} (\mathbf{G}(\alpha) - \mathfrak{m})^\top (\mathbf{G}(\alpha) - \mathfrak{m})$$

where $G_i(\alpha) = G(\alpha)(x_i) = \partial_{\mathbf{n}} u_\alpha(x_i)$,

$$\begin{cases} \Delta u_\alpha = 0 & \text{in } \Omega_c \\ u_\alpha = g & \text{on } \Gamma \\ \partial_{\mathbf{n}} u_\alpha + Z_\alpha u_\alpha = 0 & \text{on } \gamma \end{cases} .$$

The minimization problem is

$$Z_{\alpha^*} = \text{argmin}_{Z_\alpha \in \mathcal{C}_N} G_{obj}(\alpha).$$

Lemma 4.26 *The Jacobian matrix in the update step for the LM method, $\mathbb{J}(\alpha)$, is given by*

$$\mathbb{J}(\alpha) = \left[\partial_{\mathbf{n}} u_j'(x_i) \right]_{ij}$$

where u_j' solves

$$\begin{cases} \Delta u_j' = 0 & \text{in } \Omega_c \\ u_j' = 0 & \text{on } \Gamma \\ \partial_{\mathbf{n}} u_j' + Z_\alpha u_j' = -R_{e_j} u_\alpha & \text{on } \gamma \end{cases}$$

with e_j the jth vector of the standard basis of $\mathbb{R}^{2N+1}$.

Proof. We follow the proof of Lemma 4.18. Given $Z_\alpha \in \mathcal{C}_N$ consider, for sufficient small ε, the perturbation of Z_α, defined by

$$Z_\alpha^\varepsilon := Z_\alpha + \varepsilon R_{e_j} \in \mathcal{C}_N.$$

Then,

$$[\mathbb{J}(\alpha)]_{ij} = \frac{\partial G_i}{\partial \alpha_j}(x_i) = \lim_{\varepsilon \to 0} \frac{G_i(\alpha + \varepsilon e_j) - G_i(\alpha)}{\varepsilon} = (G'(Z_\alpha)R_{e_j})(x_i).$$

□

At each step of the method, we have to solve $2N + 2$ problems (one related to u_α and $2N + 1$ problems related to the Jacobian) and again we use the MFS for these problems.

For the updated coefficient $Z_{\alpha_{new}}$ some care must be taken in the choice of $\mu > 0$ in the LM method to assure that $Z_{\alpha_{new}} > 0$. To implement this restriction we evaluate $Z_{\alpha_{new}}$ at 200 equally spaced points on $[0, 2\pi]$ and denote by Ctr the vector containing this data. The update is considered valid if, besides the control conditions of the LM, we have also $\min Ctr \geq 0$.

4.4.4 Numerical simulations

We test the iterative algorithm for the previous three examples. In order to compare with the results of the decomposition method, we use the same boundary data. The strategy presented in Algorithm 1 will be used to compute the approximations.

We start from the initial guess $Z^{(0)} \equiv 1$ and compute several approximations in $\mathcal{C}_0$ (horizontal lines) until the stopping criterion

$$\frac{G_{obj}(Z_{old}) - G(Z_{new})}{G_{obj}(Z_{old})} \leq 10^{-2}$$

is reached. Then, from this last function, the approximations are computed in $\mathcal{C}_4$ again until the stopping criterion is reached.

In order to compute the MFS approximation for the arising direct problems we consider the same artificial curves used for the decomposition method and 120 collocation and source points.

We start by presenting the results for complete boundary data without noise. In Figs. 4.54 and 4.55 we present such results. As always, the dashed red lines represents the iterations, the red dotted line the final iteration and the blue line the goal. For the constant function Z_1, 5 iterations were computed in $\mathcal{C}_0$. For this example, no updates were obtained in $\mathcal{C}_4$. For the reconstruction of Z_2 and Z_3 in $\mathcal{C}_0$ no significant updates were

obtained whereas in $\mathcal{C}_4$ 5 iterations were computed.

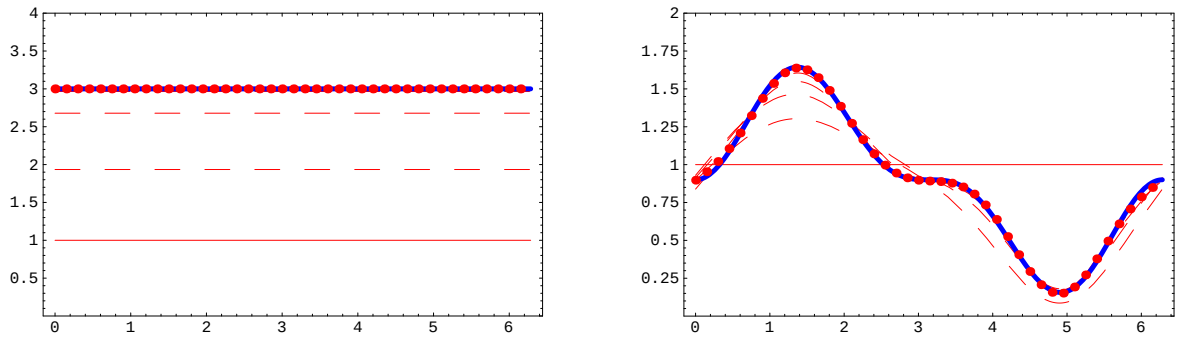

(a) Z_1. (b) Z_2.

Figure 4.54: Iterative reconstruction of the Robin coefficient in $\mathcal{C}_4$ from noise free boundary data.

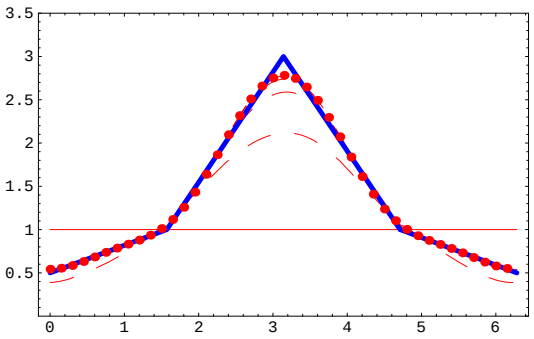

Figure 4.55: Iterative reconstruction of Z_3 in $\mathcal{C}_4$ from noise free boundary data.

For the reconstructions from noisy data we plot the last approximation (red dotted line) and also the approximation obtained with the decomposition method (green dotted line).

Concerning Z_1, we present in Fig. 4.56 the comparison for 5 % of noise (left plot) and 10% of noise (right plot). In both cases, 5 iterations were computed in $\mathcal{C}_0$ and 3 in $\mathcal{C}_4$. As we can see, the results obtained with the iterative method are slightly better.

For the smooth function Z_2, the results are equivalent. Here, 4 iterations were computed in $\mathcal{C}_4$ for both levels of 5 % (Fig. 4.57, left) and 10% (Fig. 4.57, right) of noise.

The results for the non smooth function were also equivalent. In this case, 4 and 3 iterations were computed in $\mathcal{C}_4$ for 5 % and 10 % of noise, respectively. The reconstructions are presented in Fig. 4.58 where on the left we have the results for 5 % of noise and on the right, for 10 %.

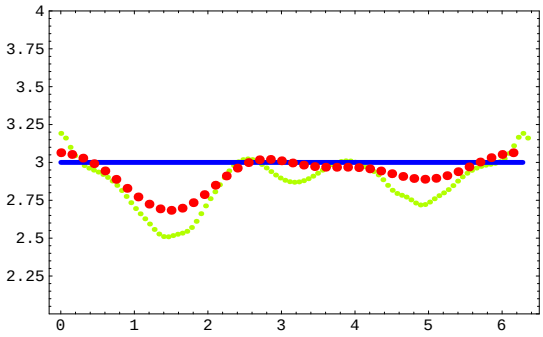

(a) 5 % of noise.

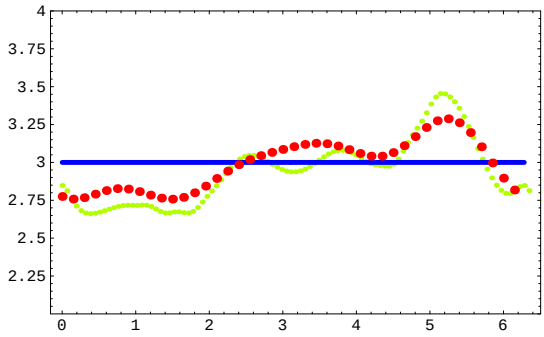

(b) 10 % of noise.

Figure 4.56: Iterative reconstruction of Z_1 in $\mathcal{C}_4$ from noisy boundary data.

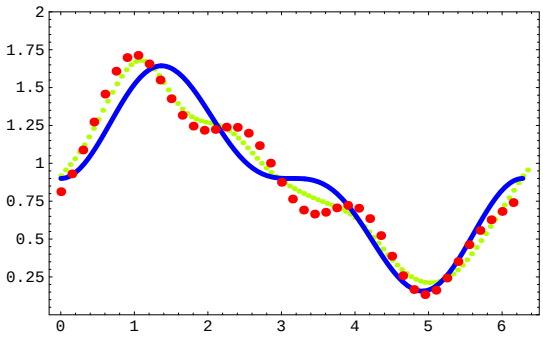

(a) 5 % of noise.

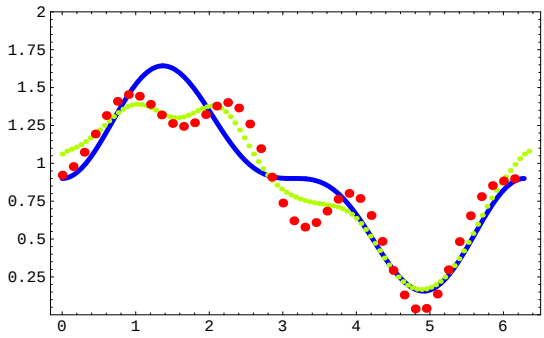

(b) 10 % of noise.

Figure 4.57: Iterative reconstruction of Z_2 in $\mathcal{C}_4$ from noisy boundary data.

We present one last numerical simulation. It regards the reconstruction of Z_2 from incomplete boundary data. The set of data was collected at 60 uniformly distributed points on the arc $[0, \pi/2]$. On the left of Fig. 4.59 is the reconstruction for noise free data and on the right for 5 % of noise. Again we notice that the function is well recovered in the first and second quadrants and also on the upper half of the fourth quadrant. In this part, the results are similar whereas on the other part of the interval the results are different. The considered data is not enough to provide a satisfactory approximation of the function in the third and part of the fourth quadrants.

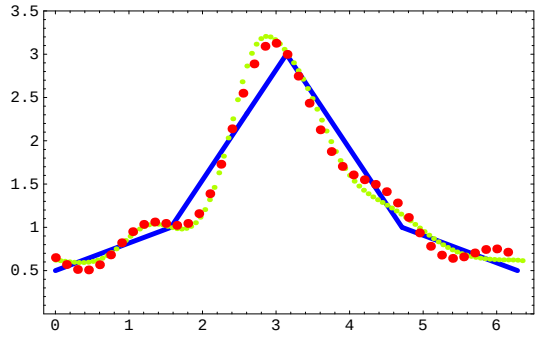

(a) 5 % of noise.

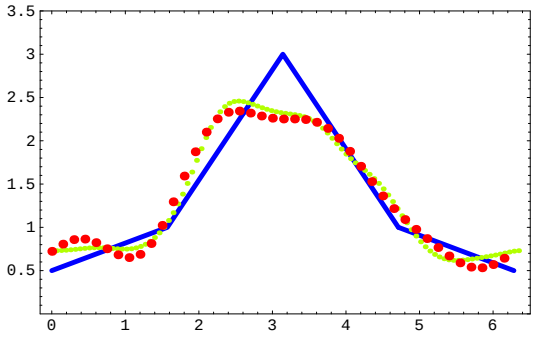

(b) 10 % of noise.

Figure 4.58: Iterative reconstruction of Z_3 in $\mathcal{C}_4$ from noisy boundary data.

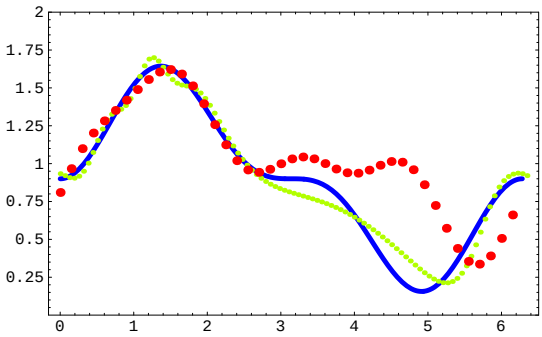

(a) Noise free.

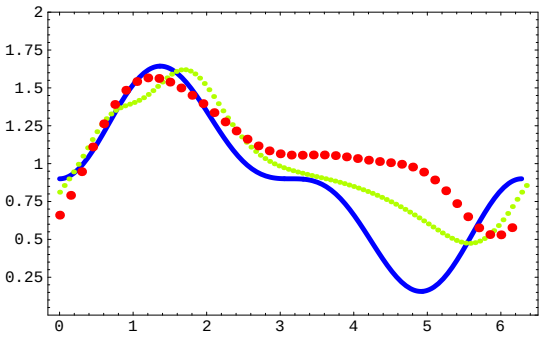

(b) 5 % of noise.

Figure 4.59: Iterative reconstruction of Z_2 in $\mathcal{C}_4$ from data measured on the arc $[0, \pi/2]$.

From the above numerical results we see that the iterative method provides good and stable results. However, no considerable gain was obtained when comparing with the decomposition method.

4.5 Conclusions

In this chapter we presented theoretical results concerning the MFS approximation for both direct and inverse problems. To support the theoretical results for the direct problems several numerical examples were presented for problems $(\mathcal{P}_D)$ and $(\mathcal{P}_R)$. Concerning the inverse geometric and coefficient problems two methods were proposed: A decomposition based method (non iterative) and a Levenberg–Marquardt based method. The proposed non iterative method is simple and requires little computational cost. However, for the geometric problem, it requires some *a priori* knowledge of the location (and di-

mension) of the obstacle. Moreover, some information of the solution's behavior inside Ω has also to be considered in order to apply the proposed method for the non linear part. On the other hand, the iterative method does not require such *a priori* information but the computation cost is bigger. The numerical examples show, as expected, that the iterative method provides better reconstruction results. From these numerical experiences we also observed that the location and dimension of the inclusion can be accurately retrieved (using the iterative method), even from noisy and incomplete boundary data.

For the inverse Robin problem, the numerical examples show the same type of results for both non iterative and iterative approaches. In this case the boundary γ is known hence the decomposition method for this problem is simpler. On the other hand, the numerical results confirms that, as expected, the (exact) information on γ should provide good reconstruction results using this decomposition method.

5

Identification and MFS reconstruction of obstacles - linear elasticity

In this chapter we address the identification and reconstruction of elastic inclusions or cavities inside an elastic body Ω from a single pair of displacement and traction boundary data. Following the electrostatic and thermal models we study an inverse geometric problem consisting in the identification and reconstruction of the inclusion's shape and a coefficient inverse problem which addresses the reconstruction of an elastic exchange coefficient (Robin coefficient). Regarding identification in the geometric inverse problem we refer the early works [20] and [22]. Since then several works for geometric inverse problems in linear elasticity containing reconstruction methods have been presented. It is the case of the reconstruction of elastic inclusions using linear sampling methods (cf. [59]), and level set methods (cf. [18]). Following the Chapter 4, we propose two methods for the reconstruction of the elastic inclusion. A decomposition method based on the MFS approximation for the inverse elastic Cauchy problem and a Quasi Newton optimization method.

Since most of the theory and methodology developed for the Laplace equation is still applicable in the elastic problem, we will mainly give a sketch of the proofs.

5.1 Geometric problem

Consider an isotropic and homogeneous elastic body $\Omega \subset \mathbb{R}^d$ $(d = 2, 3)$ with inclusions or cavities represented by ω. Again, we assume that Ω, ω are open, bounded and simply connected sets such that $\overline{\omega} \subset \Omega$. The boundaries $\Gamma = \partial\Omega$ and $\gamma = \partial\omega$ are C^2 closed curves and the domain of elastic propagation is defined by $\Omega_c := \Omega \setminus \overline{\omega}$.

Consider the following problems

$$\begin{cases} \Delta^* \mathbf{u} = \mathbf{0} & \text{in } \Omega_c \\ \mathbf{u} = \mathbf{g} & \text{on } \partial\Omega = \Gamma \\ \mathcal{B}\mathbf{u} = \mathbf{0} & \text{on } \partial\omega = \gamma \end{cases} \tag{5.1}$$

where $\mathbf{g}$ is given and $\mathcal{B}$ is either the Dirichlet or Neumann boundary operator. Following the notation introduced in Chapter 3 such problems will be denoted by $(\mathcal{P}_D)$ and $(\mathcal{P}_N)$, respectively. Regarding the well posedness of the direct problem we have the next result (see [34] for a proof).

Theorem 5.1 *Given $\mathbf{g} \in \mathbf{H}^{3/2}(\Gamma)$, problems $(\mathcal{P}_D)$ and $(\mathcal{P}_N)$ are well posed with unique solution in $\mathbf{H}^2(\Omega_c)$.*

5.1.1 Inverse problem

In this section we study the elastic geometric inverse problem (**IGP**). As in the scalar case, the problem can be formulated as

(**IGP**): *From a single pair of Cauchy data on $\Sigma \subset \Gamma$, identify the elastic inclusion ω.*

Let $\Sigma \subset \Gamma$ be an open set (in the topology of Γ) and denote by $\mathcal{G}_D(\Sigma)$ and $\mathcal{G}_N(\Sigma)$ the space of compatible Cauchy data for $(\mathcal{P}_D)$ and $(\mathcal{P}_N)$, respectively. To establish the uniqueness of (**IGP**) we start with the vectorial version of Lemma 3.5.

Denote by $\mathcal{R}_\Omega$ the set of rigid displacements, $\mathcal{R}$, in an open connected set Ω. In 2D,

$$\mathcal{R} = \text{span}\{(1,0), (0,1), (-x_2, x_1)\}$$

and in 3D,

$$\mathcal{R} = \text{span}\{(1,0,0), (0,1,0), (0,0,1), (-x_2, x_1, 0), (0, -x_3, x_2), (x_3, 0, -x_1)\}.$$

Lemma 5.2 *Let Ω be an open and connected set with regular boundary $\Gamma = \overline{\Gamma}_0 \cup \overline{\Gamma}_1$ where Γ_0, Γ_1 are open and disjoint. If $\Gamma_0 \neq \emptyset$ then, the mixed problem*

$$\begin{cases} \Delta^* \mathbf{u} = \mathbf{0} & \text{in } \Omega \\ \mathbf{u} = \mathbf{0} & \text{on } \Gamma_0 \\ \partial^*_{\mathbf{n}} \mathbf{u} = \mathbf{0} & \text{on } \Gamma_1 \end{cases} \tag{5.2}$$

has a unique solution in $\mathbf{H}^1(\Omega)$, the null vector. If $\Gamma_0 = \emptyset$, the solutions belong to $\mathcal{R}_\Omega$.

Proof. Since for $\mathbf{u} \in \mathbf{H}^1(\Omega)$

$$\lambda ||\nabla \cdot \mathbf{u}||^2_{L^2(\Omega)} + 2\mu ||\epsilon(\mathbf{u})||^2_{\mathbf{L}^2(\Omega)} = \int_\Gamma \partial^*_{\mathbf{n}} \mathbf{u} \cdot \mathbf{u} d\varsigma - \int_\Omega \Delta^* \mathbf{u} \cdot \mathbf{u} dx$$

then, if $\mathbf{u}$ solves (5.2), the right hand side of the previous equation is null and therefore we must have $||\epsilon(\mathbf{u})||_{\mathbf{L}^2(\Omega)} = 0$. This implies that $\mathbf{u} \in \mathcal{R}_\Omega$. If $\Gamma_0 \neq \emptyset$ then, in 2D, we must have $\mathbf{u} = \mathbf{0}$ in Ω. For the 3D case, since there exists at least three non collinear points on Γ_0 where $\mathbf{u}$ vanishes, the same conclusion holds. □

Theorem 5.3 *If $\mathbf{g}|_\Sigma \notin \mathcal{R}$ then a single pair of compatible data $(\mathbf{g}|_\Sigma, \mathbf{g_n}|_\Sigma)$ determines uniquely ω and*

$$\mathcal{G}^{\mathbf{g}}_D(\Sigma) \cap \mathcal{G}^{\mathbf{g}}_N(\Sigma) = \emptyset.$$

Proof. Consider two (different) domains of elastic propagation with the same exterior boundary Γ. If, for each domain, the solution of $(\mathcal{P}_D)$ or $(\mathcal{P}_N)$ generate the same Neumann data on Σ then, using the same arguments presented in the proof of Theorem 3.6, exists an open and connected set with boundary contained in Γ where one of the solutions must be a rigid displacement. Since this contradicts the hypothesis we conclude that the two domains of elastic propagation must be the same, that is Ω_c. In particular, if $(\mathbf{g}|_\Sigma, \mathbf{g_n}|_\Sigma) \in \mathcal{G}^{\mathbf{g}}_D(\Sigma) \cap \mathcal{G}^{\mathbf{g}}_N(\Sigma)$ then the solution of $(\mathcal{P}_D)$ has null Cauchy data on γ and again we obtain a rigid displacement solution. Since this contradicts the hypothesis, the second part of the result follows. □

5.2 Robin problem

Let Ω_c by a domain of elastic propagation with C^1 boundary $\partial\Omega = \Gamma \cup \gamma$. Consider the following direct problem.

Given an input function $\mathbf{g}$ on Γ, compute $\mathbf{g_n} = \partial^*_{\mathbf{n}}\mathbf{u}$ on Γ, where $\mathbf{u}$ is such that

$$(\mathcal{P}_R) \begin{cases} \Delta^*\mathbf{u} = \mathbf{0} & \text{in } \Omega_c \\ \mathbf{u} = \mathbf{g} & \text{on } \partial\Omega = \Gamma \\ \partial^*_{\mathbf{n}}\mathbf{u} + \mathbf{Z}\mathbf{u} = \mathbf{0} & \text{on } \partial\omega = \gamma \end{cases} \tag{5.3}$$

and $\mathbf{Z}$ is an $L^\infty(\gamma)$ semi positive definite diagonal matrix, ie., $\mathbf{Z} = \text{diag}(z_1, \ldots, z_d)$ with $d = 2, 3$ and each $z_i \in L^\infty(\gamma)$ is non negative.

Theorem 5.4 *If $\mathbf{g} \in \mathbf{H}^{1/2}(\Gamma)$ then $(\mathcal{P}_R)$ is well posed with solution $\mathbf{u} \in \mathbf{H}^1(\Omega_c)$.*

Proof. The bilinear form

$$\langle \mathbf{w}, \mathbf{s} \rangle_{\mathbf{V}} := \int_{\Omega_c} \epsilon(\mathbf{w}) : \epsilon(\mathbf{s}) dx, \ \forall \mathbf{w}, \ \mathbf{s} \in \mathbf{V}$$

defines an inner product in the closed space

$$\mathbf{V} := \left\{ \mathbf{s} \in \mathbf{H}^1(\Omega_c) : \mathbf{s}|_\Gamma = \mathbf{0} \right\}.$$

Endowing this space with the norm induced by the scalar product, we have by Korn's inequality that this norm is equivalent to the norm induced by $\mathbf{H}^1(\Omega_c)$. Thus, the bilinear form on $\mathbf{V} \times \mathbf{V}$

$$S(\mathbf{w}, \mathbf{s}) := \int_{\Omega_c} \sigma(\mathbf{w}) : \epsilon(\mathbf{s}) dx + \int_\gamma \mathbf{Z}\mathbf{w} \cdot \mathbf{s} d\varsigma$$

satisfies

$$S(\mathbf{s}, \mathbf{s}) = \lambda ||\nabla \cdot \mathbf{s}||^2_{L^2(\Omega_c)} + 2\mu ||\mathbf{s}||^2_{\mathbf{V}} + \int_\gamma \mathbf{Z}\mathbf{s} \cdot \mathbf{s} d\varsigma$$

We note that for a diagonal (semi positive definite) matrix $\mathbf{Z}$ we have the relation

$$\mathbf{Z}\mathbf{s} \cdot \mathbf{s} = \mathbf{Z}^{1/2}\mathbf{s} \cdot \mathbf{Z}^{1/2}\mathbf{s} \geq 0$$

whereas for a general semi positive definite matrix, $\mathbf{Z}\mathbf{s} \cdot \mathbf{s}$ may be negative. Thus, the bilinear form S can be written as

$$S(\mathbf{s}, \mathbf{s}) = \lambda ||\nabla \cdot \mathbf{s}||^2_{L^2(\Omega_c)} + 2\mu ||\mathbf{s}||^2_{\mathbf{V}} + ||\mathbf{Z}^{1/2}\mathbf{s}||^2_{L^2(\gamma)} \geq 2\mu ||\mathbf{s}||^2_{\mathbf{V}}$$

that is, S is $\mathbf{V}$-coercive. The result can now be established following the same steps of the proof of Theorem 3.13. □

5.2.1 Inverse Robin problem

Our goal is to identify $\mathbf{Z}$ (assuming that γ is known) from a pair of Cauchy data on $\Sigma \subset \Gamma$. We start with an example that shows that for a general diagonal coefficient this may not be achieved from a single boundary measurement.

Example 5.5 Consider the annular domain of propagation

$$\Omega_c := \left\{ x \in \mathbb{R}^2 : 1 < |x| < r \right\}$$

with $r > 1$ and the function

$$\mathbf{u}(x) = \left(-x_1(\rho + |x|^{-2}), x_2(1 - |x|^{-2}) \right), \quad \rho = \frac{\lambda + 4\mu}{\lambda}. \tag{5.4}$$

This function satisfies, for $\mathbf{g} = \mathbf{u}|_\Gamma$ and $\mathbf{Z}_\psi = \mathrm{diag}(2\mu, \psi)$,

$$\begin{cases} \Delta^* \mathbf{u} = \mathbf{0} & \text{in } \Omega_c \\ \mathbf{u} = \mathbf{g} & \text{in } \Gamma = \partial\Omega \\ \partial^*_{\mathbf{n}} \mathbf{u} + \mathbf{Z}_\psi \mathbf{u} = \mathbf{0} & \text{in } \gamma = \partial\omega \end{cases} .$$

In particular, $\psi > 0$ can not be identified from the single pair of boundary data $(\mathbf{g}, \partial^*_{\mathbf{n}}\mathbf{u})$ on Γ.

Let $\mathcal{G}_R(\Sigma)$ denote the space of compatible Cauchy data on the (relatively) open set $\Sigma \subset \Gamma$ and define the class

$$\mathcal{C} := \left\{ z\mathbb{I} : z \in \mathrm{C}^0(\gamma) \ \wedge \ z \geq 0 \right\}.$$

Theorem 5.6 *If $\mathbf{g}|_\Sigma$ is not the null vector and $\mathbf{Z}$ is known to be in $\mathcal{C}$ then a single pair of data $(\mathbf{g}, \mathbf{g_n}) \in \mathcal{G}_R(\Sigma)$ determines uniquely $\mathbf{Z}$.*

Proof. We follow the proof of the scalar case. Given two coefficients $z_1\mathbb{I}, z_2\mathbb{I} \in \mathcal{C}$ generating the same Cauchy data $(\mathbf{g}, \mathbf{g_n})$ on Σ, exists $\mathbf{u} \in \mathbf{H}^1(\Omega_c)$ solving $(\mathcal{P}_R)$ for both coefficients. In particular, we must have

$$(z_1 - z_2)\mathbf{u} = \mathbf{0} \text{ on } \gamma.$$

Now, if z_1 is not equal to z_2 then, by continuity, there exists a relatively open set $\sigma \subset \gamma$ where z_1 is different from z_2 and, following the scalar case, this contradicts the hypothesis. □

5.3 The MFS approximation for direct problems in linear elasticity

Let $\widehat{\Omega}_c$ be a C^1 artificial domain of propagation containing (the C^1 domain) Ω_c. Consider the single layer representation

$$\mathbf{u} = \mathbf{L}_{\widehat{\Gamma}}\phi + \mathbf{L}_{\widehat{\gamma}}\psi$$

where $\partial\widehat{\Omega}_c = \widehat{\Gamma} \cup \widehat{\gamma}$ is the admissible source set and the densities ϕ and ψ belong to $\mathbf{H}^{-1/2}(\widehat{\Gamma})$ and $\mathbf{H}^{-1/2}(\widehat{\gamma})$, respectively. We define the operator $\mathcal{B} := a\tau_\gamma^{\mathbf{n}} + \mathbf{Z_a}\tau_\gamma$, where $a \in \{0,1\}$ is constant and $\mathbf{Z}_0 = \mathbb{I}$. $\mathbf{Z}_1$ is a semi positive definite diagonal matrix with entries in $L^\infty(\gamma)$. Consider the boundary operator

$$\mathcal{M}(\Gamma,\gamma) : \mathbf{H}^{-1/2}(\widehat{\Gamma}) \times \mathbf{H}^{-1/2}(\widehat{\gamma}) \longrightarrow \mathbf{H}^{1/2}(\Gamma) \times \mathbf{H}^{-1/2}(\gamma)$$

defined as in (4.5). Again we focus on the 2D case and we denote by ${\mathcal{H}_{\mathbf{Z}}}^{1/2}(\Upsilon)$ and ${\mathcal{H}_{\mathbf{Z}}}^{-1/2}(\Upsilon)$ the vectorial versions of the spaces defined on Chapter 4. Thus,

$${\mathcal{H}_{\mathbf{Z}_a}}^{1/2}(\Upsilon) \cong \mathbf{H}^{1/2}(\Upsilon)/\mathbb{R}^{d_{\mathbf{z}_a}},\ {\mathcal{H}_{\mathbf{Z}_a}}^{-1/2}(\Upsilon) \cong \mathbf{H}^{-1/2}(\Upsilon)/\mathbb{R}^{d_{\mathbf{z}_a}}$$

where

$$d_{\mathbf{z}_a} = \begin{cases} 0 & \text{if } \mathbf{Z}_a = \mathbf{0} \\ 1 & \text{if } z_1 = 0 \,\dot{\vee}\, z_2 = 0 \\ 2 & \text{otherwise} \end{cases} .$$

Theorem 5.7 *The restriction of $\mathcal{M}(\Gamma,\gamma)$ to $\mathcal{H}_{\mathbb{I}}^{-1/2}(\widehat{\Gamma}) \times \mathcal{H}_{\mathbb{I}}^{-1/2}(\widehat{\gamma})$ is injective.*

Proof. By hypothesis, the trace operator on $\widehat{\Gamma}$ and the boundary operator $\mathcal{B}$ on $\widehat{\gamma}$ applied to the single layer potential defined on $\partial\Omega_c$ (with densities $\phi \in \mathcal{H}_{\mathbb{I}}^{-1/2}(\widehat{\Gamma})$, $\psi \in \mathcal{H}_{\mathbb{I}}^{-1/2}(\widehat{\gamma})$) is null. Since the asymptotic behavior of this single layer representation is

$$\log|x|\mathbf{c} + \mathbf{O}(1),\ |x| \to \infty$$

with

$$\mathbf{c} = -\frac{\lambda + 3\mu}{4\pi(\lambda + 2\mu)} \left(\int_{\widehat{\Gamma}} \phi d\varsigma + \int_{\widehat{\gamma}} \psi d\varsigma \right) \in \mathbb{R}^2$$

then, by hypothesis, $\mathbf{c} = \mathbf{0}$. Following the proof of Theorem 4.2 we can now establish that this single layer representation must vanish in $\mathbb{R}^2 \setminus \partial\Omega_c$ and we conclude that the densities on such representation are also null. □

Theorem 5.8 *The operator $\mathcal{M}(\Gamma,\gamma)$ has dense range in $\mathcal{H}_{\mathbb{I}}^{1/2}(\Gamma) \times \mathcal{H}_{\mathbf{Z}_a}^{-1/2}(\gamma)$.*

Proof. We prove that the restriction of the adjoint $\mathcal{M}(\Gamma,\gamma)^*$ to $\mathcal{H}_{\mathbb{I}}^{-1/2}(\widehat{\Gamma}) \times \mathcal{H}_{\mathbf{Z}_a}^{1/2}(\widehat{\gamma})$ is injective. Following the proof of Lemma 4.3, the adjoint is given by

$$\mathcal{M}(\Gamma,\gamma)^* = \begin{bmatrix} \mathbf{S}_{\widehat{\Gamma},\Gamma} & a\mathbf{K}_{\widehat{\Gamma},\gamma} + \mathbf{S}_{\widehat{\Gamma},\gamma}\mathbf{Z}_a \\ \mathbf{S}_{\widehat{\gamma},\Gamma} & a\mathbf{K}_{\widehat{\gamma},\gamma} + \mathbf{S}_{\widehat{\Gamma},\gamma}\mathbf{Z}_a \end{bmatrix}.$$

If $(\phi,\psi) \in \mathcal{H}_{\mathbb{I}}^{-1/2}(\widehat{\Gamma}) \times \mathcal{H}_{\mathbf{Z}_a}^{1/2}(\widehat{\gamma})$ are such that $\mathcal{M}(\Gamma,\gamma)^*(\phi,\psi) = \mathbf{0}$ then, defining

$$\mathbf{u} = \mathbf{L}_\Gamma\phi + (a\mathbf{M}_\gamma + \mathbf{L}_\gamma\mathbf{Z}_a)\psi$$

and following the proof of Theorem 4.4 we obtain $\mathbf{u} = \mathbf{0}$ in $\mathbb{R}^2 \setminus (\Gamma \cup \gamma)$. By the jump relations

$$[\mathbf{u}]_\Gamma = \mathbf{0}, \quad [\partial_{\mathbf{n}}^*\mathbf{u}]_\Gamma = \phi, \quad [\mathbf{u}]_\gamma = -a\psi \quad \wedge \quad [\partial_{\mathbf{n}}^*\mathbf{u}]_\gamma = \mathbf{Z}_a\psi$$

we conclude that $\psi = \phi = \mathbf{0}$. □

The remarks 4.5 remain valid for this vectorial boundary value problems. In the next section we give a description of the implementation of the MFS approximation for these problems.

5.3.1 Numerical implementation

Consider the problems

$$(\mathcal{P}) \begin{cases} \Delta^*\mathbf{u} = \mathbf{0} & \text{in } \Omega_c \\ \mathbf{u} = \mathbf{g} & \text{on } \Gamma \\ \mathcal{B}\mathbf{u} = \mathbf{0} & \text{on } \gamma \end{cases} \tag{5.5}$$

where $\mathbf{g} \in \mathbf{H}^{1/2}(\Gamma)$ is given and $\mathcal{B}$ is the boundary operator considered in the previous section. Let

$$\widetilde{\mathbf{u}} = \sum_{j=1}^{m} \mathbf{\Phi}_{y_m}\alpha_j \tag{5.6}$$

where $\alpha_j = (\alpha_{1,j}, \dots \alpha_{d,j}) \in \mathbb{R}^d$ and $y_j \in \widehat{\Gamma} \cup \widehat{\gamma}$.

Theorem 5.9 *The operator $\widetilde{M}(\Gamma,\gamma) : \mathbb{R}^{d\times m} \longrightarrow \mathbf{L}^2(\Gamma) \times \mathbf{L}^2(\gamma)$ defined by*

$$\widetilde{M}(\Gamma,\gamma)(\alpha_1,\dots,\alpha_m) := (\widetilde{\mathbf{u}}|_\Gamma, \mathcal{B}\widetilde{\mathbf{u}})$$

where $\widetilde{\mathbf{u}}$ is given by (5.6) is injective.

Proof. If $(\alpha_1,\dots,\alpha_m) \in \ker \widetilde{\mathcal{M}}(\Gamma,\gamma)$ then $\widetilde{\mathbf{u}}$ solves $(\mathcal{P})$, for $\mathbf{g} = \mathbf{0}$. Since this problem is well posed in $\mathbf{H}^1(\Omega_c)$ then $\mathbf{u} = \mathbf{0}$ in Ω_c and by analytic continuation, $\mathbf{u} = \mathbf{0}$ in the open

set $\mathbb{R}^d \setminus \{y_1, \ldots, y_m\}$. The conclusion follows from the linear independence of the vectors $\{\mathbf{\Phi}_{y_m} e_i\}$. □

Imposing the conditions

$$(\widetilde{\mathbf{u}}(x_i^\Gamma), \mathcal{B}\widetilde{\mathbf{u}}(x_i^\gamma)) = (\mathbf{g}(x_i^\Gamma), \mathbf{0})$$

on some collocation points $x_i^\Gamma \in \Gamma$ and $x_i^\gamma \in \gamma$ we obtain the linear system of equations

$$\mathbb{M}(\Gamma, \gamma)\mathbf{X} = \mathbb{D}(\Gamma, \gamma)$$

which has $d \times n$ equations and $d \times m$ variables where $d = 2, 3$ is the dimension of the space, n the number of collocation points and m the number of source points. When the system is overdetermined (ie., $n > m$) we consider the Tikhonov solution

$$(\mu \mathbb{I} + \mathbb{M}(\Gamma, \gamma)^* \mathbb{M}(\Gamma, \gamma))\, \mathbf{X} = \mathbb{M}(\Gamma, \gamma)^* \mathbb{D}(\Gamma, \gamma)$$

instead.

5.3.2 Numerical simulations

Dirichlet boundary condition

To illustrate the accuracy of the MFS approximation on the boundary $\partial\Omega_c$ for $(\mathcal{P}_D)$ we present three numerical examples. The Lamé constants are $\lambda = \mu = 1$ and the accessible part of the boundary, Γ, is $\partial B(\mathbf{0}, 3.5)$. On this part of the boundary, we consider the input function

$$\mathbf{g}(x) = x.$$

The boundary of the elastic inclusion is given by the parametrization (see Fig. 5.1):

- Example 1:
$$\gamma_1(t) = (1.2 + 0.2\sin^2(2t))(\cos t, \sin t),\ 0 \le t \le 2\pi$$

- Example 2 (bean):
$$\gamma_2(t) = (-1, -1) + \frac{1.4 + 1.3\cos t + 0.1\sin(2t)}{1 + 0.8\cos t}(\cos t, \sin t),\ 0 \le t \le 2\pi$$

- Example 3 (kite):
$$\gamma_3(t) = (-1.2, -0.5) + (-1.1 + 0.9\cos t + 0.3\cos(2t), 1.1\sin t),\ 0 \le t \le 2\pi$$

The MFS approximation was computed considering 1300 equally spaced collocation points $x_1^{\Gamma},\ldots,x_{650}^{\Gamma}\in\Gamma$, $x_1^{\gamma},\ldots,x_{650}^{\gamma}\in\gamma$ and the same amount of source points. The external source points were uniformly distributed on $\widehat{\Gamma}=\partial B(0,4.5)$ and for the internal source points we considered the strategy suggested by (4.16).

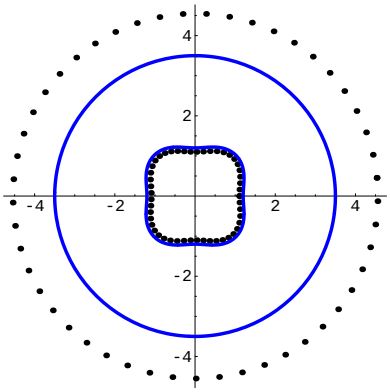

(a) Example 1.

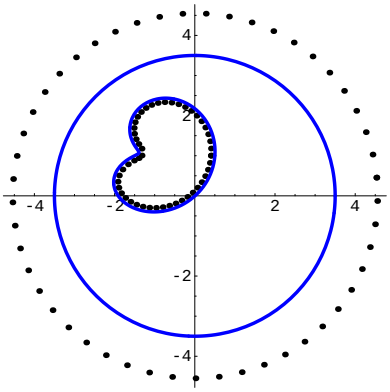

(b) Example 2.

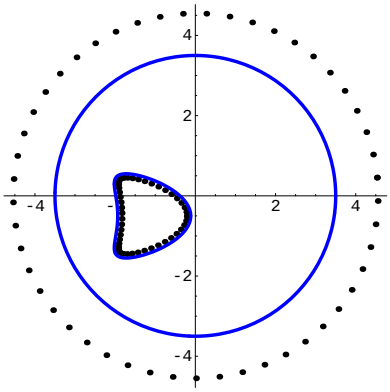

(c) Example 3.

Figure 5.1: Geometry of the domains and distribution of point sources (direct problem).

On Γ we consider the absolute error

$$|\widetilde{u}_i(x)-g_i(x)|,\ x\in\partial\Omega_c,\ i=1,2$$

and on γ,

$$|\widetilde{u}_i(x)|,\ x\in\partial\Omega_c,\ i=1,2$$

where $\widetilde{\mathbf{u}}=(\widetilde{u}_1,\widetilde{u}_2)$ is the approximation given by the MFS.

In Figs. 5.2 and 5.3 we present the absolute error of the approximation, on Γ and γ, respectively. The absolute boundary errors for the bean example can be seen in Figs. 5.4 and 5.5. Figs. 5.6 and 5.7 represent the same for the kite example.

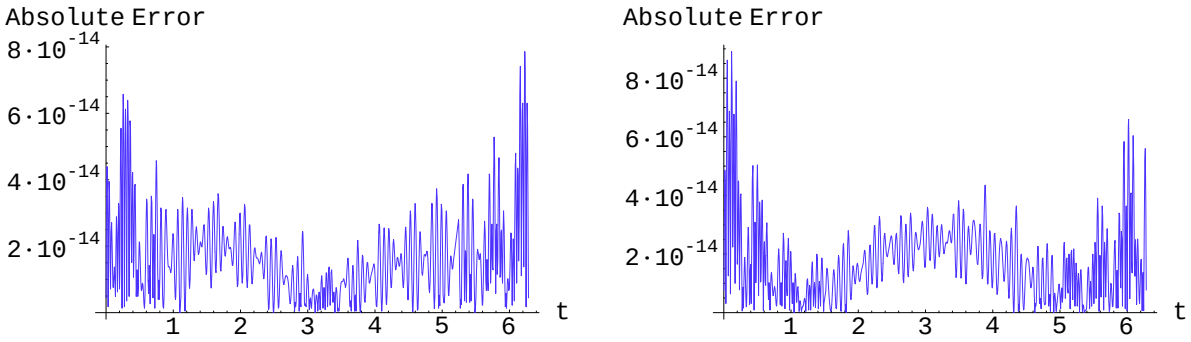

(a) First coordinate. (b) Second coordinate.

Figure 5.2: Absolute error on Γ - First example (direct problem).

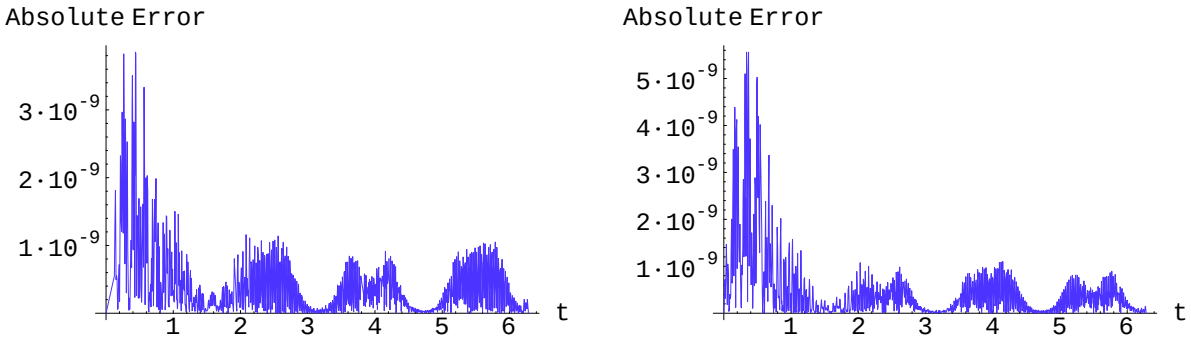

(a) First coordinate. (b) Second coordinate.

Figure 5.3: Absolute error on γ - First example (direct problem).

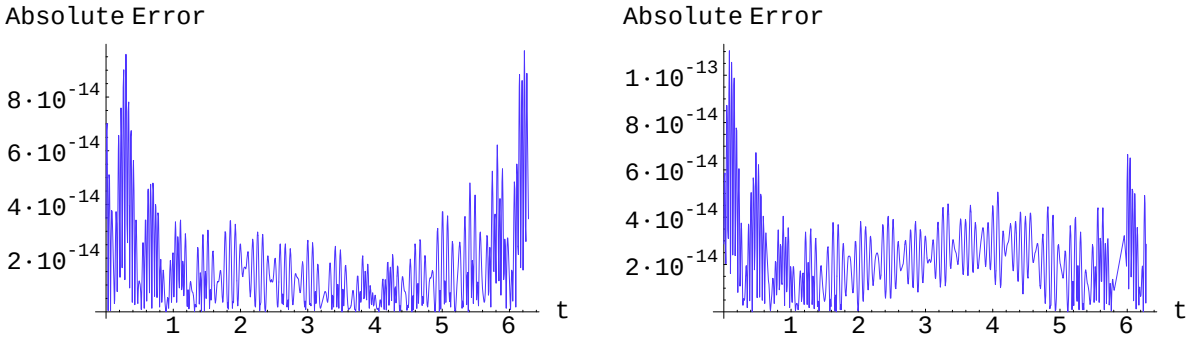

(a) First coordinate. (b) Second coordinate.

Figure 5.4: Absolute error on Γ - Second example (direct problem).

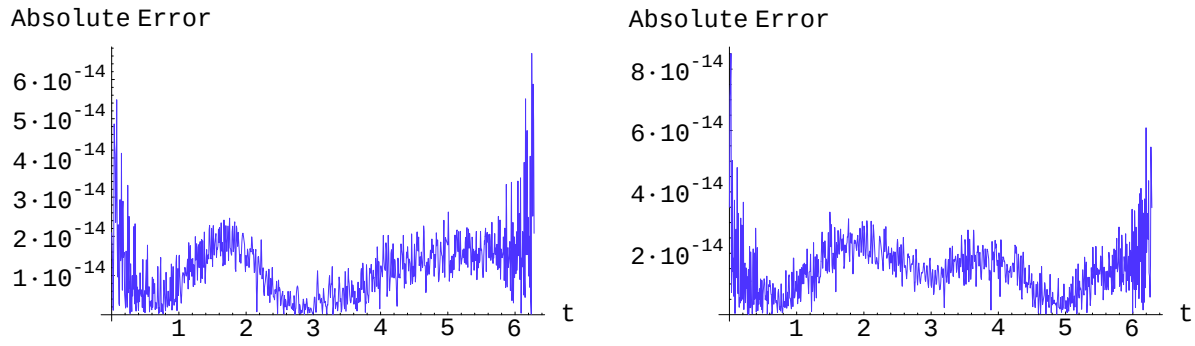

(a) First coordinate. (b) Second coordinate.

Figure 5.5: Absolute error on γ - Second example (direct problem).

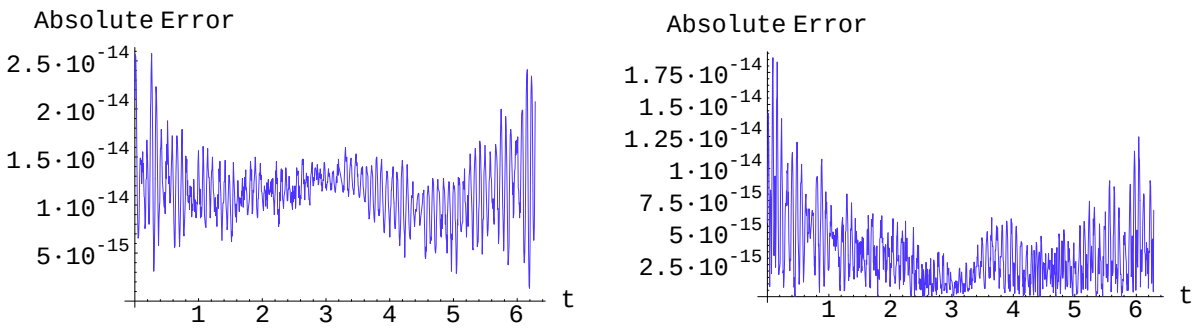

(a) First coordinate. (b) Second coordinate.

Figure 5.6: Absolute error on Γ - Third example (direct problem).

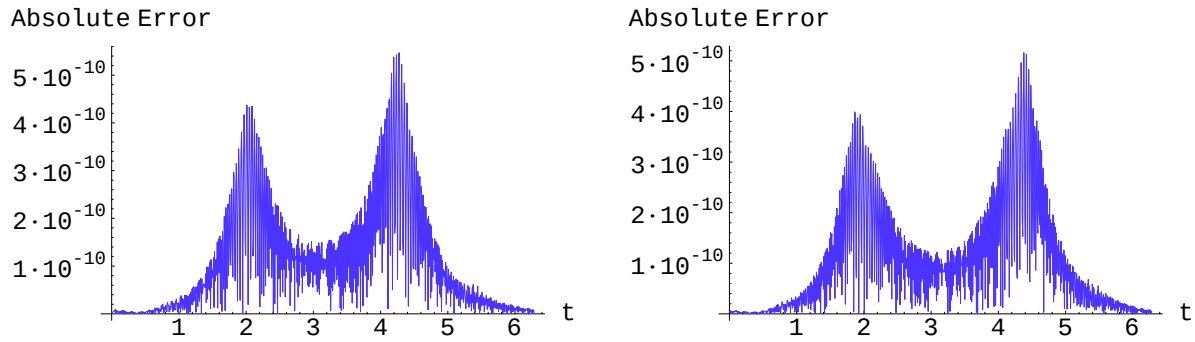

(a) First coordinate. (b) Second coordinate.

Figure 5.7: Absolute error on γ - Third example (direct problem).

Robin boundary condition

Regarding the elastic Robin problem $(\mathcal{P}_R)$ we present two examples. The Lamé constants are $\lambda = \mu = 1$ and the domain of propagation is the annulus

$$\Omega_c = \{x \in \mathbb{R}^2 : \ 1 < |x| < 3.5\}.$$

As admissible source set we considered the boundary of

$$\widehat{\Omega}_c = \{x \in \mathbb{R}^2 : \ 0.8 < |x| < 4.5\}.$$

The Robin coefficients are

- Constant coefficient:
$$\mathbf{Z}_1 = 3\mathbb{I}.$$
- Smooth coefficient:
$$\mathbf{Z}_2 = (0.9 + \sin(2t)\cos^2 t)\mathbb{I}, \ 0 \leq t \leq 2\pi.$$

The input function is $\mathbf{g}(x) = x$ and we used 600 uniformly distributed source and collocation points to compute the MFS approximation. On Γ we consider the absolute error

$$|\widetilde{u}_i(x) - g_i(x)|, \ x \in \Gamma, \ i = 1, 2$$

and on γ,

$$|\partial^*_{\mathbf{n}}\widetilde{\mathbf{u}}(x)_i + \mathbf{Z}\widetilde{u}_i(x)|, \ x \in \gamma, \ i = 1, 2$$

where $\widetilde{\mathbf{u}} = (\widetilde{u}_1, \widetilde{u}_2)$ is the approximation given by the MFS.

Regarding the constant coefficient, the absolute error on Γ is of the order of 10^{-13} (Fig. 5.8) and, on γ, the Robin condition applied to the MFS solution has an (absolute) error of the order of 10^{-12} (Fig. 5.9). For the second example the error on the boundary is higher, as can be seen in Figs. 5.10 and Fig. 5.11.

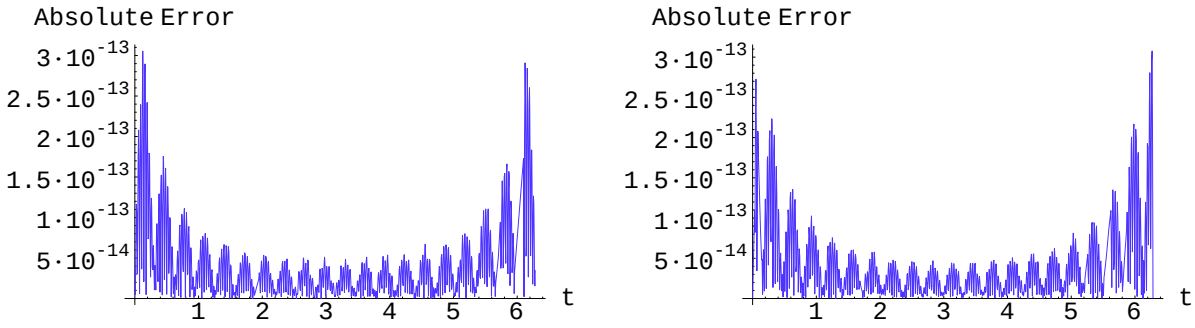

(a) First coordinate (b) Second coordinate

Figure 5.8: Error on Γ - Example 1 (direct problem).

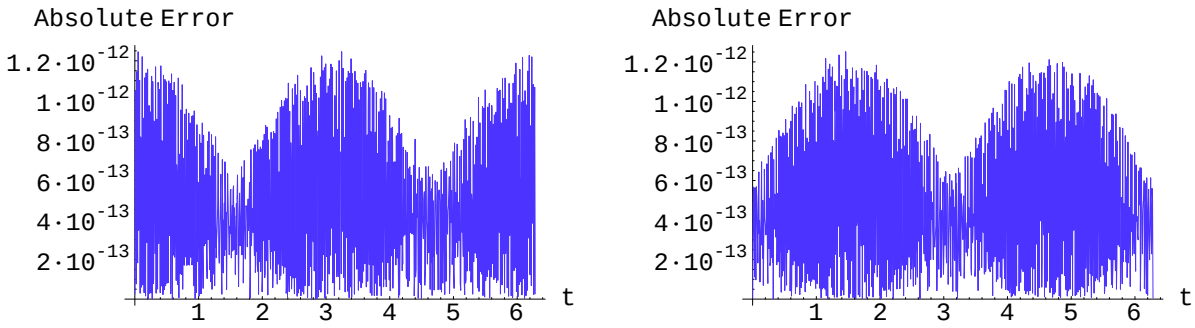

(a) First coordinate (b) Second coordinate

Figure 5.9: Error on γ - Example 1 (direct problem).

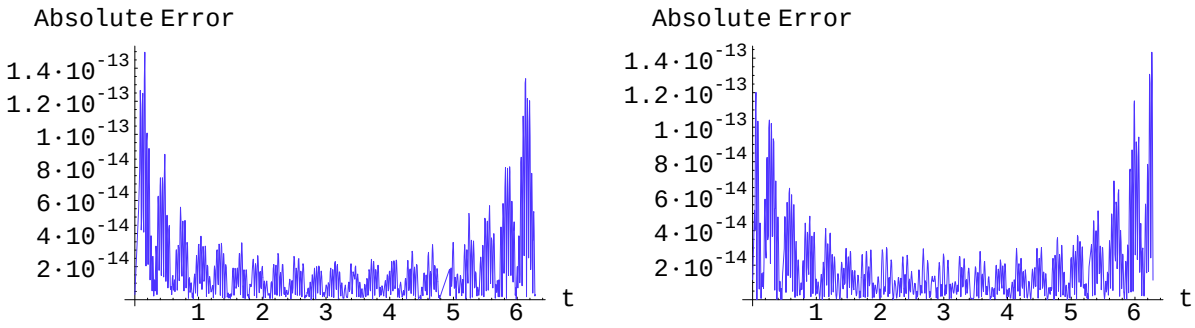

(a) First coordinate (b) Second coordinate

Figure 5.10: Error on Γ - Example 2 (direct problem).

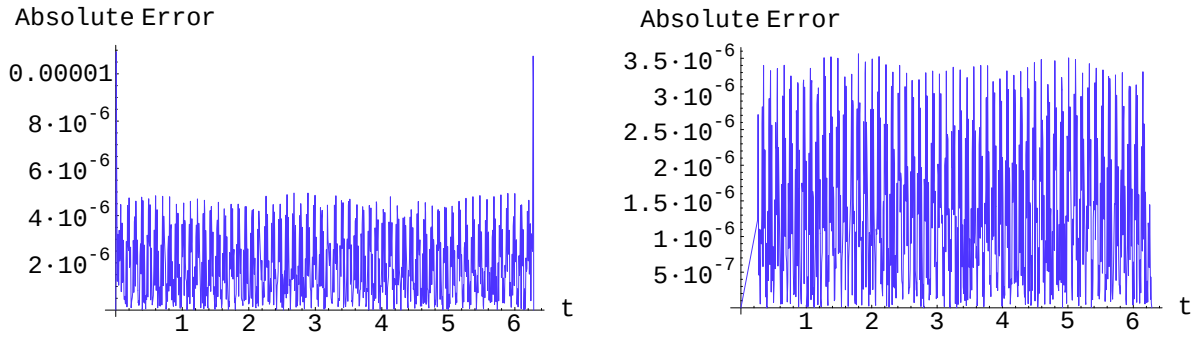

(a) First coordinate (b) Second coordinate

Figure 5.11: Error on γ - Example 2 (direct problem).

5.4 Application of the decomposition method to the elastic geometric inverse problem

In this section we present the adaptation to the elastic case of the decomposition method presented in section 4.2. We recall that the first step of the proposed method consists in fitting the Cauchy data using a single layer potential. We start with some results that justify this (MFS) approximation for the Cauchy problem in linear elasticity.

Let $\mathcal{K}(\Gamma,\Gamma) : \mathbf{H}^{-1/2}(\widehat{\Gamma}) \times \mathbf{H}^{-1/2}(\widehat{\gamma}) \longrightarrow \mathbf{H}^{1/2}(\Gamma) \times \mathbf{H}^{-1/2}(\Gamma)$,

$$\mathcal{K}(\Gamma,\Gamma)(\phi,\psi) := \begin{bmatrix} \mathbf{S}_{\Gamma,\widehat{\Gamma}} & \mathbf{S}_{\Gamma,\widehat{\gamma}} \\ \mathbf{N}_{\Gamma,\widehat{\Gamma}} & \mathbf{N}_{\Gamma,\widehat{\gamma}} \end{bmatrix} \begin{bmatrix} \phi \\ \psi \end{bmatrix}$$

be the trace and normal trace on Γ of the elastic single layer representation

$$\mathbf{u} = \mathbf{L}_{\widehat{\Gamma}}\phi + \mathbf{L}_{\widehat{\gamma}}\psi$$

where $\widehat{\Gamma} \cup \widehat{\gamma}$ is an admissible source set.

The following result is the version of Theorems 4.8 and 4.10 in linear elasticity and can be established using the same analysis of the boundary jumps.

Theorem 5.10 *We have:*

1. *The restriction of* $\mathcal{K}(\Sigma,\Sigma)$ *to* $\mathbf{H}^{-1/2}(\widehat{\Gamma})/\mathbb{R}^2 \times \mathbf{H}^{-1/2}(\widehat{\gamma})/\mathbb{R}^2$ *(*$\mathbf{H}^{-1/2}(\widehat{\Gamma}) \times \mathbf{H}^{1/2}(\widehat{\gamma})$ *in 3D) is injective and*

2. $\mathcal{K}(\Gamma,\Gamma)$ *has dense range in* $\mathbf{H}^{1/2}(\Gamma)/\mathbb{R}^2 \times \mathbf{H}^{-1/2}(\Gamma)$ *(*$\mathbf{H}^{1/2}(\Gamma) \times \mathbf{H}^{-1/2}(\Gamma)$ *in 3D).*

We now consider the discretization of the single layer potential given by

$$\widetilde{\mathbf{u}} = \sum_{j=1}^{m} \mathbf{\Phi}_{y_j} \alpha_j$$

where y_j are source points on $\widehat{\Gamma} \cup \widehat{\gamma}$ and each α_j belongs to $\mathbb{R}^d$. In order to fit the (eventually noisy) Cauchy boundary data $(\mathbf{g}, \mathbf{g_n})$ using this combination of fundamental solutions we compute the coefficients α_j by solving the Tikhonov system

$$(\mu\mathbb{I} + \mathbb{K}(\Gamma,\Gamma)^*\mathbb{K}(\Gamma,\Gamma))\,\mathbf{X} = \mathbb{K}(\Gamma,\Gamma)^*\mathbb{D}^{\mathbf{n}}(\Gamma,\Gamma)$$

with

$$\mathbb{K}(\Gamma,\Gamma) = \begin{bmatrix} \mathbf{\Phi}_{y_1}(x_1) & \cdots & \mathbf{\Phi}_{y_m}(x_1) \\ \cdots & \cdots & \cdots \\ \mathbf{\Phi}_{y_1}(x_n) & \cdots & \mathbf{\Phi}_{y_m}(x_n) \\ \partial^*_{\mathbf{n}}\mathbf{\Phi}_{y_1}(x_1) & \cdots & \partial^*_{\mathbf{n}}\mathbf{\Phi}_{y_m}(x_1) \\ \cdots & \cdots & \cdots \\ \partial^*_{\mathbf{n}}\mathbf{\Phi}_{y_1}(x_n) & \cdots & \partial^*_{\mathbf{n}}\mathbf{\Phi}_{y_m}(x_n) \end{bmatrix},\ \mathbf{X} = [\alpha_j],\ \mathbb{D}^{\mathbf{n}}(\Gamma,\Gamma) = \begin{bmatrix} \mathbf{g}(x_1) \\ \vdots \\ \mathbf{g}(x_n) \\ \mathbf{g_n}(x_1) \\ \vdots \\ \mathbf{g_n}(x_n) \end{bmatrix}$$

for some regularization parameter $\mu > 0$. We consider the external source set $\widehat{\Gamma} = B(\mathbf{0}, 5.5)$ and the internal $\widehat{\gamma} = B(\mathbf{c}, 0.3)$ where $\mathbf{c}$ is such that $\widehat{\gamma} \subset \omega$.

For the second step of the method, we use the same segment search scheme (see Fig. 4.15 , left) for the norm function $|\widetilde{\mathbf{u}}|$ and we stop at the point where the norm is the smallest. It is important to note that, even with a more regular input function $\mathbf{g}$, the inclusion

$$\gamma \subset \mathbf{u}^{-1}(0)$$

is, in general, strict.

5.4.1 Numerical simulations

The following reconstructions concerns the three domains considered in the Dirichlet problem (see section 5.3.1). We considered 120 source points, 60 collocation points and 60 observation points (measured data). As always, the red dots indicates the reconstruction and the full blue line the shape. The dashed black line represents the artificial boundary

$\widehat{\gamma}$.

We start with exact measured data on the whole Γ. For this case we obtained the reconstructions presented in Figs. 5.12, 5.13.

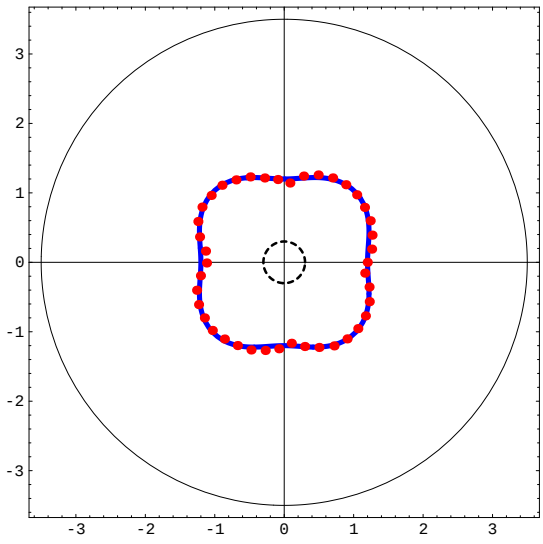

Figure 5.12: Reconstruction of the elastic inclusion for the first example using the decomposition method (noise free data).

We repeated the method for two levels of noise (norm) in the data: 5% and 10 %. For the first example, the regularization parameter was 10^{-5} and 10^{-4} for the levels of 5% and 10% of noise, respectively (Fig. 5.14).

The reconstruction of the bean shaped inclusion (example 2) does not detect the non convexity of the inclusion. Even for 5 % level of noise, the non convex part of the geometry is not retrieved (see Fig. 5.15).

For the kite (example 3) we obtained good results for the first level of noise (Fig. 5.16, left) but for the level of 10 % the reconstruction is worst (Fig. 5.16, right).

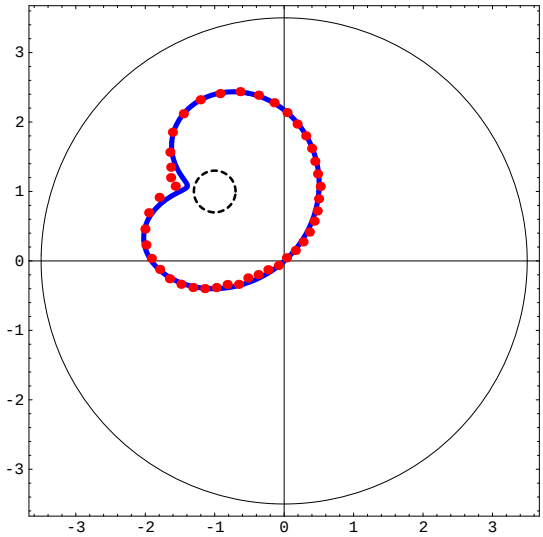

(a) Example 2.

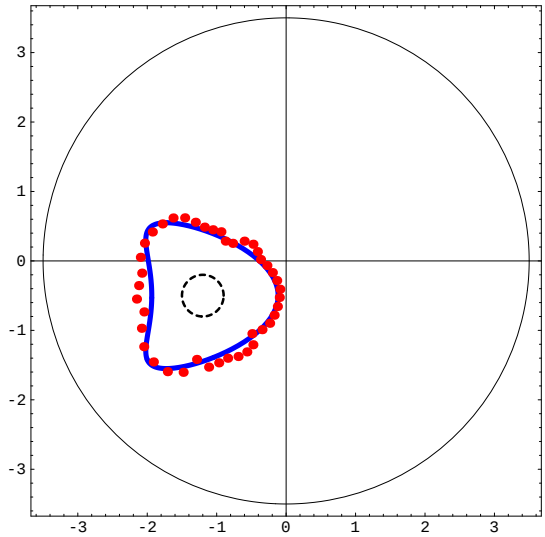

(b) Example 3.

Figure 5.13: Reconstruction of the shape considering noise free data.

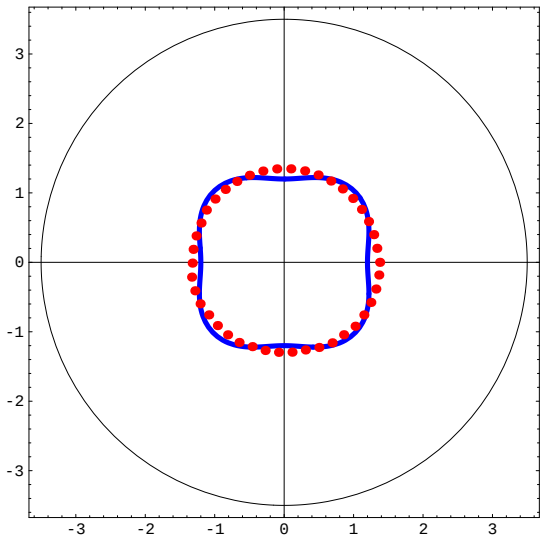

(a) 5% of noise.

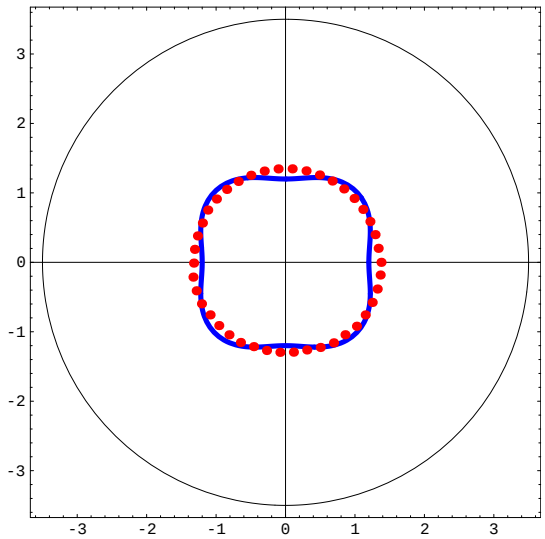

(b) 10% of noise.

Figure 5.14: Reconstruction of γ_1 from noisy data.

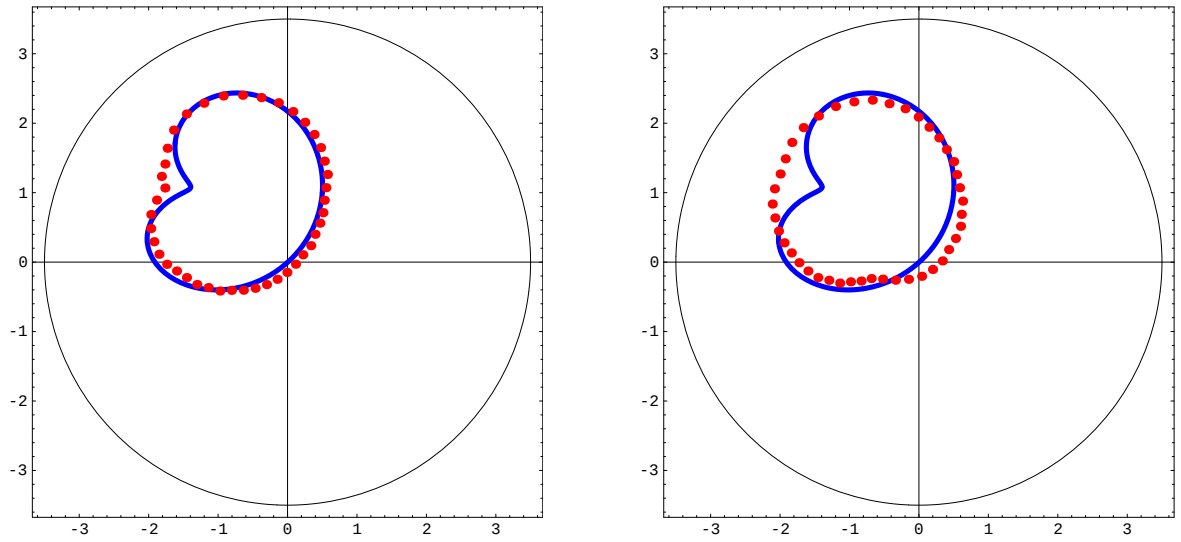

(a) 5% of noise.

(b) 10% of noise.

Figure 5.15: Reconstruction of γ_2 from noisy data.

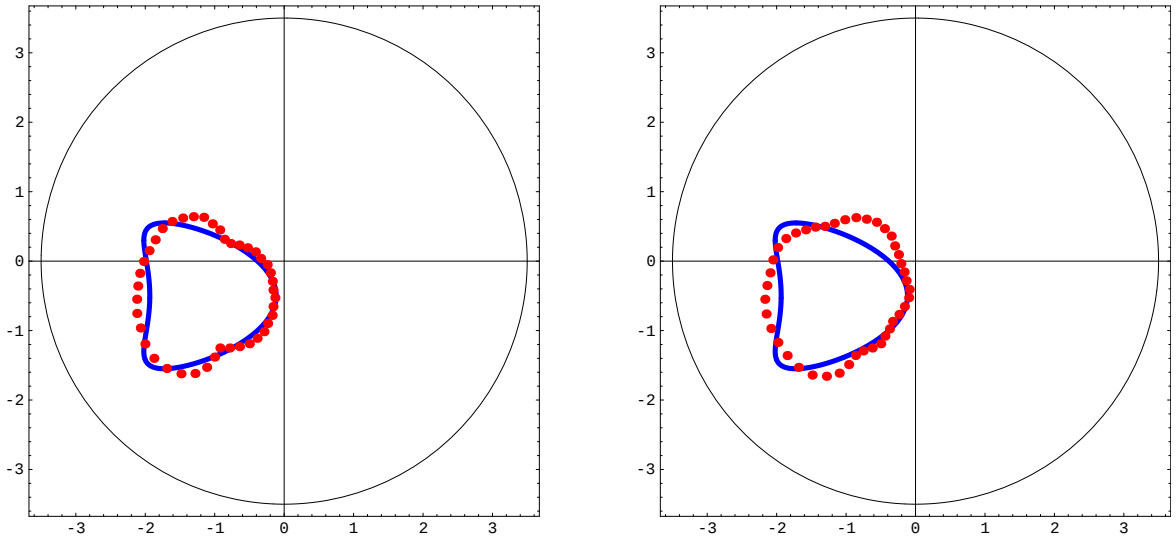

(a) 5% of noise. (b) 10% of noise.

Figure 5.16: Reconstruction of γ_3 from noisy data.

The last simulations concerns the shape reconstruction from partial boundary data. We considered 60 observation points on several parts of the boundary whose location is represented by the green dots on the following graphics. For the bean, we tested the method with boundary data on the arcs $[\pi, 3\pi/2]$ and $[\pi/2, 3\pi/2]$. For the kite, we tested on $[0, \pi/2]$ and $[0, \pi]$. Figs. 5.17, 5.18 show the reconstructions obtained for such examples in the case of exact boundary data. Finally we tested the method to reconstruct the bean shape from (incomplete) data with 5 % of noise (Fig. 5.19).

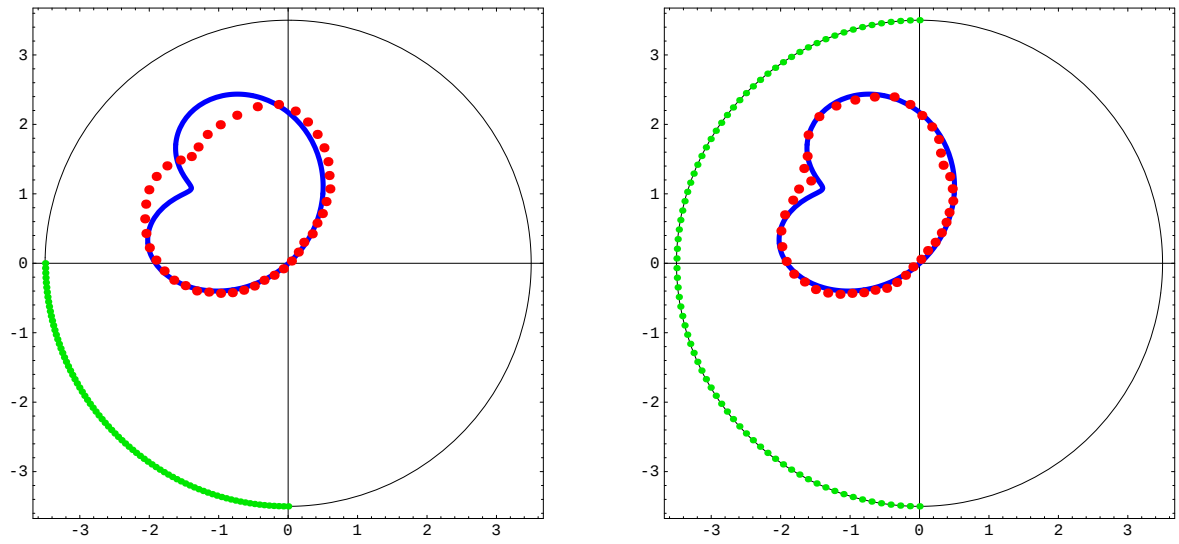

Figure 5.17: Reconstruction of γ_2 from incomplete noise free data.

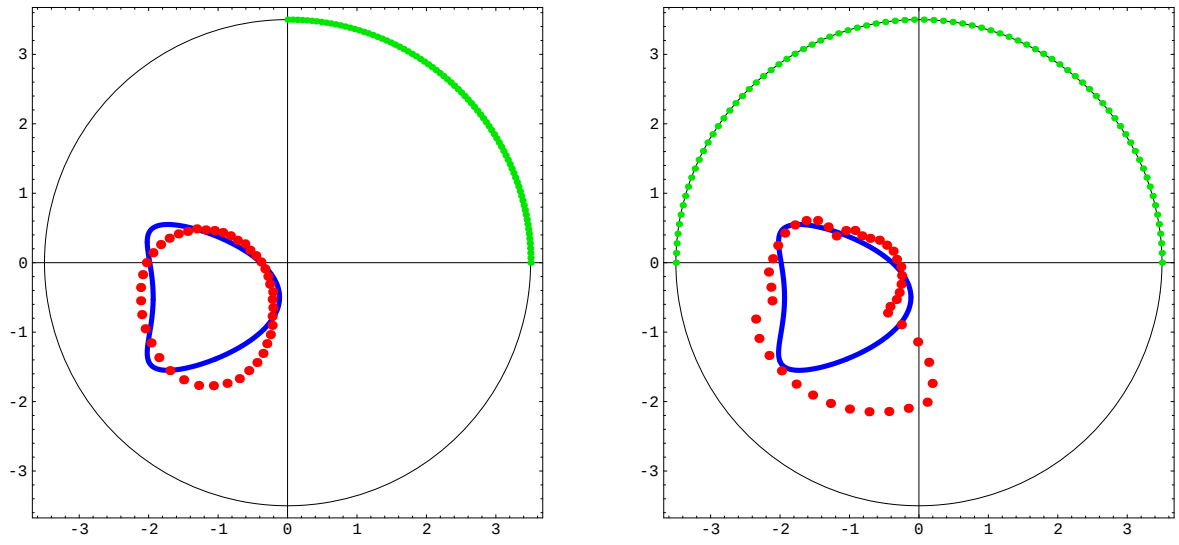

Figure 5.18: Reconstruction of γ_3 from incomplete noise free data.

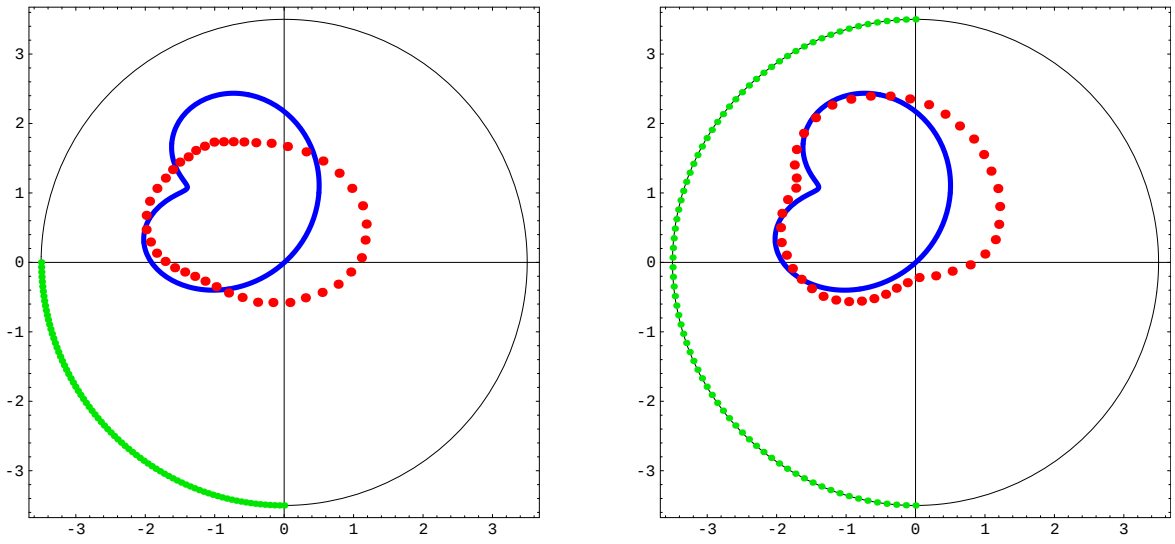

Figure 5.19: Reconstruction of γ_2 from incomplete noisy data (noise level: 5%).

Overall we obtained good and stable results using this decomposition method. Even for incomplete data, we were able to recover some parts of the boundary. As observed in the scalar case, these parts depends on the location of the measurement points. For instance, observation points only on the first quadrant enables an accurate reconstruction of the first quadrant part of the object.

5.5 Application of the optimization method to the elastic geometric problem

In this section we describe the application of the Levenberg–Marquardt method combined with the MFS approximation for direct problems to reconstruct the location and Fourier modes of a given (C^2) elastic inclusion.

Let $\mathbf{F} : \mathcal{C} \longrightarrow \mathbf{H}^{1/2}(\Gamma)$ be the map defined by $\mathbf{F}(\gamma) := \partial^*_{\mathbf{n}}\mathbf{u}$ where $\gamma \in \mathcal{C}$ is an admissible shape and $\mathbf{u}$ is the solution of $(\mathcal{P}_D)$. In this framework, the inverse problem is equivalent to the non linear ill posed equation

$$\mathbf{F}(\gamma) = \mathbf{g_n}.$$

Given an admissible vector field Ψ we have, for small $|\varepsilon|$, the following expansion.

Lemma 5.11 *For a perturbation of the boundary γ given by $\gamma_\varepsilon = \gamma + \varepsilon\Psi(\gamma)$ we have*

$$\mathbf{F}(\gamma_\varepsilon) = \mathbf{F}(\gamma) + \varepsilon\mathbf{F}'(\gamma)\Psi + \varepsilon r(\varepsilon)$$

where $\mathbf{F}'(\gamma)\Psi := \partial^*_{\mathbf{n}}\mathbf{u}' \in \mathbf{H}^{-1/2}(\Gamma)$ and $\mathbf{u}' \in \mathbf{H}^1(\Omega_c)$ is the unique solution of

$$\begin{cases} \Delta^*\mathbf{u}' = \mathbf{0} & \text{in } \Omega_c \\ \mathbf{u}' = \mathbf{0} & \text{on } \Gamma \\ \mathbf{u}' = -\nabla\mathbf{u}\Psi & \text{on } \gamma \end{cases} \tag{5.7}$$

Proof. We use the same change of variables argument of the scalar case and we give just a sketch of the proof.

Let $\widetilde{\mathbf{u}} \in H^2(\Omega)$ be such that $\widetilde{\mathbf{u}} = \mathbf{0}$ in $\mathcal{O}$ and $\widetilde{\mathbf{u}} = \mathbf{g}$ on Γ. We consider $\mathbf{w} := \mathbf{u} - \widetilde{\mathbf{u}}$ and $\mathbf{w}_\varepsilon \in \mathbf{H}^1_0(\Omega^\varepsilon_c)$ the unique solution of $\Delta^*\mathbf{w}_\varepsilon = -\Delta^*\widetilde{\mathbf{u}}$ in Ω^ε_c. In variational terms we have that $\mathbf{w}$ and $\mathbf{w}_\varepsilon$ is the solution of

$$\begin{cases} \text{Find } \mathbf{v} \in \mathbf{H}^1_0(\Omega_c) \text{ such that} \\ \mathbf{S}(\mathbf{v},\mathbf{s}) = -\displaystyle\int_{\Omega_c} \mathrm{Tr}(\sigma(\widetilde{\mathbf{u}})\nabla\mathbf{s})dx, \ \forall \mathbf{s} \in \mathbf{H}^1_0(\Omega_c) \end{cases}$$

and

$$\begin{cases} \text{Find } \mathbf{v}_\varepsilon \in \mathbf{H}^1_0(\Omega^\varepsilon_c) \text{ such that} \\ \mathbf{S}_\varepsilon(\mathbf{v}_\varepsilon,\mathbf{s}_\varepsilon) = -\displaystyle\int_{\Omega^\varepsilon_c} \mathrm{Tr}(\sigma(\widetilde{\mathbf{u}})\nabla\mathbf{s}_\varepsilon)dy, \ \forall \mathbf{s}_\varepsilon \in \mathbf{H}^1_0(\Omega^\varepsilon_c) \end{cases}$$

respectively, where

$$\mathbf{S}(\mathbf{v},\mathbf{s}) := \int_{\Omega_c} \mathrm{Tr}(\sigma(\mathbf{v})\nabla\mathbf{s})dx,$$

$$\mathbf{S}_\varepsilon(\mathbf{v}_\varepsilon,\mathbf{s}) := \int_{\Omega^\varepsilon_c} \mathrm{Tr}(\sigma(\mathbf{v}_\varepsilon)\nabla\mathbf{s}_\varepsilon)dy$$

and Tr denotes the trace of a matrix. Considering the change of variables $y = \Psi_\varepsilon(x)$ we obtain

$$\mathbf{S}_\varepsilon(\mathbf{w}_\varepsilon,\mathbf{s}) = \int_{\Omega^\varepsilon_c = {\Psi_\varepsilon}^{-1}(\Omega^\varepsilon_c)} \mathrm{Tr}(\sigma(\mathbf{w}_\varepsilon\circ\Psi_\varepsilon)\nabla(\mathbf{s}_\varepsilon\circ\Psi_\varepsilon))|\mathrm{det}J_{\Psi_\varepsilon}|dx$$

and

$$\int_{\Omega^\varepsilon_c} \mathrm{Tr}(\sigma(\widetilde{\mathbf{u}})\nabla\mathbf{s}_\varepsilon)dy = \int_{\Omega^\varepsilon_c = {\Psi_\varepsilon}^{-1}(\Omega^\varepsilon_c)} \mathrm{Tr}(\sigma(\mathbf{u}\circ\Psi_\varepsilon)\nabla(\mathbf{s}_\varepsilon\circ\Psi_\varepsilon))|\mathrm{det}J_{\Psi_\varepsilon}|dx.$$

Using the expansions for J_{Ψ_ε}, $J_{\Psi_\varepsilon}^{-1}$ and $|\det\Psi_\varepsilon|$ in the previous equations we obtain (see [70])

$$\mathbf{S}(\mathbf{w}^\varepsilon - \mathbf{w}, \mathbf{v}) = \varepsilon \int_{\Omega_c} \mathrm{Tr}(\sigma(\nabla(\mathbf{w}^\varepsilon + \widetilde{\mathbf{u}})\Psi)\nabla\mathbf{v})dx + \mathbf{O}(\varepsilon^2),\ \forall \mathbf{v} \in \mathbf{H}_0^1(\Omega_c)$$

from where it follows that $\mathbf{F}'(\gamma)\Psi = \partial_{\mathbf{n}}^* \mathbf{w}^*|_\Gamma$ where $w^* \in \mathbf{H}_0^1(\Omega_c)$ is the unique solution of the variational problem

$$\begin{cases} \text{Find } \mathbf{v} \in \mathbf{H}_0^1(\Omega_c) \text{ such that} \\ \mathbf{S}(\mathbf{v}, \mathbf{s}) = \int_{\Omega_c} \mathrm{Tr}(\sigma(\nabla(\mathbf{w} + \widetilde{\mathbf{u}})\Psi)\nabla\mathbf{s})dx,\ \forall \mathbf{s} \in \mathbf{H}_0^1(\Omega_c) \end{cases}.$$

Since $\mathbf{u} = \mathbf{w} + \widetilde{\mathbf{u}}$ then, the directional derivative $F'(\gamma)\Psi$ is the normal trace on Γ of

$$\mathbf{u}' := \mathbf{w}^* - \nabla\mathbf{u}\Psi \in \mathbf{H}^1(\Omega_c)$$

and this is the unique solution of (5.7). □

To apply the Levenberg-Marquardt method we consider the set of admissible shapes

$$\mathcal{C}_N = \{r_\alpha(t)(\cos t, \sin t) + (a, b) \in \Omega : r_\alpha > 0,\ t \in [0, 2\pi]\}$$

and vector fields

$$\Psi_{ad}^N = \{r_\alpha(t)(\cos t, \sin t) + (a, b),\ t \in [0, 2\pi]\}$$

where, for $\alpha = (\alpha_0, \ldots, \alpha_N)$, $r_\alpha(t) = \alpha_0 + \sum_{j=1}^N \alpha_j \cos(jt) + \sum_{j=1}^N \alpha_{j+N} \sin(jt)$. The objective function F_{obj} is given by

$$F_{obj}(a, b, \alpha) = \frac{1}{2}|\mathbf{F}(a, b, \alpha) - \mathfrak{m}|^2$$

where $\mathfrak{m}$ is the vector of measured data on some observation points $x_j \in \Gamma$, $\mathbf{F}(a, b, \alpha)$ is the vector with entries $F_i(a, b, \alpha) := \partial_{\mathbf{n}}^* \mathbf{u}_{(a,b,\alpha)}(x_i)$ and $\mathbf{u}_{a,b,\alpha}$ solves

$$\begin{cases} \Delta^* \mathbf{u}_{a,b,\alpha} = 0 & \text{in } \Omega_c^{a,b,\alpha} \\ \mathbf{u}_{a,b,\alpha} = \mathbf{g} & \text{on } \Gamma \\ \mathbf{u}_{a,b,\alpha} = \mathbf{0} & \text{on } \gamma_{a,b,\alpha} \end{cases}.$$

The boundary $\gamma_{a,b,\alpha}$ is parameterized by $r_\alpha(t)(\cos t, \sin t) + (a, b) \in \mathcal{C}_N$. The update step $\Psi_{(a_1,b_1,\alpha_s)} \in \Psi_{ad}^N$ is given by

$$(\mu\mathbb{I} + \mathbb{J}^\top(a, b, \alpha)\mathbb{J}(a, b, \alpha))(a_1, b_1, \alpha_s) = -\mathbb{J}^\top(a, b, \alpha)(\mathbf{F}_j(a, b, \alpha) - \mathfrak{m}_j)_j$$

where

$$\mathbb{J}(a,b,\alpha) = \left[\partial^*_{\mathbf{n}}\mathbf{u}'_j(x_i)\right]_{i,j}$$

and

$$\begin{cases} \Delta^*\mathbf{u}'_j = 0 & \text{in } \Omega_c^{a,b,\alpha} \\ \mathbf{u}'_j = \mathbf{0} & \text{on } \Gamma \\ \mathbf{u}'_j = -\nabla\mathbf{u}_{a,b,\alpha}\Psi_{e_j} & \text{on } \gamma_{a,b,\alpha} \end{cases}$$

with e_j the jth vector of the standard basis of $\mathbb{R}^{2N+3}$.

At each step of the minimization method we have $2N+4$ direct problems to solve and we use the approximation given by the MFS. Regarding the regularization parameter $\mu > 0$ we follow the strategy applied for the scalar case (see remark 4.19).

5.5.1 Numerical simulations

We test the proposed iterative method with the four examples considered for the decomposition method. Each direct problem is numerically solved with the approximation given by the MFS. We consider $\widehat{\Gamma} = \partial B(\mathbf{0}, 5.5)$ as exterior artificial boundary and the internal artificial curve is a reduction of the internal boundary by a factor of 0.9. The number of collocation and source points for the numerical implementation of the MFS is 120.

The initial shape is $\gamma^{(0)} = \partial B(\mathbf{0}, 1)$ and the first iterations are computed in $\mathcal{C}_0$ until the stopping criterion (which is the same used for the scalar case) is reached. The process is continued in $\mathcal{C}_4$.

We used the same representation scheme (dots, dashed lines, colors) in the following plots. The first plots concerns noise free measurements on the whole Γ.

For the reconstruction of the first shape, we computed 3 iterations in $\mathcal{C}_0$ and we obtained the location and dimension of the object (Fig. 5.20, left). The shape was perfectly recovered in $\mathcal{C}_4$ with 5 iterations (Fig. 5.20, right).

Regarding the reconstruction of the bean we obtained the location with 5 iterations in $\mathcal{C}_0$ and the reconstruction of the shape with 8 iterations in $\mathcal{C}_4$ (Fig. 5.21).

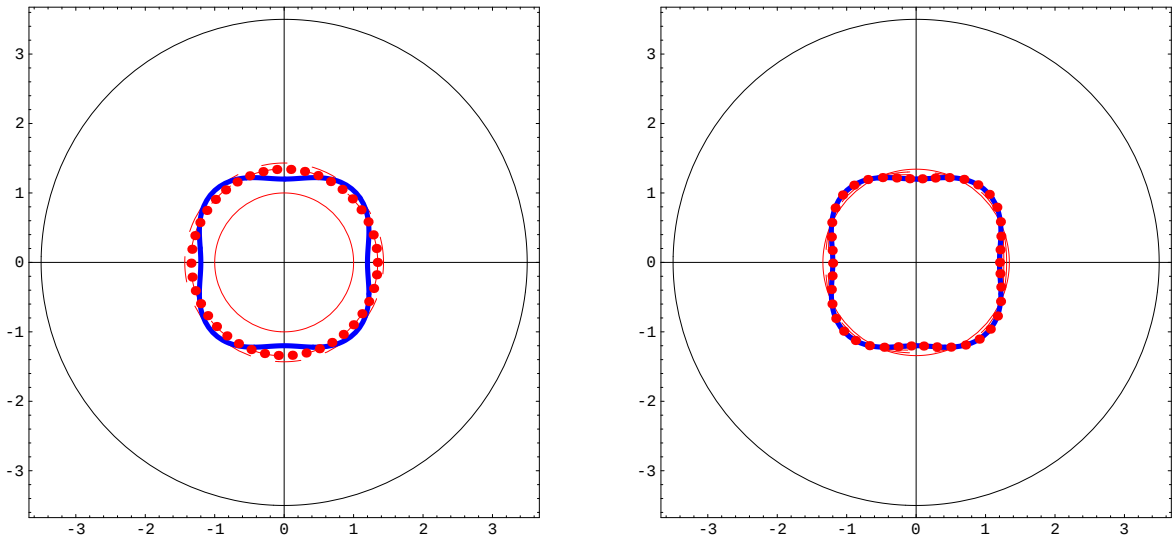

Figure 5.20: Reconstruction of γ_1 in $\mathcal{C}_0$ (left) and $\mathcal{C}_4$ (right) from data without noise.

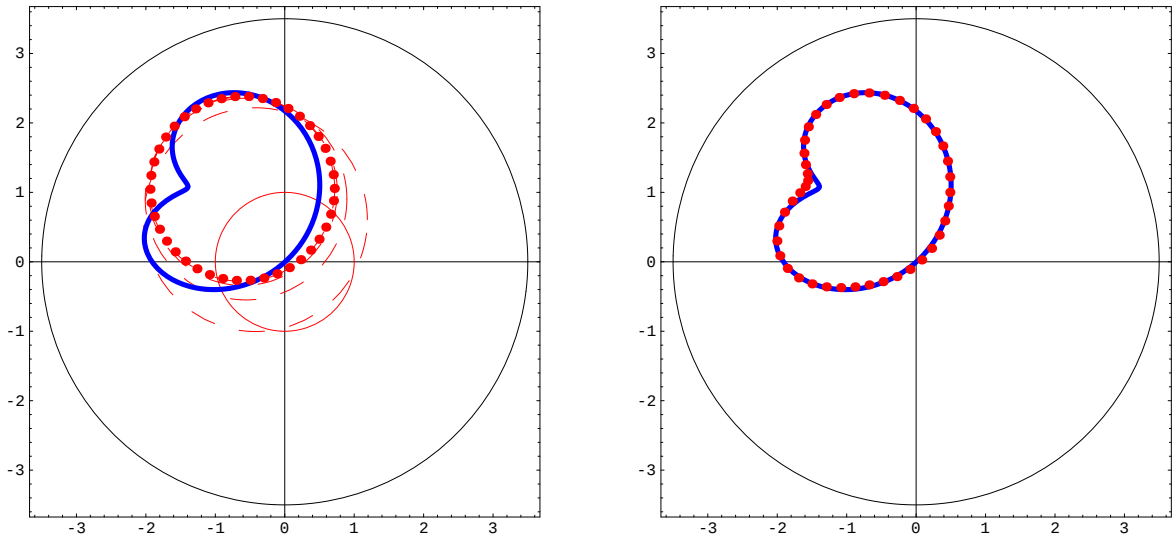

Figure 5.21: Reconstruction of γ_2 in $\mathcal{C}_0$ (left) and $\mathcal{C}_4$ (right) from data without noise.

For the kite it took 4 iterations in $\mathcal{C}_0$ to detect the location and also 4 for the shape reconstruction (Fig. 5.22).

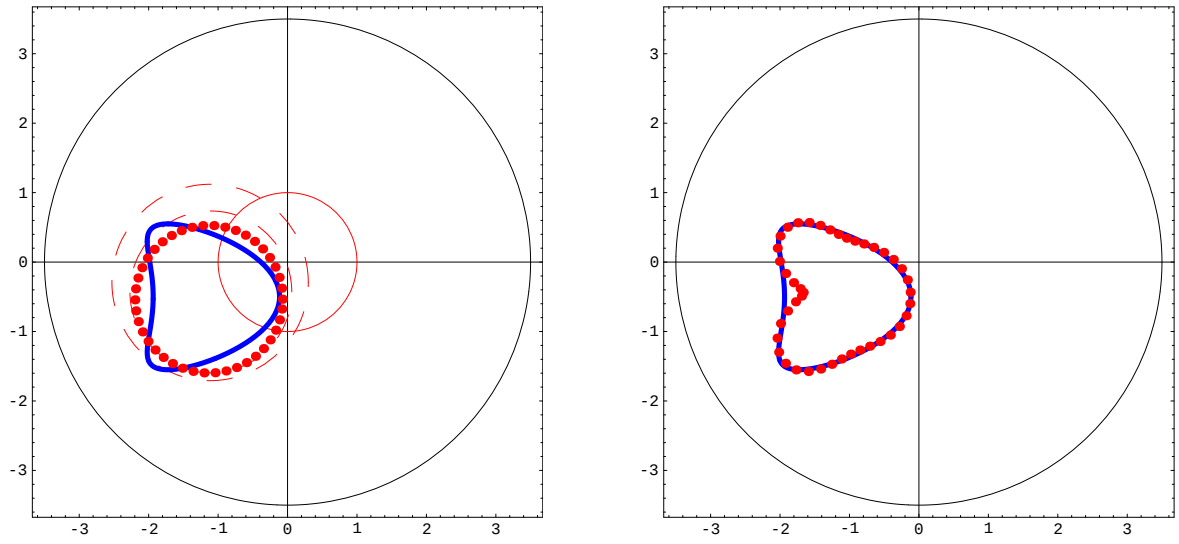

Figure 5.22: Reconstruction of γ_3 in $\mathcal{C}_0$ (left) and $\mathcal{C}_4$ (right) from data without noise.

We now compare the results of both methods for noisy data. The reconstructions obtained with the decomposition method are represented by green dotted lines and for the iterative we use red dotted lines.

For the levels of 5% and 10 % of noise we were able to retrieve the location and dimension of ω_1 with 3 iterations in $\mathcal{C}_0$ (left plots of Figs. 5.23, 5.24). For the reconstruction of the shape in $\mathcal{C}_4$ we computed 3 iterations for both levels of noise (right plots of Figs. 5.23, 5.24).

In Figs. 5.25 and 5.26 we plotted the reconstruction of the bean shaped inclusion for the considered levels of noise. In both situations we computed 4 iterations in $\mathcal{C}_0$. For the approximation of the shape in $\mathcal{C}_4$, 3 and 4 iterations were computed for 5% and 10% of noise, respectively.

For the kite we plotted the same tests in Figs. 5.27 and 5.28. In this case 4 iterations were computed in $\mathcal{C}_0$ and in $\mathcal{C}_4$ for both levels of noise.

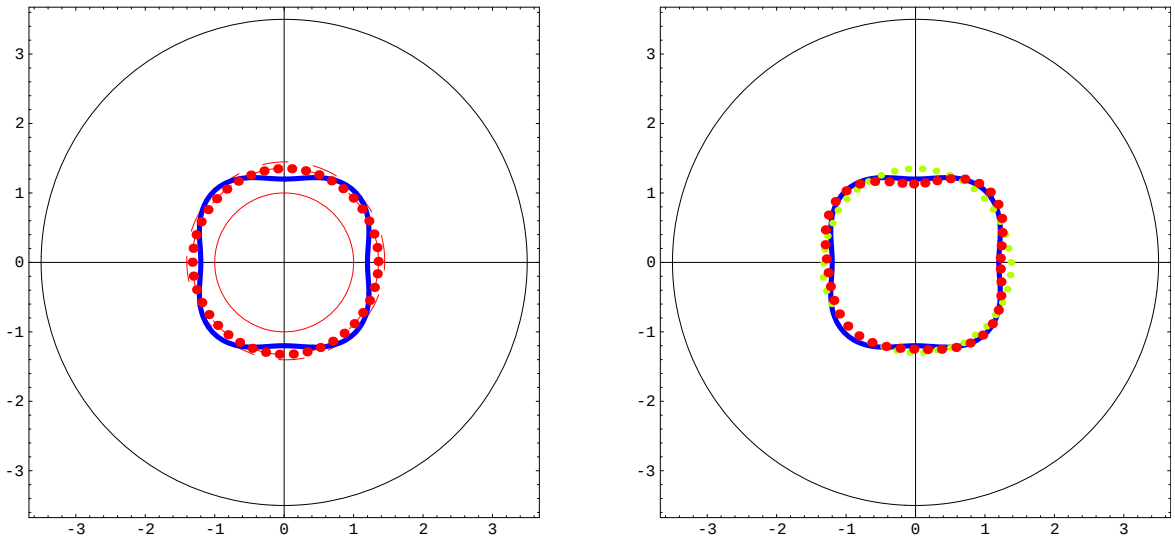

Figure 5.23: Reconstruction of γ_1 in $\mathcal{C}_0$ (left) and $\mathcal{C}_4$ (right) from data with 5% of noise.

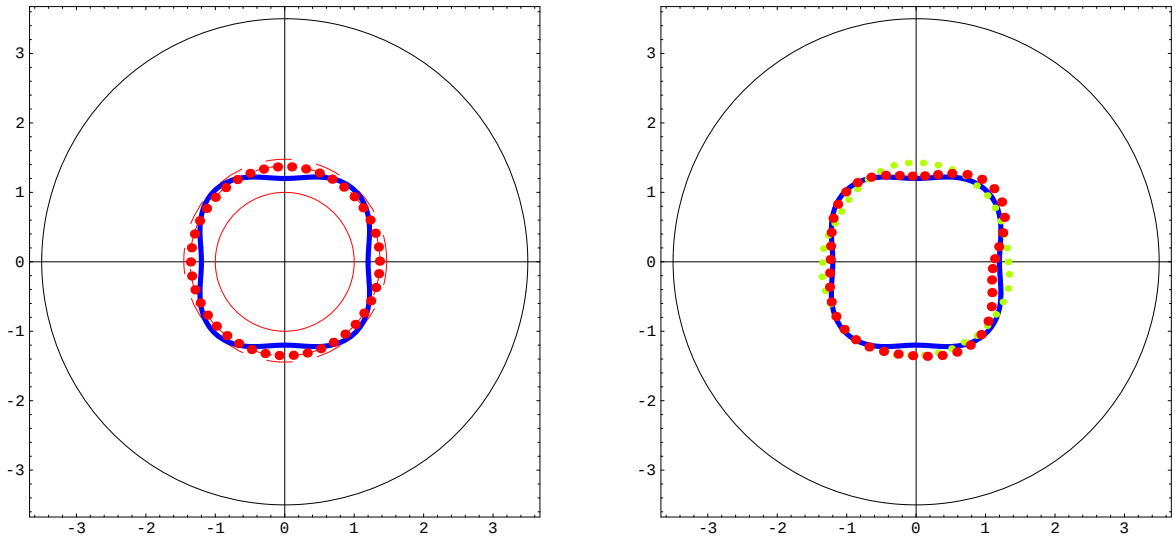

Figure 5.24: Reconstruction of γ_1 in $\mathcal{C}_0$ (left) and $\mathcal{C}_4$ (right) from data with 10% of noise.

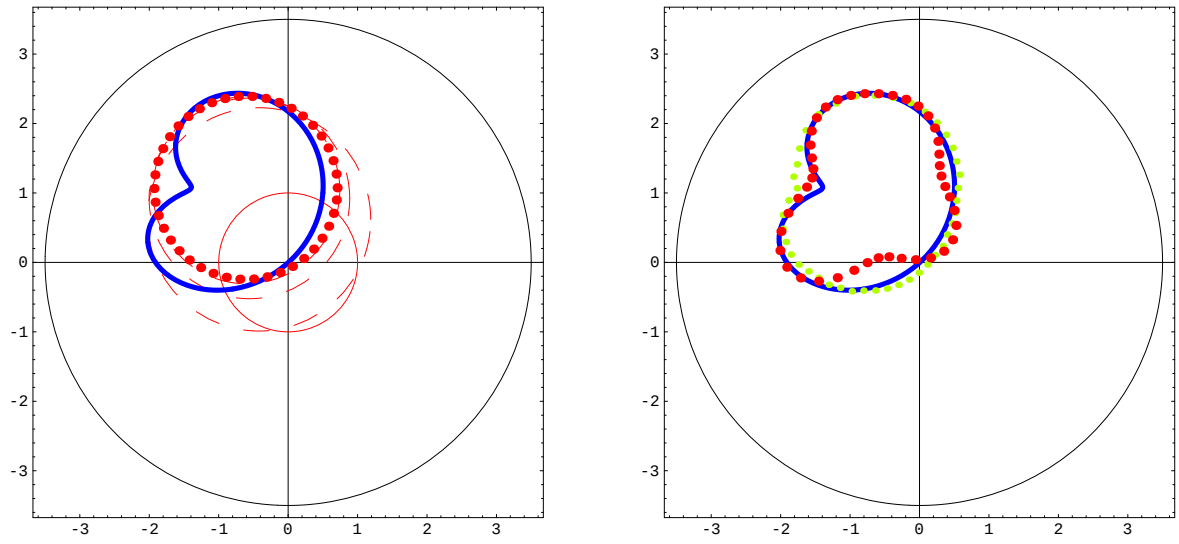

Figure 5.25: Reconstruction of γ_2 in $\mathcal{C}_0$ (left) and $\mathcal{C}_4$ (right) from data with 5% of noise.

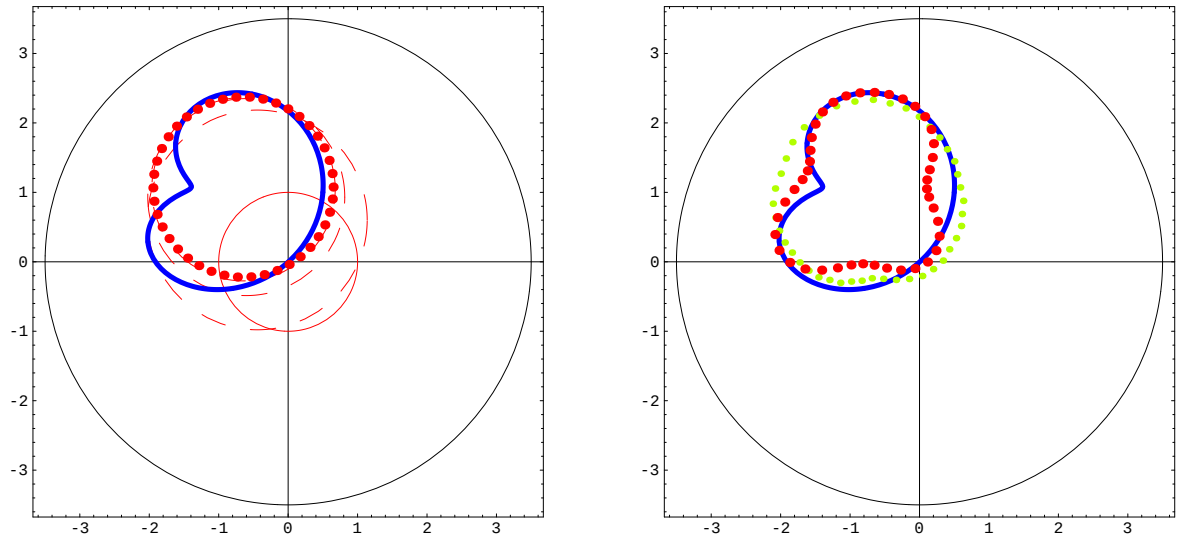

Figure 5.26: Reconstruction of γ_2 in $\mathcal{C}_0$ (left) and $\mathcal{C}_4$ (right) from data with 10% of noise.

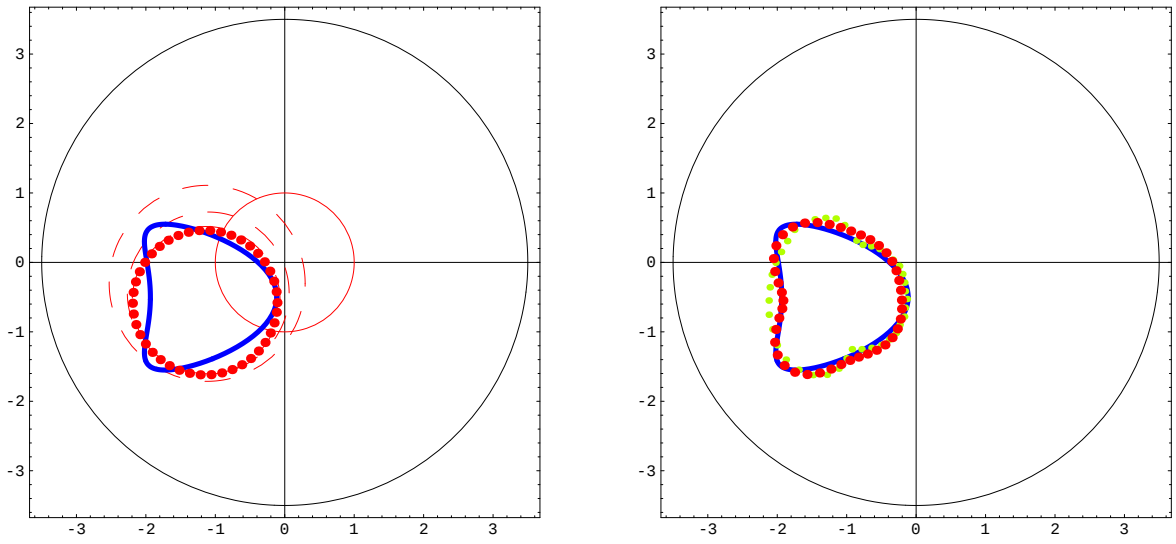

Figure 5.27: Reconstruction of γ_3 in $\mathcal{C}_0$ (left) and $\mathcal{C}_4$ (right) from data with 5% of noise.

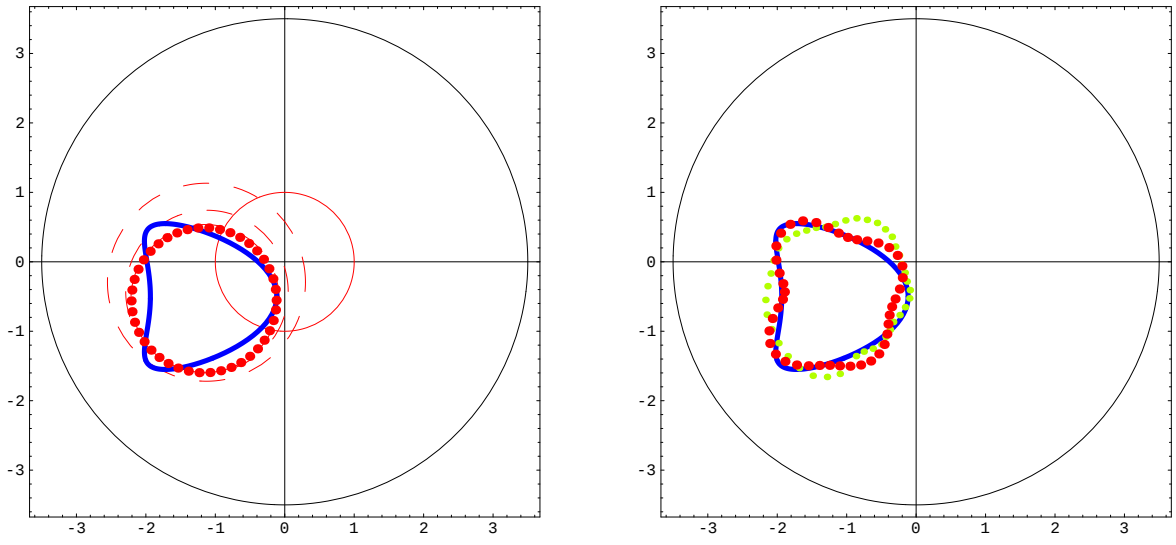

Figure 5.28: Reconstruction of γ_3 in $\mathcal{C}_0$ (left) and $\mathcal{C}_4$ (right) from data with 10% of noise.

The last tests concerns the comparison between the two methods for data measured on part of the boundary Γ. Starting with exact data, we first consider the bean reconstruction example from 60 uniformly distributed observations on $[\pi, 3\pi/2]$. In absence of noise, we obtained the results presented in Fig. 5.29 where 4 iterations were computed in both $\mathcal{C}_0$ and $\mathcal{C}_4$. Considering observation points on $[\pi/2, 3\pi/2]$ we computed 5 and 10 iterations in $\mathcal{C}_0$ and $\mathcal{C}_4$, respectively (Fig. 5.30).

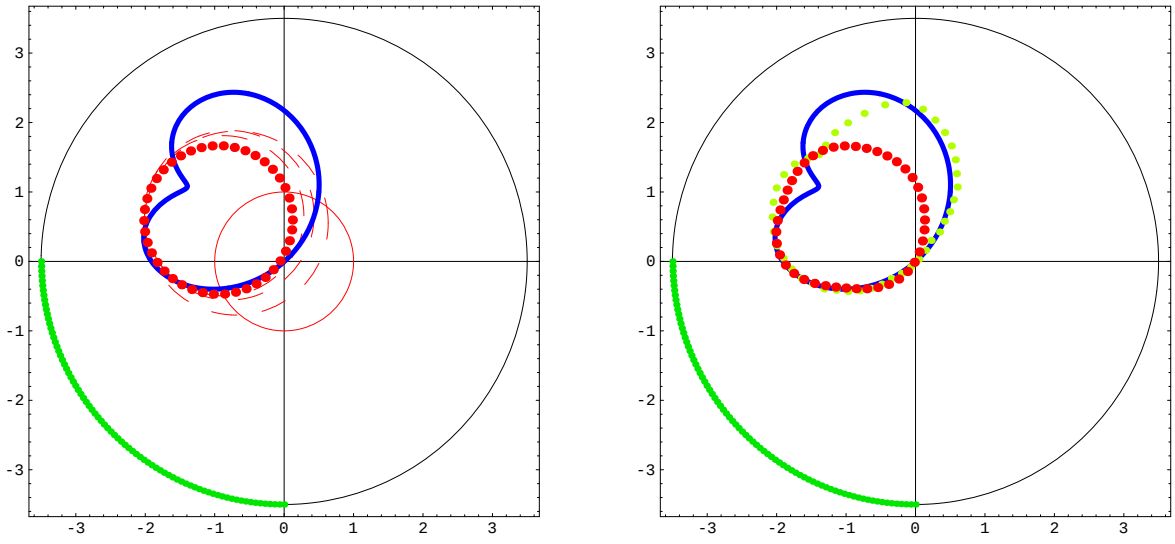

Figure 5.29: Reconstruction of γ_2 in $\mathcal{C}_0$ (left) and $\mathcal{C}_4$ (right) from incomplete noise free data.

For the kite, the observations points were on $[0, \pi/2]$ and $[\pi/2, 3\pi/2]$. Figs. 5.31 and 5.32 shows the results of the reconstructions on $\mathcal{C}_0$ and $\mathcal{C}_4$.

The last two plots (Figs. 5.33 and 5.34) compares the results of the bean shape reconstruction from incomplete data with 5% of noise.

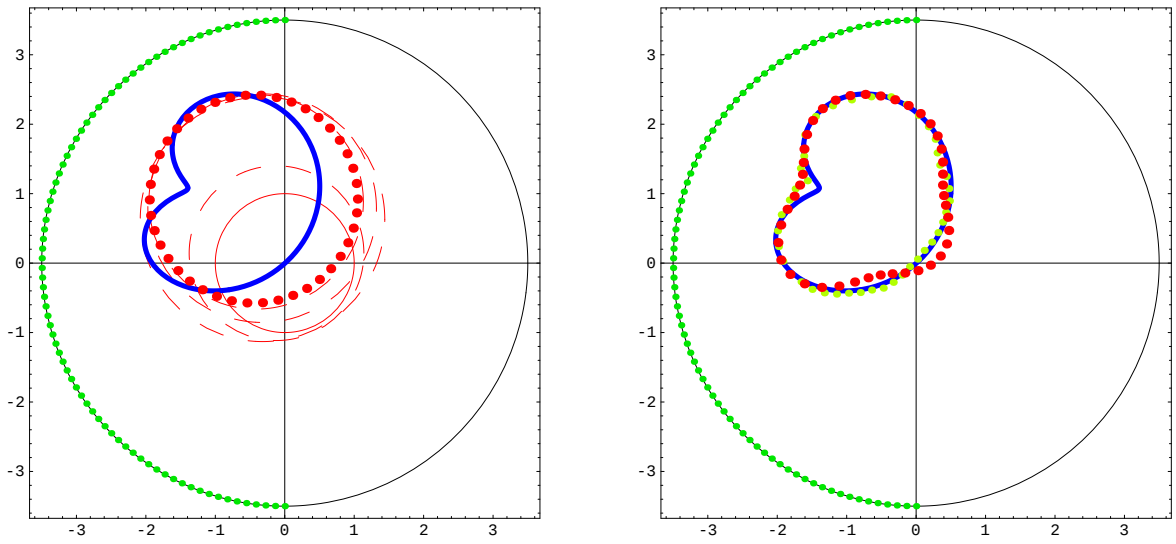

Figure 5.30: Reconstruction of γ_2 in $\mathcal{C}_0$ (left) and $\mathcal{C}_4$ (right) from incomplete noise free data.

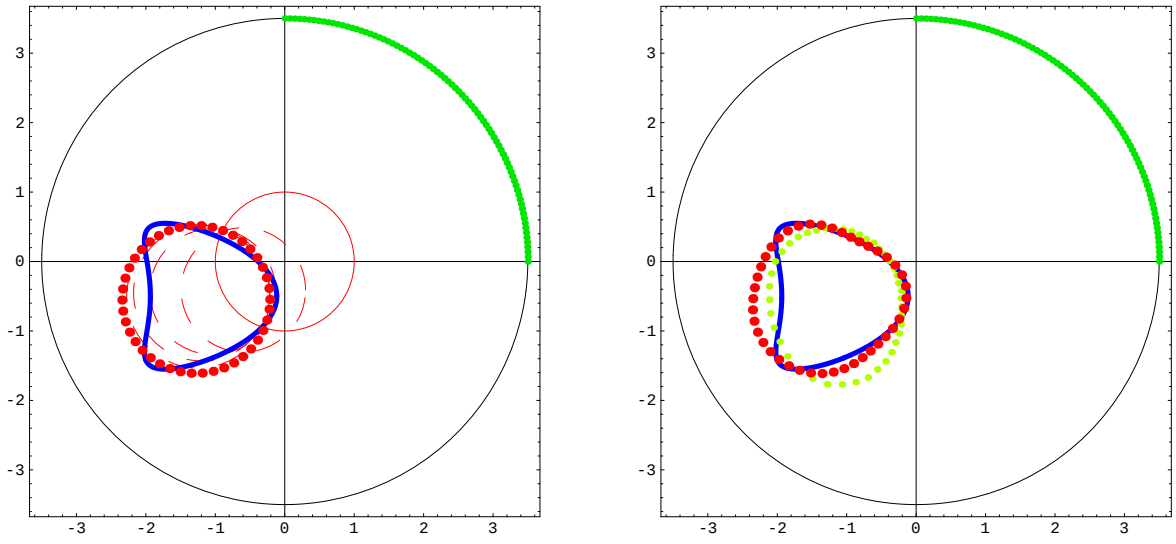

Figure 5.31: Reconstruction of γ_3 in $\mathcal{C}_0$ (left) and $\mathcal{C}_4$ (right) from incomplete noise free data.

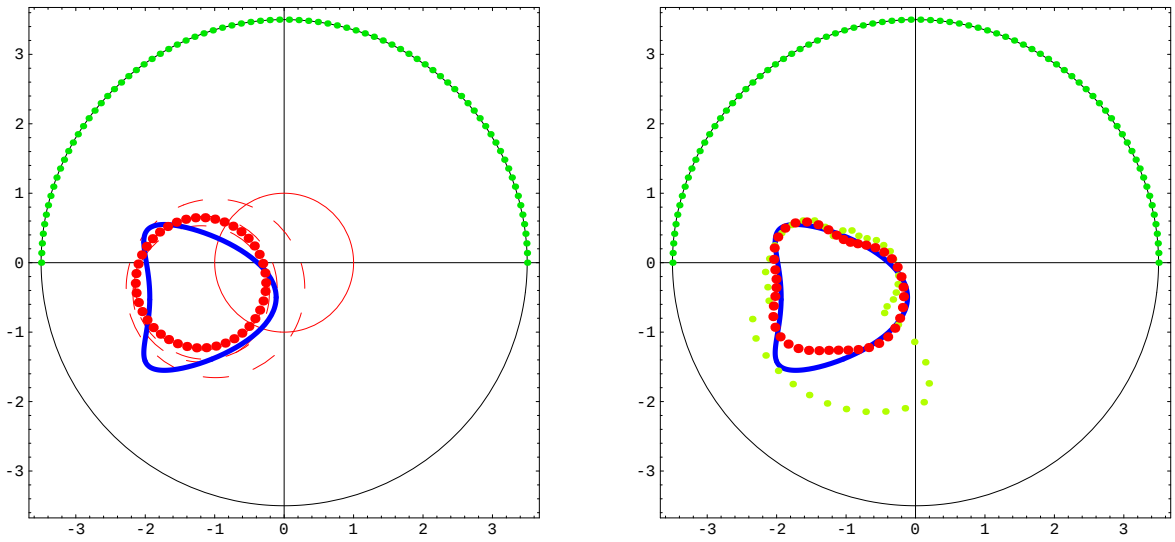

Figure 5.32: Reconstruction of γ_3 in $\mathcal{C}_0$ (left) and $\mathcal{C}_4$ (right) from incomplete noise free data.

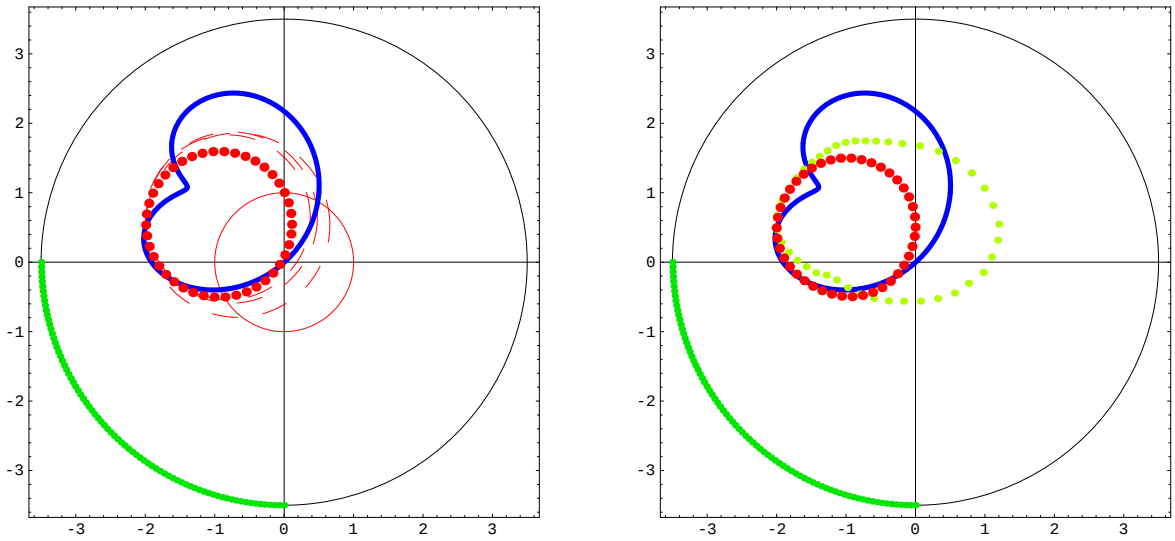

Figure 5.33: Reconstruction of γ_2 in $\mathcal{C}_0$ (left) and $\mathcal{C}_4$ (right) from incomplete data with 5% of noise.

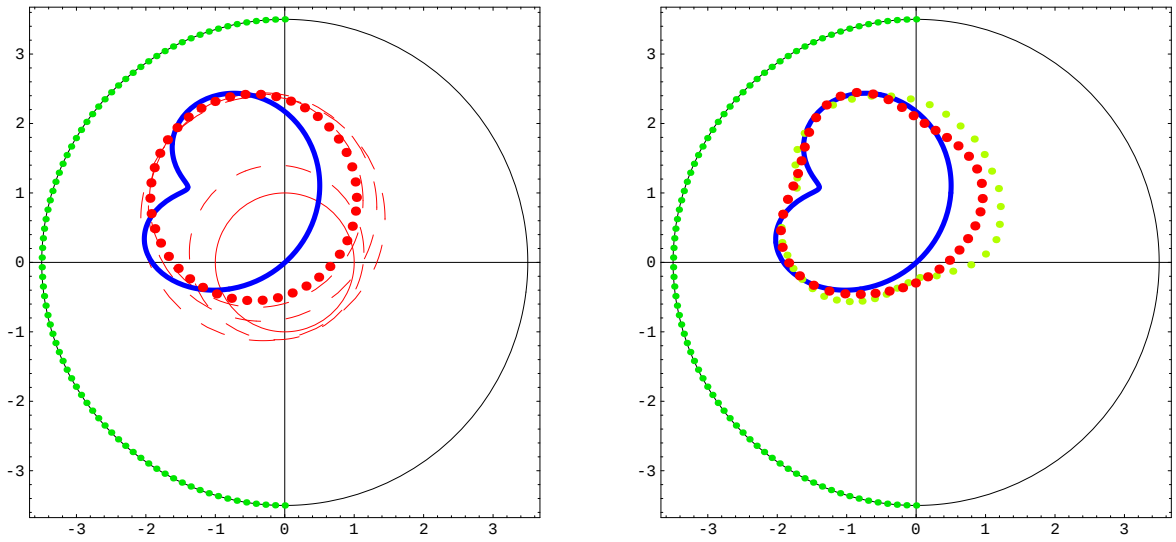

Figure 5.34: Reconstruction of γ_2 in $\mathcal{C}_0$ (left) and $\mathcal{C}_4$ (right) from incomplete data with 5% of noise.

Overall, we obtained good reconstruction results of both location and shape with this iterative method. When comparing with the decomposition method, the results shows similar reconstructions except for the non convex part of the shape, where the iterative method performs better. For incomplete boundary data we still notice that the accurately recovered part of the geometry corresponds to the location of the observation points.

In some cases, the iterative method performed worst that the decomposition method. This might be explained by the fact that in $\mathcal{C}_4$ the location is still an optimization variable. This means that two more variables are considered and thus the instability increases.

5.6 Decomposition method for the inverse Robin problem

Following the scalar case, after computing the MFS approximation for the Cauchy problem, $\widetilde{\mathbf{u}}$, we can retrieve the coefficient $z\mathbb{I} \in \mathcal{C}$ explicitly by

$$z = -\frac{\partial^*_{\mathbf{n}}\widetilde{\mathbf{u}}|_\gamma \cdot e_i}{\widetilde{\mathbf{u}}|_\gamma \cdot e_i}, \ i = 1, 2.$$

This is a componentwise reconstruction and, in the elastic problem, we can not assure that these equations have no singularities. Instead we will consider the implicit formulation

$$\text{Find } z \in \mathcal{C} : ||\partial^*_{\mathbf{n}}\widetilde{\mathbf{u}} + z\widetilde{\mathbf{u}}||_{\mathbf{L}^2(\gamma)} = 0.$$

By taking some points $x_j \in \gamma$ we transform this problem into an optimization problem, by considering, for instance, a finite number of Fourier modes for the representation of z and the objective function

$$G(\alpha) = \frac{1}{2}\sum_{i=1}^{2}\sum_{j=1}^{m}(\partial^*_{\mathbf{n}}\widetilde{\mathbf{u}}\cdot e_i + z_\alpha \widetilde{\mathbf{u}}\cdot e_i)^2$$

where $z_\alpha \in \mathcal{C}_N$ and $\mathcal{C}_N$ is the space defined in (4.30). Using the Levenberg-Marquardt method to solve the minimization problem, we obtain, by computing the derivative of the Robin boundary condition with respect to the coefficient, the (vectorial) entries of the jacobian matrix $\mathbb{J}(\alpha)$,

$$\mathbb{J}(\alpha)_{i,j} = R_{e_j}\widetilde{\mathbf{u}}(x_i)$$

where $R_{e_j} \in R^N_{ad}$ and e_j is the jth vector of the standard basis of $\mathbb{R}^{2N+1}$. We note that the computation of the jacobian does not require the resolution of any type of boundary value problem. We now test this method for the two examples considered in section 5.3.2.

5.6.1 Numerical simulations

To fit the Cauchy data using the MFS we considered 60 collocation points on the boundary Γ and 120 source points on the artificial boundary curve $\partial B(\mathbf{0}, 5.5) \cup \partial B(\mathbf{0}, 0.7)$. In the following reconstruction figures, the red dots represents the reconstruction using the optimization scheme in the space $\mathcal{C}_4$.

For noise free boundary data on the whole Γ, the two coefficients $\mathbf{Z}_1$ and $\mathbf{Z}_2$ were well recovered using both methods (Fig. 5.35).

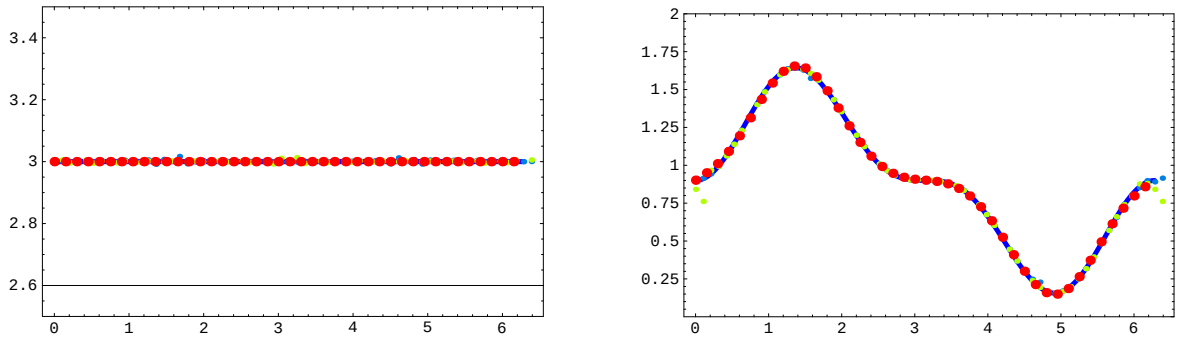

(a) $\mathbf{Z}_1$. (b) $\mathbf{Z}_2$.

Figure 5.35: Reconstruction of the Robin coefficient from noise free boundary data.

However, for data with 5 % of noise the explicit reconstruction presents several instabilities related to the zeros of $\widetilde{\mathbf{u}}$ on γ. This can be seen in Fig. 5.36, where we plotted

the reconstruction given by each component for the constant coefficient. For $\mathbf{Z}_2$, the numerical reconstruction was completely ruined by the instabilities.

Using the minimization method instead we obtained good reconstructions with a single iteration. Still for data with 5% of noise, we obtained, for $\mathbf{Z}_1$ and $\mathbf{Z}_2$, the left and right plotted results in Fig. 5.37, respectively.

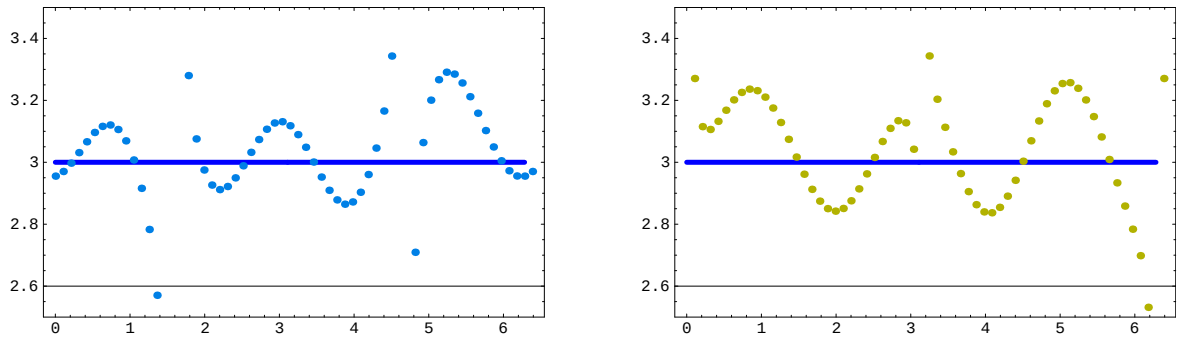

(a) First coordinate. (b) Second coordinate.

Figure 5.36: Reconstruction of $\mathbf{Z}_1$ with the explicit formulation (data with 5 % of noise).

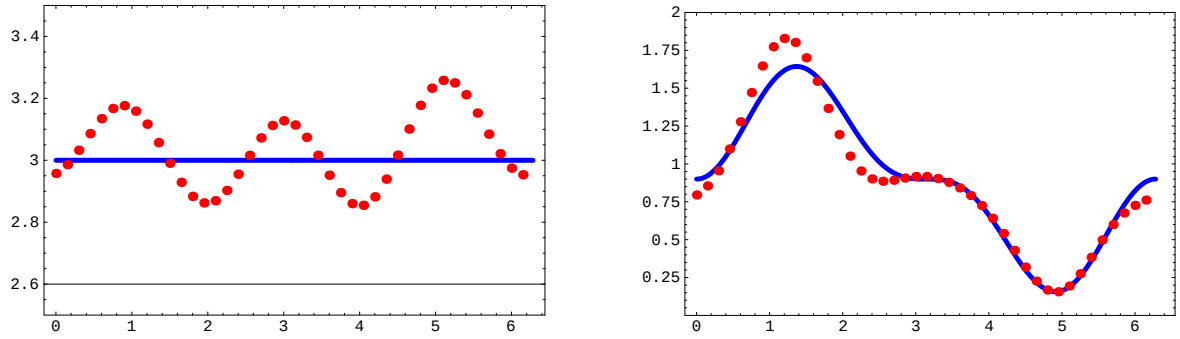

(a) $\mathbf{Z}_1$. (b) $\mathbf{Z}_2$.

Figure 5.37: Reconstruction in $\mathcal{C}_4$ from data with 5 % of noise.

The last test concerns the reconstruction of $\mathbf{Z}_2$, considering (the same amount of) observation points located on $[0, \pi]$. For noise free data, the reconstruction using the explicit method was affected by singularities. For the minimization method we obtained good results (Fig. 5.38).

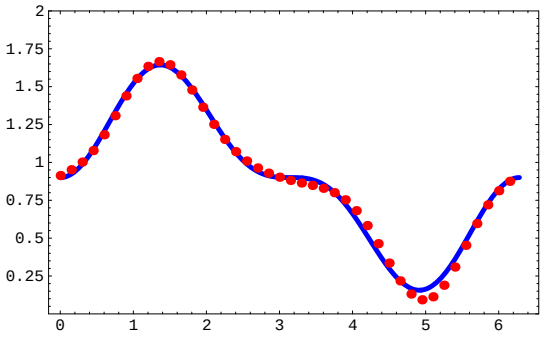

Figure 5.38: Reconstruction of $\mathbf{Z}_2$ from incomplete noise free data.

5.7 Conclusions

In this chapter, we studied of two inverse problems in linear elasticity: A geometric inverse problem and a Robin coefficient inverse problem. These are similar to the problems studied in Chapter 3 and an application of the numerical methods proposed in Chapter 4 was presented. The MFS provided good approximation results for the studied boundary value problems in linear elasticity and the decomposition method performed well, giving stable and accurate reconstructions.

For the geometric problem we tested a Newton type of method to retrieve the location and shape of the object. We were able to obtain good approximations of the location and dimension of the obstacle even for incomplete boundary data. The reconstruction of the shape was stable and again, for incomplete data, the part of the boundary that is best reconstructed corresponds to the location of observation points.

For the Robin problem, the adaptation of the decomposition method presented extra numerical difficulties and an optimization method was proposed. This approach does not affect the fast performance of the decomposition method and presented stable results. We note also that like in the scalar case, a Newton type of method could also be implemented. This was also numerically implemented and tested. Comparing both methods we obtained similar results and therefore we did not presented this approach.

6

Identification and source reconstruction from boundary data

The identification and reconstruction of sources from boundary measurements is a non destructive evaluation problem with several applications in imaging that has been often addressed in the literature. One of the most simplest settings is modeled by the Poisson equation. It is well known (eg. [38]) that, in this context, several boundary measurements do not allow identification of the right hand source term.

Depending on the underlying physical problem there might be some extra source information that, in conjunction with boundary data, enables the identification.

This is the case of: classes of characteristic functions defined on star shaped domains (eg. [51], cf. [75]); classes of point sources (cf. [39]); linear/affine classes of sources (eg. [10]). However, in many practical situations, this extra information may not be available or measurable (at least in a non destructive testing framework).

In this chapter, we investigate the identification of acoustic sources from boundary measurements. We start by showing that, in general, many boundary measurements are not sufficient to fully identify a source. For some particular cases, identification is possible from a single boundary measurement and some linear/affine classes are presented.

For the general case, the identification is achieved by considering many boundary measurements generated by different frequencies. In particular, it is showed that compactly supported sources (with support contained in the domain) can be identified from many partial boundary data.

We propose a numerical method based on the reciprocity gap functional (cf. [31], [19], for the Helmholtz equation see e.g. [1, 35]) to retrieve the source. The last part of the chapter is devoted to test this method for several numerical examples.

6.1 Direct and inverse problem

Let $\Omega \subset \mathbb{R}^d$ be a simply connected domain with C^1 boundary Γ. Given a source $f \in L^2(\Omega)$ and $g \in H^{1/2}(\Gamma)$ consider the *direct problem* of computing $g_{\mathbf{n}} := \partial_{\mathbf{n}} u|_\Gamma$, where u solves

$$(\mathcal{P}) \begin{cases} \Delta u + \kappa^2 u = f & \text{in } \Omega \\ u = g & \text{on } \Gamma \end{cases} . \tag{6.1}$$

It is well known that if $-\kappa^2$ is not an eigenvalue for the Laplace-Dirichlet operator then $(\mathcal{P})$ is well posed in $H^1(\Omega)$ (eg. [34]). Henceforth we shall assume this eigenvalue setting.

The *inverse problem* consists in the identification of the source term f from a pair of (compatible) Cauchy data $(g, g_{\mathbf{n}})$ on $\Sigma \subset \Gamma$.

We start to address the uniqueness for the inverse problem, considering a fixed wave number $\kappa \geq 0$.

6.2 Restricted identifiability with a single wave number

In this case, the identification of f from compatible Cauchy boundary data is not possible. The following example illustrates the difficulties in the identification for this inverse problem.

Example 6.1 Let $\Omega = B(0,1)$ and consider the function defined by

$$u(x) := -|x|^4 + 2|x|^2 - 1.$$

Then,

$$x \in \Gamma = \partial\Omega \Rightarrow \begin{cases} u(x) = 0 \\ \partial_{\mathbf{n}} u = (\mathbf{n} \cdot x)(-4|x|^2 + 4) = 0 \end{cases}.$$

On the other hand, since

$$\Delta u = -16|x|^2 + 8$$

then, for the non null source

$$f := -16|x|^2 + 8$$

we have

$$\begin{cases} \Delta u = f & \text{in } \Omega \\ u = 0 & \text{on } \Gamma \\ \partial_{\mathbf{n}} u = 0 & \text{on } \Gamma \end{cases}$$

and this source f can not be identified from a pair of Cauchy data on Γ. Moreover, taking

$$f_\kappa := f + \kappa^2 u \neq 0$$

we have $\Delta u + \kappa^2 u = f_\kappa$ in Ω with both trace and normal trace null on the boundary Γ.

Furthermore, we note that sources belonging to the subspace $(\Delta + \kappa^2 I)(H_0^2(\Omega)) \subset L^2(\Omega)$ can not be identified from the boundary data.

On the other hand, increasing the number of boundary measurements does not increase the information concerning the source. In fact, let $f \in L^2(\Omega)$ and, for each $g \in H^{1/2}(\Gamma)$ consider v, $w \in H^1(\Omega)$ such that

$$\begin{cases} \Delta v + \kappa^2 v = f & \text{in } \Omega \\ v = 0 & \text{on } \Gamma \end{cases} \quad \text{and} \quad \begin{cases} \Delta w + \kappa^2 w = 0 & \text{in } \Omega \\ w = g & \text{on } \Gamma \end{cases}.$$

Then, $u = v + w$ where u is the solution of $(\mathcal{P})$ and in particular

$$g_{\mathbf{n}} = \partial_{\mathbf{n}}(v + w) = \partial_{\mathbf{n}} v + \partial_{\mathbf{n}} w. \tag{6.2}$$

Thus, even with access to all possible boundary measurements, identification is not possible. It is clear that some extra information regarding the source must be considered.

We note that, from (6.2), it is sufficient to consider only the input function $g = 0$. This motivates the definition of the map

$$\begin{array}{ccccc} \Lambda : L^2(\Omega) & \longrightarrow & H^{-1/2}(\Gamma) \\ f & \mapsto & g_{\mathbf{n}} \end{array} \tag{6.3}$$

where $g_{\mathbf{n}} = \partial_{\mathbf{n}} u|_\Gamma$ and u solves $(\mathcal{P})$ considering $g = 0$.

Remark 6.2 The operator Λ is linear and continuous. Is non injective because

$$(\Delta + \kappa^2 I)(H_0^2(\Omega)) \subset \ker \Lambda.$$

As a consequence of boundary regularity results, for a domain Ω with C^2 boundary the kernel of Λ is in fact the whole $(\Delta + \kappa^2 I)(H_0^2(\Omega))$.

Moreover, we have the following density result.

Lemma 6.3 *The range of* Λ *is dense in* $H^{-1/2}(\Gamma)$.

Proof. We prove that the adjoint of Λ, $\Lambda^* : H^{1/2}(\Gamma) \longrightarrow L^2(\Omega)$ is injective. We claim that the adjoint is defined by $\Lambda^*(g_*) := u_*$ where $u_* \in H^1(\Omega)$ is the unique solution of

$$\begin{cases} \Delta u_* + \kappa^2 u_* = 0 & \text{in } \Omega \\ u_* = g_* & \text{on } \Gamma \end{cases}$$

from where it follows,

$$u_* = \Lambda^*(g_*) = 0 \Rightarrow g_* = u_*|_\Gamma = 0.$$

To prove the claim we note that,

$$\begin{aligned} \langle g_*, \Lambda(f) \rangle_{H^{1/2}(\Gamma) \times H^{-1/2}(\Gamma)} &= \int_\Gamma g_* g_{\mathbf{n}} d\varsigma = \int_\Omega (u_* \Delta u - \Delta u_* u) dx + \int_\Gamma u \partial_{\mathbf{n}} u_* d\varsigma \\ &= \int_\Omega u_* f dx = \langle u_*, f \rangle_{L^2(\Omega)}. \end{aligned}$$

□

6.2.1 Identification in linear/affine classes

We now present a type of class where identification from boundary data is possible and derive a method to retrieve the source by solving a higher order direct problem.

We recall that λ is an eigenvalue of the bilaplacian for the domain Ω if exists a non trivial solution of the fourth order problem

$$\begin{cases} \Delta^2 u - \lambda u = 0 & \text{in } \Omega \\ u = 0 & \text{on } \Gamma \\ \partial_{\mathbf{n}} u = 0 & \text{on } \Gamma \end{cases}.$$

Define the closed subspaces

$$\mathcal{H}_{\Delta\pm\kappa^2 I} := \left\{u \in L^2(\Omega) : \Delta u \pm \kappa^2 u = 0\right\}.$$

Lemma 6.4 *If κ^4 is not an eigenvalue of the bilaplacian and the boundary $\Gamma = \partial\Omega$ is C^2 then,*

$$L^2(\Omega) = \mathcal{H}_{\Delta-\kappa^2 I} \oplus (\Delta + \kappa^2 I)(H_0^2(\Omega)).$$

Proof. Let $f \in L^2(\Omega)$ and note that by the classical regularity (eg. [42]) results, $\Lambda(f)(= \partial_{\mathbf{n}} u) \in H^{1/2}(\Gamma)$ where $u \in H^2(\Omega)$ is the solution of $(\mathcal{P})$ for null input function. Since κ^4 is not an eigenvalue for the bilaplacian, the fourth order problem

$$\begin{cases} \Delta^2 v - \kappa^4 v = 0 & \text{in } \Omega \\ v = 0 & \text{on } \Gamma \\ \partial_{\mathbf{n}} v = \Lambda(f) & \text{on } \Gamma \end{cases} \tag{6.4}$$

is well posed in $H^2(\Omega)$. In particular $u - v \in H^2(\Omega)$ and since by construction, $v = u = 0$ and $\partial_{\mathbf{n}} v = \partial_{\mathbf{n}} u$ both on Γ we have $u - v \in H_0^2(\Omega)$. Thus, defining

$$w := u - v \tag{6.5}$$

we can write

$$f = (\Delta + \kappa^2)u = (\Delta + \kappa^2)(v + w) = (\Delta + \kappa^2)v + (\Delta + \kappa^2)w \in \mathcal{H}_{\Delta-\kappa^2 I} + (\Delta + \kappa^2 I)(H_0^2(\Omega))$$

and therefore $L^2(\Omega) = \mathcal{H}_{\Delta-\kappa^2 I} + (\Delta + \kappa^2 I)(H_0^2(\Omega))$.

To complete the proof we show that

$$u \in \mathcal{H}_{\Delta-\kappa^2 I} \cap (\Delta + \kappa^2 I)(H_0^2(\Omega)) \Rightarrow u = 0.$$

If $u \in \mathcal{H}_{\Delta-\kappa^2 I} \cap (\Delta + \kappa^2 I)(H_0^2(\Omega))$ then $\Delta u - \kappa^2 u = 0$ and $u = \Delta v + \kappa^2 v$ on Ω, for some $v \in H_0^2(\Omega)$. Thus,

$$0 = \Delta u - \kappa^2 u = \Delta(\Delta + \kappa^2 I)(v) - \kappa^2(\Delta + \kappa^2 I)v = \Delta^2 v - \kappa^4 v$$

and since $v \in H_0^2(\Omega)$ and κ^4 is not an eigenvalue of the bilaplacian we conclude that $v = 0$ in Ω and it follows that $u = \Delta v + \kappa^2 v = 0$. □

Remark 6.5 Note that for a domain Ω with C^2 boundary,

$$\mathcal{H}_{\Delta+\kappa^2 I}{}^{\perp} = (\Delta + \kappa^2 I)(H_0^2(\Omega)).$$

To see this, let $v \in \mathcal{H}_{\Delta+\kappa^2 I}{}^{\perp}$. Then,

$$\int_\Omega uv dx = 0, \ \forall u \in \mathcal{H}_{\Delta+\kappa^2 I}.$$

Let $v' \in H^2(\Omega)$ and $u \in H^1(\Omega)$ be a solution of

$$\left\{ \begin{array}{ll} \Delta v' + \kappa^2 v' = v & \text{in } \Omega \\ v' = 0 & \text{on } \Gamma \end{array} \right. \quad \text{and} \quad \left\{ \begin{array}{ll} \Delta u + \kappa^2 u = 0 & \text{in } \Omega \\ u = \partial_{\mathbf{n}} v' & \text{on } \Gamma \end{array} \right. \tag{6.6}$$

respectively. Since $u \in \mathcal{H}_{\Delta+\kappa^2 I}$,

$$0 = \int_\Omega uv dx = \int_\Omega (u(\Delta v' + \kappa^2 v'))dx = \int_\Omega \left(u\Delta v' + \kappa^2 uv'\right) dx. \tag{6.7}$$

Using Green's formula we can write

$$\int_\Omega u\Delta v' dx = \int_\Omega \Delta uv' dx + \int_\Gamma \left(u\partial_{\mathbf{n}} v' - \partial_{\mathbf{n}} uv'\right) d\varsigma = -\int_\Omega \kappa^2 uv' dx + ||\partial_{\mathbf{n}} v'||^2_{L^2(\Gamma)}.$$

Substituting this identity in equation (6.7) we obtain

$$||\partial_{\mathbf{n}} v'||^2_{L^2(\Gamma)} = 0$$

from where it follows that $\partial_{\mathbf{n}} v' = 0$ on Γ and therefore $v \in (\Delta + \kappa^2 I)(H_0^2(\Omega))$.

Reciprocally, we show that if $v \in (\Delta + \kappa^2 I)(H_0^2(\Omega))$ then $v \in \mathcal{H}^{\perp}_{\Delta+\kappa^2 I}$. Let $v = \Delta w + \kappa^2 w \in (\Delta + \kappa^2 I)(H_0^2(\Omega))$ and $u \in \mathcal{H}_{\Delta+\kappa^2 I}$. Then,

$$\int_\Omega uv dx = \int_\Omega u(\Delta w + \kappa^2 w)dx = \int_\Omega u\Delta w dx + \kappa^2 \int_\Omega uw dx = -\kappa^2 \int_\Omega uw dx + \int_\Omega \kappa^2 uw dx = 0$$

and the result follows.

In particular, for the Poisson equation ($\kappa = 0$) the above direct sum is in fact a sum of orthogonal subspaces (cf. [38]).

We now show that, under the same conditions of the previous result, $\mathcal{H}_{\Delta-\kappa^2 I}$ can be identified with $H^{1/2}(\Gamma)$.

Lemma 6.6 *If the conditions of the above Lemma are satisfied, the map*

$$\begin{array}{ccc} \Psi : H^{1/2}(\Gamma) & \longrightarrow & \mathcal{H}_{\Delta-\kappa^2 I} \\ g_1 & \mapsto & \Delta v + \kappa^2 v \end{array}$$

where v solves (6.4) for the input data $(0, g_1)$ is a linear homeomorphism.

Proof. The map is well defined, linear and injective because the fourth order problem (6.4) is well posed. Let g_n be a sequence in $H^{1/2}(\Gamma)$ such that

$$g_n \to 0 \text{ in } H^{1/2}(\Gamma).$$

Since the problem

$$\begin{cases} \Delta^2 v_n - \kappa^4 v_n = 0 & \text{in } \Omega \\ v_n = 0 & \text{on } \Gamma \\ \partial_{\mathbf{n}} v_n = g_n & \text{on } \Gamma \end{cases} \tag{6.8}$$

is well posed in $H^2(\Omega)$,

$$v_n \to 0 \text{ in } H^2(\Omega).$$

On the other hand, the Helmholtz operator $\Delta + \kappa^2 I : H^2(\Omega) \to L^2(\Omega)$ is bounded. Thus,

$$\Psi(g_n) = \Delta v_n + \kappa^2 v_n \to 0 \text{ in } L^2(\Omega)$$

which proves the continuity of Ψ.

Let u be in $\mathcal{H}_{\Delta-\kappa^2 I} \subset L^2(\Omega)$. Since by hypothesis $-\kappa^2$ is not an eigenvalue of the Laplace–Dirichlet operator, the problem

$$(\mathcal{P}_u) \begin{cases} \Delta v + \kappa^2 v = u & \text{in } \Omega \\ v = 0 & \text{on } \Gamma \end{cases}$$

is well posed in $H_0^1(\Omega)$. Moreover, since the boundary is C^2, by regularity, the above problem is well posed in $H^2(\Omega)$. Thus, $\partial_{\mathbf{n}} v \in H^{1/2}(\Gamma)$ and the map

$$u \mapsto \partial_{\mathbf{n}} v$$

is well defined. It is easy to see that this map is the inverse of Ψ.

Now if

$$u_n \to 0 \text{ in } L^2(\Omega)$$

then, by the well posedness of $(\mathcal{P}_{u_n})$ in $H^2(\Omega)$, we have

$$v_n \to 0 \text{ in } H^2(\Omega).$$

By the continuity of the normal trace we conclude that

$$\Psi^{-1}(u_n) = \partial_{\mathbf{n}} v_n \to 0 \text{ in } H^{1/2}(\Gamma).$$

□

This last two results show that we must consider the classes of sources where the second projection, $Q : L^2(\Omega) \longrightarrow (\Delta + \kappa^2 I)(H_0^2(\Omega))$, ie, the projection onto $\ker \Lambda$, is known. For instance, given $F \in L^2(\Omega)$, consider the affine (linear, if $F = 0$) class

$$\mathcal{C}_F := \left\{ f \in L^2(\Omega) : \Delta f - \kappa^2 f = F \right\}.$$

Theorem 6.7 *The restriction of Q to $\mathcal{C}_F$ is constant. Moreover, if a source f is known to be in the class $\mathcal{C}_F$ then a single boundary measurement $(0, \Lambda(f))$ on Γ is sufficient to identify f.*

Proof. From the decomposition

$$f = h + (\Delta + \kappa^2 I)w \in \mathcal{H}_{\Delta - \kappa^2 I} \oplus (\Delta + \kappa^2 I)(H_0^r(\Omega)) \tag{6.9}$$

we obtain, for $f \in \mathcal{C}_F$,

$$F = (\Delta - \kappa^2 I)f = (\Delta - \kappa^2 I)h + (\Delta^2 - \kappa^4 I)w = (\Delta^2 - \kappa^4 I)w. \tag{6.10}$$

Since $w \in H_0^2(\Omega)$ then w is known (because all the input data is known), unique and independent of the choice of f. Thus, Q maps $\mathcal{C}(F) \subset L^2(\Omega)$ to the singular set $\{(\Delta + \kappa^2 I)w\}$. Moreover, since $(\Delta + \kappa^2 I)v$ is uniquely determined by $\Lambda(f)$, we conclude that f is uniquely determined by this data. □

We note that in the decomposition (6.9), $h = (\Delta + \kappa^2 I)v$ where v solves (6.4). Setting

$$w_f := v + w,$$

we have

$$f = \Delta w_f + \kappa^2 w_f$$

and w_f can be computed from the available information. More precisely, for $f \in \mathcal{C}_F$, w_f is the unique solution of the fourth order problem

$$\begin{cases} \Delta^2 w_f - \kappa^4 w_f = F & \text{in } \Omega \\ w_f = 0 & \text{on } \Gamma \\ \partial_{\mathbf{n}} w_f = \Lambda(f) & \text{on } \Gamma \end{cases} .$$

6.3 Identification of sources using multiple frequencies.

In the previous section we have established that, for some fixed wave number, the identification of sources can be established in some particular cases. For the general case, we propose the use of several wave numbers to generate multiple boundary data and use such data to retrieve the source. We start with some notation.

Given $f \in L^2(\Omega)$ and $\kappa \geq 0$ we denote by $g_{\mathbf{n}}^{\kappa}$ the Neumann boundary data on Γ, generated by the solution of

$$(\mathcal{P}_\kappa) \begin{cases} \Delta u_\kappa + \kappa^2 u_\kappa = f & \text{in } \Omega \\ u_\kappa = 0 & \text{on } \Gamma \end{cases} \tag{6.11}$$

in the C^1 simply connected domain Ω. The linear map $f \mapsto g_{\mathbf{n}}^{\kappa}$ will be denoted by Λ_κ. Define, for κ in some open interval I, the map

$$\kappa \mapsto \Lambda_\kappa(f) = g_{\mathbf{n}}^{\kappa}. \tag{6.12}$$

Theorem 6.8 *The knowledge of (6.12) on some open interval $I \subset \mathbb{R}^+$ determines f, in the $L^2(\Omega)$ sense.*

Proof. Suppose that, for some $f_1,\ f_2 \in L^2(\Omega)$,

$$\Lambda_\kappa(f_1) = \Lambda_\kappa(f_2), \forall \kappa \in I. \tag{6.13}$$

Using Green's formula with test functions $v \in \mathcal{H}_{\Delta+\kappa^2 I}$ we have

$$\int_\Omega f_i v dx = \int_\Gamma \Lambda_\kappa(f_i) v d\varsigma,\ i = 1, 2.$$

Since (6.13) holds, the previous identity implies

$$\int_\Omega (f_1 - f_2) v dx = 0, \forall v \in \mathcal{H}_{\Delta+\kappa^2 I}$$

and the result is a consequence of the density of $\bigcup_{\kappa\in I}\mathcal{H}_{\Delta+\kappa^2 I}$ in $\text{Ł}^2(\Omega)$. For instance, considering plane waves $v_{\kappa,\widehat{d}}\in\mathcal{H}_{\Delta+\kappa^2 I}$ as test functions we have

$$\int_\Omega (f_1-f_2)v_{\kappa,\widehat{d}}dx=0,\forall\kappa\in I,\ \forall\widehat{d}\in S^{d-1}.$$

Therefore the Fourier transform of $(f_1-f_2)\chi_\Omega$ (where χ_Ω stands for the characteristic function of the domain Ω) gives zero evaluated at $\xi=\kappa\hat{d}$. This means that the Fourier transform is null in the set $I\times S^{d-1}$ and, by analyticity, is null everywhere. The isometry in L^2 implies $f_1=f_2$, a.e. □

6.4 Identification of a source from partial boundary data

So far, we have addressed the identification of sources from boundary measurements, assuming full access to the boundary Γ. We prove that for compactly supported sources with support $\overline{\omega}\subset\Omega$ the Cauchy data on a part of the boundary determines uniquely the full data.

Consider the following problem of data completion: Given a pair of data $(g_\Sigma, g_\Sigma^{\mathbf{n}})$ find $(g_{\Gamma\setminus\Sigma}, g_{\Gamma\setminus\Sigma}^{\mathbf{n}})$ on $\Gamma\setminus\Sigma$ such that exists $u\in H^1(\Omega)$ satisfying, for known κ,

$$(\Delta+\kappa^2 I)u=f\text{ in }\Omega,\ \ u=\begin{cases} g_\Sigma & \text{on }\Sigma\\ g_{\Gamma\setminus\Sigma} & \text{on }\Gamma\setminus\Sigma\end{cases},\ \ \partial_{\mathbf{n}}u=\begin{cases} g_\Sigma^{\mathbf{n}} & \text{on }\Sigma\\ g_{\Gamma\setminus\Sigma}^{\mathbf{n}} & \text{on }\Gamma\setminus\Sigma\end{cases}. \tag{6.14}$$

Theorem 6.9 *If f is a compactly supported source with support $\overline{\omega}\subset\Omega$ then the aforementioned Cauchy data completion problem has at most one solution.*

Proof. Suppose that this problem has two solutions i.e., that exists u_i satisfying (6.14) for a compactly supported source f_i with $\overline{\omega}_i\subset\Omega$ and the pair $(g^i_{\Gamma\setminus\sigma}, g^{i,\mathbf{n}}_{\Gamma\setminus\sigma})$, $i=1,2$. Defining $v=u_1-u_2$, we have

$$(\Delta+\kappa^2 I)v=f_1-f_2\text{ in }\Omega,$$

$$v=\begin{cases} 0 & \text{on }\Sigma\\ g^1_{\Gamma\setminus\Sigma}-g^2_{\Gamma\setminus\Sigma} & \text{on }\Gamma\setminus\Sigma\end{cases}\ \wedge\ \partial_{\mathbf{n}}v=\begin{cases} 0 & \text{on }\Sigma\\ g^{1,\mathbf{n}}_{\Gamma\setminus\Sigma}-g^{2,\mathbf{n}}_{\Gamma\setminus\Sigma} & \text{on }\Gamma\setminus\Sigma\end{cases}.$$

Since f_1-f_2 is still a compactly supported then $(\Delta+\kappa^2 I)v=0$ in the open set $\Omega_c:=\Omega\setminus\overline{\omega}$, where $\overline{\omega}$ denotes the support of f_1-f_2. Notice that v has null Cauchy data on $\Sigma\subset\partial\Omega_c$ hence, by Holmgren's lemma, $v=0$ in an open, connected set $\widetilde{\Omega}_c$ such that $\Gamma\subset\partial\widetilde{\Omega}_c$. In

particular, v has null Cauchy data on Γ and we conclude that, on $\Gamma \setminus \Sigma \subset \Gamma$,

$$g^1_{\Gamma\setminus\Sigma} = g^2_{\Gamma\setminus\Sigma} \ \wedge \ g^{1,\mathbf{n}}_{\Gamma\setminus\Sigma} = g^{2,\mathbf{n}}_{\Gamma\setminus\Sigma}.$$

□

Remark 6.10 As a consequence of theorems 6.8 and 6.9 we conclude uniqueness for the inverse source problem even from partial boundary data, when the source is compactly supported and an interval of frequencies is used.

6.5 Numerical implementation for the direct problem

To approximate the solution of $(\mathcal{P}_\kappa)$ we use the MFS–D (cf. [9]). Let

$$\widetilde{u}_\kappa(x) = \sum_{i=1}^{n}\sum_{j=1}^{m} \alpha_{i,j}\Phi_{\kappa_i}(x - y_j) \tag{6.15}$$

where Φ_κ is the fundamental solution (2.6). This expansion is justified by the following properties.

Lemma 6.11 *([9]) Let $\widehat{\Gamma}$ be an admissible source set. Then,*

(a) span$\{\Phi_\kappa(\bullet - y)|_\Omega : \kappa \in I \wedge y \in \widehat{\Gamma}\}$ is dense in $L^2(\Omega)$ and

(b) span$\{\Phi_\kappa(\bullet - y)|_\Gamma : y \in \widehat{\Gamma}\}$ is dense in $L^2(\Gamma)$.

As usual, $\widehat{\Gamma}$ will be the boundary of a regular domain $\widehat{\Omega}$ such that $\overline{\Omega} \subset \widehat{\Omega}$.

We denote by Θ_D the set of frequencies

$$\{\kappa_1, \ldots, \kappa_n\}$$

and by Ξ the set of source points, that is

$$\Xi = \{y_1, \ldots, y_m\}$$

with $y_i \in \widehat{\Gamma}$. Using the above expansion to approximate the solution of $(\mathcal{P}_\kappa)$ we obtain the system

$$\begin{cases} \sum_{i=1}^{n}\sum_{j=1}^{m}(\kappa^2-\kappa_i^2)\alpha_{i,j}\Phi_{\kappa_i}(x-y_j)=f(x) & x\in\Omega \\ \sum_{i=1}^{n}\sum_{j=1}^{m}\alpha_{i,j}\Phi_{\kappa_i}(y^\Gamma-y_j)=0 & y^\Gamma\in\Gamma \end{cases}.$$

In order the compute the coefficients $\alpha_{i,j}\in\mathbb{C}$ we consider some collocation points x_i and y_j^Γ on the domain and boundary (respectively) and solve the corresponding linear system when the number of coefficients equals the number of equations. When number of equations is higher, we apply the least squares method.

Remark 6.12 If a particular solution of

$$\Delta u_\kappa^P+\kappa^2 u_\kappa^P=f$$

is known, then $u_\kappa=u_\kappa^P+u_\kappa^H$ where u_κ^H solves the problem

$$\begin{cases} \Delta u_\kappa^H+\kappa^2 u_\kappa^H=0 & \text{in } \Omega \\ u_\kappa^H=-u_\kappa^P & \text{on } \Gamma \end{cases}. \tag{6.16}$$

In this case we only have to compute an approximation for the above homogeneous problem and we consider the MFS approximation (see section 4.1.1 for the numerical implementation procedure).

6.5.1 Numerical examples

We now test the aforementioned method for $(\mathcal{P}_\kappa)$. We consider the domain

$$\Omega=B(0,2)$$

and three sources. The first and second sources are defined by

$$f_1(x_1,x_2):=\cos(x_1^2)\sin(x_2^2)$$

and

$$f_2(x_1,x_2):=\frac{2}{e^{\frac{1}{0.4}||(x_1-0.5,x_2-0.8)||^2}}+\frac{3}{e^{10||(x_1/1.5,x_2/0.8+1.2)||^2}}$$

respectively. They are smooth functions and the second has two peaks: an elliptic and a circular. For a plot of these sources see Fig. 6.1.

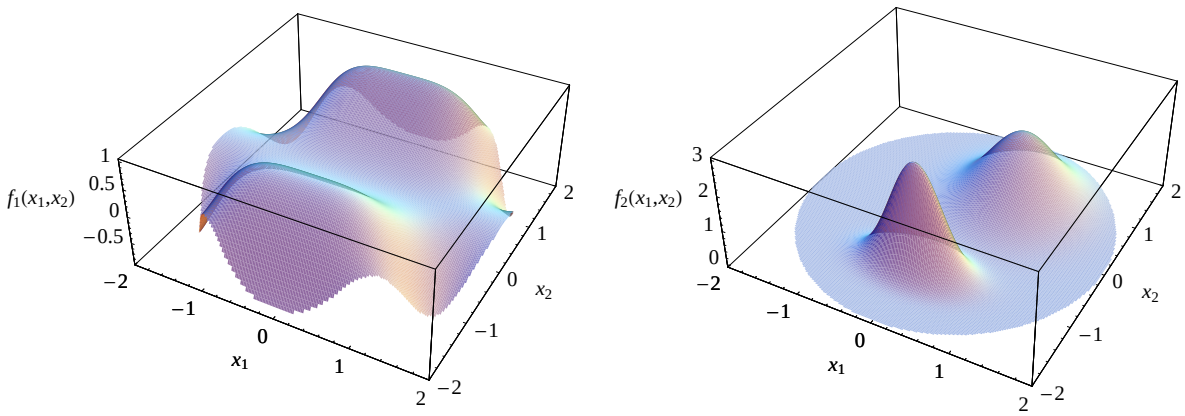

(a) f_1. (b) f_2.

Figure 6.1: Plot of the sources in Ω.

The third source is a combination of four points sources, namely

$$f_3(x) := -2\delta(x - c_1) + 6\delta(x - c_2) - 4\delta(x - c_3) - 5\delta(x - c_4)$$

with centers

$$c_1 = (1, 0),\ c_2 = (0, 1),\ c_3 = (-1, 0) \text{ and } c_4 = (0, -0.5).$$

In order to obtain an approximation for f_1 and f_2 using the MFS–D we considered the expansion (6.15) with

$$\Theta_D = \{1,\ 2,\ \ldots,\ 15\}$$

and 150 source points on $\widehat{\Gamma} := \partial B(0, 4)$. The collocation points were 1927 with the distribution suggested by Fig. 6.2.

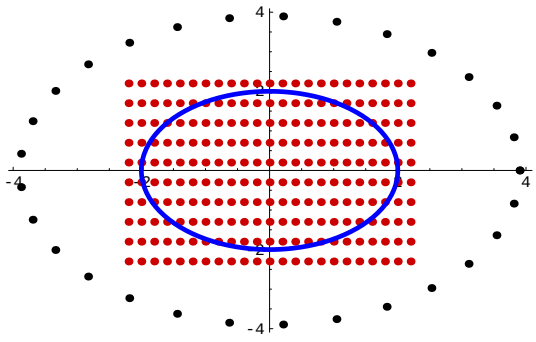

Figure 6.2: Distribution of collocation and source points. The black dots represent source points, the red dots represent collocation points and the full blue line is the boundary of the domain.

For the third example we note that

$$u_\kappa^P(x) = 2\Phi_\kappa(x - c_1) - 6\Phi_\kappa(x - c_2) + 4\Phi_\kappa(x - c_3) + 5\Phi_\kappa(x - c_4)$$

is a particular solution of the non homogeneous Helmholtz equation with right hand side f_3.

The MFS approximation for (6.16) was computed considering 150 collocation and source points.

We now present error plots to show the accuracy of the numerical method. We consider the absolute error,

$$\left|f(x) - (\Delta\widetilde{u}_{1.5} + \kappa^2\widetilde{u}_{1.5})(x)\right|, \ x \in \Omega$$

for the source approximation and the error on the boundary

$$|\widetilde{u}_{1.5}(\Gamma(t))|$$

where $\Gamma(t) := 2(\cos t, \sin t), \ t \in [0, 2\pi]$ is the parametrization of the boundary Γ.

In Figs. 6.3 and 6.4 we plot these error graphics for the first and second numerical examples, respectively. For the third example, we plot the boundary error in Fig. 6.5.

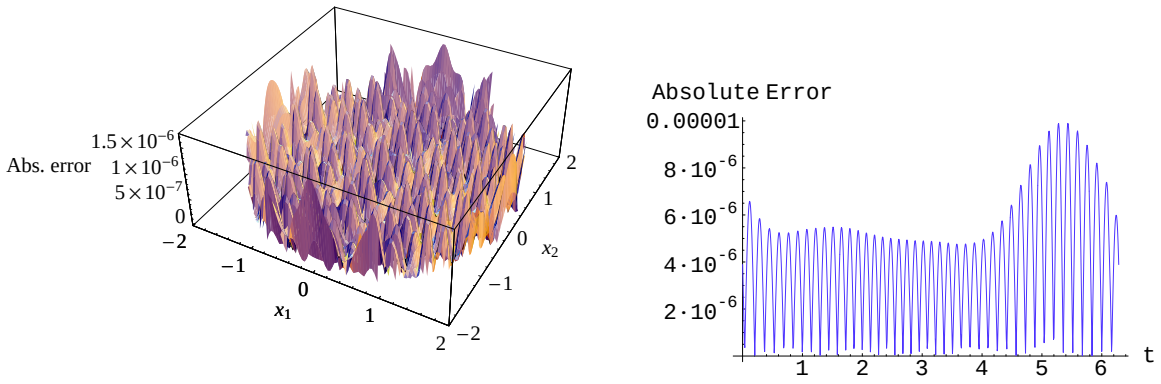

Figure 6.3: Absolute error for the approximation of f_1 (left) and the approximation of the boundary condition (right).

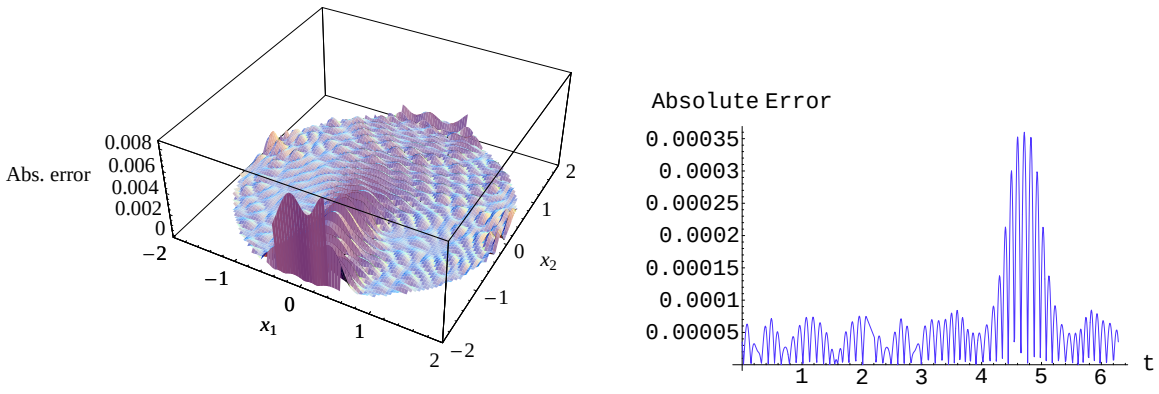

Figure 6.4: Absolute error for the approximation of f_2 (left) and the approximation of the boundary condition (right).

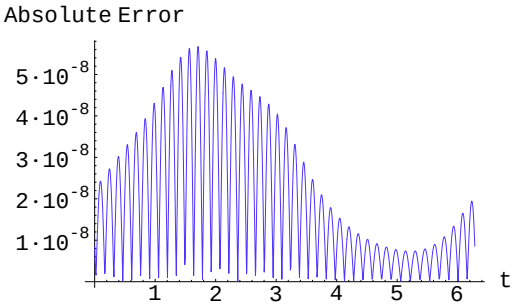

Figure 6.5: Absolute error of the boundary condition approximation for the third example.

6.6 Reconstruction of a source using the reciprocity gap functional

Since the map Λ is linear, considering a representation $\widetilde{f} = \sum_i \alpha_i \Phi_i$ of the source f, we can compute the coefficients α_i directly by solving, for instance, the linear system

$$\sum_i \alpha_i \Lambda_\kappa(\Phi_i) = \Lambda_\kappa(f) \tag{6.17}$$

for several frequencies κ. However, in a more favorable situation we choose a basis with the eigenvalue property

$$\Delta \Phi_i = -\kappa_i^2 \Phi_i$$

and $\Lambda_\kappa(\Phi_i) = \partial_{\mathbf{n}} u_i$ where $u_i = u_i^H + 1/(\kappa^2 - \kappa_i^2)\Phi_i$ and

$$\begin{cases} \Delta u_i^H + \kappa^2 u_i^H = 0 & \text{in } \Omega \\ u_i^H = -\dfrac{1}{\kappa^2 - \kappa_i^2}\Phi_i & \text{on } \Gamma \end{cases}.$$

Often, the number of basis functions is big and this approach is computational expensive. We consider instead the following weak formulation.

Given a source $f \in L^2(\Omega)$, the reciprocity functional at $v_{\kappa,\widehat{d}}(x) = e^{i\kappa x\cdot\widehat{d}}$ is

$$\mathcal{R}(v_{\kappa,\widehat{d}}) = \int_\Gamma \partial_{\mathbf{n}} u_\kappa(x) e^{i\kappa x\cdot\widehat{d}} d\varsigma_x$$

where u_κ solves $(\mathcal{P}_\kappa)$. From Green's formula we have

$$\int_\Omega f(x) e^{i\kappa x\cdot\widehat{d}} dx = \mathcal{R}(v_{\kappa,\widehat{d}}) \tag{6.18}$$

and from the proof of Theorem 6.8, the knowledge of $\mathcal{R}(v_{\kappa,\widehat{d}})$ for all $\kappa \in I$ in all directions $\widehat{d} \in S^1$ gives an identification of f in the L^2 sense.

We now use this weak form to reconstruct the source. First, a representation of f in some finite dimensional space must be considered. We take

$$\widetilde{f} = \sum_{i=1}^{n_1}\sum_{j=1}^{m_1} \alpha_{i,j} v_{\lambda_i,\widehat{c}_j},\ \lambda_i \in I \wedge \widehat{c}_i \in S^1$$

but it is clear that other basis functions could be considered. The justification for this representation is based on the density result (eg. [8])

$$L^2(\Omega) = \overline{\text{span}\{v_{\lambda,\widehat{c}}, \lambda \in I \wedge \widehat{c} \in S^1\}}.$$

For numerical implementation purposes we consider n measurements $\Lambda_{\kappa_1}(f),\ \ldots,\ \Lambda_{\kappa_n}(f)$ and $\widehat{d}_1, \ldots, \widehat{d}_m \in S^1$. The $n_1 \times m_1$ coefficients $\alpha_{i,j} \in \mathbb{C}$ are computed by solving the linear system of equations

$$(\mu\mathbb{I} + \mathbb{A}^*\mathbb{A})\mathbf{X} = \mathbb{A}^*\mathbb{B}$$

with

$$\mathbb{A} = \left[\int_\Omega e^{i(\lambda_i x\cdot\widehat{c}_j + \kappa x\cdot\widehat{d}_k)} dx\right]_{(n\times m)\times(n_1\times m_1)},\ \mathbb{B} = \left[\int_\Gamma \Lambda_\kappa(f) e^{i\kappa x\cdot\widehat{d}_k} d\varsigma\right]_{(n\times m)}$$

for some regularization parameter μ.

In the domain $\Omega = B(0,2)$ we have

$$\begin{aligned}\int_\Omega e^{i(\lambda_i x\cdot\widehat{c}_j+\kappa x\cdot\widehat{d}_k)}dx &= \int_0^{2\pi}\int_0^2 e^{i(\lambda_i(\rho\cos\theta,\rho\sin\theta)\cdot\widehat{c}_j+\kappa(\rho\cos\theta,\rho\sin\theta)\cdot\widehat{d}_k)}\rho d\rho d\theta\\ &= \int_0^{2\pi}\zeta(\theta,\lambda_i,\widehat{c}_j,\widehat{d}_k)d\theta\end{aligned}$$

with

$$\zeta(\theta,\lambda_i,\widehat{c}_j,\widehat{d}_k) := \begin{cases}\frac{-4-4ie^{i\zeta_0(\theta,\lambda_i,\widehat{c}_j,\widehat{d}_k)}(i+\zeta_0(\theta,\lambda_i,\widehat{c}_j,\widehat{d}_k))}{\zeta_0(\theta,\lambda_i,\widehat{c}_j,\widehat{d}_k)^2} & \text{if } \zeta_0(\theta,\lambda_i,\widehat{c}_j,\widehat{d}_k)\neq 0\\ 2 & \text{otherwise}\end{cases}$$

and $\zeta_0(\theta,\lambda_i,\widehat{c}_j,\widehat{d}_k) := 2(\widehat{d}_{k,1}\kappa+\widehat{c}_{j,1}\lambda_i)\cos\theta + 2(\widehat{d}_{k,2}\kappa+\widehat{c}_{j,2}\lambda_i)\sin\theta$. On the other hand,

$$\int_\Gamma \Lambda_\kappa(f)e^{i\kappa x\cdot\widehat{d}_k}d\varsigma = 2\int_0^{2\pi}(\cos\theta,\sin\theta)\cdot\nabla u_\kappa(2\cos\theta,2\sin\theta)e^{i\kappa(2\cos\theta,2\sin\theta)\cdot\widehat{d}_k}d\theta$$

and we use the trapezoidal rule with 80 points to approximate both integrals on θ.

Remark 6.13 We note that if $f=\sum_{i=1}^n a_i\delta_{c_i}$ and the centers c_i are known, then this method allows also the reconstruction of the intensities a_i. In fact for this particular type of sources, the intensities satisfy the system of equations

$$\sum_{i=1}^n a_i v_{\kappa,\widehat{d}}(c_i) = \mathcal{R}(v_{\kappa,\widehat{d}}), \forall\kappa\in I\wedge\widehat{d}\in S^1. \tag{6.19}$$

6.6.1 Numerical examples

The following numerical tests concerns the reconstruction of f_1, f_2 and f_3. For each case, we considered

$$\lambda_i = 0.3+i,\ i=0,\ldots 13$$

$\widehat{c}_1,\ldots,\widehat{c}_{20}$ and $\widehat{d}_1,\ldots,\widehat{d}_{100}$ both uniformly distributed on S^1. We tested the method for up to six measurements (with and without noise) and considered 80 uniformly distributed observation points on Γ.

For the first example, assuming noise free data, we plotted the reconstructions using one two and three boundary measurements. Starting with a single measurement corresponding to the frequency $\kappa = 1.5$ we obtained the results in Fig. 6.6. On the left we have the real part of $\widetilde{f}_1$ and on the right the imaginary part. Fig. 6.7 a) presents the reconstruction considering two measurements $\kappa = 1.5,\ 3.5$ and Fig. 6.7 b) three measurements.

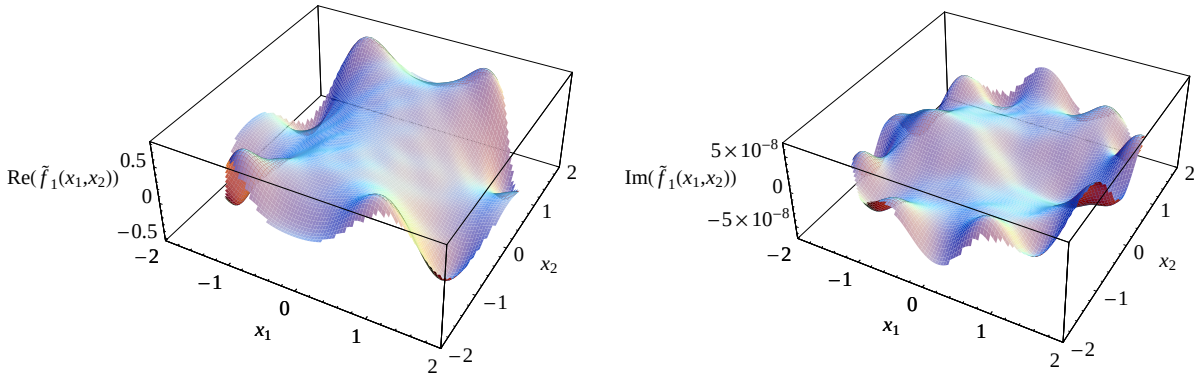

(a) $\kappa = 1.5$ (b) $\kappa = 1.5$

Figure 6.6: Reconstruction of f_1 considering noise free data obtained from a single measurement.

Still considering three boundary measurements for $\kappa = 1.5,\ 3.5,\ 5.5$ we observe that the noise does not affect much the reconstructions. This can be seen in Fig. 6.8 where we plotted the reconstruction for several levels of noise. The regularization parameter was $\mu = 10^{-3}$ for data with 3 % of noise, $\mu = 10^{-2}$ for 5 % and 8 % of noise level and $\mu = 10^{-1}$ for 10 %.

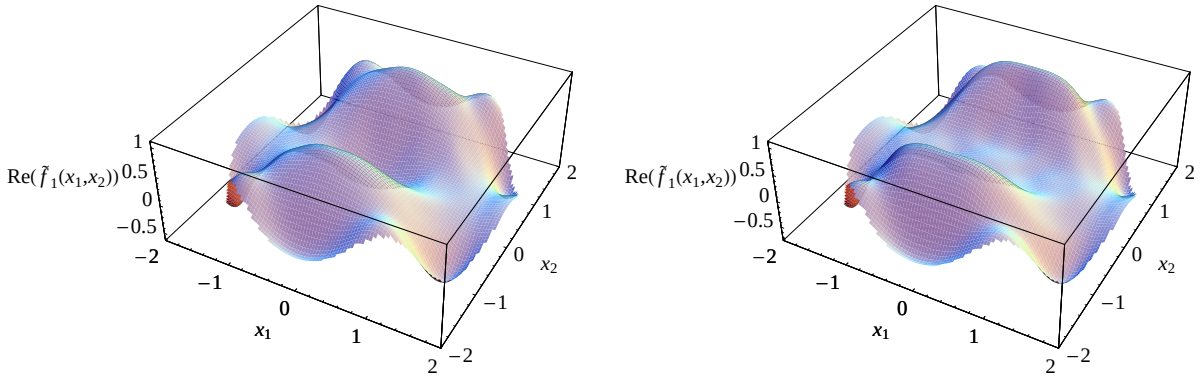

(a) $\kappa = 1.5,\ 3.5$ (b) $\kappa = 1.5,\ 3.5,\ 5.5$

Figure 6.7: Reconstruction of f_1 considering noise free data obtained from several measurements.

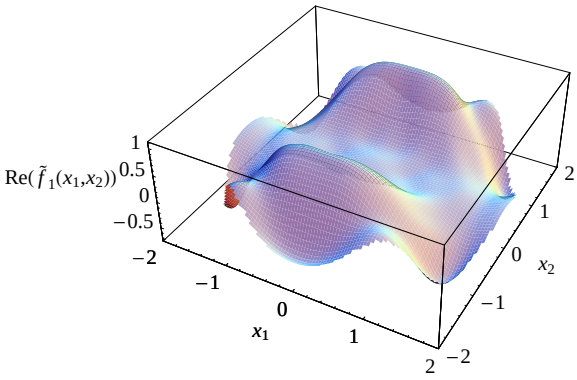

(a) 3 % of noise.

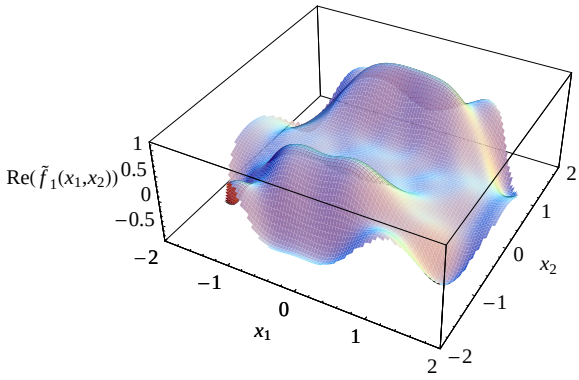

(b) 5 % of noise.

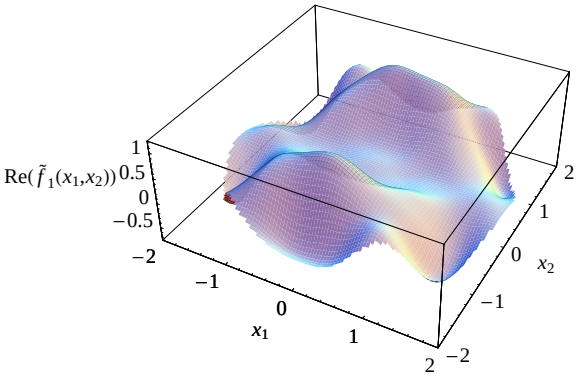

(c) 8 % of noise.

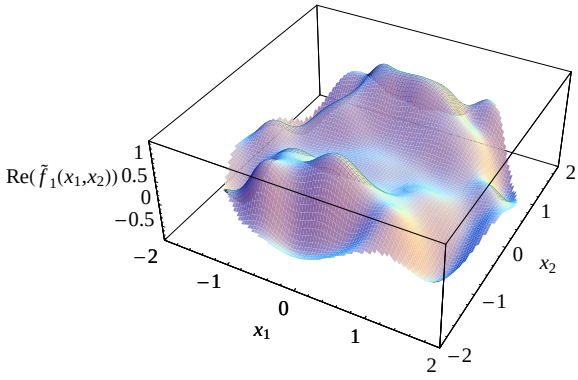

(d) 10 % of noise.

Figure 6.8: Reconstruction of f_1 considering data with several levels of noise, obtained from three measurements.

The source f_2 is fairly retrieved using two (noise free) boundary measurements (Fig. 6.8, plot (b)). With three measurements, the shape and location of the peaks were well recovered (Fig. 6.8, plot (c)) and with six the full source is well approximated (Fig. 6.8, plot (f)).

If we consider noisy data, we obtain, with three measurements, a good reconstruction of the location and peaks shape. In this case we plot in Fig. 6.9 the reconstruction for data with 5 % of noise. The regularization parameter was $\mu = 10^{-1}$.

To better visualize the location and shape of the peaks we show in Fig. 6.10 three contour plots. Plot (a) is the contour plot of f_2 while plots (b) and (c) are contour plots of the (real part) computed approximations from noise free and noisy data, respectively.

For the last example, taking three (noise free) measurements we were able to identify the number and location of the point sources (Fig. 6.12, plot (b)). However, this is more clear with four measurements (Fig. 6.12, plot (c)). In order to see the negative part of the function presented in Fig. 6.12, plot (d) we show the inversion of this graphic with respect to the plane xoy (Fig. 6.12, plot (e)).
The same test was performed considering noisy data obtained from four measurements (see Fig. 6.13). Using a built in function to locate extrema we obtained

$$\widetilde{c}_1 = (0.94, -0.022),\ \widetilde{c}_2 = (0.011, 0.98),\ \widetilde{c}_3 = (-0.97, 0.006) \text{ and } \widetilde{c}_4 = (-0.0005, -0.47).$$

Since

$$f_3 = -2\delta_{(1,0)} + 6\delta_{(0,1)} - 4\delta_{(-1,0)} - 5\delta_{(0,0.5)},$$

the point sources are being well recovered. This can also be seen in the contour plots of Fig. 6.14. Using these locations and following remark 6.13 we obtain, for $\kappa = 1.5$ and the aforementioned directions $\widehat{d}_1, \ldots, \widehat{d}_{100}$, a 100×4 system which, solved in a least squares sense gives the intensities

$$\begin{array}{ll} \widetilde{a}_1 \approx -2.09 + 3 \times 10^{-12} i & \widetilde{a}_2 \approx 6.2 - 4 \times 10^{-13} i \\ \widetilde{a}_3 \approx -4.02 + 3 \times 10^{-12} i & \widetilde{a}_4 \approx -4.9 - 2 \times 10^{-12} i \end{array}.$$

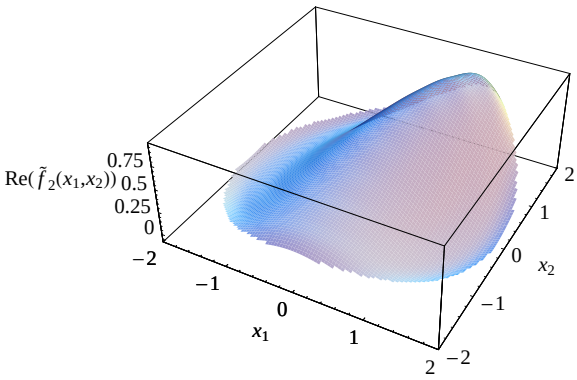

(a) $\kappa = 1.5$

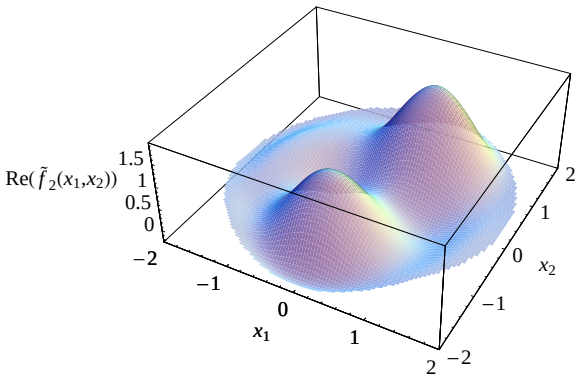

(b) $\kappa = 1.5,\ 3.5$

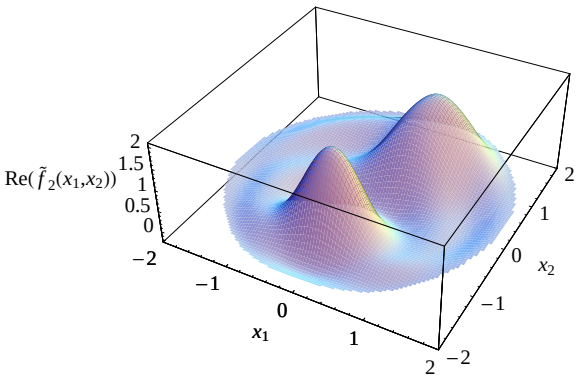

(c) $\kappa = 1.5,\ 3.5,\ 5.5$

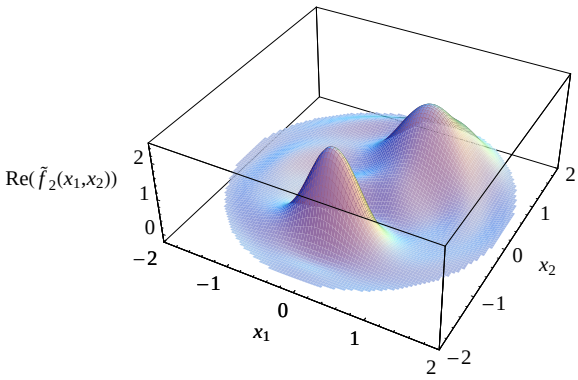

(d) $\kappa = 1.5,\ 3.5,\ 5.5,\ 7.5$

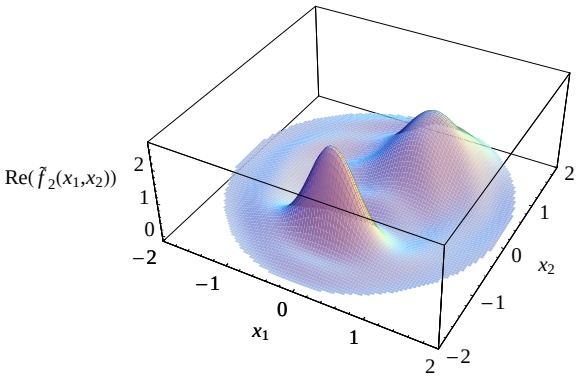

(e) $\kappa = 1.5,\ 3.5,\ 5.5,\ 7.5,\ 9.5$

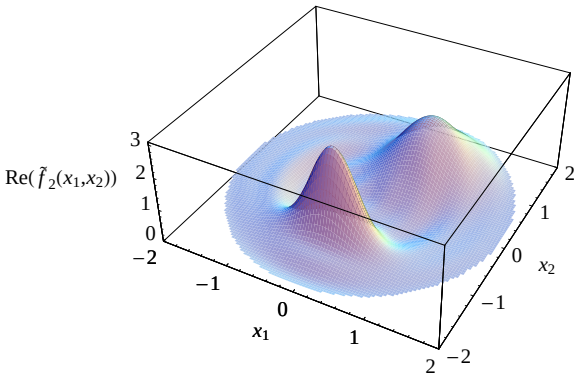

(f) $\kappa = 1.5,\ 3.5,\ 5.5,\ 7.5,\ 9.5,\ 11.5$

Figure 6.9: Reconstruction of f_2 considering noise free data obtained from several measurements.

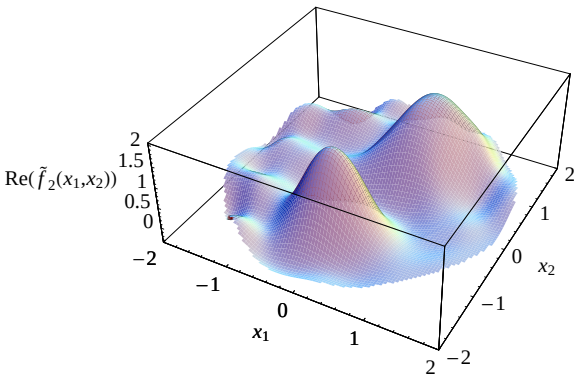

Figure 6.10: Reconstruction of f_2 considering data with 5% of noise obtained from three measurements.

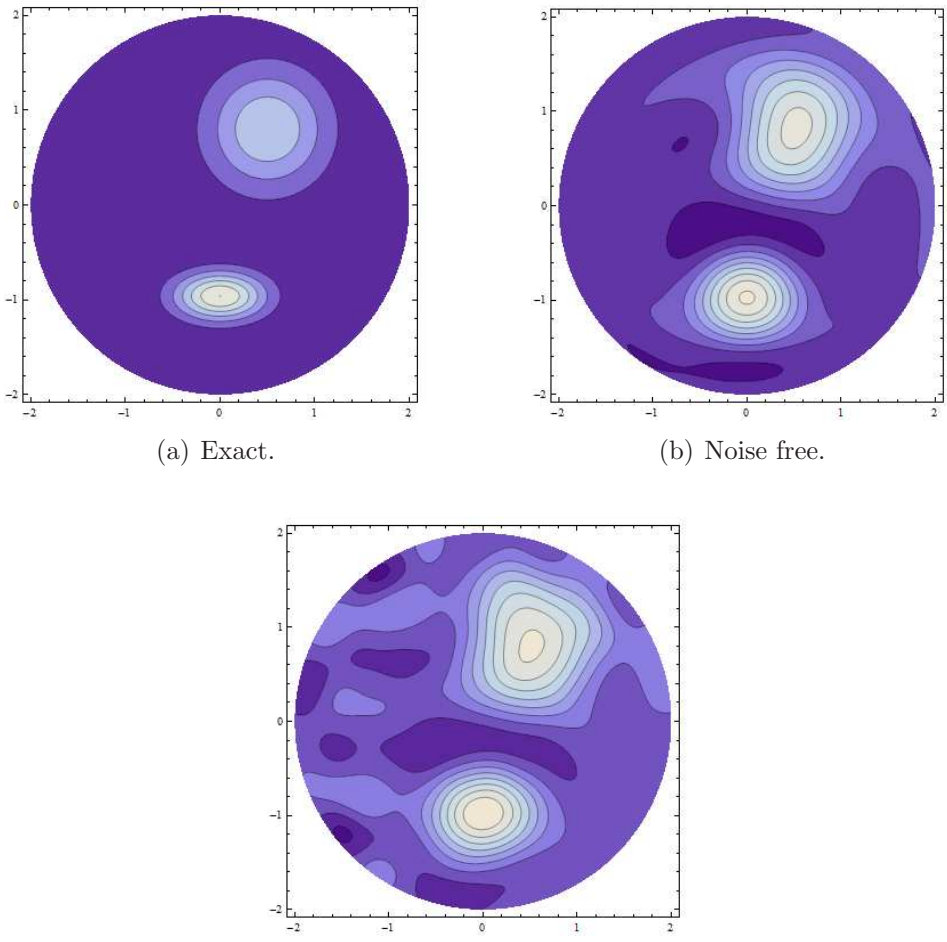

(a) Exact.

(b) Noise free.

(c) 5% of noise.

Figure 6.11: Contour plot regarding the reconstructions of f_2 considering three boundary measurements.

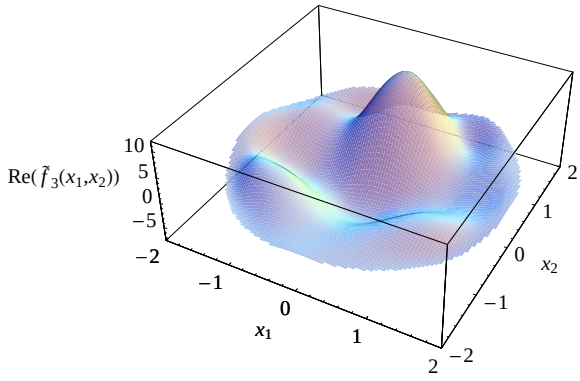

(a) $\kappa = 1.5,\ 3.5$

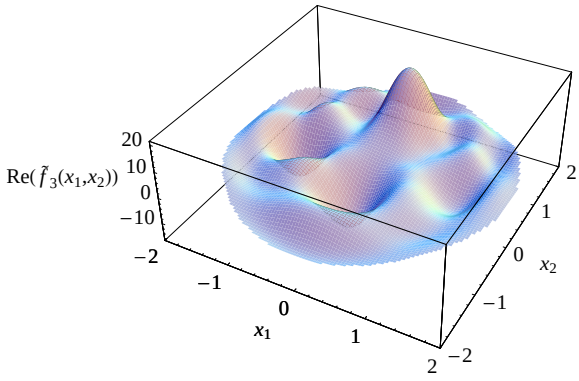

(b) $\kappa = 1.5,\ 3.5,\ 5.5$

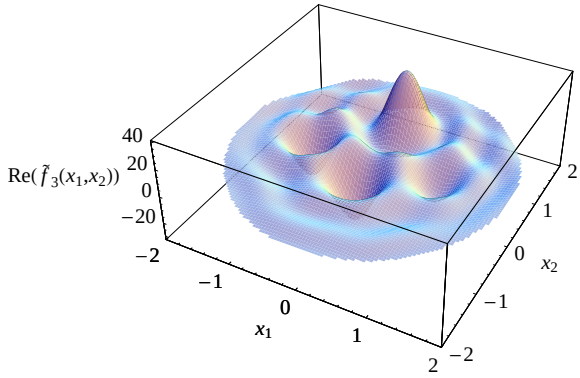

(c) $\kappa = 1.5,\ 3.5,\ 5.5,\ 7.5$

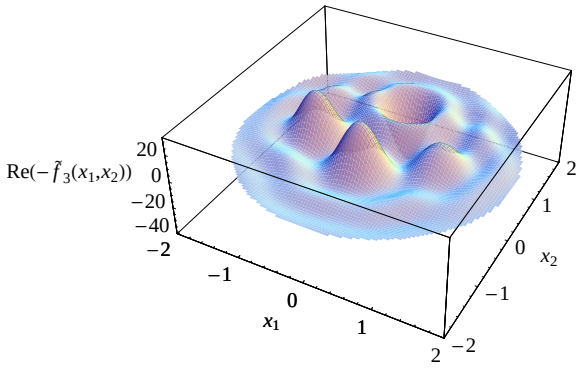

(d) the same as (c)

Figure 6.12: Reconstruction of four points sources considering noise free data obtained from several boundary measurements.

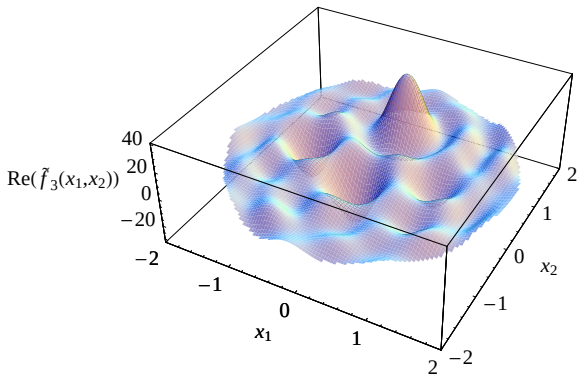

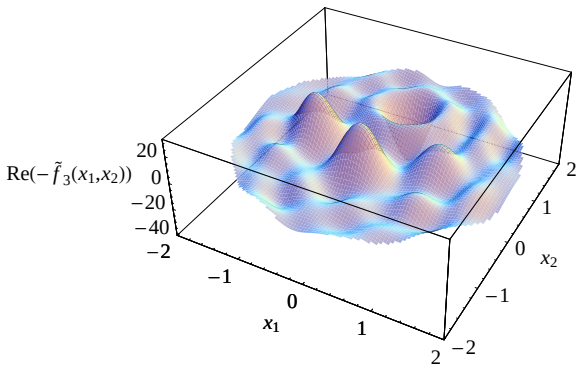

Figure 6.13: Reconstruction of four points sources considering data with 5% of noise obtained from four boundary measurements.

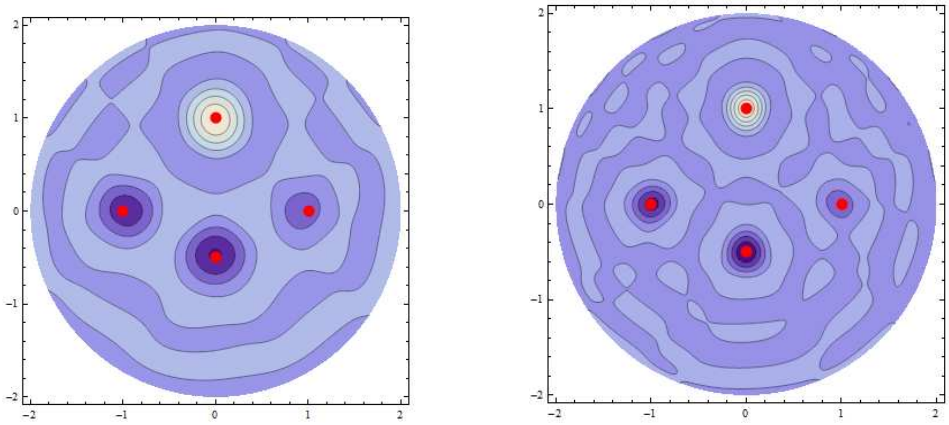

(a) Noise free. (b) 5 % of noise.

Figure 6.14: Contour plot regarding the reconstruction of four points sources (red dots) considering data obtained from four boundary measurements.

6.7 Conclusions

In this Chapter we studied the identification of acoustic sources from boundary measurements. It was established that identification (in the L^2 sense) can be obtained if the boundary data generated by all the frequencies on some open interval is known. Several numerical simulations showed the feasibility and stability of the method based on the reciprocity functional. With a few number of boundary measurements we were able to identify some properties of the source and in some cases we obtained good reconstructions. This can be useful if one wants to identify a class where the source belongs. Depending on such class, a single boundary may be sufficient (eg. point sources) and other (more efficient) methods can be applied. Since our method requires integrations on the boundary, the number and location of the observation points must provide accurate numerical integrations. Thus, for incomplete boundary data, a completion method must be implemented first.

Final remarks and future work

In the first part of this work we addressed the identification and reconstruction of shapes and (Robin) coefficients from a single boundary measurement. The MFS based decomposition method performed well for simply connected inclusions and we aim to develop a method to reconstruct a non connected inclusion. No numerical tests have been carried out for this situation but it is clear that with the proposed line search some shadow effects may lead to poor reconstructions.

We provided an example that shows the non identifiability of both shape and coefficient from a single measurement. This is still an open problem even for several boundary measurements. Recently Rundell showed in [79] a local identifiability result for this problem using two appropriate measurements (in the 2D case). Following the ideas developed in Chapter 4, we want to study the application of the MFS based decomposition method to this inverse problem and eventually to a similar acoustic setting.

In a second part of the work we applied the developed methods and techniques to similar inverse problems in the context of linear elasticity. The methods performed well and the main difficulties were the results based on the maximum principle and Hopf's lemma. Although several numerical tests suggest that some of the results hold, we were not able to establish the corresponding theoretical results. In particular, we are interested in developing a criterion to distinguish elastic cavities from inclusions and in the implementation of a numerical method to retrieve multiple inclusions or cavities. Other line of work will be transmission problems in linear elasticity. In particular we are interested in the identification of elastic inclusions with different (and unknown) elastic properties of the domain of propagation. Despite some examples that show the difficulties in the identification of both Lamé parameters and elastic inclusion, we obtained good numerical results for this problem.

Regarding the sources inverse problem, we will study the application of the MFS for the Cauchy problem as a data completion method, in order to use the integral method to retrieve compactly supported sources from partial data. A possible extension to the elastic case will also be investigated.

Appendix
Levenberg–Marquardt method for non linear least squares problems

Given a vector function $\mathbf{F} : \mathbb{R}^n \to \mathbb{R}^m$ with $m \geq n$ we want to solve the following global optimization problem

$$x^* = \text{argmin}_x F_{obj}(x)$$

where the objective function F_{obj} is

$$F_{obj}(x) = \frac{1}{2}\sum_{i=1}^{m} F_i(x)^2 = \frac{1}{2}\mathbf{F}(x) \cdot \mathbf{F}(x),$$

with $\mathbf{F}(x) = (F_1(x), \ldots, F_m(x))$. The methods for such optimization problems are iterative and usually enforce a descent condition,

$$F_{obj}(x_{k+1}) < F_{obj}(x_k)$$

in order to avoid the convergence to a maximizer. These descent methods can be described as:

Algorithm 2

`Give` x_0

h_k :=`search direction(`x_k`)`

α_k :=`step length(`h_k`,`x_k`)`

$x_{k+1} := x_k + \alpha_k h_k$

Supposing that $\mathbf{F}$ has continuous second order partial derivatives, we can write

$$\mathbf{F}(x+h) = \mathbf{F}(x) + \mathbb{J}(x)h + O(|h|^2) \tag{6.20}$$

where

$$\mathbb{J}(x) = \left[\frac{\partial F_i}{\partial x_j}(x)\right]$$

is the Jacobian. In terms of F_{obj}, the gradient is given by

$$F'_{obj}(x) = \mathbb{J}(x)^\top \mathbf{F}(x)$$

and the Hessian by

$$F''_{obj}(x) = \mathbb{J}(x)^\top \mathbb{J}(x) + \sum_{i=1}^{m} F_i(x) F''_i(x).$$

From the Taylor expansion (6.20) we have, for small $|h|$, the linear approximation

$$\mathbf{F}(x+h) \approx \ell(h) := \mathbf{F}(x) + \mathbb{J}(x)h.$$

Inserting this approximation in the definition of F_{obj} we have

$$F_{obj}(x+h) \approx L(h) := \frac{1}{2}\ell(h)^\top \ell(h) = F_{obj}(x) + h^\top \mathbb{J}(x)^\top \mathbf{F}(x) + \frac{1}{2} h^\top \mathbb{J}^\top(x)\mathbb{J}(x)h. \tag{6.21}$$

The gradient and Hessian of L are

$$L'(h) = \mathbb{J}(x)^\top \mathbf{F}(x) + \mathbb{J}(x)^\top \mathbb{J}(x)h \ \wedge \ L''(h) = \mathbb{J}(x)^\top \mathbb{J}(x)$$

respectively. If $\mathbb{J}$ has full rank then L admits a unique minimizer h_{min}, solution of the equation

$$L'(h_{min}) = 0.$$

If instead we solve the penalized system

$$L'(h_{lm}) + \mu \mathbb{I} h_{lm} = 0,\ \mu \geq 0$$

we obtain the Levenberg–Marquardt method (LM). The damping parameter $\mu \geq 0$ has several effects:

- For all $\mu > 0$ the coefficient matrix is positive definite and this ensures that h_{min} is a descent direction.
- For large values of μ, h_{min} is a short step in the descent direction.
- If μ is very small then we have a Newton method and we get a good step when the approximation is near x^*.
- Can be used to implement constrains in the optimization problem.

The initial choice of μ is usually given by

$$\mu = \tau \max\{a_{ii}^{(0)}\}$$

where τ is given (typically $\tau = 10^{-3}$) and $\mathbb{A}^{(0)} = \mathbb{J}(x_0)^\top \mathbb{J}(x_0)$. During the iterative process the updating is controlled by the gain ratio

$$\rho := \frac{F_{obj}(x) - F_{obj}(x + h_{lm})}{L(0) - L(h_{lm})}$$

according to the strategy:

Algorithm 3

`If` $\rho > 0$

$\mu := \mu \times \max\{1/3, 1 - (2\rho - 1)^3\}; \nu := 2$

`else`

$\mu := \mu \times \nu; \nu := 2\nu$

`endif`

If $\rho > 0$, then $x_{new} := x + h_{lm}$ is an admissible iteration and the dumping parameter is decreased. Otherwise, the iteration is not admissible and the penalized system is solved for a higher value of μ.

As stopping criteria we use, for a given tolerance tol,

$$\frac{F_{obj}(x_{new}) - F_{obj}(x)}{F_{obj}(x)} \leq tol$$

where x, x_{new} are two consecutive admissible iterations. Finally the condition $k \geq k_{\max}$ to avoid infinite loops. In conclusion:

Algorithm 4 `Levenberg--Marquardt method`

`Begin`

`Given:` x_0, $k_{\max}$, tol, $\tau := 10^{-3}$

$k := 0;\ \nu := 2;\ x = x_0\ \mathbb{A} := \mathbb{J}^\top(x)\mathbb{J}(x);\ \mathbf{g} := \mathbb{J}^\top(x)\mathbf{F}(x)$

found `:=false;` $\mu = \tau \max\{a_{ii}\}$

`While (not` ***found***`)` `and` $k < k_{\max}$

$k := k + 1;$ `Solve` $(\mathbb{A} + \mu\mathbb{I})h_{lm} = -\mathbf{g}$

$x_{new} := x + h_{lm}$

$\rho := \dfrac{F_{obj}(x) - F_{obj}(x_{new})}{L(0) - L(h_{lm})}$

`If` $\rho > 0$

`If` $(F_{obj}(x_{new}) - F_{obj}(x))/F_{obj}(x) \leq tol$

`found:=true`

`else`

$x := x_{new}$

$\mathbb{A} := \mathbb{J}^\top(x)\mathbb{J}(x);\ \mathbf{g} := \mathbb{J}^\top(x)\mathbf{F}(x)$

$\mu = \mu \times \max\{1/3, 1 - (2\rho - 1)^3\};\ \nu := 2$

`endif`

`else`

$\mu = \mu \times \nu;\ \nu := 2\nu$

`endif`

```
    endWhile

End
```

References

[1] Abda A.B., Delbary F. and Haddar H. *On the use of the reciprocity-gap functional in inverse scattering from planar cracks*, Math. Models Methods Appl. Sci. **15** (10) (2005) 1553– 1574.

[2] Abda A.B., Chaabane S., El Dabaghi F. and Jaoua M., *On a Non-linear Geometrical Inverse Problem of Signorini Type: Identifiability and Stability*, Math. Meth. Appl. Sci. **21** (1998) 1379–1398.

[3] Adams R.A., *Sobolev Spaces*, Academic Press, New York, 1975.

[4] Alifanov O.M., *Inverse Heat Transfer Problems*, Springer-Verlag, Berlin, 1994.

[5] Alessandrini G. and Rondi L., *Optimal stability for the inverse problem of multiple cavities*, J. Diff. Eqns **176** (2001) 356-386.

[6] Alvarez C., Conca C., Friz L., Kavian O. and Ortega J.H., *Identification of immersed obstacles via boundary measurements*, Inverse Problems 21 (2005) 1531-1552.

[7] Alves C.J.S., *Density results for the Helmholtz equation and the method of fundamental solutions*, Advances in Computational Engineering & Sciences Vol. I (Editors: Atluri S.N. and Brust F.W.) Tech. Sc. Press. (2000) 45–50.

[8] Alves C.J.S., *Density results on partial differential equations and the derivation of meshless methods*, Proceedings of the International Conference in Engineering & Science (Editors: Atluri S.N., Beskos D. and Polyzos D.), Los Angeles, USA (2003) in CDROM.

[9] Alves C.J.S. and Chen C.S., *A new method of fundamental solutions applied to non-homogeneous elliptic problems*, Advances in Computational Mathematics **23** (2005) 125–142.

[10] Alves C.J.S., Colaço M.J., Leitão V.M.A., Martins N.F.M., Orlande H.R.B. and Roberty N.C., *Recovering the source term in a linear diffusion problem by the Method of Fundamental Solutions*, Inv. Probl. in Sci. and Eng. **16** (8) (2008) 1005–1021.

[11] Alves C.J.S. and Ha Duong T., *On inverse scattering by screens*, Inverse Problems **13** (1997) 1161-1176.

[12] Alves C.J.S. and Martins N.F.M., *The method of fundamental solutions applied to a heat conduction inverse problem*, Proceedings of the III European Conference on Computational Mechanics, Solids, Structures and Coupled Problems in Engineering (Editors: Soares C.A.M., Martins J.A.C., Rodrigues H.C. and Ambrósio J.A.C.), Lisbon, Portugal (2006), in CDROM.

[13] Alves C.J.S. and Martins N.F.M., *The direct Method of Fundamental Solutions and the inverse Kirsch-Kress Method for the reconstruction of elastic inclusions or cavities*, To appear in J. Integral Eq. and Appl.

[14] Alves C.J.S. and Martins N.F.M., *On the determination of a Robin boundary coefficient in an elastic cavity*, Progress on meshless methods (Editors: Ferreira A., Kansa E., Fasshauer G. and Leitão V.), Springer (2008) 125–139.

[15] Alves C.J.S. and Martins N.F.M., *Reconstruction of inclusions or cavities in potential problems using the MFS*, To appear in "The method of Fundamental Solutions - A Meshless Method" (Editors: Chen C.S., Karageorghis A. and Smyrlis Y.S.).

[16] Alves C.J.S., Martins N.F.M. and Roberty N.C., *Full identification of acoustic sources with multiple frequencies and boundary measurements*, submitted.

[17] Alves C.J.S., Martins N.F.M., Roberty N.C., Colaço M.J. and Orlande H.R.B. *Solving an inverse source problem with the MFS and a higher order direct problem*, Proceedings of the Inverse Problems, Design and Optimization Symposium, Miami, Florida (2007) pp. 548-555.

[18] Ameur H.B., Burger M. and Hackl B., *Level set methods for geometric inverse problems in linear elasticity*, Inverse Problems **20** (2004) 673-696.

[19] Andrieux S. and Ben Abda A., *The reciprocity gap: a general concept for flaws identification problems*, Mechanical Research Communications **20** (5) (1993) 415–20.

[20] Andrieux S., Ben Abda A. and Bui H.D., *Sur lidentification de fissures planes via le concept décart à la réciprocité en élasticité*, C. R. Acad. Sci. Paris Sér. I Math. **324** (1997) 1431-1438.

[21] Andrieux S., Baranger T.N. and Ben Abda A., *Solving Cauchy problems by minimizing an energy-like functional*, Inverse Problems **22** (2006) 115–133.

[22] Ang D.D., Trong D.D. and Yamamoto M., *Unique continuation and identification of boundary of an elastic body*, J. Inverse Ill-posed Problems **3** (1995) 417-428.

[23] Ang D.D., Trong D.D. and Yamamoto M., *Identification of cavities inside two-dimensional heterogeneous isotropic elastic bodies*, Journal of elasticity **56** (1999) 371–385.

[24] Arantes e Oliveira E.R., *Plane stress analysis by a general integral method*, Proc. ASCE Eng. Mech. Div. **94** (1968) 79–101.

[25] Argyropoulos E. and Kiriaki K., *Modified Green's function technique for disjoint bodies in two-dimensional linear elasticity*, Bull. Greek Math. Soc. **47** (2003) 137–151.

[26] Bogomolny A., *Fundamental solution method for elliptic boundary value problems* , SIAM J. Numer. Anal. **22** (1985) 644–669.

[27] Bonnet M. and Constantinescu A., *Inverse problems in elasticity*, Inverse Problems 21 (2005) R1–R50.

[28] Bryan K. and Caudill L.F., *An inverse problem in thermal imaging*, SIAM J. Appl. Math. **56** (1996) 715-735.

[29] Bukhgeim A.L., Cheng J. and Yamamoto M., *Stability for an inverse boundary problem of determining a part of a boundary*, Inverse Problems **15** (1999) 1021-1032.

[30] Cakoni F. and Kress R., *Integral equations for inverse problems in corrosion detection from partial Cauchy data*, Inverse Problems and Imaging, vol. 1, **2** (2007) 229-245.

[31] Calderon A.P., *On an inverse boundary value problem*, Seminar on Numerical Analysis and its Application to Continuum Physics: Rio de Janeiro,(1980) pp 65-73.

[32] Chaabane S., Elhechmi C. and Jaoua M., *A stable recovery method for the Robin inverse problem*, Mathematics and Computers in Simulation **66** (2004) 367-383.

[33] Chaabane S. and Jaoua M., *Identification of Robin coefficients by the means of boundary measurements*, Inverse Problems **15** (1999) 1425-1438.

[34] Chen G. and Zhou J. , *Boundary Element Methods*, Academic Press, London, 1992.

[35] Colton D. and Haddar H., *An application of the reciprocity gap functional to inverse scattering theory*, Inverse Problems **21** (2005) 383–398.

[36] Colton D. and Kress R., *Inverse acoustic and electromagnetic scattering theory*, Applied mathematical sciences **93**, 2nd ed., Springer, Berlin, 1998.

[37] Dautray R. and Lions J.– L., *Analyse mathématique et calcul numérique pour les sciences et les techniques*, tome 1, Serie scientifique, Masson, Paris, 1984.

[38] El Badia A. and Ha Duong T., *Some remarks on the problem of source identification from boundary measurements*, Inverse Problems 14 (1998) 883–891.

[39] El Badia A. and Ha Duong T., *An inverse source problem in potential analysis*, Inverse Problems 16 (2000) 651–663.

[40] Cheney M., Isaacson D. and Newell J.C., *Electrical Impedance Tomography*, SIAM Review **41** (1) (1999) 85–101.

[41] Colaço M.J., Orlande H.R.B., Roberty N.C., Alves C.J.S. and Leitão V.M.A., *On the use of MFS in Linear Inverse Diffusion Problems*, CIT06-0732, Proceeding of the 11th Brazilian Congress on Thermal Science and Engineering Dec-5-8 2006, Curitiba, Brazil.

[42] Evans L.C., *Partial differential equations*, Graduate Studies in Mathematics, vol. 19, AMS, 1998.

[43] Fairweather G. and Karageorghis A., *The Method of Fundamental Solutions for Elliptic Boundary Value Problems*, Advances in Comp. Math. Vol. 9 (1998) 69–95.

[44] Fasino D. and Inglese G., *Discrete methods in the study of an inverse problem for Laplace's equation*, IMA Journal of Numerical Analysis **19** (1999) 105–118.

[45] Fritz J., *Partial differential equations*, Applied Mathematical Sciences **1**, 4th edition, Springer–Verlag, New York, 1982.

[46] Hadamard J., *Lectures on the Cauchy Problem in Linear Partial Differential Equations*, Yale University Press, New Haven, 1923.

[47] Hanke M., *Limitations of the L–curve method in ill–posed problems*, BIT **36** (1996) 287–301.

[48] Hansen P.C., *Analysis of discrete ill–posed problems by means of the L–curve*, SIAM Review **34** (4) (1992) 561–580.

[49] Hettlich F. and Rundell W., *Iterative methods for the reconstruction of an inverse potential problem*. Inverse Problems **12** (1996) 251-266.

[50] Inglese G., *An inverse problem in corrosion detection*, Inverse Problems **13** (1997) 977-994.

[51] Isakov V., *Inverse Problems for Partial diferential Equations*, Applied Mathematical Sciences **127**, Springer-Verlag, New-York, 1998.

[52] Jin B. and Marin L., *The method of fundamental solutions for inverse source problems associated with steady-state heat conduction*, Int. J. Numer. Meth. Engng. **69** (2007) 1570–1589.

[53] Kansa E. J., *Multiquadrics– A scattered data approximation scheme with applications to computational fluid mechanics – II: Solutions to parabolic, hyperbolic and elliptic partial differential equations*, Comput. Math. Appl. **19** (1990) 147–161.

[54] Katsurada M., *Asymptotic error analysis of the charge simulation method in a Jordan region with an analytic boundary*, J. Fac. Sci. Univ. Tokyo, Sect. IA **37** (1990) 635–657.

[55] Katsurada M. and Okamoto H., *The collocation points of the fundamental solution method for the potential problem*, Computers Math. Applic. **31**(1) (1996) 123–137.

[56] Kaup P.G. and Santosa F., *Nondestructive evaluation of corrosion damage using electrostatic measurements*, Journal of Nondestructive Evaluation, vol. 14, **3** (1995) 127–135.

[57] Kaup P.G., Santosa F. and Vogelius M., *A method for imaging corrosion damage in thin plates from electrostatic data*, Inverse Problems, **12** (1996), 279–293.

[58] Kirsch A., *The domain derivative and two applications in inverse scattering theory*, Inverse Problems, **9** (1993), 81–96.

[59] Kirsch A., *The Detection of Holes by Elasto-Static Measurements*, Fakultt fr Mathematik, Universitt Karlsruhe, Preprint 10 (2001).

[60] Kirsch A. and Kress R., *On an integral equation of the first kind in inverse acoustic scattering*, Inverse Problems ISNM **77** (1986) 93–102.

[61] Kitagawa T., *On the numerical stability of the method of fundamental solution applied to the Dirichlet problem*, Japan J. Appl. Math. **5** (1988) 123–133.

[62] Kress R., *Linear integral equations*, 2nd Edition, Springer, New York, 1999.

[63] Kress R. and Rundell W., *Nonlinear integral equations and the iterative solution for an inverse boundary value problem*, Inverse Problems **21** (2005) 1207-1223.

[64] Kupradze V.D. and Aleksidze M.A., *The Method of Functional Equations for the Approximate Solution of Certain Boundary Value Problems*, U.S.S.R. Computational Mathematics and Mathematical Physics **4** (1964) 82–126.

[65] Lawson C.L. and Hanson R.J., *Solving least squares problems*, Englewood Cliffs, Prentice–Hall, NJ, 1974.

[66] Madsen K., Nielsen H.B. and Tingleff O., *Methods for non-linear Least Squares Problems*, IMM, 60 pages, Denmark, 2004.

[67] Marin L., *A meshless method for solving the Cauchy problem in three-dimensional elastostatics*, Comput. Math. Appl. **50** (2005) 73–92.

[68] Martins N.F.M. and Silvestre A.L., *An iterative MFS approach for the detection of immersed obstacles*, Eng. Anal. Bound. Elem. **32** (6) (2008) 517–524.

[69] Mathon R. and Johnston R.L., *The approximate solution of elliptic boundary-value problems by fundamental solutions*, SIAM J. Numer. Anal. **14** (1977) 638-650.

[70] Menif F., *Identification de cavités par les ondes acoustiques et élastiques*, Thèse de Doctorat, 2006.

[71] Morassi A. and Rosset E., *Detecting rigid inclusions or cavities, in an elastic body*, Journal of elasticity **73** (2003) 101–126.

[72] Morozov V. A., *The error principle in the solution of operator equations by the regularization method*, USSR Comput. Math. and Math. Phus. **8** (2) (1968) 63–87.

[73] Murat F., and Simon J., *Sur le contrôle par un domaine géometrique*, Rapport du L.A. 189 no. 76015 (1976) Univ. Paris VI.

[74] Nakamura G. and Uhlmann G., *Identification of Lamé parameters by boundary measurements*, American Journal of Mathematics **115** (1993) 1161–1187.

[75] Novikov P., *Sur le probleme inverse du potentiel,* Dokl. Akad. Nauk **18** (1938) 165–168.

[76] Ramm A.G., *Inverse problems- mathematical and analytic techniques with applications to engineering* , Springer, New York, 2005.

[77] Raviart P.A. and Thomas J.M., *Introduction à l'analyse numérique des équations aux derivées partielles*, Masson, Paris, 1988.

[78] Rudin W., *Functional Analysis*, International series in pure and applied mathematics, 2nd. ed., McGraw–Hill, 1991.

[79] Rundell W., *Recovering an obstacle and its impedance from Cauchy data*, Inverse Problems **24** (2008).

[80] Schaback R., *Error estimates and condition numbers for radial basis function interpolation.* Adv. Comp. Math. **3** (1995) 251–264.

[81] Simon J., *Differentiation with respect to the domain in boundary value problems*, Numer. Funct. and Optimiz. **2** (1980), 649–687.

[82] Sokolowski J. and Zolesio J.P., *Introduction to shape optimization : shape sensitivity analysis*, Springer-Verlag, Berlin, 1992.

[83] Trong D.D. and Ang D.D., *Domain identification for semilinear elliptic equations in the plane: the zero flux case*, Z. An. Anw. **19** (2000)(1) 109-120.

[84] Valtchev S.S., *Numerical analysis of methods with fundamental solutions for acoustic and elastic wave propagation problems*, Ph.D. thesis IST-UTL, 2008.

[85] Vladimirov V.S., *Equations of Mathematical Physics*, MIR Publishers, Moscow, 1992.